UNIVERSIDAD DE CÓRDOBA

INSTITUTO DE AGRICULTURA SOSTENIBLE IAS

CSIC
CONSEJO SUPERIOR DE INVESTIGACIONES CIENTÍFICAS

TESIS DOCTORAL

MONITORIZACIÓN 3D DE CULTIVOS Y CARTOGRAFÍA DE MALAS HIERBAS MEDIANTE VEHÍCULOS AÉREOS NO TRIPULADOS PARA UN USO SOSTENIBLE DE FITOSANITARIOS

Jorge Torres Sánchez

Directores
Francisca López Granados
José Manuel Peña Barragán

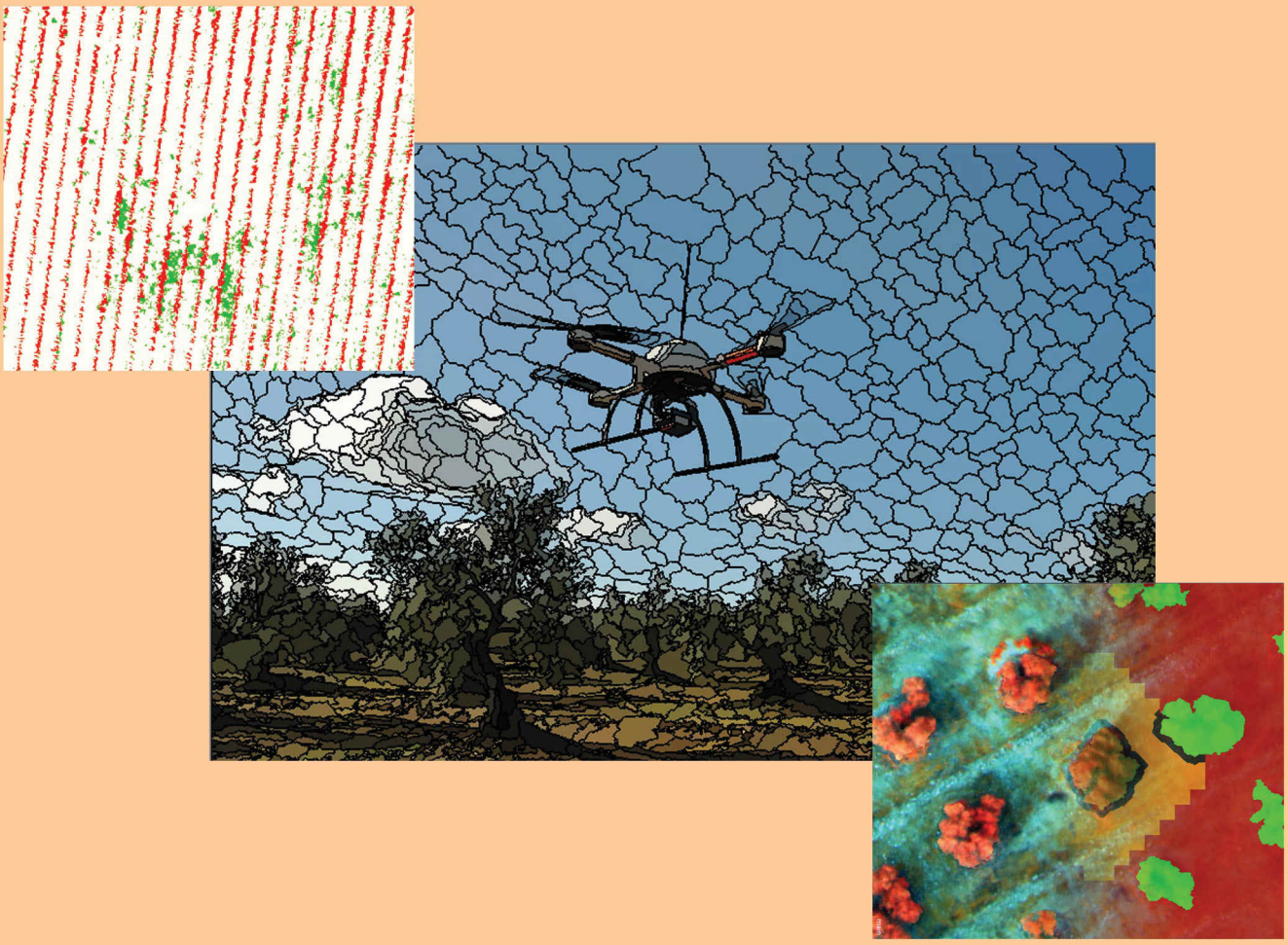

UNIVERSIDAD DE CÓRDOBA

DEPARTAMENTO DE INGENIERÍA GRÁFICA Y GEOMÁTICA

TESIS DOCTORAL

MONITORIZACIÓN 3D DE CULTIVOS Y CARTOGRAFÍA DE MALAS HIERBAS MEDIANTE VEHÍCULOS AÉREOS NO TRIPULADOS PARA UN USO SOSTENIBLE DE FITOSANITARIOS

Presentada por Jorge Torres Sánchez para la obtención del título de
Doctor Ingeniero de Montes

Directores:
Francisca López Granados
José Manuel Peña Barragán
Tutor:
Alfonso García-Ferrer Porras

Córdoba, Enero de 2.017

TÍTULO DE LA TESIS: Monitorización 3D de cultivos y cartografía de malas hierbas mediante vehículos aéreos no tripulados para un uso sostenible de fitosanitarios

DOCTORANDO/A: Jorge Torres Sánchez

INFORME RAZONADO DEL/DE LOS DIRECTOR/ES DE LA TESIS

La **Dra. Francisca López Granados, Investigadora Científica**, y el **Dr. José Manuel Peña Barragán, investigador Ramón y Cajal**, ambos adscritos al Instituto de Agricultura Sostenible de Córdoba (IAS-CSIC), como directores de la Tesis Doctoral titulada "MONITORIZACIÓN 3D DE CULTIVOS Y CARTOGRAFÍA DE MALAS HIERBAS MEDIANTE VEHÍCULOS AÉREOS NO TRIPULADOS PARA UN USO SOSTENIBLE DE FITOSANITARIOS" realizada por Jorge Torres Sánchez,

INFORMAN QUE:

- Dicha Tesis Doctoral ha sido realizada bajo nuestra dirección.
- Ha tenido como principal objetivo el desarrollo de metodologías robustas para la cartografía de malas hierbas en cultivos herbáceos en fase temprana y la monitorización tridimensional de cultivos leñosos, con el fin último de contribuir a la implementación de estrategias de técnicas de aplicación variable en el ámbito de la agricultura de precisión que permitan un uso sostenible de los productos fitosanitarios.
- Tanto la metodología como el trabajo de investigación, las conclusiones y los resultados obtenidos son satisfactorios.
- En el desarrollo de su etapa predoctoral, Jorge Torres Sánchez ha colaborado en numerosas líneas de trabajo que se han desarrollado expresamente en su Tesis Doctoral así como en otros Proyectos de Investigación del grupo en los que el doctorando se ha incorporado. De estos trabajos se han derivado las siguientes publicaciones, señalándose con asterisco las directamente relacionadas con los objetivos de su Tesis Doctoral:

Revistas incluidas en el Science Citation Index:

1. López-Granados, F., **Torres-Sánchez, J.**, de Castro, A.I., Serrano-Pérez, A., Mesas-Carrascosa, F.J., Peña, J.M. (2016) Object-based early monitoring of a grass weed in a grass crop using high resolution UAV-imagery. En prensa, *Agronomy for Sustainable Development*.
2. Mesas-Carrascosa, F.J., Clavero, I., **Torres-Sánchez, J.**, García-Ferrer, A., Peña, J.M., López-Granados, F. (2016). Accurate ortho-mosaicked six-band

multispectral UAV images as affected by mission planning for precision agriculture proposes. En prensa, *International Journal of Remote Sensing*.

3. Pérez-Ortiz, M., Peña, J.M., Gutiérrez, P.A., **Torres-Sánchez, J.**, Hervás-Martínez, C., López-Granados, F. (2016). Selecting patterns and features for between- and within- crop-row weed mapping using UAV-imagery. *Expert Systems with Applications*, 47:85-94.
4. Mesas-Carrascosa, F.-J., **Torres-Sánchez, J.**, Clavero-Rumbao, I., García-Ferrer, A., Peña, J.-M., Borra-Serrano, I., & López-Granados, F. (2015). Assessing Optimal Flight Parameters for Generating Accurate Multispectral Orthomosaicks by UAV to Support Site-Specific Crop Management. *Remote Sensing*, 7(10), 12793–12814.
5. Borra-Serrano, I., Peña, J. M., **Torres-Sánchez, J.**, Mesas-Carrascosa, F. J., & López-Granados, F. (2015). Spatial Quality Evaluation of Resampled Unmanned Aerial Vehicle-Imagery for Weed Mapping. *Sensors*, 15(8), 19688–19708.
6. * López-Granados, F., **Torres-Sánchez, J.**, Serrano-Pérez, A., Castro, A. I. de, Mesas-Carrascosa, F.-J., & Peña, J.-M. (2016). Early season weed mapping in sunflower using UAV technology: variability of herbicide treatment maps against weed thresholds. *Precision Agriculture*, 17, 183-199.
7. Pérez-Ortiz, M., Peña, J. M., Gutiérrez, P. A., **Torres-Sánchez, J.**, Hervás-Martínez, C., & López-Granados, F. (2015). A semi-supervised system for weed mapping in sunflower crops using unmanned aerial vehicles and a crop row detection method. *Applied Soft Computing*, 37, 533–544.
8. * **Torres-Sánchez, J.**, López-Granados, F., Serrano, N., Arquero, O., & Peña, J. M. (2015). High-Throughput 3-D Monitoring of Agricultural-Tree Plantations with Unmanned Aerial Vehicle (UAV) Technology. *PLoS ONE*, 10(6), e0130479.
9. * **Torres-Sánchez, J.**, López-Granados, F., & Peña, J. M. (2015). An automatic object-based method for optimal thresholding in UAV images: Application for vegetation detection in herbaceous crops. *Computers and Electronics in Agriculture*, 114, 43–52.
10. * Peña, J. M., **Torres-Sánchez, J.**, Serrano-Pérez, A., de Castro, A. I., López-Granados, F. (2015). Quantifying Efficacy and Limits of Unmanned Aerial Vehicle (UAV) Technology for Weed Seedling Detection as Affected by Sensor Resolution. Sensors, 15, 5609-5626.
11. * **Torres-Sánchez, J.**, Peña, J. M., de Castro A. I., López-Granados, F. (2013). Multi-temporal mapping of the vegetation fraction in early-season wheat fields using images from UAV. *Computers and electronics in agriculture*, 103, 104–113.
12. * Peña, J. M., **Torres-Sánchez, J.**, de Castro, A. I., Kelly , M., López-Granados, F. (2013). Weed mapping in early-season maize fields using object-based analysis of unmanned aerial vehicle (UAV) images. *PLoS ONE*, 8, e77151.
13. * **Torres-Sánchez, J.**, López-Granados, F., de Castro A. I., Peña-Barragán, J. M. (2013). Configuration and specifications of an unmanned aerial vehicle (UAV) for early site specific weed management. *PLoS ONE*, 8, e58210.

Revistas incluidas en el Science Citation Index (artículos en revisión):

1. * **Torres-Sánchez, J.**, López-Granados, F., Jiménez-Brenes, F.M., Borra-Serrano, I., de Castro, A.I., Peña, J.M. (2016). 3-D vineyard monitoring with UAV images and a novel OBIA procedure for precision viticulture applications. *Computers and Electronics in Agriculture,* en revisión.
2. **Torres-Sánchez, J.**, López-Granados, F., Borra-Serrano, I., Peña, J.M. (2016). Assessment of forward overlap influence in the computation time for DSM generation of woody crops from UAV imagery. *Precision Agriculture*, en revision.

Revistas no incluidas en el Science Citation Index:

1. Peña, J.M., **Torres-Sánchez, J.**, Serrano-Pérez, A., López-Granados, F. (2014). Detección de malas hierbas en girasol en fase temprana mediante imágenes tomadas con un vehículo aéreo no tripulado (UAV). *Revista de Teledetección* 42, 39-47.

Aportaciones en Congresos Internacionales:

1. Jiménez-Brenes, F.M., **Torres-Sánchez, J.**, López-Granados, F., de Castro, A.I., Serrano, N., Peña, J.M. (2016). Assessment of pruning intensity from 3-D olive-tree models generated with UAV technology*. 8th Olive International Symposium*. Publicación on-line. Split, Croacia.
2. Gómez-Candón, D., **Torres-Sánchez, J.**, Labbe, S., Jolivot, A., Martinez, S., Regnard, J.L. (2015) Water stress assessment at tree scale: high-resolution thermal UAV imagery acquisition and processing. *VIII International Symposium on Irrigation of Horticultural Crops*. Publicación on-line. Lleida, Spain
3. * **Torres-Sánchez, J.**, López-Granados, F., Peña, J.M. (2015) Mapping olive-tree geometric features from 3-D models generated with an Unmanned Aerial Vehicle (UAV). *10th European Congress of Precision Agriculture*. Pp: 321-329. Tel Aviv, Israel.
4. * **Torres-Sánchez, J.**, López-Granados, F., Serrano, N., Arquero, O., Peña, J.M. (2014). Characterizing olive tree geometric features using unmanned aerial vehicle (UAV) images. *Olivebioteq 2014*. Publicación on-line. Amman, Jordania.
5. * **Torres-Sánchez, J.**, Peña, J. M., de Castro, A.I., Serrano-Pérez, A., López-Granados, F. (2014). Weed seedlings detection in winter cereals for site-specific control: use of UAV imagery to overcome the challenge. *12th International Conference on Precision Agriculture*. Publicación on-line. Sacramento, USA.
6. Peña, J. M., **Torres-Sánchez, J.**, de Castro, A.I., López-Granados, F. (2014). The TOAS project: UAV technology for optimizing herbicide applications in weed-crop systems. *12th International Conference on Precision Agriculture*. Publicación on-line. Sacramento, USA.
7. * Peña, J. M., **Torres-Sánchez, J.**, de Castro, A.I., Serrano-Pérez, A., López-Granados, F. (2014). Comparing visible and color-infrared UAV imagery for early-season weed mapping: the case of maize as a wide row crop. *2nd International Conference on Robotics and associated High-technologies and Equipment for Agriculture and Forestry*. Pp: 319-328. Madrid, Spain.
8. * **Torres-Sánchez, J.**, Peña, J.M., de Castro, A.I., López-Granados, F.. 2014. Multitemporal weed mapping using UAV imagery for early site-specific control:

the case of wheat as a narrow row crop*. 2nd International Conference on Robotics and associated High-technologies and Equipment for Agriculture and Forestry*. Pp: 269-278. Madrid, Spain.

9. Mesas-Carrascosa, F.J., **Torres-Sánchez, J**., Peña, J.M., García-Ferrer, A., Castillejo-González, I.L., López-Granados, F. 2014. Generating UAV accurate ortho-mosaicked images using a six-band multispectral camera arrangement. *2nd International Conference on Robotics and associated High-technologies and Equipment for Agriculture and Forestry*. Pp: 299-308. Madrid, Spain.
10. * **Torres-Sánchez, J.**, Peña-Barragán, J. M., de Castro, A. I., López-Granados, F. (2013) Imagery from unmanned aerial vehicles (UAV) for early site specific weed management (ESSWM). *9th European Congress of Precision Agriculture*. Pp: 193-199. Lleida, Spain.
11. Labbé, S., Gómez-Candón, D., El-Natour, G., Dorado, J., Fernández-Quintanilla, C., López-Granados, F., Peña-Barragán, J. M., de-Castro, A. I., **Torres-Sánchez, J.,** Rabatel, G. (2012) Automatic mosaicking of very high spatial resolution UAV multispectral images for precision agriculture: Test of MICMAC freeware. *First International Conference on Robotics and associated High-technologies and Equipment for Agriculture (RHEA-2012)*. Pp: 269-274. Pisa, Italy.

Aportaciones en Congresos Nacionales:

1. * **Torres-Sánchez J.**, Peña J.M., Serrano-Pérez Á., López-Granados F. (2015). Detección automática de vegetación en estado de plántula en imágenes procedentes de un vehículo aéreo no tripulado (UAV): aplicación para la discriminación de malas hierbas. *XV Congreso de la Sociedad Española de Malherbología.* Pp: 249-255. Sevilla, España.
2. Borra I., Peña J.M., **Torres-Sánchez J.**, López-Granados F. (2015). Evaluación de la técnica de resampling en imágenes UAV para la discriminación de malas hierbas mediante análisis OBIA. *XV Congreso de la Sociedad Española de Malherbología*. Pp: 209-216. Sevilla, España.
3. Caballero-Novella J.J., Peña J.M., **Torres-Sánchez J.**, López-Granados F. Optimización de algoritmos de segmentación por valor umbral aplicado a detección de malas hierbas en imágenes procedentes de vehículos aéreos no tripulados. *XV Congreso de la Sociedad Española de Malherbología*. Pp: 217-222. Sevilla, España.
4. Pérez-Ortiz M., Peña J.M., Gutiérrez P.A., **Torres-Sánchez J.**, Hervás-Martínez C., López-Granados F. A weed monitoring system using UAV-imagery and the Hough transform. *XV Congreso de la Sociedad Española de Malherbología*. Pp: 233-239. Sevilla, España.
5. * **Torres-Sánchez, J.**, Peña-Barragán, J.M., de Castro-Megías, A.I., López-Granados, F. (2013). Seguimiento multitemporal de trigo para la detección de malas hierbas en imágenes tomadas desde un vehículo aéreo no tripulado (UAV). *XV Congreso de la Asociación Española de Teledetección*. Pp: 43-48. Alcalá de Henares, Spain.
6. * **Torres-Sánchez, J.**, Peña-Barragán, J.M., de Castro-Megías, A.I., López-Granados, F. (2013). Puesta a punto de un vehículo aéreo no tripulado (UAV) para detección de malas hierbas en fase temprana: resolución espacial y altura de vuelo. *XIV Congreso de la Sociedad Española de Malherbología*. Pp: 43-47. Valencia, Spain.

7. * Peña-Barragán, J.M., de Castro-Megías, A.I., **Torres-Sánchez, J.**, López-Granados, F. (2013). Imágenes multiespectrales procedentes de un vehículo aéreo no tripulado (UAV): Una innovación tecnológica para la detección de malas hierbas en fase temprana. *XIV Congreso de la Sociedad Española de Malherbología*. Pp: 49-53. Valencia, Spain.

Premios recibidos en Congresos Internacionales:

1. Premio 2015 **"Best paper"** a la mejor comunicación del 10th European Conference on Precision Agriculture por el trabajo "Mapping olive-tree geometric features from 3-D models generated with an Unmanned Aerial Vehicle (UAV)". (Autores: J. Torres-Sánchez, F. López-Granados y J.M. Peña-Barragán). 10th European Conference on Precision Agriculture (ECPA) (12-16 Julio, 2015. Tel Aviv, Israel).
2. Premio 2014 que bianualmente otorga la INTERNATIONAL SOCIETY OF PRECISION AGRICULTURE. El premio 2014 se concedió en el 12th Conference on Precision Agriculture a J. Torres-Sánchez como **"Outstanding Graduate Student Award"** por la comunicación: Weed seedlings detection in winter cereals for site-specific control: use of UAV imagery to overcome the challenge (Autores: J. Torres-Sánchez, J.M. Peña, A.I. de Castro and F. López-Granados). 12th International Conference on Precison Agriculture, CD ROM, 20-23 July 2014, Sacramento (EEUU).
3. Premio 2013 **"2nd Best Oral Communication Award"** concedido en 9th International Congress on Precision Agriculture por la comunicación: Imagery from unmanned aerial vehicles (UAV) for early site specific weed management (ESSWM). (Autores: J. Torres-Sánchez, J.M. Peña-Barragán, D. Gómez-Candón, A. I. De Castro, F. López-Granados). 9th European Conference on Precision Agriculture (ECPA) pp 193-199, Lleida, Fecha: 7-11 July, 2013.

Estancias internacionales

1. Departamento Z-GIS de Geoinformática de la University of Salzburg (Austria). Bajo la supervisión del Dr. Stefan Lang. En el período del 01/08/2016 al 31/10/2016. Perfeccionamiento de técnicas de análisis de imagen.
2. Maison de la Télédétection dependiente de IRSTEA, Montpellier (Francia). Bajo la supervisión del Dr. Sylvain Labbé. En el período del 01/06/14 al 15/08/14. Manejo de sensores térmicos embarcados en UAVs.

- Consideramos que el trabajo realizado cumple los requisitos necesarios para su presentación y lectura.

Por todo ello, se autoriza la presentación de la tesis doctoral.

Córdoba, ____ de Noviembre de 2016

Firma del/de los director/es

Fdo.:_____ Fdo.: _____

TÍTULO DE LA TESIS: Monitorización 3D de cultivos y cartografía de malas hierbas mediante vehículos aéreos no tripulados para un uso sostenible de fitosanitarios

DOCTORANDO/A: Jorge Torres Sánchez

ESCRITO RAZONADO DEL RESPONSABLE DE LA LÍNEA DE INVESTIGACIÓN

(Ratificando el informe favorable de los directores. Sólo cuando no pertenezcan a la Universidad de Córdoba).

D. ALFONSO GARCÍA-FERRER PORRAS, Catedrático del Departamento de Ingeniería Gráfica y Geomática de la Universidad de Córdoba

INFORMA:

Que la investigación sobre **"Monitorización 3D de cultivos y cartografía de malas hierbas mediante vehículos aéreos no tripulados para un uso sostenible de fitosanitarios"** llevada a cabo por el Ingeniero de Montes D. Jorge Torres Sánchez, bajo la dirección de los Drs. Francisca López Granados, Investigadora Científica, y José Manuel Peña Barragán, investigador Ramón y Cajal, ambos adscritos al Instituto de Agricultura Sostenible de Córdoba (IAS-CSIC), y la tutoría del que subscribe, ha sido desarrollada con éxito y alcanzado los objetivos inicialmente propuestos. Los resultados de la investigación realizada constituyen una aportación científica innovadora y relevante para la cartografía de malas hierbas en cultivos herbáceos en fase temprana y la monitorización tridimensional de cultivos leñosos, con el fin último de contribuir a la implementación de estrategias basadas en técnicas de aplicación variable en el ámbito de la agricultura de precisión que permitan un uso sostenible de los productos fitosanitarios. En consecuencia, como tutor de la Tesis Doctoral que comprende dicha investigación, considero que puede ser presentada para su exposición y defensa públicas en la Universidad de Córdoba y ratifico la consideración favorable emitida por los Directores de la Tesis Doctoral a tal efecto.

Por todo ello, se autoriza la presentación de la Tesis Doctoral.

Córdoba 9 de Noviembre de 2016

Firma del responsable de línea de investigación

NOMBRE GARCIA FERRER PORRAS ALFONSO - NIF 30417127H

Firmado digitalmente por NOMBRE GARCIA FERRER PORRAS ALFONSO - NIF 30417127H
Nombre de reconocimiento (DN): c=ES, o=FNMT, ou=FNMT Clase 2 CA, ou=500780156, cn=NOMBRE GARCIA FERRER PORRAS ALFONSO - NIF 30417127H
Fecha: 2016.11.07 08:59:53 +01'00'

Fdo.: Alfonso García-Ferrer Porras

A mis padres y a Loles
por todo

AGRADECIMIENTOS

En primer lugar quisiera agradecer a Paquita y José Manuel su dedicación a la dirección de esta tesis, todo lo que me han ayudado y apoyado con sus conocimientos y consejos. Quiero agradecerles también la buena relación que hemos desarrollado, que ha sido la culpable de que haya visto demasiado frío poner su cargo y haya preferido poner sus nombres (espero que perdonen este sacrilegio doctoral). Gracias a mi tutor en la Universidad, Alfonso, con el que también puedo presumir de tener una buena relación y al que debo agradecerle su buena disposición a echar una mano siempre que ha hecho falta.

Ya que he mencionado a Alfonso quiero dar las gracias también a los componentes del departamento de Ingeniería Gráfica y Geomática, Javier Mesas, Ignacio García-Ferrer e Isa, con los que he compartido reuniones, jornadas de trabajo y conversaciones. Pero no sólo con miembros de la UCO he compartido trabajo y charlas, de igual forma hay un hueco aquí para la gente con la que he trabajado del ICA, CAR, Universidad de Lleida y otros centros.

Haciendo un inciso internacional quisiera dar las gracias a los doctores Sylvain Labbé y Stefan Lang, de la Maison de la Télédétection de Montpellier y la Universidad de Salzburgo, respectivamente. Ellos hicieron posibles mis estancias en sus centros de investigación, facilitándome la infraestructura y contactos que necesité para conseguir que mis estancias fueran fructíferas.

Volviendo al IAS debo acordarme de todo el grupo de investigación en el que he trabajado, pero no sólo por la investigación, sino también por los desayunos en los que se habla de lo divino y lo humano, y por los eventos de la “Concejalía de Festejos”. Gracias a todos los que habéis compartido conmigo esos ratos: Amparo, Ana, Angélica, David, Irene, Juanjo, Luis, María, Montse y Paco.

Ahora viene la gente con la que no he trabajado, quiero agradecer a mis amistades los buenos ratos que hemos tenido, pero sobre todo su apoyo en los malos, que por fortuna no han sido muchos. Poner todos sus nombres aquí no tiene sentido, y mencionar sólo a los más cercanos no me parece justo porque siempre me dejaría a alguien atrás. Así que gracias a todos, nos vemos en los bares.

En el penúltimo párrafo, lo mejor. Gracias a mi padre y mi madre, sin ellos no estaría aquí en el sentido literal ni en el figurado. Gracias por haber hecho de mí una persona curiosa y

crítica. Gracias a Loles, con ella a mi lado los buenos momentos son mejores, y los malos se suavizan.

Finalmente, el apartado pecuniario. Gracias al programa FPI (BES-2012-052424) y a los proyectos AGL2011-30442-CO2-01 y AGL2014-52465-C4-4R del Ministerio de Economía y Competitividad por haber proporcionado la financiación que ha hecho posible la realización de las diferentes líneas de investigación incluidas en esta Tesis Doctoral.

ÍNDICE

INTRODUCCIÓN 7

1. Interés económico y agro-ambiental del uso sostenible de fitosanitarios en el marco europeo y español 9
2. Agricultura de precisión 11
3. Teledetección en agricultura 13
4. Vehículos aéreos no tripulados: características de las imágenes 14
5. Vehículos aéreos no tripulados: aplicaciones en agricultura 16
6. Análisis de imagen orientado a objetos 16
7. Cartografía de malas hierbas en fase temprana 19
8. Monitorización 3D de cultivos leñosos 22
9. Objetivos de la tesis doctoral 23
10. Bibliografía 25

CAPÍTULO 1. Configuration and Specifications of an Unmanned Aerial Vehicle (UAV) for Early Site Specific Weed Management 39

1. Resumen 41
2. Abstract 41
3. Introduction 42
4. Materials and methods 44
   - 4.1. UAV description 44
   - 4.2. Sensors description 46
   - 4.3. Study site and field sampling 47
   - 4.4. UAV flight and sensors tests 48
     - *4.4.1. Mission planning* 48
     - *4.4.2. UAV flight and image acquisition* 49
     - *4.4.3. Multispectral band alignment* 51
     - *4.4.4. Spatial resolution and flight length as affected by flight altitude* 51
     - *4.4.5. Spectral resolution as affected by flight altitude* 51
5. Results and discussion 53
   - 5.1. Image pre-processing 53
     - *5.1.1. Band alignment of multispectral imagery* 53
     - *5.1.2. Image orthorectification and mosaicking* 54
   - 5.2. Effect of flight altitude on image spatial resolution and flight time 55

5.3. Effect of flight altitude on image spectral resolution 58
6. Conclusions 63
7. Acknowledgements 64
8. References 64

CAPÍTULO 2. Multi-temporal mapping of the vegetation fraction in early-season wheat fields using images from UAV 69
1. Resumen 71
2. Abstract 71
3. Introduction 72
4. Materials and methods 74
4.1. Study site 74
4.2. UAV flights and remote images 75
4.3. Image mosaicking 76
4.4. Quantification of vegetation fraction 77
4.5. Evaluation of VF mapping 79
5. Results 81
5.1. Classification accuracy of VF as affected by VI and spatial factor 81
5.2. Classification accuracy of VF as affected by VI and temporal factors 81
5.3. Classification accuracy of VF as affected by VI and the flight altitude 83
5.4. Automatic thresholding by using Otsu´s method 83
5.5. VF mapping from the best VIs 83
6. Discussion 86
7. Conclusions 89
8. Acknowledgments 90
9. References 90

CAPÍTULO 3. An automatic object-based method for optimal thresholding in UAV images: Application for vegetation detection in herbaceous crops 95
1. Resumen 97
2. Abstract 97
3. Introduction 98
4. Materials and methods 99
4.1. Description of the automatic thresholding OBIA algorithm 99
4.2. Rule set application for vegetation detection 101
4.3. Image analysis 103
4.3.1. Influence of scale parameter on segmentation and thresholding rule set 103
4.3.2. Evaluation of the OBIA algorithm for quantifying vegetation coverage 104

5. Results and discussion 104
5.1. Object size as affected by the segmentation scale parameter 104
5.2. Automatic threshold value as affected by the scale parameter 106
5.3. Influence of the scale parameter on the vegetation index histograms 107
5.4. Vegetation detection 110
5.4.1. Classification accuracy as affected by segmentation scale 110
5.4.2. Classification accuracy as affected by segmentation shape and compactness parameters 112
6. Conclusions 113
7. Acknowledgments 114
8. References 114

CAPÍTULO 4. Weed mapping in early-season maize fields using object-based analysis of Unmanned Aerial Vehicle (UAV) images 117
1. Resumen 119
2. Abstract 119
3. Introduction 120
4. Materials and methods 122
4.1. Study site 122
4.2. UAV flights and remote images 122
4.3. Weed mapping by object-based image analysis (OBIA) 123
4.3.1. Crop row classification 125
4.3.2. Discrimination of crop and weeds 125
4.3.3. Weed coverage mapping 127
4.4. The evaluation of the methodology 127
5. Results and discussion 129
5.1. Weed map information provided by the OBIA procedure 129
5.1.1. Whole field: upper segmentation level 129
5.1.2. Crop row structure: Intermediate segmentation level 130
5.1.3. Weed infestation in grid units: lower segmentation level 130
5.2. The evaluation of the weed map 131
6. Conclusions 133
7. Acknowledgements 134
8. References 134

CAPÍTULO 5. Quantifying efficacy and limits of Unmanned Aerial Vehicle (UAV) technology for weed seedling detection as affected by sensor resolution 137
1. Resumen 139
2. Abstract 139

3. Introduction 140
4. Experimental section 142
4.1. Study Site 142
4.2. UAV Flights: Camera, Altitudes and Dates 142
4.3. OBIA Algorithm 144
4.4. Evaluation of OBIA Algorithm Performance 147
5. Results and discussion 148
5.1. Image Spatial Resolution and Covered Area As Affected by Flight Altitude 148
5.2. Accuracy Assessment on Classification of Crop-Rows 151
5.3. Weed Discrimination As Affected by Camera, Date and Flight Altitude 153
6. Conclusions 156
7. Acknowledgments 156
8. References 157

CAPÍTULO 6. Early season weed mapping in sunflower using UAV technology: variability of herbicide treatment maps against weed thresholds 161
1. Resumen 163
2. Abstract 163
3. Introduction 164
4. Materials and methods 167
4.1. Sites 167
4.2. UAV flights: cameras and altitudes 168
4.3. Image mosaicking 170
4.4. OBIA algorithm 171
4.5. Evaluation of OBIA algorithm performance 173
5. Results and discussion 173
5.1. Spatial resolution and area covered by ortho-mosaicked imagery 173
5.2. Classification of sunflower crop rows 175
5.3. Effect of cameras and flight altitudes on mapping of weed-patches and weed-free areas 176
6. Conclusions 180
7. Acknowledgments 181
8. References 181

CAPÍTULO 7. High-throughput 3-D monitoring of agricultural-tree plantations with Unmanned Aerial Vehicle (UAV) technology 185
1. Resumen 187
2. Abstract 187
3. Introduction 188

4. Materials and methods 189
4.1. Description of the UAV and the sensors 189
4.2. Study sites and UAV flight missions 191
4.3. Generation of the ortho-mosaics and of the Digital Surface Models (DSM) 193
4.4. Object-based image analysis (OBIA) procedure 194
4.5. Training and validation of the methodology 197
5. Results and discussion 198
5.1. Quality of ortho-mosaic and DSM generation 198
5.2. Classification accuracy as affected by the flight altitude 199
5.3. Quantification of the tree geometric features (canopy area, tree height and crown volume) 201
5.3.1. Canopy area 201
5.3.2. Tree height 202
5.3.3. Crown volume 203
5.4. Detailed map information provided by the OBIA algorithm 205
5.5. Time consumption 206
6. Conclusions 207
7. Acknowledgements 208
8. References 208

CAPÍTULO 8. 3-D vineyard monitoring with UAV images and a novel OBIA procedure for precision viticulture applications 213
1. Resumen 215
2. Abstract 215
3. Introduction 216
4. Materials and methods 217
4.1. Study fields and UAV flights 217
4.2. DSM and orthomosaic generation 219
4.3. OBIA algorithm 219
4.4. Validation 221
4.4.1. Grapevine classification and gap detection 221
4.4.2. Grapevine height 222
5. Results and discussion 223
5.1. Vine classification 223
5.2. Vine gaps detection 224
5.3. Vine height quantification 225
5.4. Volume mapping 227
6. Conclusions 228

7. Acknowledgments 228
8. References 228

CAPÍTULO 9. Conclusiones 233

INTRODUCCIÓN

1. INTERÉS ECONÓMICO Y AGRO-AMBIENTAL DEL USO SOSTENIBLE DE FITOSANITARIOS EN EL MARCO EUROPEO Y ESPAÑOL

La agricultura europea se caracteriza, de una forma general, por una alta productividad ligada a una elevada mecanización y al empleo de productos agroquímicos aplicados de forma uniforme en las parcelas (Figura 1). Estas prácticas presentan un coste agro-económico notable y una relevante huella de carbono, producida tanto por las emisiones directas de la maquinaria agrícola, como por las indirectas derivadas de la producción de insumos agrícolas (fertilizantes, fitosanitarios, semillas, entre otros) (Schieffer y Dillon 2014). En concreto, la actual producción agraria requiere el consumo de fitosanitarios (principalmente herbicidas, fungicidas e insecticidas) como herramienta esencial para mantener las necesidades de calidad y cantidad de alimentos que demanda la población. Los gastos en herbicidas ascendieron en 2015 en España a 312 M € mientras que los referidos al resto de fitosanitarios llegaron a los 547 M € (AEPLA 2016).

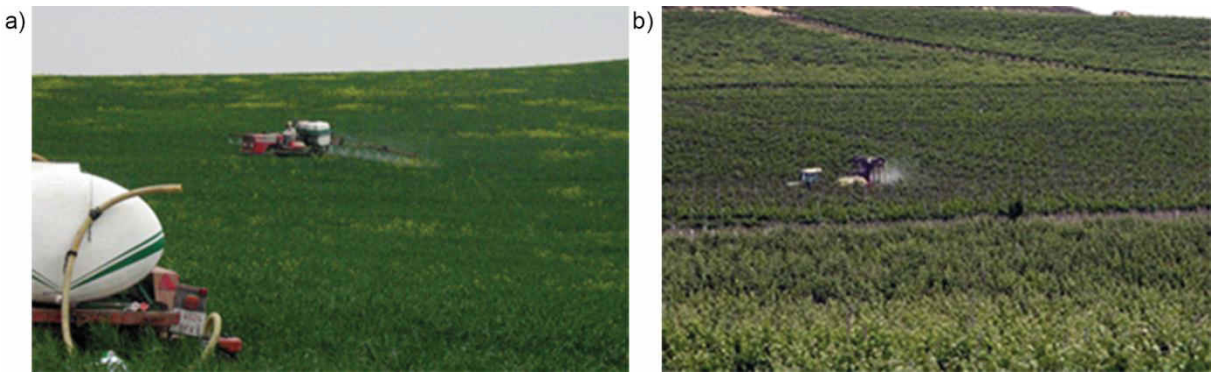

Figura 1. *Tratamiento herbicida en cereal (a) y fungicida en viñedo (b) realizado de forma uniforme sin tener en cuenta la distribución espacial de las malas hierbas ni del hongo que se deben controlar ni la arquitectura de las cepas en el caso de la viña.*

Este elevado coste de las aplicaciones propiamente dichas junto con el de los fitosanitarios, así como sus potenciales efectos medioambientales, han originado una gran preocupación en distintos ámbitos administrativos cuya consecuencia ha sido la creación de Normativas Europeas como el **REGLAMENTO (CE) 1107/2009 para la comercialización de Productos Fitosanitarios** y la **DIRECTIVA 2009/128/CE para el Uso Sostenible de Fitosanitarios**. Dentro de esta Directiva se destacan como elementos clave "el fomento del bajo consumo (**reducción de las aplicaciones**) y la utilización de **dosis adecuadas** en función de las infestaciones de malas hierbas, insectos-plaga y enfermedades". Esta Directiva ha sido traspuesta a cada país miembro de la Unión y en España se publicó el Real Decreto 1311/2012 (BOE nº 223, 15/09/2012: 65127-65171) en el que se define el Marco de Actuación para un **Uso Sostenible de los Productos Fitosanitarios**. Concretamente se establece que "las poblaciones de los insectos-plaga, enfermedades y malas hierbas deben ser objeto de

seguimiento mediante métodos e instrumentos adecuados" y como objetivo se menciona el "desarrollo de herramientas de gestión… y sistemas de apoyo a las decisiones basados en **SIG y teledetección**". Estos últimos componentes están incluidos en el fundamento agronómico de dos técnicas integradas en la **Agricultura de Precisión** y que son de gran importancia para alcanzar las metas propuestas en la legislación anteriormente comentada**:**

1. En el ámbito de los cultivos herbáceos, la tecnología basada en **tratamientos localizados de herbicidas** (en inglés **SSWM**: *Site-Specific Weed Management*) según la distribución de las malas hierbas. Esta forma de acometer el control de malas hierbas se basa en que éstas se suelen distribuir en **rodales dentro de los cultivos,** tal como prueban numerosos trabajos científicos, lo que permite cartografiar zonas de infestación y de no infestación de forma que los tratamientos puedan definirse según la densidad **de malas hierbas y composición de grupos** (por ejemplo, monocots *vs* dicots; malas hierbas resistentes o de difícil control; Heijting *et al*. 2007; Jurado-Expósito *et al*. 2004, 2009).
2. En el ámbito de los cultivos leñosos, la tecnología de aplicación de fitosanitarios (en inglés **VA**: *Variable Application*) se puede realizar en función de su volumen y arquitectura considerando si un árbol o conjunto de árboles (o cepas en el caso de viñedo) están o no afectados por determinado problema que necesite la aplicación dirigida a su parte aérea en esa zona del campo. La utilización del volumen de copa de estos cultivos como base para el cálculo y optimización de las aplicaciones de estos fitosanitarios fue discutido y evaluado por Sutton y Unrath (1984). Estas aplicaciones necesitan ser precisas y estar adaptadas a la arquitectura y volumen del cultivo, de lo contrario el agricultor utiliza producto por elevación, aplicándolo de forma inadecuada y provocando un exceso de tratamiento (Figura 1) que puede llevar a gastos agro-económicos innecesarios y a potenciales riesgos medioambientales de diversa índole (Miranda-Fuentes *et al*. 2016).

Además de la legislación comentada anteriormente se han creado los cauces para generar el conocimiento científico y los desarrollos tecnológicos de forma que la estrategia agronómica que subyace en la **aplicación sostenible de fitosanitarios** se contempló como objetivo en el **7º Programa Marco Europeo**, concretamente en los Programas **7FP-NMP-2009** (*Nanosciences, Nanotechnologies, Materials and New Production Technologies)* y **7FP-KBBE-2008** (*Food, Agriculture and Fisheries, and Biotechnology*). Actualmente y dentro del vigente **Programa H2020** también se incorporó este objetivo en el Reto Social "*Food security, sustainable agriculture and forestry, marine and maritime and inland water research and the bioeconomy*", en el que se incluyen dos acciones: (a) Acción "SFS3-2014: *Practical solutions for pests and invasive alien species affecting plants*" en la que se persigue avanzar en el desarrollo de soluciones fiables para la gestión de insectos-plaga, enfermedades y

malas hierbas utilizando las últimas tecnologías y mediante enfoques biológicos e integrados; y (b) Acción "SFS2-2014/2015: *Sustainable crop production*" en la que se pretende alcanzar una mejora en la sostenibilidad de diferentes sistemas intensivos de producción de cultivos, disminuyendo el impacto negativo sobre el medio ambiente, empleando nuevas tecnologías (sistemas automatizados, aplicaciones localizadas, teledetección, sensores terrestres, TICs). Esta acción se centra en la racionalización de las necesidades de nutrientes y de fitosanitarios mediante la **minimización del uso de fertilizantes, herbicidas y otros fitosanitarios.** Ello se debe lograr definiendo nuevas estrategias de manejo de los cultivos que reduzcan su uso y, al mismo tiempo, garanticen un nivel adecuado de fertilización y control así como unos rendimientos económicos y medioambientales satisfactorios. Es decir, es necesario compatibilizar **productividad con sostenibilidad** lo cual es sin duda un reto fundamental en los actuales sistemas agrícolas. En esta Tesis Doctoral se proponen una serie de desarrollos cuya finalidad es aportar conocimiento y tecnologías para avanzar en la consecución de este desafío.

A continuación se recogen los principales conceptos que se desarrollan en la presente Tesis Doctoral para la elaboración de mapas de prescripción de tratamientos herbicidas, y para la caracterización tridimensional de cultivos leñosos. Se presenta asimismo la bibliografía más relevante sobre dichas temáticas y las tecnologías relacionadas con éstas.

2. AGRICULTURA DE PRECISIÓN

Como se ha mencionado anteriormente, uno de los métodos posibles que permiten aumentar la sostenibilidad de las explotaciones agrícolas es el abandono de las prácticas más comunes en la agricultura convencional consistentes en la aplicación de manera uniforme en todo el campo de las labores y los insumos (dosis de siembra, fertilizantes, herbicidas, insecticidas, fungicidas, riego, entre otros). Es necesario tener en cuenta que un sistema agrícola se compone de elementos muy diversos y que en una parcela existen variaciones que se pueden agrupar en tres tipos (Hatfield 2000): 1) natural, como el suelo y la topografía; 2) aleatoria, como las precipitaciones; y 3) manejada, como la aplicación de agroquímicos. La interacción entre estas fuentes de heterogeneidad provoca la variación que se observa en los cultivos. Considerando dicha variabilidad, surgió a finales del siglo XX la **Agricultura de Precisión**, consistente en la aplicación de técnicas geoespaciales para el manejo del cultivo de manera que se incremente la eficiencia mediante la aplicación de insumos donde y cuando sean necesarios y en la cantidad requerida (Robert 2002). Esta forma de afrontar la producción agrícola hace que la agricultura de precisión ofrezca grandes ventajas en lo referente a sostenibilidad, calidad de las cosechas, protección medioambiental, seguridad alimentaria, desarrollo económico rural, calidad de vida en las zonas rurales, rentabilidad y productividad (Liaghat 2010). Los

protocolos para la implementación de la agricultura de precisión pueden ser resumidos en tres pasos generales (Liaghat 2010): 1) recopilación de información sobre la variabilidad; 2) procesado y análisis de la información para comprenderla; y 3) implementación de cambios en el manejo de los insumos.

En el caso de **SSWM**, los últimos años se ha avanzado en las etapas 2 y 3 (toma de decisiones y aplicación localizada de herbicidas), de tal forma que hay maquinaria agronómica disponible para realizar con éxito ambas fases. Sin embargo, el paso 1) es decir, **la monitorización de las malas hierbas en los cultivos** es aún uno de los **componentes críticos** para la adopción de SSWM y está identificado a nivel empresarial y científico como el **principal cuello de botella** de esta tecnología. La razón fundamental es que los tratamientos se realizan habitualmente en post-emergencia, en estados fenológicos tempranos del cultivo y malas hierbas, en base a las infestaciones presentes que son muy diversas y que varían según cultivos y épocas del año. Dada la complejidad de estos tratamientos, la estimación o monitorización de las infestaciones de malas hierbas en estado de **plántula** es una cuestión a resolver y un requisito crucial para el desarrollo de SSWM. Según la revisión de López Granados (2011), diversos autores manifiestan que la monitorización de las infestaciones de malas hierbas se puede realizar mediante técnicas de detección remota o próxima basándose en que: 1) existen (y son cuantificables) diferencias espectrales entre las malas hierbas y el cultivo; 2) la resolución espacial (tamaño del píxel) de las imágenes es la adecuada para su discriminación; y 3) hay disponibilidad del tipo de imágenes con las resoluciones espacial y espectral que se requieren. A pesar de los numerosos trabajos reseñados en dicha revisión siguen sin solución las diferentes dificultades inherentes a la detección temprana de malas hierbas y se concluye que muchos estudios presentan resultados en condiciones muy limitadas (ej.: una mala hierba en un cultivo concreto; condiciones de iluminación muy específicas al momento de la toma de imágenes terrestres, entre otros) lo que reduce el interés comercial ya que cualquier herramienta que se desarrolle tendría un mercado muy restringido. En el **apartado 7** de esta Introducción se detallarán las investigaciones que recientemente se han publicado sobre cartografía de malas hierbas.

En el desarrollo de técnicas **VA para cultivos leñosos**, se han realizado contribuciones científicas relevantes en lo referente a los tres pasos generales para la implementación de la agricultura de precisión: tanto en la recopilación de información sobre la variabilidad del cultivo (Rosell y Sanz 2012), como en la toma de decisiones en función de ésta y en la aplicación de tratamientos en base a estas decisiones (Doruchowski *et al*. 2009). De hecho, hay numerosas investigaciones que se basan en la detección on-ground o próxima, ya sea mediante sensores ultrasónicos (Hu y Fu 2012; Zaman y Schumann 2005) o LiDAR (Arnó *et al*. 2012; Escolà *et al*. 2016; Méndez *et al*. 2013; Rosell *et al*. 2009). Sin embargo, hasta el momento existe escasa bibliografía

(Burgos *et al*. 2015; Zarco-Tejada *et al*. 2014) sobre la adquisición de información para determinar la variabilidad morfológica del cultivo desde plataformas aéreas y las ventajas que esta podría aportar. Esta carencia está ligada al hecho de que hasta hace unos pocos años las plataformas aéreas disponibles no cumplían con los requisitos necesarios en cuanto a resolución espacial para estas tareas. En el **apartado 8** de esta Introducción se detallarán las investigaciones que recientemente se han publicado sobre monitorización 3D de cultivos leñosos.

La presente Tesis Doctoral se ocupa del primero de los pasos en la agricultura de precisión, la **adquisición de información georreferenciada**, centrándose en el uso de Teledetección como uno de los métodos que más se han extendido para ello. Asimismo, se presentarán los trabajos realizados para abordar el segundo paso y la toma de decisiones para el control localizado de malas hierbas.

3. TELEDETECCIÓN EN AGRICULTURA

La teledetección es la ciencia que se ocupa de obtener e interpretar información desde la distancia mediante sensores que no están en contacto con el objeto de observación (Jensen 2006). Esta forma de recolectar información tiene ventajas únicas (Jensen 2006) que son de gran importancia en la agricultura y entre las que cabe destacar:

- Es un método no destructivo.
- Los datos pueden ser obtenidos sistemáticamente sobre grandes áreas en vez de mediante muestreos de puntos singulares.
- La adquisición de datos sistemática puede eliminar el sesgo de los muestreos.
- Permite generar información de lugares que no son accesibles.

Por lo anterior, la teledetección es una herramienta ampliamente utilizada en la agricultura y la agronomía con diferentes propósitos (Atzberger 2013). Según Becker-Reshef *et al*. (2010), la investigación y el desarrollo de la monitorización de la agricultura con imágenes de satélite empezó a comienzos de los 70 del siglo pasado debido a que una drástica carestía de trigo en Rusia atrajo la atención sobre la importancia de tener estimaciones sobre la producción agrícola de manera exacta y a tiempo. Como resultado, en 1974 el USDA junto a la NASA y NOAA iniciaron un experimento para mejorar los métodos de predicción de cosecha. Desde ese momento, la teledetección ha sido frecuentemente utilizada en estudios agrícolas. Por citar algunos de ellos, se ha cartografiado una gran variedad de factores (Lee *et al*. 2010) incluyendo el estado del cultivo (Houborg *et al*. 2009), las propiedades del suelo (López-Granados *et al*. 2005), el contenido de agua (Meron *et al*. 2010), la distribución de malas hierbas (de Castro *et al*. 2013), la detección de enfermedades (de Castro *et al*. 2015), entre otros. Los aviones tripulados y los satélites han sido las principales plataformas remotas

utilizadas para obtener imágenes y facilitar la toma de datos a escala local o global. Sin embargo, los continuos avances y mejoras en plataformas no tripuladas junto al desarrollo de sensores susceptibles de ser embarcados en ellas, han proporcionado grandes oportunidades para su aplicación en teledetección.

4. VEHÍCULOS AÉREOS NO TRIPULADOS: CARACTERÍSTICAS DE LAS IMÁGENES

Tradicionalmente, la teledetección ha sido asociada con satélites o aviones tripulados con sensores a bordo. Sin embargo, estas plataformas presentan carencias para el desarrollo de muchos aspectos de la agricultura de precisión debido a sus limitaciones para proporcionar imágenes de adecuadas resoluciones espacial y temporal, y a que se ven fuertemente afectadas por las condiciones meteorológicas en el momento de la toma de imágenes (Herwitz *et al*. 2004). Los drones, **UAV o RPAS** (por las siglas en inglés de **Unmanned Aerial Vehicle** o **Remotely Piloted Aerial Systems**) son plataformas aéreas cuya principal característica es la ausencia de piloto, aparte de esto, pueden ser remotamente controladas, autónomas, semi-autónomas o presentar una combinación de estas características (Eisenbeiss 2009). Como todos los desarrollos en teledetección, los UAVs tuvieron sus inicios en el ámbito militar, pero los avances en electrónica y miniaturización junto a la bajada de sus precios, han hecho posible que se extienda su uso a aplicaciones civiles. Los UAVs ofrecen las siguientes ventajas como plataformas para la teledetección:

- Versatilidad y flexibilidad. Los recientes progresos en electrónica, customización y miniaturización han hecho posible que haya un gran abanico de sensores disponibles para ser embarcados en un UAV (Tabla 1). Estos sensores tienen la ventaja de que pueden ser intercambiados o instalados simultáneamente con facilidad en la mayoría de las ocasiones. Esto contrasta con los satélites, en los que no es posible cambiar de sensor, y con los aviones tripulados, en los que el mayor coste de los sensores embarcados hace que no todas las empresas de toma de imágenes puedan ofrecer un amplio rango de sensores.
- Costes más asumibles que las plataformas tradicionales (Hardin y Jensen 2011), con lo que se puede obtener información multitemporal dentro de una temporada de cultivo, pudiéndose así realizar un seguimiento y evaluación exhaustivos del mismo que permitan la adopción de medidas en el momento preciso.
- Pueden operar rápidamente sin necesidad de planificación previa, esto es de gran importancia ya que en agricultura la ventana temporal de actuación es en ocasiones muy estrecha ya que puede ser necesario adquirir información y evaluarla para tomar medidas en un breve margen de tiempo. Esto no es posible con los satélites debido a que sus periodos de

revisita sobre áreas concretas están establecidos de antemano y no pueden ser cambiados. Además, los satélites con mayor frecuencia de revisita suelen ser aquellos que tienen menor resolución espacial. En el caso de los vuelos tripulados, las imágenes son normalmente obtenidas por un número limitado de empresas que poseen los aviones y sensores, por lo tanto es necesario concertar la toma de datos con una gran antelación. Ello contrasta con los condicionantes propios de la agricultura ya que no siempre es posible conocer con precisión el momento en que se deberán tomar los datos.

Tabla 1. Sensores a borde de UAVs en la bibliografía. Adaptado de (Pajares 2015)

Auxiliares	Específicos	
GPS	Cámaras de vídeo (espectro visible)	Cámaras térmicas
IMU	Cámaras fotográficas (espectro visible)	Colectores electrostáticos
Giroscopios	Cámaras multiespectrales	Higrómetros
Estabilizadores	Cámaras hiperespectrales	Termómetros
Altímetros	LIDAR	Barómetros
Acelerómetros	Radar/SAR	Sonar
	Radiómetros	Contadores de partículas
	Nariz electrónica	Sensores magnéticos
	Detectores de gases	Detectores de humo

- Pueden volar bajo las nubes, facilitando la generación de información mediante la teledetección en zonas con gran cobertura nubosa a lo largo del todo el año, en las que esta incidencia meteorológica impedía o dificultaba la toma de imágenes por parte de satélites y aviones tripulados.
- Pueden volar a bajas alturas y velocidades, lo que permite adquirir datos de alta resolución espacial y ver pequeñas plantas y rodales así como detalles del follaje de los cultivos leñosos, lo que no había sido posible con anterioridad (Xiang y Tian 2011).

Debido a la baja altura de vuelo que permite conseguir resoluciones espaciales muy altas, las imágenes procedentes de los UAVs abarcan normalmente una superficie reducida y menor que la superficie que suelen tener las parcelas. Por tanto, al igual que en los vuelos fotogramétricos tradicionales, suele ser necesario realizar rutas de vuelo con diferentes pasadas sobre el cultivo objeto de estudio, a fin de tomar una **secuencia o colección** de imágenes que deben poseer solapamiento transversal y longitudinal y que deben ser combinadas para obtener una **única imagen del campo**. Para unir todas las imágenes y obtener lo que se conoce como la **ortofoto** completa de la parcela, hay que realizar un proceso de **ortorrectificación** y posterior "**mosaicado**" (*mosaicking* en inglés). Uno de los aspectos clave durante el diseño del plan de vuelo para conseguir un mosaicado correcto es determinar el **porcentaje de solapamiento** que requiere cada objetivo agronómico. A fin de que la ortofoto sea de utilidad para los propósitos para los que se ha generado, es necesario asegurar que tendrá la **métrica y la precisión** necesarias para que los errores de georreferenciación

estén minimizados al máximo y no afecten a las técnicas análisis de imagen que le serán aplicadas (Laliberte *et al*. 2010).

5. VEHÍCULOS AÉREOS NO TRIPULADOS: APLICACIONES EN AGRICULTURA

Las ventajas comentadas previamente han hecho que el número de usos civiles de los UAVs no pare de crecer y parezca casi ilimitado. Una gran cantidad de estas aplicaciones puede observarse en diversas revisiones bibliográficas que sobre los UAVs se han publicado recientemente: Colomina y Molina (2014); Pajares (2015); Shahbazi *et al*. (2014); Whitehead *et al*. (2014). Sin embargo, en esta Tesis Doctoral nos vamos a centrar en sus aplicaciones a la agricultura.

Como se ha indicado en párrafos anteriores, el UAV puede ser programado a voluntad del usuario, puede volar con gran flexibilidad y tomar imágenes de cultivos en momentos críticos del periodo de crecimiento, mejorando por tanto los procesos de toma de decisiones de los agricultores (Lelong *et al*. 2008). Los últimos años, los UAVs han sido utilizados para un gran abanico de aplicaciones en agricultura, del que pueden servir como muestra los siguientes ejemplos: medición de parcelas de cultivo (Mesas-Carrascosa *et al*. 2014), generación de mosaicos multiespectrales para agricultura de precisión (Mesas-Carrascosa *et al*. 2015), estudio del estado hídrico de viñedos (Baluja *et al*. 2012); caracterización de la cubierta de viña (Ballesteros *et al*. 2015; Mathews y Jensen 2013); estudio de la variabilidad espacial y composición de la uva (Rey-Caramés *et al*. 2015); estimación de biomasa y contenido de nitrógeno en cultivos (Geipel *et al*. 2016); detección de enfermedades (Calderón *et al*. 2013; Garcia-Ruiz *et al*. 2013); monitorización del crecimiento de cultivos herbáceos (Bendig *et al*. 2013); cálculo del índice de área foliar (Mathews y Jensen 2013).

En definitiva, la bibliografía consultada concluye que los sistemas UAVs proporcionan resultados prometedores para la agricultura de precisión e identifican varios aspectos clave para la elección del equipo: máxima carga de pago, fiabilidad y estabilidad de la plataforma, capacidad del sensor, autonomía de vuelo y su maniobrabilidad, entre otras (Hardin y Hardin 2010; Hardin y Jensen 2011; Laliberte *et al*. 2010), así como para programar la misión (altitud de vuelo, porcentaje de solapamiento) para acometer cada uno de los objetivos agronómicos que se planteen.

6. ANÁLISIS DE IMAGEN ORIENTADO A OBJETOS

Como se puede ver en la figura 2, con el incremento en la resolución espacial de las imágenes alcanzado en los últimos años, se ha evolucionado de situaciones en las que las entidades a detectar y los píxeles de la imagen eran de tamaños parecidos (Figura 2a) a imágenes en que cada una de estas entidades está compuesta por multitud de píxeles (Figura 2b). Por tanto, en imágenes de muy alta resolución espacial como las obtenidas por sensores a bordo de UAVs para aplicaciones

agrícolas, uno de los problemas inherentes del análisis de las imágenes es que los píxeles ya no representan las características de los objetivos de la clasificación (Yu *et al*. 2006). Es decir, estas imágenes presentan una mayor variabilidad intra-clase (Aplin 2006; Woodcock y Strahler 1987) y, consecuentemente, una reducción en la separabilidad estadística entre clases si se usan métodos de clasificación tradicionales basados tan sólo en los valores espectrales de los píxeles. Ello puede llevar a una reducción en la precisión de clasificación en comparación a la obtenida en imágenes de menor resolución (Yu *et al*. 2006). Por tanto, la simple aplicación de las metodologías basadas en píxeles utilizadas tradicionalmente en el análisis de las imágenes de satélite o de aviones tripulados puede no ser la forma más satisfactoria de desarrollar las aplicaciones de UAVs para la agricultura (Hunt *et al*. 2013).

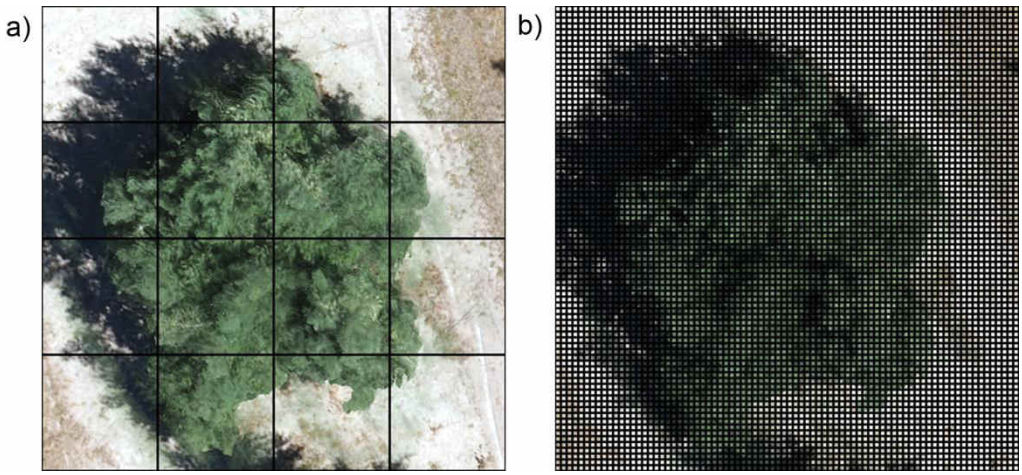

Figura 2. *Ejemplo sobre una imagen de olivar de la relación entre objetos y resolución espacial de las imágenes en teledetección: a) píxel de 2 m, b) píxel de 5 cm. Adaptado de* (Blaschke 2010).

Para solucionar esta variabilidad espectral intra-clase, un nuevo paradigma ha surgido en los últimos años, el **análisis de imagen orientado a objetos** (**OBIA** por las siglas en inglés de ***Object-Based Image Analysis***), cuyo uso se ha venido extendiendo entre la comunidad de investigadores dedicados a la teledetección desde el año 2000 (Blaschke 2010). Los objetos son agrupaciones de píxeles adyacentes y fueron definidos por Hay *et al*. (2001) como entidades básicas de las imágenes, donde cada grupo de píxeles está compuesto de valores digitales similares que poseen de manera intrínseca una forma, tamaño, y relación con los demás componentes de la escena que modela. Por tanto, los objetos son más homogéneos espectralmente en su interior que con respecto a sus vecinos. De esta manera se ha progresado del análisis de la imagen utilizando el **píxel**, en el que la única información disponible para la clasificación era el valor espectral de cada píxel (o también la textura en caso de que se aplicaran análisis por kernels o ventanas), al análisis por **objetos** en el que cada uno de ellos tiene información espectral más amplia (ya que se le añaden valores medios, desviaciones típicas, ratios entre medias, entre otros estadísticos) y además información espacial,

contextual y jerárquica. Tal y como se puede ver en la figura 3, la información contextual hace referencia a las relaciones que existen entre un objeto y sus vecinos, y la información jerárquica se refiere al hecho de que se pueden establecer distintos niveles de objetos en los que estos se van agrupando de manera que en niveles superiores se pueden establecer comparaciones entre los objetos de un grupo con los de otro (Figura 3). Por tanto, el primer paso de los procedimientos OBIA es la **segmentación en objetos** de la imagen.

Sin embargo, la segmentación no es un fin en sí misma de tal forma que existen otros pasos importantes en el análisis OBIA que se pueden dividir en las siguientes fases: 1) segmentar una imagen automáticamente en objetos; 2) combinar su información espectral, contextual, morfológica y jerárquica; y 3) clasificar la imagen usando los objetos como unidades mínimas de trabajo (Blaschke 2010). Para realizar la clasificación de la imagen se deben tener en cuenta qué características de los objetos son las que pueden aportar mayor información para una clasificación correcta, teniendo en cuenta que estas características variarán de un problema de clasificación a otro. Además y con el fin de conseguir buenos resultados, el analista de imágenes debe plasmar su conocimiento y su forma de reconocer los objetos en algoritmos que imiten la manera en que el cerebro humano reconoce los objetos en el mundo real. Una vez logrado lo anterior, se alcanza otra de las ventajas del OBIA, la transferibilidad de los algoritmos (Laliberte *et al*. 2011). En otras palabras, el objetivo último es que una vez que un algoritmo se ha desarrollado para cierta aplicación en una zona concreta, pueda ser transferido con pequeños cambios para su utilización con el mismo objetivo en otras áreas.

Las técnicas OBIA han sido utilizadas con éxito en diferentes aplicaciones dentro del ámbito de la teledetección como clasificación de usos del suelo en zonas mixtas de terreno urbano y agrícola (Ma *et al*. 2015), análisis de campos de refugiados (Tiede *et al*. 2010), detección de canales de agua en humedales (Moffett y Gorelick 2013), clasificación de árboles y arbustos en zonas forestales (Hellesen y Matikainen 2013), o clasificación de manglares (Heumann 2011). Dentro del ámbito de la agricultura, el paradigma OBIA también ha sido aplicado a diversos objetivos como por ejemplo la cartografía de cultivos (Castillejo-González *et al*. 2009; Peña-Barragán *et al*. 2011), la detección de líneas de cultivo (Peña-Barragán *et al*. 2012) o la caracterización de viñedos (Mathews 2014); siendo además estos dos últimos ejemplos casos de aplicación de la metodología OBIA a información obtenida mediante UAVs en agricultura

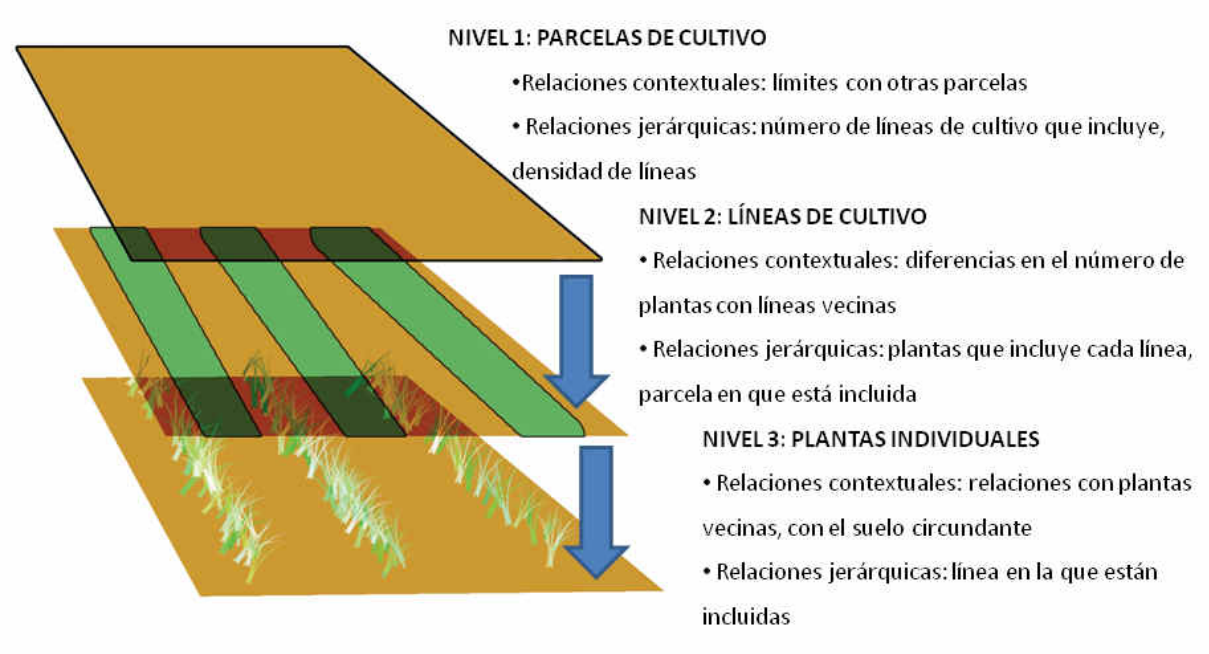

Figura 3. *Representación gráfica de las relaciones entre objetos, ejemplo con parcela de cultivo herbáceo.*

7. CARTOGRAFÍA DE MALAS HIERBAS EN FASE TEMPRANA

Como se ha mencionado anteriormente, un control eficiente y a tiempo de las malas hierbas en cultivos en post-emergencia temprana es una tarea crítica debido a que un uso inapropiado de herbicidas y por tanto un manejo inadecuado de las malas hierbas pueden originar una reducción en el rendimiento y un incremento de potenciales impactos negativos en el medioambiente. Muestra de ello es el hecho de que los herbicidas sean el grupo de fitosanitarios más frecuentemente detectado en análisis de aguas subterráneas y superficiales (Carter 2000). El riesgo de contaminación del agua y del medioambiente en general podría ser reducido mediante el SSWM **dirigiendo las aplicaciones herbicidas únicamente a los rodales de malas hierbas presentes en el cultivo**.

El control deficiente de las malas hierbas está relacionado en ocasiones con un uso incorrecto de los herbicidas resultante de tres problemas principales. El primero es aplicar herbicidas cuando las malas hierbas no están en el momento fenológico adecuado (generalmente cuando tienen de 2 a 6 hojas verdaderas, aunque depende de la especie o grupo de especies), el segundo es la aplicación de herbicidas sin considerar ningún umbral de aplicación (*i.e.*, el nivel de infestación por encima del cual es necesario tratar (Swanton *et al*. 1999), y el tercero es aplicar herbicidas sobre todo el campo, incluso cuando hay zonas libres de malas hierbas debido a su distribución en rodales (Jurado-Expósito *et al*. 2003; Jurado-Exposito *et al*. 2005). El primer inconveniente es normalmente resuelto mediante la experiencia de los agricultores o técnicos. Los otros dos problemas pueden ser solucionados mediante el desarrollo de estrategias SSWM de acuerdo a umbrales de infestación

(Longchamps *et al*. 2014). Estas estrategias pueden consistir en un tratamiento con un solo herbicida a los rodales donde sólo un grupo de malas hierbas está presente (por ejemplo de hoja estrecha o de hoja ancha), o en el uso de varios herbicidas de acuerdo a la presencia de especies resistentes o diferentes especies de malas hierbas o de diferentes grupos o una mala hierba específica problemática como *Orobanche*, la cual puede ser un serio problema en la producción del girasol (García-Torres *et al*. 1994; Molinero-Ruiz *et al*. 2014). Las estrategias de control localizado, además de tener incidencia sobre la producción del cultivo y el medioambiente, podrían tener un fuerte impacto económico al ayudar a reducir la inversión que los agricultores realizan en herbicidas, la cual representó alrededor el 36% del gasto total en fitosanitarios en España en 2015 (AEPLA 2016), y en torno al 28% del consumo total medio en toneladas de productos fitosanitarios en el periodo 1999-2014 (Figura 4).

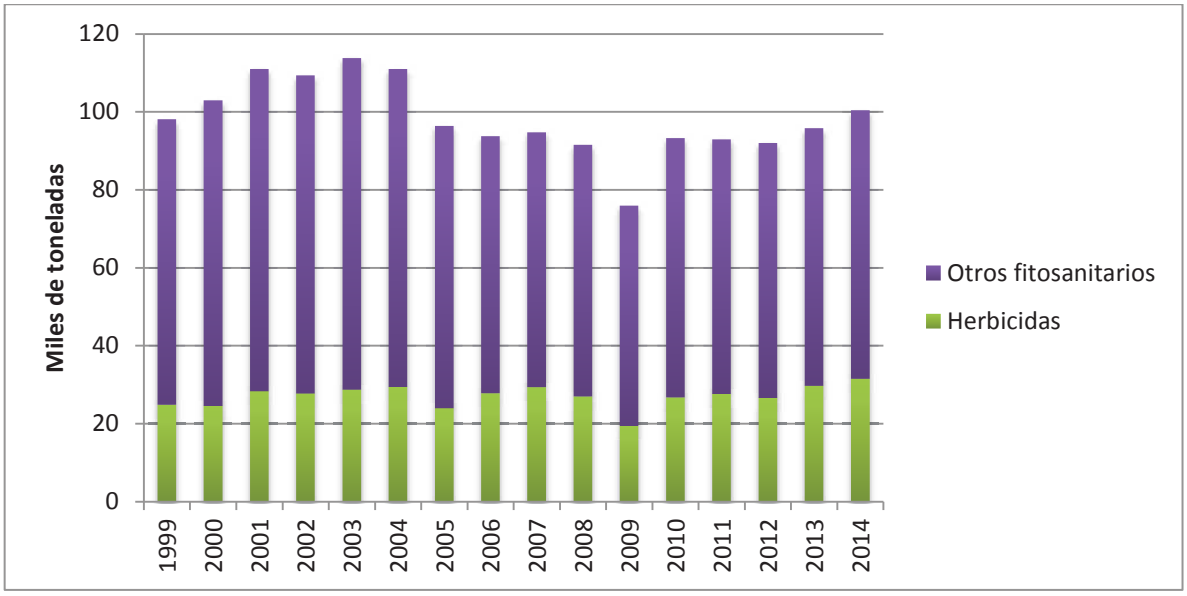

Figura 4. *Comparación entre el consumo de herbicidas y el resto de fitosanitarios en España en el periodo 1999-2014 (Instituto Aragonés de Estadística 2016)*

Para llegar a aplicar métodos SSWM, en primer lugar es necesario proceder a la detección y cartografía de las infestaciones de malas hierbas. Éstas pueden ser afrontadas de dos maneras, mediante la detección próxima desde **vehículos terrestres** que recorren el campo o mediante la detección remota desde **satélite o plataformas aéreas** (López-Granados 2011). Los orígenes de la teledetección de malas hierbas desde plataformas aéreas se pueden situar en Thornton *et al*. (1990) en una investigación preliminar de técnicas de vigilancia aérea usando un globo de helio a baja altura para tomar imágenes de la distribución de la avena loca en un campo de trigo.

De forma general, la discriminación de las malas hierbas mediante detección remota (o teledetección) puede abordarse según dos aproximaciones metodológicas diferentes: considerando

las malas hierbas en **estado fenológico temprano** (desde el estado de plántula hasta 2 - 6 hojas verdaderas) o en **estado fenológico tardío** (desde el inicio de la floración o inicio de senescencia). Utilizando esta última aproximación, se han obtenido resultados satisfactorios en la detección de malas hierbas utilizando imágenes aéreas (López-Granados *et al*. 2006; Peña-Barragán *et al*. 2007) y de satélite (Castillejo-González *et al*. 2014; de Castro *et al*. 2013), reportándose ahorros en herbicida de hasta el 50%. En estos trabajos se detectaban las malas hierbas en fase tardía para aplicar el herbicida al año siguiente en época temprana ya que en la mayoría de los escenarios agrícolas el momento óptimo para el control de las malas hierbas es justo unas pocas semanas después de la emergencia del cultivo. Esta idea se basa en que las malas hierbas persisten en su localización de un año para otro si no se controlan (Barroso *et al*. 2004; Jurado-Expósito *et al*. 2004). Sin embargo, si el objetivo es detectar infestaciones de malas hierbas en fase temprana, las dificultades son mayores que en el caso de la fase tardía principalmente por las siguientes tres razones (López-Granados 2011): 1) las malas hierbas son de pequeño tamaño, lo que hace necesario trabajar con imágenes remotas de gran resolución espacial, a veces píxeles < 5 cm (Robert 1996); 2) las malas hierbas de hoja estrecha presentes en los cultivos monocotiledóneos (*e.g.,* avena en trigo) o las malas hierbas de hoja ancha en cultivos dicotiledóneos (*e.g*., *Chenopodium* en girasol), generalmente tienen propiedades espectrales parecidas en fase temprana, lo que disminuye la posibilidad de discriminar entre clases de vegetación usando sólo información espectral; y 3) la reflectancia del suelo puede interferir con la detección (Thorp y Tian 2004).

Los problemas comentados anteriormente han ocasionado que, cuando sólo se podía trabajar con imágenes procedentes de satélites y aviones tripulados, la teledetección en fase temprana de malas hierbas para el desarrollo de estrategias de control localizado no fuera posible. Hoy en día la tecnología UAV ha hecho que la necesidad de una resolución espacial centimétrica ya no sea una limitación. Asimismo, la gran flexibilidad existente en la programación de vuelos permite que se tomen las imágenes en el momento que el agricultor estime más adecuado para la detección y posterior tratamiento de las malas hierbas. Para afrontar los problemas de separabilidad espectral es la tecnología OBIA la que aporta las herramientas necesarias para la adecuada clasificación de las malas hierbas, permitiendo su discriminación del cultivo utilizando parámetros que van más allá de la información espectral. De hecho, con anterioridad a esta Tesis Doctoral, algunos trabajos con UAV ya habían abordado objetivo parecidos, como la distribución de malas hierbas acuáticas (Göktoğan *et al*. 2010) o la invasión de plantas en la monitorización de grandes fincas (Laliberte *et al*. 2011), trabajo en el que se incorporó, además de tecnología UAV, una metodología OBIA.

8. MONITORIZACIÓN 3D DE CULTIVOS LEÑOSOS

Tras exponer los conceptos básicos del SSWM en relación a la teledetección mediante imágenes-UAV, a continuación se explican los fundamentos en los que se basa la importancia de **monitorizar de forma precisa la arquitectura 3D de los cultivos leñosos**. Los resultados en olivar de Miranda-Fuentes *et al*. (2016) han demostrado que carece de base científica la extendida creencia de que aumentar el volumen de aplicación mejora la homogeneidad y la penetración de la aplicación en la copa, ya que los valores óptimos de cobertura en su estudio se obtuvieron utilizando los volúmenes de aplicación más bajos. Pero además, la aplicación de fitosanitarios necesita ser precisa porque los tratamientos inadecuados pueden llevar a serios problemas como la contaminación medioambiental, la presencia de residuos en los alimentos y problemas de salud en los responsables de la aplicación. Los tratamientos que se realizan sin tener en cuenta la variabilidad espacial de la arquitectura foliar de los cultivos leñosos pueden contribuir a la contaminación de acuíferos y aguas subterráneas. Sin embargo, los agricultores a menudo aplican los productos hasta que se produce escorrentía como supuesta garantía de alta eficacia biológica.

El uso del volumen de copa de los cultivos como base para el cálculo y optimización de las aplicaciones de productos químicos fue discutido y evaluado por Sutton y Unrath (1984). El concepto del **volumen del seto** de árboles mantiene que la tasa de aplicación de productos químicos debe estar basada en el volumen del cultivo en vez de en su área. Siguiendo esta metodología desarrollada en manzanos, se han obtenido resultados satisfactorios para adaptar el volumen de aplicación a las dimensiones en el caso del viñedo (Llorens *et al*. 2010; Pergher y Petris 2008). En los casos mencionados, una medición precisa de las dimensiones del cultivo fue vital para el éxito final. En el caso de olivar, el desafío de los árboles aislados y con gran volumen de copa, como es el caso tanto de los olivares tradicionales como de los intensivos, es que la forma irregular de la copa hace difícil la implementación de los métodos establecidos para la estimación de su volumen (Miranda-Fuentes *et al*. 2016). Normalmente, las principales dimensiones del árbol son medidas de manera manual con un intenso trabajo de campo. A continuación, el volumen de copa es estimado con modelos empíricos o con ecuaciones que consideran que los árboles son sólidos geométricos (West 2009). Sin embargo, realizar estos muestreos a escala de campo exige una inversión de tiempo considerable y generalmente se generan resultados inciertos debido a la falta de ajuste de los árboles reales a los modelos geométricos, o a la gran variabilidad presente en los cultivos que puede afectar la adecuación de modelos basados en mediciones en campo.

Entre las alternativas tecnológicas, los escáneres LiDAR y los sistemas de visión estereoscópica ya sea desde el terreno o embarcados en plataformas aéreas convencionales han sido hasta la fecha los métodos más relevantes (Arnó *et al*. 2012; Escolà *et al*. 2016; Rosell y Sanz 2012), aunque estas

técnicas también presentan también sus limitaciones en condiciones de campo. Por una parte, aunque los equipos terrestres son muy precisos en la medición de la arquitectura arbórea (Fernández-Sarría *et al*. 2013; Moorthy *et al*. 2011; Rovira-Más *et al*. 2008), son menos eficientes en grandes superficies de terreno y no son fáciles de usar en áreas de difícil acceso. Por otra parte, la resolución espacial de los datos tomados con aviones tripulados y satélites es aún insuficiente para detectar las características 3D de los árboles en la mayoría de los casos (Rosell y Sanz 2012).

Como se ha comentado en esta Introducción, los UAVs pueden volar automáticamente a baja altura y con gran solape. Ello permite la toma de imágenes de muy alta resolución espacial (en el rango de centímetros) y facilita la generación de modelos digitales de superficies (MDS) mediante métodos automáticos de reconstrucción basados en los modelos "**Structure from Motion**". Lo anterior es relevante ya que investigaciones recientes se han centrado en la generación de MDSs con UAVs (Nex y Remondino 2014) y su interpretación sobre áreas agrícolas para la caracterización tridimensional de cultivos herbáceos y leñosos con el objetivo de monitorizar el estado del cultivo y su crecimiento (Bendig *et al*. 2014; Burgos *et al*. 2015).

Sin embargo, para explotar al máximo la tecnología UAV hay que incorporar la adopción de procedimientos automáticos y robustos de análisis de imagen que sean capaces de extraer la inmensa cantidad de información que ofrecen las imágenes. Para alcanzar un alto nivel de automatización y adaptabilidad en esta Tesis Doctoral se propone la aplicación de técnicas OBIA.

9. OBJETIVOS DE LA TESIS DOCTORAL

Por todo lo recogido anteriormente, el objetivo general de la presente Tesis ha sido el desarrollo de metodologías automatizadas y robustas para la cartografía de malas hierbas en cultivos herbáceos en fase temprana y la monitorización tridimensional de cultivos leñosos, con el fin último de contribuir a la implementación de estrategias de técnicas de aplicación variable en el ámbito de la agricultura de precisión que permitan un uso sostenible de los productos fitosanitarios.

Este objetivo general se ha desarrollado a través de los siguientes objetivos específicos:

1. Estudiar la configuración y las especificaciones técnicas de un UAV y de los sensores embarcados para su aplicación en la detección temprana de malas hierbas y contribuir a la generación de mapas para un control localizado.
2. Evaluar los índices espectrales en el rango visible existentes en la literatura científica para su uso en la discriminación de vegetación en imágenes tomadas con un UAV sobre cultivos de trigo en fase temprana.

3. Implementar en un entorno OBIA un método de cálculo automático de umbrales para la detección de vegetación en imágenes procedentes de UAV tomadas en cultivos herbáceos en fase temprana.
4. Desarrollar una metodología OBIA automática y robusta para la discriminación de malas hierbas en cultivos herbáceos en fase temprana, así como evaluar la influencia sobre su funcionamiento de distintos parámetros relacionados con la toma de imágenes UAV.
5. Desarrollar una metodología OBIA automática y robusta para la caracterización tridimensional de cultivos leñosos usando imágenes y MDS generados a partir de imágenes procedentes de un UAV.

La presente Tesis Doctoral está organizada en 9 capítulos:

- En el **capítulo 1** se estudian la configuración y las especificaciones de un UAV para la detección temprana de malas hierbas y contribuir a la generación de mapas para un control localizado, lo que corresponde al artículo: Torres-Sánchez, J., López-Granados, F., De Castro, A. I., & Peña-Barragán, J. M. (2013). Configuration and Specifications of an Unmanned Aerial Vehicle (UAV) for Early Site Specific Weed Management. *PLoS ONE*, 8(3), e58210. doi:10.1371/journal.pone.0058210.
- El **capítulo 2** refleja el estudio de una serie de índices de vegetación para la cartografía de la fracción de vegetación en cultivos herbáceos usando imágenes UAV, que fue publicado en el artículo: Torres-Sánchez, J., Peña, J. M., de Castro, A. I., & López-Granados, F. (2014). Multi-temporal mapping of the vegetation fraction in early-season wheat fields using images from UAV. *Computers and Electronics in Agriculture*, 103, 104–113. doi:10.1016/j.compag.2014.02.009.
- En el **capítulo 3** se presenta la implementación en un entorno OBIA de un método automático de cálculo de umbrales y su aplicación a la detección de vegetación en imágenes UAV, trabajo correspondiente al artículo: Torres-Sánchez, J., López-Granados, F., & Peña, J. M. (2015). An automatic object-based method for optimal thresholding in UAV images: Application for vegetation detection in herbaceous crops. *Computers and Electronics in Agriculture*, 114, 43–52. doi:10.1016/j.compag.2015.03.019.
- En el **capítulo 4** se desarrolla un algoritmo OBIA para la detección de malas hierbas en un cultivo de maíz en fase temprana usando imágenes tomadas por un UAV, recogido en el artículo: Peña, J. M., Torres-Sánchez, J., de Castro, A. I., Kelly, M., & López-Granados, F. (2013). Weed Mapping in Early-Season Maize Fields Using Object-Based Analysis of Unmanned Aerial Vehicle (UAV) Images. *PLOS ONE*, 8(10), e77151. doi:10.1371/journal.pone.0077151.

- En el **capítulo 5** se estudió la influencia de la resolución espectral y espacial sobre el algoritmo para la detección de malas hierbas en fase temprana, reflejando el artículo: Peña, J. M., Torres-Sánchez, J., Serrano-Pérez, A., de Castro, A. I., & López-Granados, F. (2015). Quantifying Efficacy and Limits of Unmanned Aerial Vehicle (UAV) Technology for Weed Seedling Detection as Affected by Sensor Resolution. *Sensors*, 15(3), 5609–5626. doi:10.3390/s150305609.
- En el **capítulo 6** se aplicó el algoritmo anteriormente diseñado a ortoimágenes tomadas sobre campos de girasol, y se estudiaron los diferentes mapas prescripción de herbicida fruto de la aplicación de un rango de umbrales de tratamiento, trabajo que fue descrito en el artículo: López-Granados, F., Torres-Sánchez, J., Serrano-Pérez, A., Castro, A. I. de, Mesas-Carrascosa, F.-J., & Peña, J.-M. (2015). Early season weed mapping in sunflower using UAV technology: variability of herbicide treatment maps against weed thresholds. *Precision Agriculture*, 17(2), 183–199. doi:10.1007/s11119-015-9415-8.
- El **capítulo 7** presenta una metodología para la caracterización tridimensional de cultivos arbóreos usando tecnología UAV, correspondiente al artículo: Torres-Sánchez, J., López-Granados, F., Serrano, N., Arquero, O., & Peña, J. M. (2015). High-Throughput 3-D Monitoring of Agricultural-Tree Plantations with Unmanned Aerial Vehicle (UAV) Technology. *PLOS ONE*, 10(6), e0130479. doi:10.1371/journal.pone.0130479.
- En **el capítulo 8** se aplica una metodología OBIA para la monitorización 3D de viñedos, trabajo presentado en el artículo: Torres-Sánchez, J., López-Granados, F., Jiménez-Brenes, F.M., Borra-Serrano, I., de Castro, A.I., Peña, J.M. (2016). 3-D vineyard monitoring with UAV images and a novel OBIA procedure for precision viticulture applications. *Computers and Electronics in Agriculture,* en revisión.
- Por último, en el **capítulo 9**, se enumeran las conclusiones generales obtenidas de los trabajos anteriormente descritos sobre tecnología UAV y el desarrollo de metodologías robustas para la cartografía de malas hierbas en cultivos herbáceos en fase temprana y la monitorización tridimensional de cultivos leñosos con el fin último de contribuir a la implementación de estrategias de técnicas de aplicación variable en el ámbito de la agricultura de precisión que permitan un uso sostenible de los productos fitosanitarios.

10.BIBLIOGRAFÍA

AEPLA. (2016). Memoria AEPLA 2015. http://www.aepla.es/tmp/images/publicaciones/P0022_Memoria_AEPLA_2015.pdf. Accessed 30 September 2016

Aplin, P. (2006). On scales and dynamics in observing the environment. *International Journal of Remote Sensing*, *27*(11), 2123–2140. doi:10.1080/01431160500396477

Arnó, J., Escolà, A., Vallès, J. M., Llorens, J., Sanz, R., Masip, J., et al. (2012). Leaf area index estimation in vineyards using a ground-based LiDAR scanner. *Precision Agriculture*, *14*(3), 290–306. doi:10.1007/s11119-012-9295-0

Atzberger, C. (2013). Advances in Remote Sensing of Agriculture: Context Description, Existing Operational Monitoring Systems and Major Information Needs. *Remote Sensing*, *5*(2), 949–981. doi:10.3390/rs5020949

Ballesteros, R., Ortega, J. F., Hernández, D., & Moreno, M. Á. (2015). Characterization of Vitis vinifera L. Canopy Using Unmanned Aerial Vehicle-Based Remote Sensing and Photogrammetry Techniques. *American Journal of Enology and Viticulture*, ajev.2014.14070. doi:10.5344/ajev.2014.14070

Baluja, J., Diago, M. P., Balda, P., Zorer, R., Meggio, F., Morales, F., & Tardaguila, J. (2012). Assessment of vineyard water status variability by thermal and multispectral imagery using an unmanned aerial vehicle (UAV). *Irrigation Science*, *30*(6), 511–522. doi:10.1007/s00271-012-0382-9

Barroso, J., Fernàndez-Quintanilla, C., Ruiz, D., Hernaiz, P., & Rew, L. (2004). Spatial stability of Avena sterilis ssp. ludoviciana populations under annual applications of low rates of imazamethabenz. *Weed Research*, *44*(3), 178–186. doi:10.1111/j.1365-3180.2004.00389.x

Becker-Reshef, I., Justice, C., Sullivan, M., Vermote, E., Tucker, C., Anyamba, A., et al. (2010). Monitoring Global Croplands with Coarse Resolution Earth Observations: The Global Agriculture Monitoring (GLAM) Project. *Remote Sensing*, *2*(6), 1589–1609. doi:10.3390/rs2061589

Bendig, J., Bolten, A., & Bareth, G. (2013). UAV-based Imaging for Multi-Temporal, very high Resolution Crop Surface Models to monitor Crop Growth Variability Monitoring.

Photogrammetrie - Fernerkundung - Geoinformation, *2013*(6), 551–562. doi:10.1127/1432-8364/2013/0200

Bendig, J., Bolten, A., Bennertz, S., Broscheit, J., Eichfuss, S., & Bareth, G. (2014). Estimating Biomass of Barley Using Crop Surface Models (CSMs) Derived from UAV-Based RGB Imaging. *Remote Sensing*, *6*(11), 10395–10412. doi:10.3390/rs61110395

Blaschke, T. (2010). Object based image analysis for remote sensing. *ISPRS Journal of Photogrammetry and Remote Sensing*, *65*(1), 2–16. doi:10.1016/j.isprsjprs.2009.06.004

Burgos, S., Mota, M., Noll, D., & Cannelle, B. (2015). Use of Very High-Resolution Airborne Images to Analyse 3d Canopy Architecture of a Vineyard. *The International Archives of Photogrammetry, Remote Sensing and Spatial Information Sciences*, *40*(3), 399.

Calderón, R., Navas-Cortés, J. A., Lucena, C., & Zarco-Tejada, P. J. (2013). High-resolution airborne hyperspectral and thermal imagery for early detection of Verticillium wilt of olive using fluorescence, temperature and narrow-band spectral indices. *Remote Sensing of Environment*, *139*, 231–245. doi:10.1016/j.rse.2013.07.031

Carter. (2000). Herbicide movement in soils: principles, pathways and processes. *Weed Research*, *40*(1), 113–122. doi:10.1046/j.1365-3180.2000.00157.x

Castillejo-González, I. L., López-Granados, F., García-Ferrer, A., Peña-Barragán, J. M., Jurado-Expósito, M., de la Orden, M. S., & González-Audicana, M. (2009). Object- and pixel-based analysis for mapping crops and their agro-environmental associated measures using QuickBird imagery. *Computers and Electronics in Agriculture*, *68*(2), 207–215. doi:10.1016/j.compag.2009.06.004

Castillejo-González, I. L., Peña-Barragán, J. M., Jurado-Expósito, M., Mesas-Carrascosa, F. J., & López-Granados, F. (2014). Evaluation of pixel- and object-based approaches for mapping wild oat (Avena sterilis) weed patches in wheat fields using QuickBird imagery for site-specific management. *European Journal of Agronomy*, *59*, 57–66. doi:10.1016/j.eja.2014.05.009

Castro, A. I. de, Ehsani, R., Ploetz, R. C., Crane, J. H., & Buchanon, S. (2015). Detection of Laurel Wilt Disease in Avocado Using Low Altitude Aerial Imaging. *PLOS ONE*, *10*(4), e0124642. doi:10.1371/journal.pone.0124642

Castro, A. I. de, López-Granados, F., & Jurado-Expósito, M. (2013). Broad-scale cruciferous weed patch classification in winter wheat using QuickBird imagery for in-season site-specific control. *Precision Agriculture*, *14*(4), 392–413. doi:10.1007/s11119-013-9304-y

Colomina, I., & Molina, P. (2014). Unmanned aerial systems for photogrammetry and remote sensing: A review. *ISPRS Journal of Photogrammetry and Remote Sensing*, *92*, 79–97. doi:10.1016/j.isprsjprs.2014.02.013

Doruchowski, G., Balsari, P., & Van de Zande, J. (2009). Development of a crop adapted spray application system for sustainable plant protection in fruit growing. *Acta Horticulturae*, (824), 251–260. doi:10.17660/ActaHortic.2009.824.29

Eisenbeiss, H. (2009). *UAV photogrammetry*. Inst. für Geodäsie und Photogrammetrie, Zürich.

Escolà, A., Martínez-Casasnovas, J. A., Rufat, J., Arnó, J., Arbonés, A., Sebé, F., et al. (2016). Mobile terrestrial laser scanner applications in precision fruticulture/horticulture and tools to extract information from canopy point clouds. *Precision Agriculture*, 1–22. doi:10.1007/s11119-016-9474-5

Fernández-Sarría, A., Martínez, L., Velázquez-Martí, B., Sajdak, M., Estornell, J., & Recio, J. A. (2013). Different methodologies for calculating crown volumes of Platanus hispanica trees using terrestrial laser scanner and a comparison with classical dendrometric measurements. *Computers and Electronics in Agriculture*, *90*, 176–185. doi:10.1016/j.compag.2012.09.017

Garcia-Ruiz, F., Sankaran, S., Maja, J. M., Lee, W. S., Rasmussen, J., & Ehsani, R. (2013). Comparison of two aerial imaging platforms for identification of Huanglongbing-infected citrus trees. *Computers and Electronics in Agriculture*, *91*, 106–115. doi:10.1016/j.compag.2012.12.002

García-Torres, L., López-Granados, F., & Castejón-Muñoz, M. (1994). Pre-emergence herbicides for the control of broomrape (Orobanche cernua Loefl.) in sunflower (Helianthus annus L.). *Weed Research*, *34*(6), 395–402. doi:10.1111/j.1365-3180.1994.tb02035.x

Geipel, J., Link, J., Wirwahn, J. A., & Claupein, W. (2016). A Programmable Aerial Multispectral Camera System for In-Season Crop Biomass and Nitrogen Content Estimation. *Agriculture*, *6*(1), 4. doi:10.3390/agriculture6010004

Göktoğan, A., Sukkarieh, S., Bryson, M., Randle, J., Lupton, T., & Hung, C. (2010). A Rotary-wing Unmanned Air Vehicle for Aquatic Weed Surveillance and Management. *Journal of Intelligent & Robotic Systems*, *57*(1), 467–484. doi:10.1007/s10846-009-9371-5

Hardin, P. J., & Hardin, T. J. (2010). Small-Scale Remotely Piloted Vehicles in Environmental Research. *Geography Compass*, *4*(9), 1297–1311. doi:10.1111/j.1749-8198.2010.00381.x

Hardin, P. J., & Jensen, R. R. (2011). Small-Scale Unmanned Aerial Vehicles in Environmental Remote Sensing: Challenges and Opportunities. *GIScience & Remote Sensing*, *48*(1), 99–111. doi:10.2747/1548-1603.48.1.99

Hatfield, J. L. (2000). *Precision agriculture and environmental quality: challenges for research and education*. USDA National Resources Conservation Service Ames, IA. https://www.researchgate.net/profile/Jerry_Hatfield2/publication/265008087_Precision_Agriculture_and_Environmental_Quality_Challenges_for_Research_and_Education/links/5464ca9d0cf267ed84f25c16.pdf. Accessed 21 September 2016

Hay, G. J., Marceau, D. J., Dubé, P., & Bouchard, A. (2001). A multiscale framework for landscape analysis: Object-specific analysis and upscaling. *Landscape Ecology*, *16*(6), 471–490. doi:10.1023/A:1013101931793

Heijting, S., Van Der Werf, W., Stein, A., & Kropff, M. J. (2007). Are weed patches stable in location? Application of an explicitly two-dimensional methodology. *Weed Research*, *47*(5), 381–395. doi:10.1111/j.1365-3180.2007.00580.x

Hellesen, T., & Matikainen, L. (2013). An Object-Based Approach for Mapping Shrub and Tree Cover on Grassland Habitats by Use of LiDAR and CIR Orthoimages. *Remote Sensing*, *5*(2), 558–583. doi:10.3390/rs5020558

Herwitz, S. ., Johnson, L. ., Dunagan, S. ., Higgins, R. ., Sullivan, D. ., Zheng, J., et al. (2004). Imaging from an unmanned aerial vehicle: agricultural surveillance and decision support. *Computers and Electronics in Agriculture*, *44*(1), 49–61. doi:10.1016/j.compag.2004.02.006

Heumann, B. W. (2011). An Object-Based Classification of Mangroves Using a Hybrid Decision Tree—Support Vector Machine Approach. *Remote Sensing*, *3*(11), 2440–2460. doi:10.3390/rs3112440

Houborg, R., Anderson, M., & Daughtry, C. (2009). Utility of an image-based canopy reflectance modeling tool for remote estimation of LAI and leaf chlorophyll content at the field scale. *Remote Sensing of Environment*, *113*(1), 259–274. doi:10.1016/j.rse.2008.09.014

Hu, K., & Fu, Z. (2012). Research On The Performance Of The Ultrasonic Measurement System Of The Tree Canopy Volume. *Intelligent Automation & Soft Computing*, *18*(5), 591–600. doi:10.1080/10798587.2012.10643268

Hunt, E. R., Daughtry, C. S. T., Mirsky, S. B., & Hively, W. D. (2013). Remote sensing with unmanned aircraft systems for precision agriculture applications. In *2013 Second International Conference on Agro-Geoinformatics (Agro-Geoinformatics)* (pp. 131–134). Presented at the 2013 Second International Conference on Agro-Geoinformatics (Agro-Geoinformatics). doi:10.1109/Argo-Geoinformatics.2013.6621894

Instituto Aragonés de Estadística. (2016). Estadísticas de consumo de fertilizantes y pesticidas. http://www.aragon.es/DepartamentosOrganismosPublicos/Institutos/InstitutoAragonesEstadistica/AreasTematicas/14_Medio_Ambiente_Y_Energia/01_SectoresProductivos/ci.01_Agricultura_medio_ambiente.detalleDepartamento. Accessed 1 October 2016

Jensen, J. R. (2006). *Remote Sensing of the Environment: An Earth Resource Perspective* (2 edition.). Upper Saddle River, NJ: Pearson.

Jurado-Expósito, M., López-Granados, F., García-Torres, L., García-Ferrer, A., Sánchez de la Orden, M., & Atenciano, S. (2003). Multi-species weed spatial variability and site-specific management maps in cultivated sunflower. *Weed Science*, *51*(3), 319–328. doi:10.1614/0043-1745(2003)051[0319:MWSVAS]2.0.CO;2

Jurado-Exposito, M., Lopez-Granados, F., Gonzalez-Andujar, J. L., & Garcia-Torres, L. (2005). Characterizing population growth rate of Convolvulus arvensis in wheat-sunflower no-tillage systems. *Crop science*, *45*(5), 2106–2112.

Jurado-Expósito, M., López-Granados, F., González-Andújar, J. L., & García-Torres, L. (2004). Spatial and temporal analysis of Convolvulus arvensis L. populations over four growing seasons. *European Journal of Agronomy*, *21*(3), 287–296. doi:10.1016/j.eja.2003.10.001

Jurado-Expósito, M., López-Granados, F., Peña-Barragán, J. M., & García-Torres, L. (2009). A digital elevation model to aid geostatistical mapping of weeds in sunflower crops. *Agronomy for Sustainable Development*, *29*(2), 391–400. doi:10.1051/agro:2008045

Laliberte, A. S., Goforth, M. A., Steele, C. M., & Rango, A. (2011). Multispectral Remote Sensing from Unmanned Aircraft: Image Processing Workflows and Applications for Rangeland Environments. *Remote Sensing*, *3*(11), 2529–2551. doi:10.3390/rs3112529

Laliberte, A. S., Herrick, J. E., Rango, A., & Winters, Craig. (2010). Acquisition, orthorectification, and classification of unmanned aerial vehicle (UAV) imagery for rangeland monitoring. *Photogrammetric Engineering and Remote Sensing*, *76*, 661–672.

Lee, W. S., Alchanatis, V., Yang, C., Hirafuji, M., Moshou, D., & Li, C. (2010). Sensing technologies for precision specialty crop production. *Computers and Electronics in Agriculture*, *74*(1), 2–33. doi:10.1016/j.compag.2010.08.005

Lelong, C. C. D., Burger, P., Jubelin, G., Roux, B., Labbé, S., & Baret, F. (2008). Assessment of Unmanned Aerial Vehicles Imagery for Quantitative Monitoring of Wheat Crop in Small Plots. *Sensors*, *8*(5), 3557–3585. doi:10.3390/s8053557

Liaghat. (2010). A Review: The Role of Remote Sensing in Precision Agriculture. *American Journal of Agricultural and Biological Sciences*, *5*(1), 50–55. doi:10.3844/ajabssp.2010.50.55

Llorens, J., Gil, E., Llop, J., & Escolà, A. (2010). Variable rate dosing in precision viticulture: Use of electronic devices to improve application efficiency. *Crop Protection*, *29*(3), 239–248. doi:10.1016/j.cropro.2009.12.022

Longchamps, L., Panneton, B., Simard, M.-J., & Leroux, G. D. (2014). An Imagery-Based Weed Cover Threshold Established Using Expert Knowledge. *Weed Science*, *62*(1), 177–185. doi:10.1614/WS-D-13-00050.1

López-Granados, F. (2011). Weed detection for site-specific weed management: mapping and real-time approaches. *Weed Research*, *51*(1), 1–11. doi:10.1111/j.1365-3180.2010.00829.x

López-Granados, F., Jurado-Expósito, M., Peña-Barragán, J. M., & García-Torres, L. (2005). Using geostatistical and remote sensing approaches for mapping soil properties. *European Journal of Agronomy*, *23*(3), 279–289. doi:10.1016/j.eja.2004.12.003

López-Granados, F., Jurado-Expósito, M., Peña-Barragán, J. M., & García-Torres, L. (2006). Using remote sensing for identification of late-season grass weed patches in wheat. *Weed Science*, *54*(2), 346–353. doi:10.1614/WS-05-54.2.346

Ma, L., Cheng, L., Li, M., Liu, Y., & Ma, X. (2015). Training set size, scale, and features in Geographic Object-Based Image Analysis of very high resolution unmanned aerial vehicle imagery. *ISPRS Journal of Photogrammetry and Remote Sensing*, *102*, 14–27. doi:10.1016/j.isprsjprs.2014.12.026

Mathews, A. J. (2014). Object-based spatiotemporal analysis of vine canopy vigor using an inexpensive unmanned aerial vehicle remote sensing system. *Journal of Applied Remote Sensing*, *8*(1), 85199. doi:10.1117/1.JRS.8.085199

Mathews, A. J., & Jensen, J. L. R. (2013). Visualizing and Quantifying Vineyard Canopy LAI Using an Unmanned Aerial Vehicle (UAV) Collected High Density Structure from Motion Point Cloud. *Remote Sensing*, *5*(5), 2164–2183. doi:10.3390/rs5052164

Méndez, V., Catalán, H., Rosell-Polo, J. R., Arnó, J., & Sanz, R. (2013). LiDAR simulation in modelled orchards to optimise the use of terrestrial laser scanners and derived vegetative measures. *Biosystems Engineering*, *115*(1), 7–19. doi:10.1016/j.biosystemseng.2013.02.003

Meron, M., Tsipris, J., Orlov, V., Alchanatis, V., & Cohen, Y. (2010). Crop water stress mapping for site-specific irrigation by thermal imagery and artificial reference surfaces. *Precision Agriculture*, *11*(2), 148–162. doi:10.1007/s11119-009-9153-x

Mesas-Carrascosa, F. J., Notario-García, M. D., Meroño de Larriva, J. E., Sánchez de la Orden, M., & García-Ferrer Porras, A. (2014). Validation of measurements of land plot area using UAV imagery. *International Journal of Applied Earth Observation and Geoinformation*, *33*, 270–279. doi:10.1016/j.jag.2014.06.009

Mesas-Carrascosa, F.-J., Torres-Sánchez, J., Clavero-Rumbao, I., García-Ferrer, A., Peña, J.-M., Borra-Serrano, I., & López-Granados, F. (2015). Assessing Optimal Flight Parameters for Generating Accurate Multispectral Orthomosaicks by UAV to Support Site-Specific Crop Management. *Remote Sensing*, *7*(10), 12793–12814. doi:10.3390/rs71012793

Miranda-Fuentes, A., Llorens, J., Rodríguez-Lizana, A., Cuenca, A., Gil, E., Blanco-Roldán, G. L., & Gil-Ribes, J. A. (2016). Assessing the optimal liquid volume to be sprayed on isolated olive trees according to their canopy volumes. *Science of The Total Environment*, *568*, 296–305. doi:10.1016/j.scitotenv.2016.06.013

Moffett, K. B., & Gorelick, S. M. (2013). Distinguishing wetland vegetation and channel features with object-based image segmentation. *International Journal of Remote Sensing*, *34*(4), 1332–1354. doi:10.1080/01431161.2012.718463

Molinero-Ruiz, L., García-Carneros, A. B., Collado-Romero, M., Raranciuc, S., Domínguez, J., & Melero-Vara, J. M. (2014). Pathogenic and molecular diversity in highly virulent populations of the parasitic weed Orobanche cumana (sunflower broomrape) from Europe. *Weed Research*, *54*(1), 87–96. doi:10.1111/wre.12056

Moorthy, I., Miller, J. R., Berni, J. A. J., Zarco-Tejada, P., Hu, B., & Chen, J. (2011). Field characterization of olive (Olea europaea L.) tree crown architecture using terrestrial laser scanning data. *Agricultural and Forest Meteorology*, *151*(2), 204–214. doi:10.1016/j.agrformet.2010.10.005

Nex, F., & Remondino, F. (2014). UAV for 3D mapping applications: a review. *Applied Geomatics*, *6*(1), 1–15. doi:10.1007/s12518-013-0120-x

Pajares, G. (2015). Overview and Current Status of Remote Sensing Applications Based on Unmanned Aerial Vehicles (UAVs). *Photogrammetric Engineering & Remote Sensing*, *81*(4), 281–329. doi:10.14358/PERS.81.4.281

Peña-Barragán, J. M., López-Granados, F., Jurado-Expósito, M., & García-Torres, L. (2007). Mapping Ridolfia segetum patches in sunflower crop using remote sensing. *Weed Research*, *47*(2), 164–172. doi:10.1111/j.1365-3180.2007.00553.x

Peña-Barragán, J. M., Ngugi, M. K., Plant, R. E., & Six, J. (2011). Object-based crop identification using multiple vegetation indices, textural features and crop phenology. *Remote Sensing of Environment*, *115*(6), 1301–1316. doi:10.1016/j.rse.2011.01.009

Peña-Barragán, Kelly, M., de Castro, & López-Granados. (2012). Object-based approach for crop row characterizatioin in UAV images for site-specific weed management. In *Proceedings of the 4th GEOBIA* (pp. 426–430). Presented at the International Conference on Geographic Object-Based Image Analysis, Rio de Janeiro, Brazil.

Pergher, G., & Petris, R. (2008). Pesticide Dose Adjustment in Vineyard Spraying and Potential for Dose Reduction. *Agricultural Engineering International: CIGR Journal*. http://cigrjournal.org/index.php/Ejounral/article/view/1254. Accessed 23 September 2016

Rey-Caramés, C., Diago, M. P., Martín, M. P., Lobo, A., & Tardaguila, J. (2015). Using RPAS Multi-Spectral Imagery to Characterise Vigour, Leaf Development, Yield Components and Berry Composition Variability within a Vineyard. *Remote Sensing*, *7*(11), 14458–14481. doi:10.3390/rs71114458

Robert, P. C. (1996). Use of remote sensing imagery for precision farming. In *Proc of 26th Int. Symposium on Rem. Sens. of Env* (pp. 596–599).

Robert, P. C. (2002). Precision agriculture: a challenge for crop nutrition management. *Plant and Soil*, *247*(1), 143–149. doi:10.1023/A:1021171514148

Rosell, J. R., Llorens, J., Sanz, R., Arnó, J., Ribes-Dasi, M., Masip, J., et al. (2009). Obtaining the three-dimensional structure of tree orchards from remote 2D terrestrial LIDAR scanning. *Agricultural and Forest Meteorology*, *149*(9), 1505–1515. doi:10.1016/j.agrformet.2009.04.008

Rosell, J. R., & Sanz, R. (2012). A review of methods and applications of the geometric characterization of tree crops in agricultural activities. *Computers and Electronics in Agriculture*, *81*, 124–141. doi:10.1016/j.compag.2011.09.007

Rovira-Más, F., Zhang, Q., & Reid, J. F. (2008). Stereo vision three-dimensional terrain maps for precision agriculture. *Computers and Electronics in Agriculture*, *60*(2), 133–143. doi:10.1016/j.compag.2007.07.007

Schieffer, J., & Dillon, C. (2014). The economic and environmental impacts of precision agriculture and interactions with agro-environmental policy. *Precision Agriculture*, *16*(1), 46–61. doi:10.1007/s11119-014-9382-5

Shahbazi, M., Théau, J., & Ménard, P. (2014). Recent applications of unmanned aerial imagery in natural resource management. *GIScience & Remote Sensing*, *51*(4), 339–365. doi:10.1080/15481603.2014.926650

Sutton, T. B., & Unrath, C. R. (1984). Evaluation of the tree-row-volume concept with density adjustments in relation to spray deposits in apple orchards. *Plant disease*, *68*(6), 480–484.

Swanton, C. J., Weaver, S., Cowan, P., Acker, R. V., Deen, W., & Shreshta, A. (1999). Weed Thresholds. *Journal of Crop Production*, *2*(1), 9–29. doi:10.1300/9785529

Thornton, P. K., Fawcett, R. H., Dent, J. B., & Perkins, T. J. (1990). Spatial weed distribution and economic thresholds for weed control. *Crop Protection*, *9*(5), 337–342. doi:10.1016/0261-2194(90)90003-P

Thorp, K. R., & Tian, L. F. (2004). A Review on Remote Sensing of Weeds in Agriculture. *Precision Agriculture*, *5*(5), 477–508. doi:10.1007/s11119-004-5321-1

Tiede, D., Lang, S., Hölbling, D., & Füreder, P. (2010). Transferability of OBIA rulesets for IDP camp analysis in Darfur. In *Proceedings of GEOBIA 2010—Geographic Object-Based Image Analysis.* Presented at the Geographic Object-Based Image Analysis, Ghent.

West, P. W. (2009). *Tree and forest measurements* (2nd ed.). Berlin, Germany: Springer-Verlag.

Whitehead, K., Hugenholtz, C. H., Myshak, S., Brown, O., LeClair, A., Tamminga, A., et al. (2014). Remote sensing of the environment with small unmanned aircraft systems (UASs), part 2: scientific and commercial applications. *Journal of Unmanned Vehicle Systems*, *2*(3), 86–102. doi:10.1139/juvs-2014-0007

Woodcock, C. E., & Strahler, A. H. (1987). The factor of scale in remote sensing. *Remote Sensing of Environment*, *21*(3), 311–332. doi:10.1016/0034-4257(87)90015-0

Xiang, H., & Tian, L. (2011). Development of a low-cost agricultural remote sensing system based on an autonomous unmanned aerial vehicle (UAV). *Biosystems Engineering*, *108*(2), 174–190. doi:10.1016/j.biosystemseng.2010.11.010

Yu, Q., Gong, P., Clinton, N., Biging, G., Kelly, M., & Schirokauer, D. (2006). Object-based detailed vegetation classification. with airborne high spatial resolution remote sensing imagery. *Photogrammetric Engineering and Remote Sensing*, *72*(7), 799–811.

Zaman, Q.-, & Schumann, A. W. (2005). Performance of an Ultrasonic Tree Volume Measurement System in Commercial Citrus Groves. *Precision Agriculture*, *6*(5), 467–480. doi:10.1007/s11119-005-4243-x

Zarco-Tejada, P. J., Diaz-Varela, R., Angileri, V., & Loudjani, P. (2014). Tree height quantification using very high resolution imagery acquired from an unmanned aerial vehicle (UAV) and automatic

3D photo-reconstruction methods. *European Journal of Agronomy*, *55*, 89–99. doi:10.1016/j.eja.2014.01.004

CAPÍTULO 1

CONFIGURATION AND SPECIFICATIONS OF AN UNMANNED AERIAL VEHICLE (UAV) FOR EARLY SITE SPECIFIC WEED MANAGEMENT

Torres-Sánchez, J., López-Granados, F., De Castro, A. I., & Peña-Barragán, J. M. (2013). Configuration and Specifications of an Unmanned Aerial Vehicle (UAV) for Early Site Specific Weed Management. *PLoS ONE*, 8(3), e58210. doi:10.1371/journal.pone.0058210

1. RESUMEN

Una nueva plataforma aérea para la toma de imágenes remotas ha surgido en los últimos años, el vehículo aéreo no tripulado (UAV por sus siglas en inglés). Este artículo describe la configuración y las especificaciones técnicas de un UAV utilizado para tomar imágenes para el control localizado de malas hierbas en fase temprana. También se ha evaluado si las imágenes tomadas por el UAV, al contrario que las tomadas por satélites y plataformas tripuladas, cumplen los requisitos necesarios para la detección en fase temprana de malas hierbas en cuanto a resolución espacial y espectral. Dos sensores diferentes, una camára convencional y una cámara multiespectral de 6 bandas, y tres alturas de vuelo (30, 60 y 100 m) fueron evaluados sobre un campo de girasol naturalmente infestado de malas hierbas. Las principales fases del flujo de trabajo con el UAV fueron: 1) planificación de la misión, que incluye consideraciones sobre el área a volar, las especificaciones del sensor y las tareas a realizar por el UAV; 2) vuelo UAV y toma de imágenes; y 3) preprocesamiento de las imágenes, que incluyó la correcta alineación de las seis bandas de la cámara multiespectral capturadas en cada vuelo. Del estudio de las imágenes se pudo extraer que la resolución espacial, el área cubierta por cada imagen y el tiempo de vuelo fueron muy sensibles a la altura de vuelo. A menor altitud, el UAV tomó imágenes de mayor resolución espacial, aunque el número de imágenes necesitado para cubrir el campo entero podría ser un factor limitante debido a la energía necesaria para una mayor duración de vuelo y a los requerimientos computacionales para el posterior mosaicado de las imágenes. A partir de las imágenes tomadas se calcularon tres índices espectrales. Las diferencias espectrales entre malas hierbas, cultivo y suelo fueron significativas para los índices de vegetación estudiados (ExG, NGRDI, NDVI), principalmente a 30 m de altura. Sin embargo, la mayor separabilidad espectral se dio para vegetación y suelo desnudo con el NDVI. Estos resultados sugieren que es necesario llegar a un balance entre la resolución espacial y espectral para optimizar el plan de vuelo de acuerdo al objetivo agronómico buscado, teniendo en cuenta el tamaño del menor objeto que se necesita detectar (malas hierbas individuales o rodales de malas hierbas).

2. ABSTRACT

A new aerial platform has risen recently for image acquisition, the Unmanned Aerial Vehicle (UAV). This article describes the technical specifications and configuration of a UAV used to capture remote images for early season site- specific weed management (ESSWM). Image spatial and spectral properties required for weed seedling discrimination were also evaluated. Two different sensors, a still visible camera and a six-band multispectral camera, and three flight altitudes (30, 60 and 100 m)

were tested over a naturally infested sunflower field. The main phases of the UAV workflow were the following: 1) mission planning, 2) UAV flight and image acquisition, and 3) image pre-processing. Three different aspects were needed to plan the route: flight area, camera specifications and UAV tasks. The pre-processing phase included the correct alignment of the six bands of the multispectral imagery and the orthorectification and mosaicking of the individual images captured in each flight. The image pixel size, area covered by each image and flight timing were very sensitive to flight altitude. At a lower altitude, the UAV captured images of finer spatial resolution, although the number of images needed to cover the whole field may be a limiting factor due to the energy required for a greater flight length and computational requirements for the further mosaicking process. Spectral differences between weeds, crop and bare soil were significant in the vegetation indices studied (Excess Green Index, Normalised Green-Red Difference Index and Normalised Difference Vegetation Index), mainly at a 30 m altitude. However, greater spectral separability was obtained between vegetation and bare soil with the index NDVI. These results suggest that an agreement among spectral and spatial resolutions is needed to optimise the flight mission according to every agronomical objective as affected by the size of the smaller object to be discriminated (weed plants or weed patches).

3. INTRODUCTION

Precision agriculture (PA) is defined as "*a management strategy that uses information technology to bring data from multiple sources to bear on decisions associated with crop production"* (National Research Council (U.S.) 1997). PA encompasses all the techniques and methods for crop and field management by taking into account their local and site-specific heterogeneity and variability (Lelong *et al*. 2008). Within the context of PA, early season site-specific weed management (ESSWM) involves the development of techniques to detect the weeds growing in a crop and the application of new technologies embedded in specific agricultural machinery or equipment to control them successfully, taking action to maximise economic factors and reduce the environmental impact of the control measurements applied (Christensen *et al*. 2009). The efficient development of these practices somehow relies on the use of remote sensing technology for collecting and processing spatial data from sensors mounted in satellite or aerial platforms. This technology has been widely applied in agricultural studies, allowing the mapping of a variety of factors (Lee *et al*. 2010), including crop conditions (Houborg *et al*. 2009), soil properties (López-Granados *et al*. 2005), water content (Meron *et al*. 2010) and weed distribution (de Castro *et al*. 2012), among others. Piloted aircraft and satellites are traditionally the primary platforms used to obtain remote images for local to global

data acquisition. However, these platforms present problems for many aspects of precision agriculture because they are limited in their ability to provide imagery of adequate spatial and temporal resolutions and are strongly affected by weather conditions (Herwitz *et al*. 2004). In the case of ESSWM, good results have been obtained in late growth stages (normally at the flowering stage) using aerial (López-Granados *et al*. 2006; Peña-Barragán *et al*. 2007) and satellite (de Castro *et al.* 2013) images, with herbicide savings of more than 50% reported. Nevertheless, in most weed-crop scenarios, the optimal weed treatment is recommended at an early growth stage of the crop, just a few weeks after crop emergence. In this stage, mapping weeds using remote sensing presents much greater difficulties than in the case of the late-stage season for three main reasons (López-Granados 2011): 1) weeds are generally distributed in small patches, which makes it necessary to work with remote images at very small pixel sizes, often on the order of centimetres (Robert 1996); 2) grass weeds and monocotyledonous crops (e.g., *Avena* spp. in wheat) or broad-leaved weeds and many dicotyledonous crops (e.g., *Chenopodium* spp. in sunflower) generally have similar reflectance properties early in the season, which decreases the possibility of discriminating between vegetation classes using only spectral information; and 3) soil background reflectance may interfere with detection (Thorp and Tian 2004).

Today, difficulties related to spatial and temporal resolutions can be overcome using an Unmanned Aerial Vehicle (UAV) based remote sensing system, which has progressed in recent years as a new aerial platform for image acquisition. UAVs can fly at low altitudes, allowing them to take ultra-high spatial resolution imagery and to observe small individual plants and patches, which has not previously been possible (Xiang and Tian 2011). Moreover, UAVs can supply images even on cloudy days, and the time needed to prepare and initiate the flight is reduced, which allows greater flexibility in scheduling the imagery acquisition. Other advantages of UAVs are their lower cost, and the lower probability of serious accidents compared with piloted aircraft.

Examples of applications of UAVs in agricultural studies are becoming more noticeable in the literature. For instance, Hunt *et al*. (2005) evaluated an aerobatic model aircraft for acquiring high-resolution digital photography to be used in estimating the nutrient status of corn and crop biomass of corn, alfalfa, and soybeans. In other cases, an unmanned helicopter was tested to monitor turf grass glyphosate application (Xiang and Tian 2011), demonstrating its ability to obtain multispectral imaging. Other UAV models have been developed, such as the six-rotor aerial platform used by Primicerio *et al.* (2012) to map vineyard vigour with a multi-spectral camera. Recently, Zhang and Kovacs (2012) reviewed the advances in UAV platforms for PA applications. In this review, they indicated the phases in the production of the remote images (including acquisition, georeferencing

and mosaicking) and the general workflow for information extraction. Generally, all these authors concluded that these systems provide very promising results for PA and identified some key factors for equipment and system selection, such as maximum UAV payload capacity, platform reliability and stability, sensor capability, flight length and UAV manoeuvrability, among others (Hardin and Hardin 2010; Hardin and Jensen 2011; Andrea S. Laliberte *et al*. 2010).

To our knowledge, however, no detailed investigation has been conducted regarding the application of this technology in the field of ESSWM, in which remote images at centimetre-scale spatial resolution and a narrow temporal window for image acquisition are required (Gray *et al*. 2008). Therefore, this paper defines the technical specifications and configuration of a quadrocopter UAV and evaluates the spatial and spectral requirements of the images captured by two different sensors (a commercial scale camera and a multispectral 6-channel camera) with the ultimate aim of discriminating weed infestations in a sunflower crop-field in the early growing season for post-emergence treatments. Moreover, the steps for preparing and performing UAV flights with both cameras are described as well as the relationships amongst flight altitude, pixel size, sensor properties and image spectral information.

4. MATERIALS AND METHODS

4.1. UAV description

A quadrocopter platform with vertical take-off and landing (VTOL), model md4-1000 (microdrones GmbH, Siegen, Germany), was used to collect a set of aerial images at several flight altitudes over an experimental crop-field (Figure 1). This UAV is equipped with four brushless motors powered by a battery and can fly by remote control or autonomously with the aid of its Global Position System (GPS) receiver and its waypoint navigation system. The VTOL system makes the UAV independent of a runway, so it can be used in a wide range of different situations and flight altitudes. The UAV's technical specifications and operational conditions, provided by the manufacturer, are shown in Table 1.

The whole system consists of the vehicle, the radio control transmitter, a ground station with the software for mission planning and flight control, and a telemetry system. The radio control transmitter is a handheld device whose main tasks are to start the vehicle's engines, manage take-off and landing, control the complete flight in the manual mode, and activate the autonomous navigation system. The control switchboard consists of several triggers, pushbuttons, scroll bars, a display, and an antenna, and it is equipped with a RF-module synthesiser, which enables the

selection of any channel in the 35 MHz band. The ground station works as an interface between the operator and the vehicle and includes the support software mdCockpit (MDC). MDC allow the UAV settings to be configured, implements the flight route plan with the Waypoint Editor (WPE) module, and monitors the flight. The telemetry system collects relevant flight data and retrieves a stream of information in a plain text scheme that includes GPS position data, attitude, altitude, flight time, battery level, and motor power output, among many others. All sensors and control devices for flight and navigation purposes are embedded on-board the vehicle and are managed by a computer system, which can listen telemetry data and make decisions according to the momentary flight situation and machine status, thus avoiding that occasional loss of critical communication between the UAV and the ground station resulting in the vehicle crashing.

Figure 1. *The quadrocopter UAV, model md4-1000, flying over the experimental crop-field.*

Table 1. *Technical specifications and operational conditions of the UAV, model md4-1000.*

UAV specification	Value
Technical specifications	
Climb rate	7.5 m/s
Cruising speed	15.0 m/s
Peak thrust	118 N
Vehicle mass	2.65 Kg approx. (depends on configuration)
Recommended payload mass	0.80 Kg
Maximum payload mass	1.25 Kg
Maximum take-off weight	5.55 Kg
Dimensions	1.03 m between opposite rotor shafts
Flight time	Up to 45 min (depends on payload and wind)
Operational conditions	
Temperature	- 10º C to 50º C
Humidity	Maximum 90%
Wind tolerance	Steady pictures up to 6 m/s
Flight radius	Minimum 500 m using radiocontrol, with waypoints up to 40 km
Ceiling altitude	Up to 1,000 m
Take-off altitude	Up to 4,000 m about sea level

Source: UAV manufacturer (microdrones GmbH, Siegen, Germany).

Three persons were employed for the secure use of the UAV: a radio control pilot, a ground station operator and a visual observer. The radio control pilot manually takes off and lands the UAV and activates the programmed route during the flight operation. The ground station operator controls the information provided by the telemetry system, i.e., UAV position, flight altitude, flight speed, battery level, radio control signal quality and wind speed. The visual observer is on the lookout for potential collision threats with other air traffic.

4.2. Sensors description

The md4-1000 UAV can carry any sensor weighing less than 1.25 kg mounted under its belly, although the maximum recommended payload is 0.80 kg. Two sensors with different spectral and spatial resolutions were separately mounted on the UAV to be tested in this experiment: a still point-and-shoot camera, model Olympus PEN E-PM1 (Olympus Corporation, Tokyo, Japan), and a six-band multispectral camera, model Tetracam mini-MCA-6 (Tetracam Inc., Chatsworth, CA, USA). The Olympus camera acquires 12-megapixel images in true colour (Red, R; Green, G; and Blue, B, bands) with 8-bit radiometric resolution and is equipped with a 14-42 mm zoom lens. The camera's sensor is 4,032 × 3,024 pixels, and the images are stored in a secure digital SD-card. The mini-MCA-6 is a lightweight (700 g) multispectral sensor composed of six individual digital channels arranged in a 2×3 array. The slave channels are labelled from "1" to "5", while the sixth "master" channel is used to define the global settings used by the camera (e.g., integration time). Each channel has a focal length

of 9.6 mm and a 1.3 megapixel (1,280 × 1,024 pixels) CMOS sensor that stores the images on a compact flash CF-card. The images can be acquired with 8-bit or 10-bit radiometric resolution. The camera has user configurable band pass filters (Andover Corporation, Salem, NH, USA) of 10-nm full-width at half-maximum and centre wavelengths at B (450 nm), G (530 nm), R (670 and 700 nm), R edge (740 nm) and near-infrared (NIR, 780 nm). These bandwidth filters were selected across the visible and NIR regions with regard to well-known biophysical indices developed for vegetation monitoring (Kelcey and Lucieer 2012). Image triggering is activated by the UAV according to the programmed flight route. At the moment of each shoot, the on-board computer system records a timestamp, the GPS location, the flight altitude, and vehicle principal axes (pitch, roll and heading).

4.3. Study site and field sampling

The UAV system was tested in a sunflower field situated at the private farm La Monclova, in La Luisiana (Seville, southern Spain, coordinates 37.527N, 5.302W, datum WGS84). The flights were authorized by a written agreement between the farm owners and our research group. We selected sunflower because this is the major oil-seed crop grown in Spain, with a total surface of 850,000 ha in 2012 (MAGRAMA 2012) [25], and because weed control operations (either chemical or physical) with large agricultural machinery represent a significant proportion of production costs, create various agronomic problems (soil compaction and erosion) and represent a risk for environmental pollution. The sunflower seeds were planted at the end of March 2012 at 6 kg ha^{-1} in rows 0.7 m apart. The set of aerial images were collected on May 15th, just when post-emergence herbicide or other control techniques are recommended in this crop. Several visits were periodically made to the field from crop sowing to monitor crop growth and weed emergence and, finally, to select the best moment to take the set of remote images. The sunflower was at the stage of 4-6 leaves unfolded. The weed plants had a similar size or, in some cases, were smaller than the crop plants (Figure 1).

An experimental plot of 100×100 m was delimited within the crop-field to perform the flights. The coordinates of each corner of the flight area were collected using GPS to prepare the flight route in the mission-planning task. A systematic on-ground sampling procedure was carried out the day of the UAV flights. The procedure consisted of placing 49 square white frames of 1×1 m distributed regularly throughout the studied surface (Figure 2A). Every frame was georeferenced with a GPS and photographed in order to compare on-ground weed infestation (observed weed density) and outputs from image classification (estimated weed density). These numbered cards were also utilised as artificial terrestrial targets (ATTs) to perform the imagery orthorectification and mosaicking process. In the course of the UAV flights, a barium sulphate standard spectralon® panel (Labsphere Inc., North

Sutton, NH, USA) of 1×1 m was also placed in the middle of the field to calibrate the spectral data (Figure 2B).

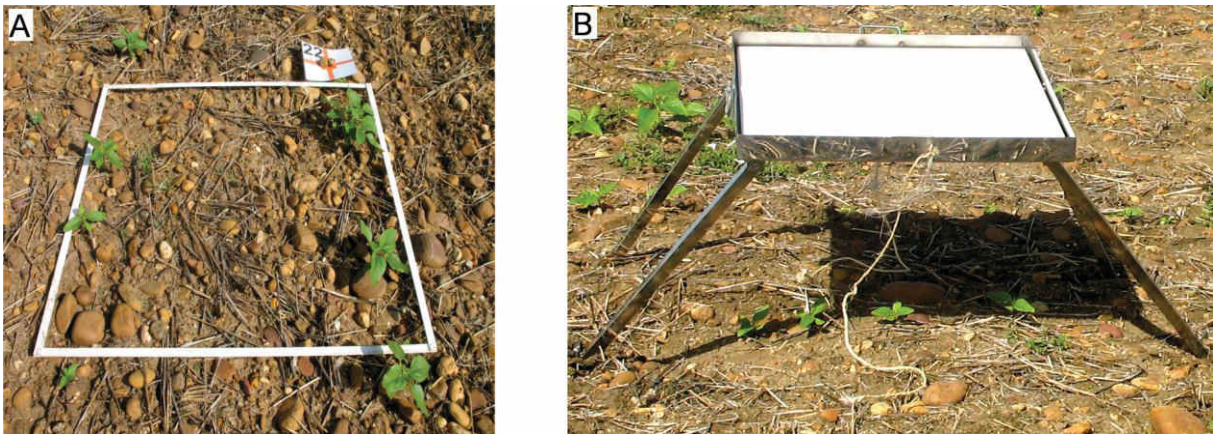

Figure 2. *Details of the experimental set. a) 1x1 m frame used in the ground-truth field sampling, and b) reference panel for image spectral calibration.*

4.4. UAV flight and sensors tests

4.4.1. Mission planning

The flight mission was planned with the WPE module of the MDC software installed at the ground station. The flight route was designed over the orthoimages and the digital elevation model (DEM) of the flight area previously imported from the application Google Earth™ (Keyhole Inc., Mountain View, CA, USA). Three different parameters were needed to plan the route: flight area, camera specifications and UAV tasks (Table 2). The flight area information includes width and length, the direction angle of the main side, and the desired overlap in the imagery. The images were acquired at 60% forward-lap and 30% side-lap. The camera specifications are the focal length and the sensor size. The UAV tasks refer to the actions that the UAV has to perform once it arrives at each point for image acquisition, and it includes the number of photos and dwell time in each point. Once both, this information and the flight altitude were introduced in the WPE module, it automatically generated the flight route and estimated the flight duration according to the total number of images planned (Figure 3). The route file was exported to a memory card embedded in the UAV via a standard serial link.

Table 2. *Data required by the Waypoint Editor software and the route settings used in the experimental field.*

Data type	Setting value*
Flight area	
Width	100 m
Length	100 m
Direction angle	65°
Horizontal overlapping	60 %
Vertical overlapping	30 %
Camera specifications	
Focal length	
RGB camera	14 mm
Multispectral camera	9.6 mm
Sensor size (width x length)	
RGB camera	17.3 x 13 mm
Multispectral camera	6.66 x 5.32 mm
UAV tasks	
Dwell	5 s
Number of images	1
*** Values used in the experimental field.**	

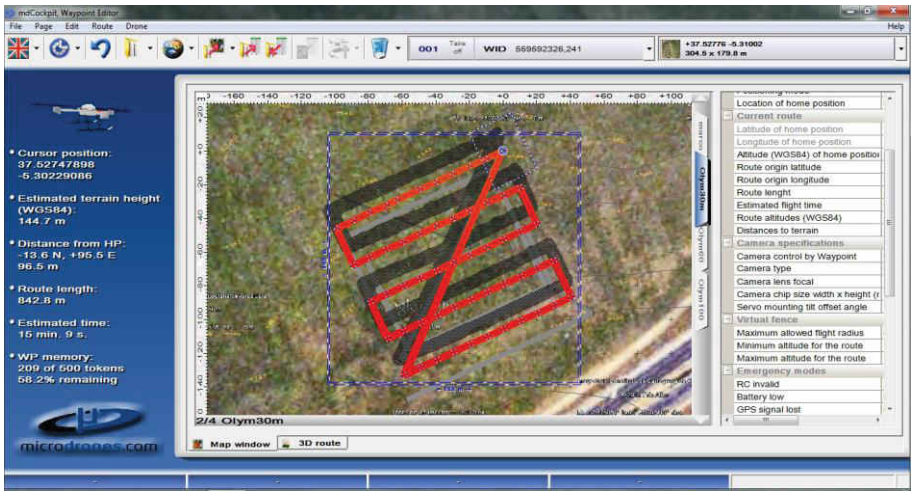

Figure 3. *Screen shot of the Waypoint Editor module showing the flight planning.*

4.4.2. UAV flight and image acquisition

The preliminary steps before starting the flight were to upload the flight route to the UAV computer system, attach the camera to the vehicle and check the connectivity and the proper functioning of the whole system. After these steps, the pilot manually launches the UAV with the radio control transmitter and next activates the automatic flight route, making the vehicle go to the first waypoint and then fly along the flight lines until the entire study area is completely covered. Once all the images are taken, the pilot manually lands the UAV, and the ground station operator

prepares the vehicle for the next route. During the flight, the ground station operator watches the UAV telemetry data using the downlink decoder, another component of the MDC software (Figure 4). This program gives information about: 1) operating time of the UAV, 2) current flight time, 3) distance from take-off point to the UAV, 4) quality of the remote control signal received by the UAV, 5) downlink quality, 6) battery status, and 7) GPS accuracy.

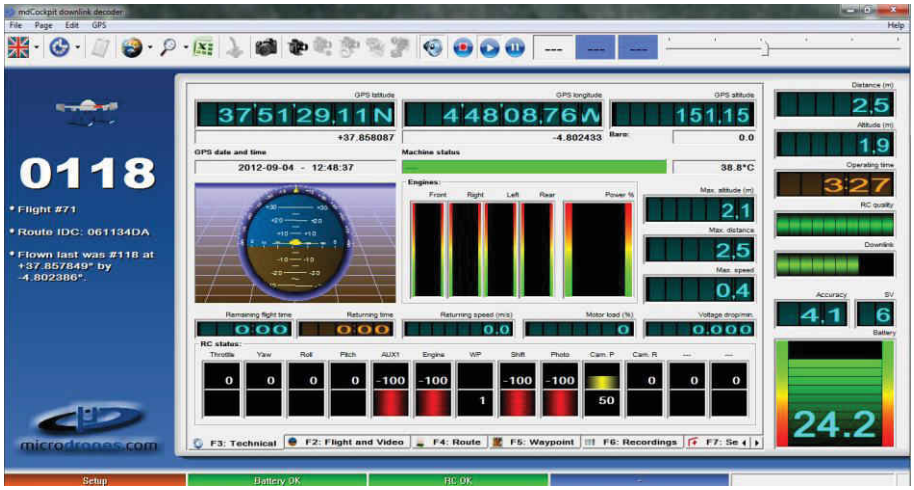

Figure 4. *Screen shot of the Downlink Decoder module showing the information displayed during a programmed flight.*

In addition to this information, the downlink decoder supports several important dialog pages, as follows:

- Flight and video. This page shows the video stream captured by the sensor attached to the UAV, making it easier to control the UAV when it is manually driven. Additional data displayed in this page are: 1) distance to the UAV, 2) flight altitude above the take-off position, 3) speed of the UAV, 4) artificial horizon, 5) compass, and 6) roll and tilt angles.
- Technical. This page supplies information about: 1) UAV position (GPS latitude and longitude), 2) UAV altitude (GPS altitude above sea level), 3) current navigation mode, 4) magnetometer status, 5) barometer status, 6) motor power, 7) momentary status of all the radio control channels, and 8) limit values of flight altitude, distance and speed.
- Route. This page shows a tridimensional display of the flight path.
- Waypoint. This section shows information about: 1) the flying route followed by the UAV, 2) the UAV GPS position, and 3) the waypoint command that is being executed at each moment.
- Sensor-payload. This page displays a diagram with sensor data received from the payload.

- Recordings. Three diagrams are displayed in this section: 1) comprising motor power and battery voltage over time, 2) comprising flight attitude (roll, pitch and yaw angles) with GPS data, and 3) comprising velocity, distance, wind profile, flight altitude and radio-control link quality.

4.4.3. Multispectral band alignment

The images taken by the still camera (Olympus model) can be used directly after downloading to the computer, but those taken by the multispectral camera (mini-MCA-6 Tetracam model) require some pre-processing. This camera takes the images of each channel in raw format and stores them separately on six individual CF cards embedded in the camera. Therefore, an alignment process is needed to group the six images taken in each waypoint. The Tetracam PixelWrench 2 (PW2) software (Tetracam Inc., Chatsworth, CA, USA), supplied with the multispectral camera, was used to perform the alignment process. The PW2 software provides a band-to-band registration file that contains information about the translation, rotation and scaling between the master and slave channels. Two different options were tested: 1) basic configuration of the PW2 software, as applied by Laliberte *et al.* (Laliberte *et al*. 2011), and 2) advanced configuration of PW2, which includes the newest field of view (FOV) optical calculator, which calculates additional offsets to compensate the alignment for closer distances. The quality of the alignment process was evaluated with the help of the spectralon® panel data captured in the images at a 30 m altitude. Spatial profiles were taken across the reference panel for each method and compared with the non-aligned image. The spatial profiles consisted of graphics representing the spectral values for each band along a line 45 pixels long drawn in the multi-band images using the ENVI image processing software (Research System Inc., Boulder, CO, USA).

4.4.4. Spatial resolution and flight length as affected by flight altitude

Three independent flight routes were programmed for each type of camera to cover the whole experimental field at 30, 60 and 100 m altitude above ground level. The effects of flight altitude and camera resolution with respect to pixel size, area coverage (number of images per hectare) and flight duration were studied, and their implications for weed discrimination in the early season were discussed.

4.4.5. Spectral resolution as affected by flight altitude

To perform weed mapping based on UAV images, two consecutive phases are usually required (López-Granados 2011): 1) bare soil and vegetation discrimination, which would allow obtaining a

two-classes image with vegetal cover (crop and weeds together) and bare soil, 2) crop and weeds discrimination, in which the zones corresponding to crop are identified and masked, and finally, the detection and location of weeds are obtained. To determine the limitations of each sensor with regard to both phases, spectral values of the three covers present in the field (bare soil, crop and weeds) were extracted. These spectral values were collected in 15 randomly selected sampling areas for each soil use from the images taken during all the flight missions (i.e., both sensors at 30, 60 and 100 m altitudes).

Three well-known vegetation indices (VIs) were derived from these values:

- Normalised Difference Vegetation Index (NDVI, (Rouse *et al*. 1974))

  $NDVI = (NIR-R)/(NIR+R)$ (1)

- Normalised Green-Red Difference Index (NGRDI, (Gitelson *et al*. 2002)),

  $NGRDI = (G-R)/(G+R)$ (2)

- Excess Green Index (ExG, (Ribeiro et al. 2005; Woebbecke *et al*. 1995)).

  $ExG = 2g - r - b$ (3)

The potential of the VIs for spectral discrimination was evaluated by performing a least significant difference (LSD) test at $p \leq 0.01$ through a one-way analysis of variance (ANOVA), and applying the M-statistic (equation 4) presented by Kaufman and Remer (1994) in order to quantify the histogram´s separation of vegetation indices. JMP software (SAS, Cary, NC, USA) was employed to perform the statistical analysis.

$$M = (MEAN_{class1} - MEAN_{class2}) / (\sigma_{class1} - \sigma_{class2}) \quad (4)$$

M expresses the difference in the means of the class 1 and class 2 histograms normalized by the sum of their standard deviations (σ). Following the research strategy and steps mentioned before, class 1 and class 2 were either, vegetation and bare soil, where vegetation was weeds and crop studied together, or weeds and crop. *M* values are indicative of the separability or discriminatory power of classes 1 and 2 considered in every step. Two classes exhibit moderate separability when *M* exceeds 1, showing easier separation for larger *M* values which will provide a reasonable discrimination (Smith *et al*. 2007). According to Kaufman and Remer (1994), the same difference in means can give different measures of separability depending on the spread of the histograms. Wider histograms (larger σ) will cause more overlap and less separability than narrow histograms (smaller σ) for the same difference in means.

5. RESULTS AND DISCUSSION

5.1. Image pre-processing

5.1.1. Band alignment of multispectral imagery

The images acquired by both cameras were downloaded to a computer by inserting their memory cards into a card reader and copying the data. An alignment process was performed on the multispectral images to match the six bands into a single readable file. The alignment results were examined visually and evaluated using spatial profiles (Figure 5).

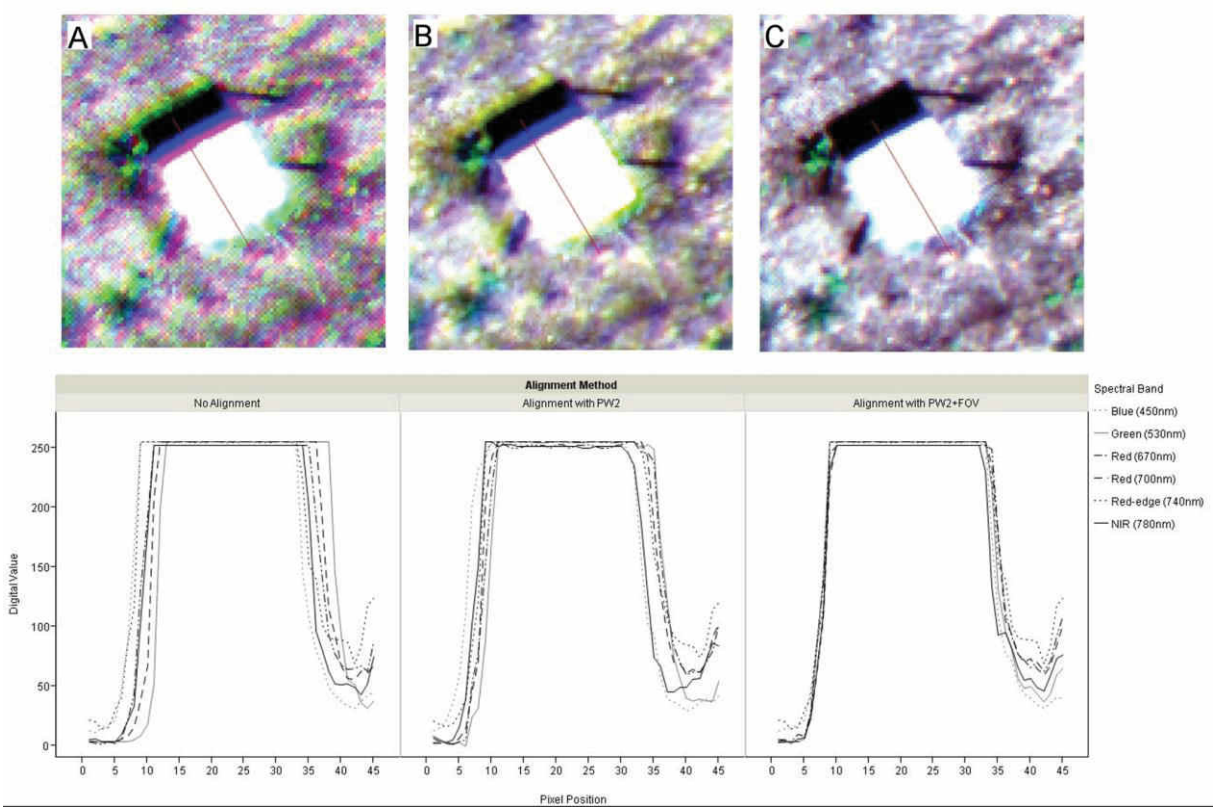

Figure 5. *Images captured by the multispectral camera and spatial profiles depicting comparison of band-to-band alignment. a) No alignment, b) Alignment by using the basic configuration of the PW2 software, and c) Alignment by using the PW2 software plus the field of view (FOV) optical calculator.*

The displacement among the curves for each channel in the spatial profiles makes evident the band misalignment of the original non-aligned images. The non-aligned images showed halos around the reference objects (Spectralon and vegetation) and noise in the soil background (Figure 5A). These halos and noise were still recognisable in the image aligned using the basic configuration of the PW2 software (Figure 5B), although they were lesser than in the non-aligned image. These results are similar to those obtained by Laliberte *et al.* (2011), who reported poor alignment results using PW2 software with the mini-MCA imagery. To solve this problem, they developed the local weighted

mean transform (LMWT) method and obtained a satisfactory alignment. However, the latest version of the PW2 software, launched in 2012, which includes the FOV optical calculator, performed a good alignment and allowed elimination of the halos and a high reduction of the background noise (Figure 5C). In fact, these results seem to be quite similar to those achieved using the LMWT method. A good alignment of all the individual bands is crucial for subsequent image analysis, especially when spectral values of different objects of the image are extracted. The vegetation objects present in a weed-crop scenario in the early season are very small, as a consequence a poor alignment might include pixels not belonging to the objects of interest, drastically reducing the success of the image analysis and classification.

Next to the alignment process, the PW2 software generated a unique multi-band image file that is incompatible with the mosaicking software. Therefore, the last step was to convert this multi-band file to a TIFF-readable format using the ENVI software.

5.1.2. Image orthorectification and mosaicking

A sequence of images was collected in each flight mission to cover the whole experimental crop-field. An important task prior to image analysis was the combination of all these individual and overlapped images by applying two consecutive processes of orthorectification and mosaicking. The Agisoft Photoscan Professional Edition (Agisoft LLC, St. Petersburg, Russia) software was employed in this task. In the first step, the software asks for the geographical position and principal axes (roll, pitch and yaw) of the vehicle in each acquired image. Next, the software automatically aligns the photos. Finally, some ATT's coordinates are added to assign geographical coordinates to the image. Then, the software automatically performs the orthorectification and mosaicking of the imagery set into a single image of the whole experimental field (Figure 6). The resultant ortho-mosaic shows a high-quality landscape metric and accurate crop row matching between consecutive images, which guarantees good performance of the subsequent image classification.

Figure 6. *Ortho-mosaic of the whole experimental field. Composed from six individual images taken by the still RGB camera at 100 meters altitude.*

5.2. Effect of flight altitude on image spatial resolution and flight time

The image spatial resolution and the area covered by each image as affected by the UAV flight altitude and the type of camera are shown in Figure 7. The imagery pixel size was directly proportional to the flight altitude. The still RGB camera captured images with pixel sizes of 1.14 cm and 3.81 cm, while the multispectral camera captured images with pixel sizes of 1.63 cm and 5.42 cm at flight altitudes of 30 and 100 m, respectively (Figure 8). At these altitudes, the area covered by each image of the still RGB camera increased from 0.16 ha (46 × 35 m) to 1.76 ha (153 × 115 m) and of the multispectral camera from 0.04 (21 × 17 m) to 0.38 ha (69 × 55 m), respectively. The differences between both types of images were due to the cameras' technical specifications (Table 2). The camera focal length affects both the pixel size and the area covered by each image, while the camera sensor size only influences the imagery pixel size.

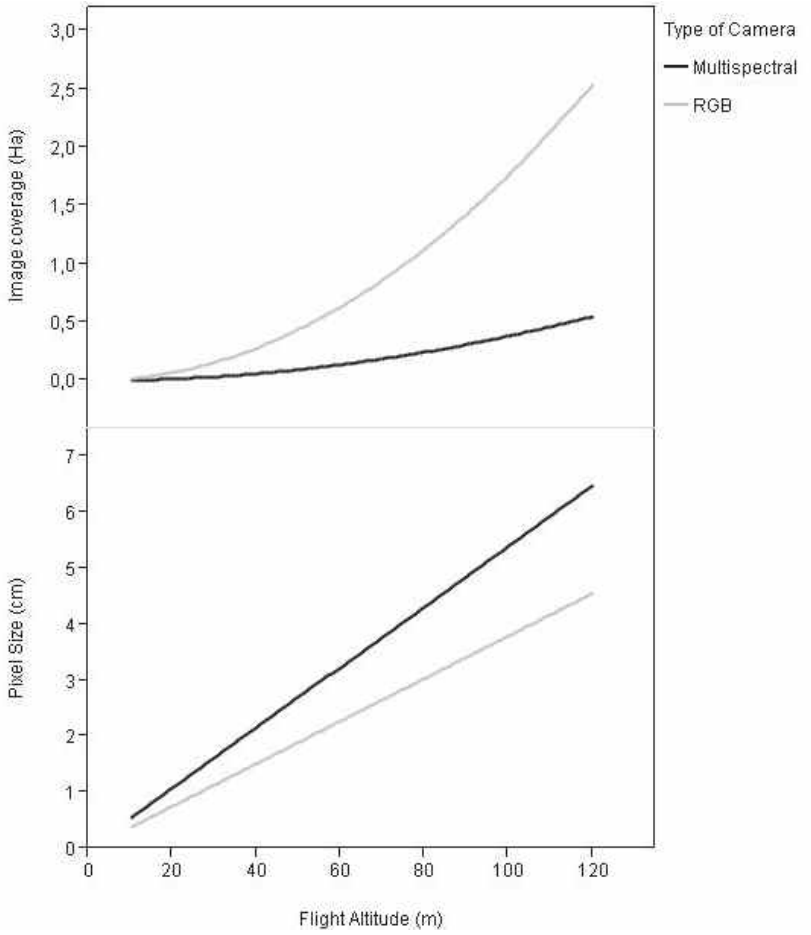

Figure 7. *Image spatial resolution and coverage as affected by flight altitude and type of camera.*

A crucial feature of the remote images for weed mapping in the early season is their high spatial resolution, which can be achieved with low-altitude flights. Of great importance is defining the optimum pixel size needed according to each specific objective, which is calculated from the size of the weed seedlings to be discriminated, the distance between crop rows and the crop type. In general, at least four pixels are required to detect the smallest objects within an image (Hengl 2006). Accordingly, if the objective is the discrimination of individual weed plants, the pixel size should be approximately 1-4 cm, which corresponds to flight altitudes of 27 to 105 m in the case of the still RGB camera and from 19 to 74 m in the case of the multispectral camera. However, when weed patch detection is aimed, the remote images could have a pixel size of 5 cm or even greater, which corresponds to a flight altitude higher than 100 m in both cameras.

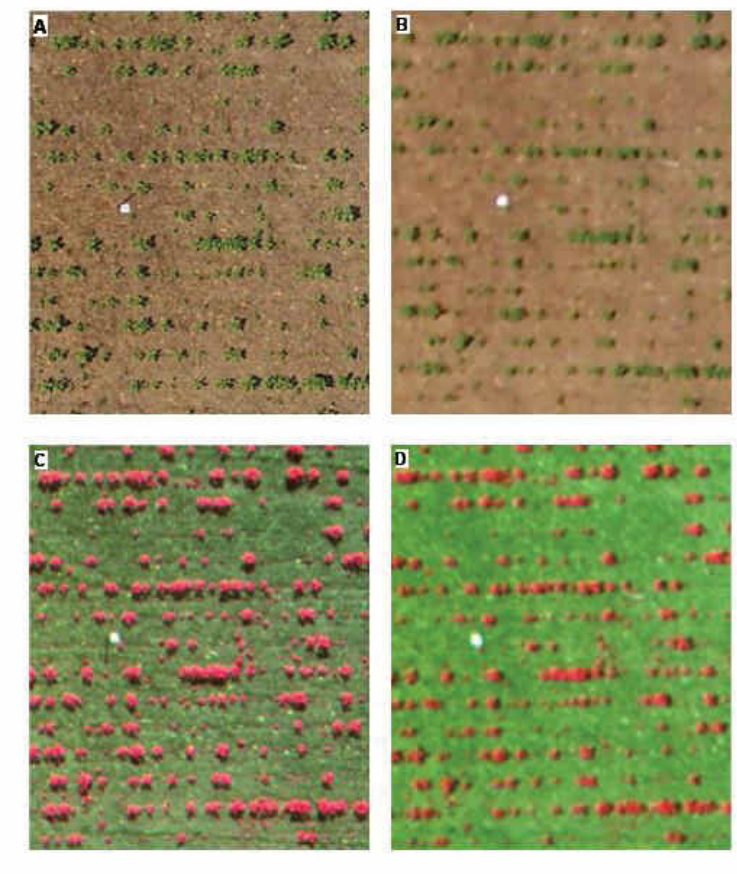

Figure 8. *UAV images collected by the two cameras. Still RGB camera (a, b) and multispectral camera (c, d) at 30 m (a, c) and 100 m (b, d) flight altitude.*

The UAV acquired imagery with 60% forward lap and 30% side lap. From this overlapping and the camera sensor size, the WPE module calculated the number of images needed to capture the whole experimental field and, consequently, the time taken by the UAV to collect them at each flight altitude (Figure 9). The number of images per ha and the flight length were greater when using the multispectral camera, decreasing from 117 images ha^{-1} and 27 min at a 30 m altitude to 12 images ha^{-1} and 6 min at a 100 m altitude. For the still RGB camera, these variables ranged from 42 images ha^{-1} and 12 min at 30 m altitude to 6 images ha^{-1} 5 min at 100 m. A very large number of images can limit the mosaicking process because the number of images per hectare strongly increased at very low altitudes following an asymptotic curve. In addition, the operation timing is limited by the UAV battery duration. All these variables have strong implications in the configuration of the optimum flight mission for weed mapping in the early season, which involves two main conditions: 1) to provide remote images with a fine spatial resolution to guarantee weed discrimination, and 2) to minimise the operating time and the number of images to reduce the limitation of flight duration and image mosaicking, respectively.

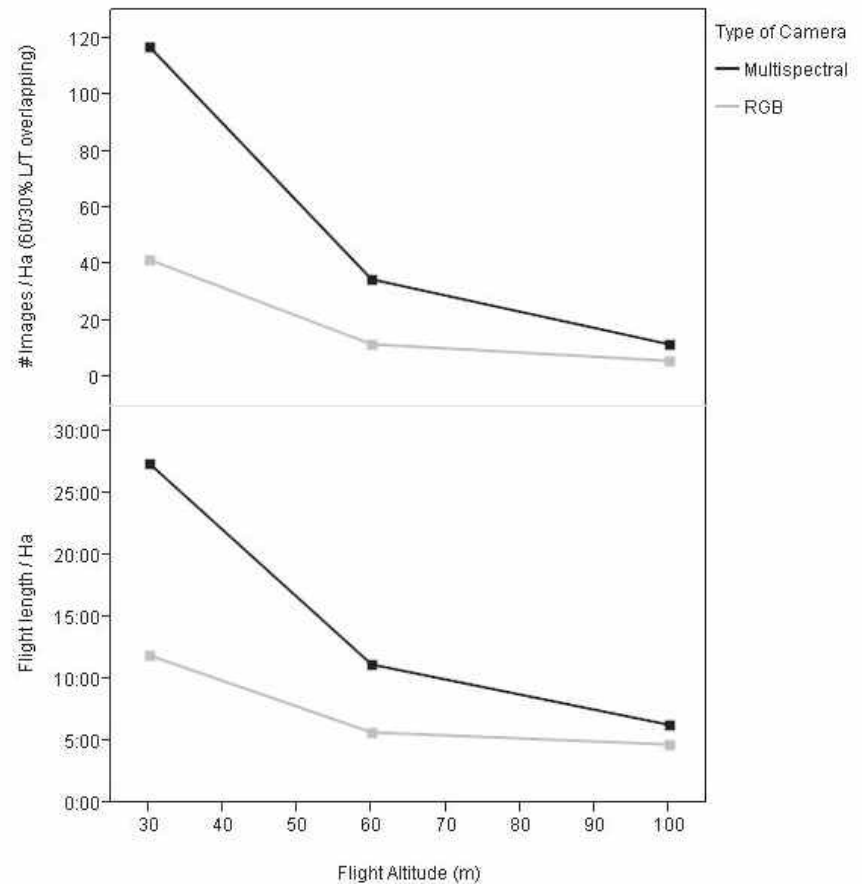

Figure 9. *Flight length and number of images per ha as affected by flight altitude and camera.*

5.3. Effect of flight altitude on image spectral resolution

Spectral information captured by each camera at three flight altitudes was studied to determine significant differences at the pixel level between class 1 and class 2 in the two phases previously mentioned, i.e. between vegetation cover and bare soil, and between weeds and crop. The range and average spectral pixel values of the VIs, and M-statistics are shown in Table 3.

First of all, it was crucial to explore the spectral differences between vegetation and bare soil to identify the potential to perform the first step of our research scheme, such an approach should point out the significant variations in spectral data of both classes, indicating which set of VIs, cameras and altitudes were able for their discrimination. All the indices showed significant differences between vegetation and soil and, in most cases, M-statistics performed reasonably well exceeding 2, being NDVI the index that achieved the highest spectral separability at the three flight altitudes. This is due to NDVI emphasises the spectral response of the NIR band which characterises vegetation vigour and it is less sensitive to soil background effects than the other two indices. The magnitude of M-statistic, usually higher than 2.5 (excepting for ExG at 30 m and 60 altitudes and

multispectral camera), offer satisfactory results for a high robustness of vegetation discrimination in all the scenarios. Kaufman and Remer (1994) reported *M* values ranging from 1.5 to 0.5 for mapping dense vegetation in forests, whereas Smith *et al*. (2007) obtained *M* values between 0.24 and 2.18 for mapping burned areas. According to our findings, the *M* achieved a much higher value (*M* = 8.9 for multispectral camera and NDVI index) suggesting robust separability of classes. NDVI could be the best index to perform the first phase of the proposed classification strategy, although NGRDI and ExG also showed an overall good capacity for distinguishing vegetal cover, which would be very relevant due to RGB camera is much cheaper and easier to use than the multispectral camera.

In order to perform the second proposed phase, it is necessary to test if weeds and crop can be discriminated using either RGB camera or the multispectral sensor. As a general statement, the multispectral camera showed much higher capacity to discriminate crop and weeds than the RGB camera. The better performance of the multispectral camera may be caused by its narrow sensor bandwidth. This camera uses filters with a 10 nm bandwidth, which reduces the interferences caused by other wavelengths, while the RGB camera acquires information in three wider spectral wavebands from the entire visible spectrum. Thus, means of NGRDI and ExG were not significantly different for crop and weeds at any flight altitude and M-statistic values were the lowest ones, excepting for ExG at 30 m altitude where *M* = 1.61. However, even at this altitude, M-statistic value is quite lower than the obtained for ExG and the multispectral camera (*M* = 3.02). A preliminary conclusion could be that the RGB camera is able to discriminate weeds and crop using images from ExG at 30 m altitude. However, one of the key question to elucidate at this point is to determine if *M* = 1.61 provides enough robustness for mapping weeds and crop. That doubt could be clarified going to Figure 10 which shows the significant spectral differences among soil, weeds and crop in all the scenarios. Note that spectral differences among soil, and weeds and crop at 30 m altitude for ExG and RGB camera are clearly significant; however, the range of the standard deviation (see points in Fig. 10) of weeds and crop causes an overlapping which could produce a deficient discrimination between weeds and crop. Therefore, Table 3 offers an overall overview of separation between vegetation and soil, and weeds and crop; however these results must be deeply studied observing the ranges of minimum and maximum spectral values of every VI (Table 3) and ranges of standard deviation (Figure 10).

Table 3. *Least Significant Differences (LSD) test at P≤0.01 and Spectral Separability according to the M-statistic between crop and weed plants and vegetation and bare soil as affected by vegetation index, type of camera and flight altitude*

			Vegetation *vs.* Bare soil discrimination										Crop *vs.* Weed discrimination									
			Vegetation				Bare soil				LSD test (Prob > F)	M [(b)]	Crop				Weed				LSD test (Prob > F)	M [(b)]
Flight altitude	Type of camera	VIs [(a)]	Max	Min	Mean	±SD	Max	Min	mean	±SD			Max	Min	mean	±SD	Max	Min	Mean	±SD		
30-m	RGB	NGRDI	0.11	-0.02	0.04	± 0.03	-0.08	-0.11	-0.09	± 0.01	<0.01	3.61	0.09	0.00	0.05	± 0.02	0.11	-0.02	0.03	± 0.03	0.10	0.32
		ExG	0.34	0.10	0.21	± 0.06	0.02	-0.01	0.00	± 0.01	<0.01	2.93	0.34	0.20	0.27	± 0.04	0.20	0.10	0.16	± 0.01	<0.01	1.61
	Multispectral	NDVI	0.73	0.45	0.58	± 0.07	-0.15	-0.19	-0.16	± 0.01	<0.01	8.90	0.73	0.52	0.61	± 0.06	0.68	0.45	0.55	± 0.07	0.03	0.42
		NGRDI	0.35	-0.04	0.14	± 0.12	-0.20	-0.27	-0.23	± 0.02	<0.01	2.75	0.35	0.15	0.24	± 0.06	0.17	-0.04	0.05	± 0.06	<0.01	1.59
		ExG	0.18	-0.01	0.08	± 0.07	-0.05	-0.09	-0.06	± 0.01	<0.01	1.94	0.18	0.11	0.15	± 0.02	0.06	-0.01	0.02	± 0.02	<0.01	3.02
60-m	RGB	NGRDI	0.06	-0.03	0.01	± 0.02	-0.08	-0.10	-0.09	± 0.01	<0.01	3.53	0.06	-0.03	0.01	± 0.02	0.06	-0.02	0.01	± 0.02	0.85	0.03
		ExG	0.26	0.11	0.18	± 0.04	0.03	-0.01	0.01	± 0.01	<0.01	3.50	0.26	0.14	0.20	± 0.04	0.20	0.11	0.15	± 0.03	<0.01	0.79
	Multispectral	NDVI	0.51	0.15	0.35	± 0.09	-0.08	-0.11	-0.10	± 0.01	<0.01	4.52	0.51	0.23	0.38	± 0.09	0.46	0.15	0.33	± 0.08	0.10	0.31
		NGRDI	0.23	-0.04	0.08	± 0.07	-0.11	-0.13	-0.12	± 0.01	<0.01	2.77	0.23	0.03	0.12	± 0.06	0.11	-0.04	0.04	± 0.04	<0.01	0.81
		ExG	0.28	0.10	0.18	± 0.05	0.07	0.05	0.06	± 0.01	<0.01	1.91	0.28	0.13	0.22	± 0.04	0.19	0.10	0.14	± 0.02	<0.01	1.19
100-m	RGB	NGRDI	0.04	-0.09	-0.02	± 0.04	-0.09	-0.12	-0.10	± 0.01	<0.01	1.67	0.04	-0.07	-0.01	± 0.04	0.04	-0.09	-0.03	± 0.03	0.13	0.28
		ExG	0.23	0.05	0.14	± 0.05	0.02	-0.01	0.01	± 0.01	<0.01	2.20	0.23	0.12	0.16	± 0.05	0.22	0.05	0.12	± 0.05	0.02	0.46
	Multispectral	NDVI	0.64	0.23	0.43	± 0.10	-0.13	-0.16	-0.14	± 0.01	<0.01	5.25	0.64	0.34	0.47	± 0.09	0.56	0.23	0.39	± 0.09	0.04	0.40
		NGRDI	0.20	-0.12	0.01	± 0.09	-0.21	-0.24	-0.21	± 0.01	<0.01	2.40	0.20	-0.05	0.08	± 0.07	0.02	-0.12	-0.05	± 0.04	<0.01	1.16
		ExG	0.23	0.07	0.14	± 0.05	0.03	0.00	0.02	± 0.01	<0.01	2.28	0.23	0.12	0.18	± 0.03	0.12	0.07	0.10	± 0.02	<0.01	1.90

[(a)] Vegetation indices: NGRDI = (G-R)/(G+R); ExG = 2g – r – b; NDVI = (NIR-R)/(NIR+R)

[(b)] M-statistic = $(MEAN_{class1} - MEAN_{class2}) / (\sigma_{class1} + \sigma_{class2})$

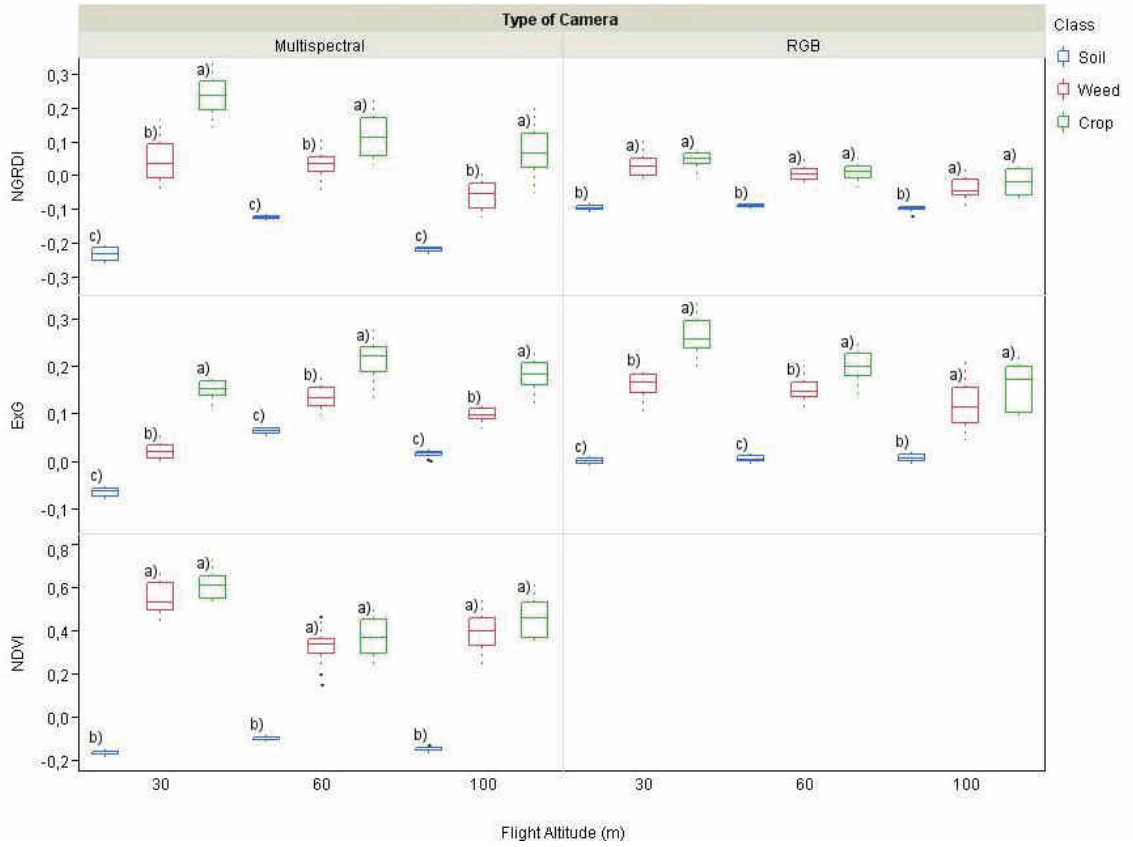

Figure 10. *Vegetation index values of each class of soil cover (bare soil, weed and crop). The index values are affected by flight altitude and type of camera. Within a group, box-plots followed by the same letter do not differ significantly according to LSD test at P ≤ 0.01.*

In the multispectral camera, NGRDI and ExG were significantly different for weeds and crop in all the flight altitudes tested. However, despite these significant differences observed and as stated before, the M-statistic and Figure 10 must be taken into account since both help to quantify the risk of misclassification due to the overlapping between value ranges of the vegetation indices studied. For instance, at 60 m altitude, NGRDI showed a significant spectral difference for weeds and crop; however M-statistic was lower than 1 (*M* = 0.81). This indicates that, apart from a significant spectral difference, a poor separation is expected between pixels from weeds and crop. This can be clearly appreciated in Figure 10 where the range of the standard deviation between weeds and crop involves an overlapping of values and this is the reason for which having a significant spectral discrimination this is not sufficient to achieve a satisfactory separability (*M* higher than 1).

The case of ExG is different since this vegetation index showed significant spectral differences and *M* values higher than 1 at any flight altitude, although *M* was only slightly superior than 1 (*M* = 1.19) at 60 m altitude. This points out that a good separation would be expected at 30 m and probably at 100 m; however, have the significant spectral differences and *M* = 1.19 obtained in Table

3 sufficient discriminatory power to properly separate crop and weeds at 60 m altitude. Figure 10 again shows that this magnitude of *M* probably is not as much as required to successfully reach this objective due to the apparent overlapping of box-plots of weeds and crop and, consequently, a much more difficult separation would be expected at 60 m altitude. The only index studied using the NIR band was NDVI and it was not able to discriminate between crop and weeds at any flight altitude; in fact, NDVI showed the lowest M-statistic values among the indices calculated from the multispectral camera.

As mentioned in the previous section and according to the objective of minimising the operating time and the number of images taken to reduce the limitation of UAV flight duration and image mosaicking, the optimum flight mission may be to capture images at the highest altitude possible. However, the highest spectral differences and *M* values of pixels were obtained at the lowest altitudes, i.e., pixel-based methods may be unsuccessful in weeds and crop discrimination in seedling stages at altitudes higher than 30 m due to the spectral similarity among these vegetation classes. Currently, spectral limitations may be solved by implementing advanced algorithms such as the object-based image analysis (OBIA) methodology (Laliberte and Rango 2009). The OBIA methodology identifies spatially and spectrally homogenous units named *objects* created by grouping adjacent pixels according to a procedure known as segmentation. Afterwards, multiple features of localisation, texture, proximity and hierarchical relationships are used that drastically increase the success of image classification (Blaschke 2010; Peña-Barragán *et al*. 2011). In crop fields at an early stage, the relative position of the plants in the crop rows, rather than their spectral information, may be the key feature to distinguishing them. Consequently, every plant that is not located in the crop row can be assumed to be a weed. Therefore, according our results a strategy for a robust classification of UAV images could be developed involving two steps: 1) discriminating vegetation (weeds and crop) from bare soil by using spectral information, and 2) discriminating weeds from crop-rows using the OBIA methodology. Therefore, future investigations will be essential to determine the potential of OBIA techniques to distinguish and map weeds and crop using UAV imagery at higher flight altitudes and taken when weeds and crop are at the early phenological stages. Our recent research using OBIA methodology has shown the improvement of using satellite imagery for mapping crops (Castillejo-González *et al*. 2009; Peña-Barragán *et al*. 2011) or weeds at late phenological stages in winter wheat (de Castro *et al*. 2013). Our hypothesis for further work is based on the idea that the OBIA methodology has confirmed to be a powerful and flexible algorithm adaptable in a number of agricultural situations. The main aim would be to discriminate and map early weeds to enhance the decision making process for developing in-season ESSWM at high

altitudes using RGB and ExG index compared to multispectral camera and the pixel-based image analysis. This would allow reducing the number of UAV imagery to improve the performance of the UAV (flight length and efficiency of energy supply) and the mosaicking process. This approach could be a more profitable method for mapping early weed infestations due to both, the covering of larger crop surface area and RGB cameras are cheaper and economically more affordable than multispectral cameras. Considering that the UAV development is a substantial investment, the possibility of using RGB cameras would reduce significantly the additional costs.

6. CONCLUSIONS

Weeds are distributed in patches within crops and this spatial structure allows mapping infested-uninfested areas and herbicide treatments can be developed according to weed presence. The main objectives of this research were to deploy an UAV equipped with either, RBG or multispectral cameras, and to analyze the technical specifications and configuration of the UAV to generate images at different altitudes with the high spectral resolution required for the detection and location of weed seedlings in a sunflower field for further applications of ESSWM. Due to its flexibility and low flight altitude, the UAV showed ability to take ultra-high spatial resolution imagery and to operate on demand according to the flight mission planned.

The image spatial resolution, the area covered by each image and the flight timing varied according to the camera specifications and the flight altitude. The proper spatial resolution was defined according to each specific objective. A pixel lower than 4 cm was recommended to discriminate individual weed plants, which corresponded to flight altitudes below 100 m. If the objective was weed patch detection, the UAV can fly to a higher altitude to obtain remote images with pixels of 5 cm or greater. However, the number of images needed to cover the whole field could limit the flight mission at a lower altitude due to the increased flight length, problems with the energy supply, and the computational capacity of the mosaicking software.

Spectral differences between weeds, crop and bare soil were significant for NGRDI and ExG indices, mainly at a 30 m altitude. At higher altitudes, many weed and crop pixels had similar spectral values, which may increase discrimination errors. Greater spectral separability was obtained between vegetation and bare soil with the index NDVI, suggesting the employment of multispectral images for a more robust discrimination. In this case, the strategy for improving the image mosaicking and classification could be to implement the OBIA methodology to include features of localisation and proximity between weed and crop plants. An agreement among spectral and spatial

resolutions is needed to optimise the flight mission according to the size of the smaller objects to be discriminated (weed plants or weed patches).

The information and results herein presented can help in the selection of an adequate sensor and to configure the flight mission for ESSWM in sunflower crops and other similar crop row scenarios (e.g., corn, sugar beet, tomato). Despite the initial complexity of management of the UAV and its components and software, and after a period of training the pilots and operators, the described workflow can be applied recursively.

7. ACKNOWLEDGEMENTS

The authors thank Dr. David Gómez-Candón for his very useful help during field work, and Mr. Íñigo de Arteaga y Martín and Mr. Iván de Arteaga del Alcázar for allowing developing our field work in La Monclova farm.

8. REFERENCES

Blaschke, T. (2010). Object based image analysis for remote sensing. *ISPRS Journal of Photogrammetry and Remote Sensing*, *65*(1), 2–16. doi:10.1016/j.isprsjprs.2009.06.004

Castillejo-González, I. L., López-Granados, F., García-Ferrer, A., Peña-Barragán, J. M., Jurado-Expósito, M., de la Orden, M. S., & González-Audicana, M. (2009). Object- and pixel-based analysis for mapping crops and their agro-environmental associated measures using QuickBird imagery. *Computers and Electronics in Agriculture*, *68*(2), 207–215. doi:10.1016/j.compag.2009.06.004

Castro, A. I. de, Jurado-Expósito, M., Peña-Barragán, J. M., & López-Granados, F. (2012). Airborne multi-spectral imagery for mapping cruciferous weeds in cereal and legume crops. *Precision Agriculture*, *13*(3), 302–321. doi:10.1007/s11119-011-9247-0

Castro, A. I. de, López-Granados, F., & Jurado-Expósito, M. (2013). Broad-scale cruciferous weed patch classification in winter wheat using QuickBird imagery for in-season site-specific control. *Precision Agriculture*, *14*(4), 392–413. doi:10.1007/s11119-013-9304-y

Christensen, S., Søgaard, H. T., Kudsk, P., Nørremark, M., Lund, I., Nadimi, E. S., & Jørgensen, R. (2009). Site-specific weed control technologies. *Weed Research*, *49*(3), 233–241. doi:10.1111/j.1365-3180.2009.00696.x

Gitelson, A. A., Kaufman, Y. J., Stark, R., & Rundquist, D. (2002). Novel algorithms for remote estimation of vegetation fraction. *Remote Sensing of Environment*, *80*(1), 76–87. doi:10.1016/S0034-4257(01)00289-9

Gray, C. J., Shaw, D. R., Gerard, P. D., & Bruce, L. M. (2008). Utility of Multispectral Imagery for Soybean and Weed Species Differentiation. *Weed Technology*, *22*(4), 713–718. doi:10.1614/WT-07-116.1

Hardin, P. J., & Hardin, T. J. (2010). Small-Scale Remotely Piloted Vehicles in Environmental Research. *Geography Compass*, *4*(9), 1297–1311. doi:10.1111/j.1749-8198.2010.00381.x

Hardin, P. J., & Jensen, R. R. (2011). Small-Scale Unmanned Aerial Vehicles in Environmental Remote Sensing: Challenges and Opportunities. *GIScience & Remote Sensing*, *48*(1), 99–111. doi:10.2747/1548-1603.48.1.99

Hengl, T. (2006). Finding the right pixel size. *Computers & Geosciences*, *32*(9), 1283–1298. doi:10.1016/j.cageo.2005.11.008

Herwitz, S. ., Johnson, L. ., Dunagan, S. ., Higgins, R. ., Sullivan, D. ., Zheng, J., et al. (2004). Imaging from an unmanned aerial vehicle: agricultural surveillance and decision support. *Computers and Electronics in Agriculture*, *44*(1), 49–61. doi:10.1016/j.compag.2004.02.006

Houborg, R., Anderson, M., & Daughtry, C. (2009). Utility of an image-based canopy reflectance modeling tool for remote estimation of LAI and leaf chlorophyll content at the field scale. *Remote Sensing of Environment*, *113*(1), 259–274. doi:10.1016/j.rse.2008.09.014

Hunt, E. R., Cavigelli, M., Daughtry, C. S. T., Mcmurtrey, J. E., & Walthall, C. L. (2005). Evaluation of Digital Photography from Model Aircraft for Remote Sensing of Crop Biomass and Nitrogen Status. *Precision Agriculture*, *6*(4), 359–378. doi:10.1007/s11119-005-2324-5

Kaufman, Y. J., & Remer, L. A. (1994). Detection of forests using mid-IR reflectance: an application for aerosol studies. *IEEE Transactions on Geoscience and Remote Sensing*, *32*(3), 672–683. doi:10.1109/36.297984

Kelcey, J., & Lucieer, A. (2012). Sensor Correction of a 6-Band Multispectral Imaging Sensor for UAV Remote Sensing. *Remote Sensing*, *4*(5), 1462–1493. doi:10.3390/rs4051462

Laliberte, A. S., Goforth, M. A., Steele, C. M., & Rango, A. (2011). Multispectral Remote Sensing from Unmanned Aircraft: Image Processing Workflows and Applications for Rangeland Environments. *Remote Sensing*, *3*(11), 2529–2551. doi:10.3390/rs3112529

Laliberte, A. S., Herrick, J. E., Rango, A., & Winters, Craig. (2010). Acquisition, orthorectification, and classification of unmanned aerial vehicle (UAV) imagery for rangeland monitoring. *Photogrammetric Engineering and Remote Sensing*, *76*, 661–672.

Laliberte, A. S., & Rango, A. (2009). Texture and Scale in Object-Based Analysis of Subdecimeter Resolution Unmanned Aerial Vehicle (UAV) Imagery. *IEEE Transactions on Geoscience and Remote Sensing*, *47*(3), 761–770. doi:10.1109/TGRS.2008.2009355

Lee, W. S., Alchanatis, V., Yang, C., Hirafuji, M., Moshou, D., & Li, C. (2010). Sensing technologies for precision specialty crop production. *Computers and Electronics in Agriculture*, *74*(1), 2–33. doi:10.1016/j.compag.2010.08.005

Lelong, C. C. D., Burger, P., Jubelin, G., Roux, B., Labbé, S., & Baret, F. (2008). Assessment of Unmanned Aerial Vehicles Imagery for Quantitative Monitoring of Wheat Crop in Small Plots. *Sensors*, *8*(5), 3557–3585. doi:10.3390/s8053557

López-Granados, F. (2011). Weed detection for site-specific weed management: mapping and real-time approaches. *Weed Research*, *51*(1), 1–11. doi:10.1111/j.1365-3180.2010.00829.x

López-Granados, F., Jurado-Expósito, M., Peña-Barragán, J. M., & García-Torres, L. (2005). Using geostatistical and remote sensing approaches for mapping soil properties. *European Journal of Agronomy*, *23*(3), 279–289. doi:10.1016/j.eja.2004.12.003

López-Granados, F., Jurado-Expósito, M., Peña-Barragán, J. M., & García-Torres, L. (2006). Using remote sensing for identification of late-season grass weed patches in wheat. *Weed Science*, *54*(2), 346–353. doi:10.1614/WS-05-54.2.346

MAGRAMA. (2012). http://www.magrama.gob.es/es/agricultura/temas/producciones-agricolas/cultivos-herbaceos/leguminosas-y-oleaginosas/#para3. Accessed 18 August 2012

Meron, M., Tsipris, J., Orlov, V., Alchanatis, V., & Cohen, Y. (2010). Crop water stress mapping for site-specific irrigation by thermal imagery and artificial reference surfaces. *Precision Agriculture*, *11*(2), 148–162. doi:10.1007/s11119-009-9153-x

National Research Council (U.S.) (Ed.). (1997). *Precision agriculture in the 21st century: geospatial and information technologies in crop management*. Washington, D.C: National Academy Press.

Peña-Barragán, J. M., López-Granados, F., Jurado-Expósito, M., & García-Torres, L. (2007). Mapping Ridolfia segetum patches in sunflower crop using remote sensing. *Weed Research*, *47*(2), 164–172. doi:10.1111/j.1365-3180.2007.00553.x

Peña-Barragán, J. M., Ngugi, M. K., Plant, R. E., & Six, J. (2011). Object-based crop identification using multiple vegetation indices, textural features and crop phenology. *Remote Sensing of Environment*, *115*(6), 1301–1316. doi:10.1016/j.rse.2011.01.009

Primicerio, J., Di Gennaro, S., Fiorillo, E., Genesio, L., Lugato, E., Matese, A., & Vaccari, F. (2012). A flexible unmanned aerial vehicle for precision agriculture. *Precision Agriculture*, *13*(4), 517–523. doi:10.1007/s11119-012-9257-6

Ribeiro, A., Fernández-Quintanilla, C., Barroso, J., García-Alegre, M. C., & others. (2005). Development of an image analysis system for estimation of weed pressure. *Precision Agriculture*, *5*, 169–174.

Robert, P. C. (1996). Use of remote sensing imagery for precision farming. In *Proc of 26th Int. Symposium on Rem. Sens. of Env* (pp. 596–599).

Rouse, J. W., Jr., Haas, R. H., Schell, J. A., & Deering, D. W. (1974). Monitoring Vegetation Systems in the Great Plains with Erts. *NASA Special Publication*, *351*, 309.

Smith, A. M. S., Drake, N. A., Wooster, M. J., Hudak, A. T., Holden, Z. A., & Gibbons, C. J. (2007). Production of Landsat ETM+ reference imagery of burned areas within Southern African savannahs: comparison of methods and application to MODIS. *International Journal of Remote Sensing*, *28*(12), 2753–2775. doi:10.1080/01431160600954704

Thorp, K. R., & Tian, L. F. (2004). A Review on Remote Sensing of Weeds in Agriculture. *Precision Agriculture*, *5*(5), 477–508. doi:10.1007/s11119-004-5321-1

Woebbecke, D. M., Meyer, G. E., Von Bargen, K., & Mortensen, D. A. (1995). Color indices for weed identification under various soil, residue, and lighting conditions. *Transactions of the ASAE*, *38*(1), 259–269.

Xiang, H., & Tian, L. (2011). Development of a low-cost agricultural remote sensing system based on an autonomous unmanned aerial vehicle (UAV). *Biosystems Engineering*, *108*(2), 174–190. doi:10.1016/j.biosystemseng.2010.11.010

Zhang, C., & Kovacs, J. M. (2012). The application of small unmanned aerial systems for precision agriculture: a review. *Precision Agriculture*, *13*(6), 693–712. doi:10.1007/s11119-012-9274-5

CAPÍTULO 2

MULTI-TEMPORAL MAPPING OF THE VEGETATION FRACTION IN EARLY-SEASON WHEAT FIELDS USING IMAGES FROM UAV

Torres-Sánchez, J., Peña, J. M., de Castro, A. I., & López-Granados, F. (2014). Multi-temporal mapping of the vegetation fraction in early-season wheat fields using images from UAV. *Computers and Electronics in Agriculture*, 103, 104–113. doi:10.1016/j.compag.2014.02.009.

1. RESUMEN

Cartografiar la vegetación en campos de cultivo es un primer paso importante en las aplicaciones de la teledetección a la agricultura de precisión. Las plataformas aéreas tradicionales como aviones y satélites no son adecuadas para estas tareas en fase temprana debido a su baja resolución temporal y espacial. En este artículo, un vehículo aéreo no tripulado (UAV por sus siglas en inglés) equipado con una cámara convencional (que toma imágenes en el espectro visible) fue usado para tomar imágenes de muy alta resolución espacial sobre un campo de trigo en fase temprana. En estas imágenes, seis índices espectrales (CIVE, ExG, ExGR, índice de Woebbecke, NGRDI, VEG) y dos combinaciones de estos índices fueron calculados y evaluados para la cartografía de la fracción de vegetación. También se estudió la influencia en la precisión de la clasificación de la altura de vuelo (30 y 60 m) y de los días después de la siembra (DDS) del 35 al 75. Los índices ExG y VEG consiguieron la mayor precisión en la cartografía de la fracción de vegetación, con valores desde 87,73% a 91,99% a 30 m de altura de vuelo y del 83,74% al 87,82% a 60 m de altura. Estos índices fueron también espacial y temporalmente consistentes, permitiendo una cartografía precisa de la vegetación sobre todo el campo de trigo y en cualquier fecha. Esto proporciona evidencias de que los índices espectrales en el rango visible, calculados usando una cámara de bajo coste a bordo de un UAV volando a baja altura, son una herramienta apropiada para discriminar la vegetación en campos de trigo en fase temprana. Esto abre la puerta a la utilización de esta tecnología en aplicaciones de la agricultura de precisión como el manejo localizado de malas hierbas en fase temprana, en el cual una precisa detección de la vegetación es esencial para clasificar cultivo y mala hierba.

2. ABSTRACT

Mapping vegetation in crop fields is an important step in remote sensing applications for precision agriculture. Traditional aerial platforms such as planes and satellites are not suitable for these applications due to their low spatial and temporal resolutions. In this article, a UAV equipped with a commercial camera (visible spectrum) was used for ultra-high resolution image acquisition over a wheat field in the early-season period. From these images, six visible spectral indices (CIVE, ExG, ExGR, Woebbecke Index, NGRDI, VEG) and two combinations of these indices were calculated and evaluated for vegetation fraction mapping, to study the influence of flight altitude (30 and 60 m) and days after sowing (DAS) from 35 to 75 DAS on the classification accuracy. The ExG and VEG indices achieved the best accuracy in the vegetation fraction mapping, with values ranging from 87.73% to 91.99% at a 30 m flight altitude and from 83.74% to 87.82% at a 60 m flight altitude. These indices were also spatially and temporally consistent, allowing accurate vegetation mapping over the entire wheat field at any date. This provides evidence that visible spectral indices derived from

images acquired using a low-cost camera onboard a UAV flying at low altitudes are a suitable tool to use to discriminate vegetation in wheat fields in the early season. This opens the doors for the utilisation of this technology in precision agriculture applications such as early site specific weed management in which accurate vegetation fraction mapping is essential for crop-weed classification.

3. INTRODUCTION

The mapping of the percentage of green vegetation per unit of ground surface, i.e., the vegetation fraction (VF), is a major issue in remote sensing. Monitoring the temporal and spatial variations in the VF in a specific area has many ecological and agricultural applications, such as the identification of land degradation and desertification (Xiao and Moody 2005), the estimation of the phenological and physiological status of vegetation (Yu *et al*. 2013) and the prediction of crop yields (Yang et al. 2006), among others. In precision agriculture (PA), quantifying the distribution of VF within a crop-field is a first and crucial step prior to addressing further objectives. One of these objectives is the detection and mapping of weeds in crop fields, with the ultimate goal of applying site-specific weed management (SSWM) techniques and controlling weed patches according to their coverage at each point of the crop-field. In this context, remote imagery for mapping weeds has been traditionally provided by piloted airborne (de Castro *et al*. 2012; Peña-Barragán *et al*. 2011) or satellite platforms (de Castro *et al*. 2013; Martín *et al*. 2011). However, these platforms are limited in their ability to provide images with adequate spatial resolution for differentiating crop and weed vegetation in early development stages for early site specific weed management ESSWM) (López-Granados 2011). In most crop-weed scenarios and for post-emergence herbicide application, the optimal date for weed control is when the crop and weeds are in their seedling growth stages (García Torres and Fernández Quintanilla 1991), and consequently images at very high spatial resolution (often on the order of mm or very few cm) are needed (Hengl 2006).

Limitations associated with traditional aerial imagery platforms can be overcome by using Unmanned Aerial Vehicles (UAV), which have been developed in recent years into a new aerial platform for image acquisition with a tremendous potential for mapping vegetation cover for detailed vegetation studies with environmental (Bryson *et al*. 2010; Laliberte and Rango 2006) and agricultural objectives (Garcia-Ruiz *et al*. 2013; Herwitz *et al*. 2004). UAVs can fly at low altitudes, allowing them to take ultra-high spatial resolution images (e.g., pixels of a few mm or cm) and to observe small individual plants and patches, which has not previously been possible (Xiang and Tian 2011). Moreover, UAVs can supply images even on cloudy days, and the time needed to prepare and initiate the flight is reduced, which allows greater flexibility in scheduling the imagery acquisition. Other advantages of UAVs are their lower cost and their great flexibility of configuration compared

with piloted aircraft, which allows the utilisation and testing of low-cost sensors such as conventional digital cameras. For example, there is widespread agreement among researchers that commercial cameras have been a powerful tool for assessing green vegetation cover using on-ground imagery taken with terrestrial platforms (Guijarro *et al*. 2011; Meyer and Neto 2008; Romeo *et al*. 2013) and masts (Motohka *et al*. 2010; Sakamoto *et al*. 2011; Yu *et al*. 2013). Together with their low cost, another advantage of conventional digital cameras is their high resolution, which is needed when working in narrow row crops such as wheat. However, to the best of our knowledge, they have not been used for VF assessment in images collected with an UAV for agricultural proposes.

Image analysis techniques for quantifying vegetation cover are generally based on the use of vegetation indices (VIs) (Xiao and Moody 2005), which are the product of arithmetic operations performed with spectral information from the radiation reflected by the vegetation at different wavelengths. Information derived from VIs is usually less sensitive to illumination and other factors affecting reflectance (Gitelson *et al*. 2002). The underlying mechanisms of VIs are well understood, and they emphasise some features of vegetation cover and facilitate obtaining relevant information from digital imagery (Delegido *et al*. 2013). In images at ultra-high spatial resolution, it is necessary to determine the VI that enhances the differences among pixels containing vegetation and pixels containing non-vegetation, as well as the threshold value that sets the breakpoint between both classes. The classification output is necessary for the thresholding operation, which needs to be optimised for a successful result. There are several automatic methods for threshold calculation, among which Otsu's (Otsu 1979) method is one of the most utilised for agronomical issues (Guijarro *et al*. 2011; Meyer and Neto 2008). It assumes that the image contains two classes of pixels (bare soil and vegetation when considering crop scenarios) and then calculates the optimum threshold based on minimising combined spread (intra-class variance).

To date, VF has been estimated by relating it to VI values in image pixels from airborne and satellite platforms, in which the pixels include vegetated and non-vegetated zones due to the large size (from a few square metres to square kilometres) (Barati *et al*. 2011; Gitelson *et al*. 2002). Today, the ultra-high resolution of UAV imagery allows images in which almost every pixel covers only vegetation or bare soil, with a low proportion of pixels representing a mixed coverage. Therefore, VF can be calculated as the percentage of pixels classified as vegetation per unit of ground surface. This is particularly relevant when working with crops such as cereals which are sown in narrow crop rows because the surface distance between such rows is usually not wider than 15-17 cm.

In addition to adequate thresholding and good spatial and temporal resolution, another important issue in VF mapping is accurate spatial and temporal consistency. Spatial stability is needed to assure that VF mapping is accurate in the whole studied area because a VI that works

appropriately in only a few zones is useless. Temporal stability is recommendable because it makes it possible to obtain VF maps whenever they are needed. Both parameters make possible the construction of VF maps without any quality loss in the most adequate moment according to the objective.

Although previously reported methods have been mostly applied to on-ground images, they could also be suitable for the remote images captured with UAVs, mainly due to the spatial resolution of on-ground and UAV images being on the same order of magnitude. Investigations about detailed evaluation of remote images captured with UAV platforms and their spectral information or derived vegetation indices with the objective of quantifying VF are currently scarce, although recently Peña *et al*. (2013) developed a method for weed mapping in early-season maize fields using UAV images.

As part of an overall research program to investigate the opportunities and limitations of UAV imagery in accurately mapping weeds in early season winter wheat, it is crucial to explore the potential of generating VF maps from multiple overlapped frames that were mosaicked as a first step in the proper discrimination of crop rows and weeds. Such an approach should demonstrate the ability to accurately discriminate weeds grown between crop rows to design a field program of ESSWM. Consequently, this work evaluated the accuracy, spatial and temporal consistency and sensitivity of different vegetation indices for a wheat crop that were extracted from visible images acquired with a low-cost camera installed in an UAV flying. We focused on several acquisition dates (temporal analysis) and two different flight altitudes. Additionally, to the best of our knowledge, this is the first work to evaluate the adequate performance of Otsu's thresholding method for VF mapping in UAV imagery.

4. MATERIALS AND METHODS

4.1. Study site

The study was performed in a wheat field with flat ground (average slope <1%) situated at the public farm Alameda del Obispo, in Córdoba (southern Spain, coordinates 37,856N, 4,806W, datum WGS84). The wheat crop was sown on November 22th 2012 at 6 kg ha^{-1} in rows 0.15 m apart, and emergence of the wheat plants started by 15 days after sowing (DAS). The field had an area of about 0.5 ha, and was naturally infested by ryegrass (*Lolium rigidum*), which is a monocotyledoneus weed with an appearance very similar to wheat and an analogous phenological evolution. Weed and crop plants were in the principal stage 1 (leaf development) from the BBCH extended scale (Meier *et al*. 1997) in the beginning of the experiment, whereas plants were at the principal stage 2 (tillering) in the last days of the study.

4.2. UAV flights and remote images

A quadrocopter platform with vertical take-off and landing (VTOL), model md4-1000 (microdrones GmbH, Siegen, Germany), was used to collect a set of aerial images at two flight altitudes over the experimental crop-field. This UAV (Figure 1) is equipped with four brushless motors powered by a battery and can fly by remote control or autonomously with the aid of its Global Position System (GPS) receiver and its waypoint navigation system. The VTOL system makes the UAV independent of a runway, so it can be used in a wide range of different situations. The sensor mounted on the UAV to acquire the imagery was a still point-and-shoot camera, model Olympus PEN E-PM1 (Olympus Corporation, Tokyo, Japan). The camera acquires 12-megapixel images in true colour (Red, R; Green, G; and Blue, B, bands) with 8-bit radiometric resolution and is equipped with a 14-42 mm zoom lens. The camera's sensor is 4,032 × 3,024 pixels, and the images are stored in a secure digital SD-card. The camera was set to operate in the automatic mode, which adjusts the exposure time (shutter speed) and F-stop (aperture) optimally. Image triggering is activated by the UAV according to the programmed flight route. At the moment of each shoot, the on-board computer system records a timestamp, the GPS location, the flight altitude, and vehicle principal axes (pitch, roll and heading). Detailed information about the configuration of the UAV flights and specification of the vehicle and the camera used can be found in (Torres-Sánchez *et al*. 2013).

Figure 1. *Microdrone MD4-1000 flying over the experimental crop.*

The first set of aerial images was collected at 35 DAS, and then sets were collected at 7-10 day intervals; the last set was collected at 75 DAS. Therefore, images were obtained at different growth stages. On every date, two flights were performed at different altitudes: 30 m and 60 m. These flight altitudes resulted in spatial resolutions of 1.14 and 2.28 cm, respectively. The flight routes were programmed into the UAV software so that the vehicle stopped 5 s at every image acquisition point to ensure that the camera took a good light measurement. With this configuration, the flights at 30 m and 60 m altitude took 10 and 5 minutes, respectively; and the UAV acquired 36 and 10 images at 30 and 60 m flight altitude, respectively.

In the course of the UAV flights, a barium sulphate standard Spectralon® panel (Labsphere Inc., North Sutton, NH, USA) of 1×1 m was also placed in the middle of the field (Figure 2) to calibrate the spectral data. Digital images captured by each camera channel were spectrally corrected by applying an empirical linear relationship (Hunt, Jr. *et al*. 2010). Equation coefficients were derived by fitting digital numbers of the images located in the Spectralon panel to the Spectralon ground values.

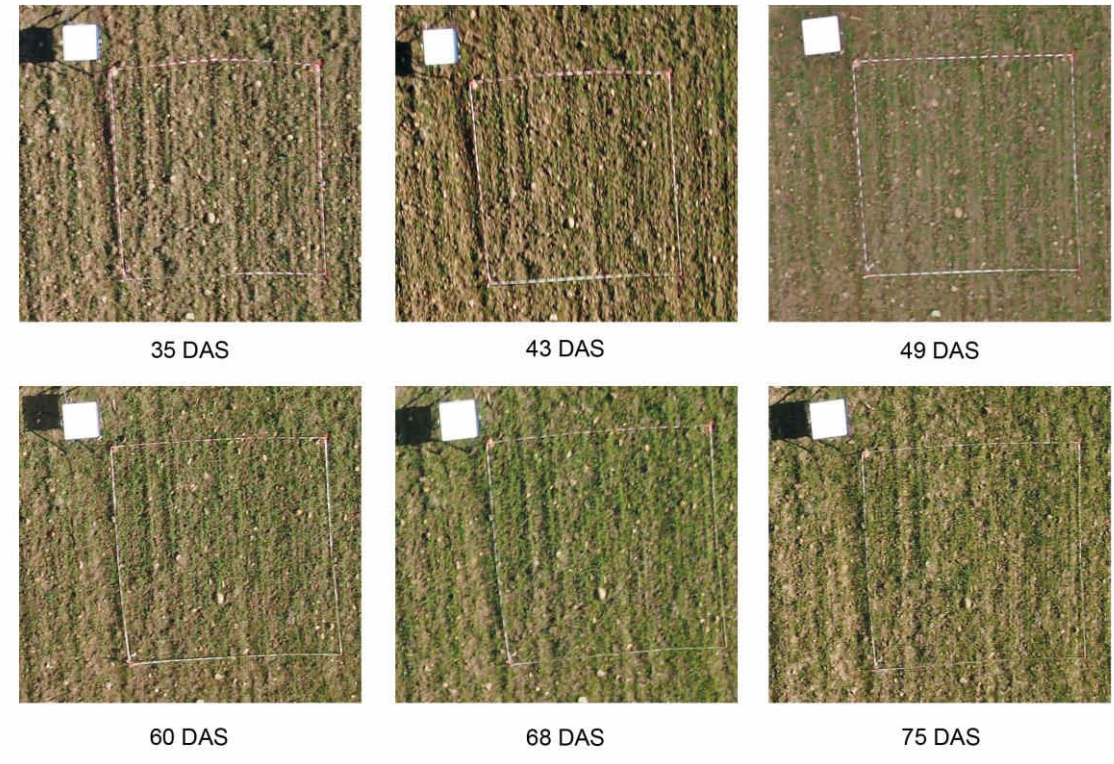

Figure 2. *Spectralon and frames in the wheat field.*

4.3. Image mosaicking

A sequence of overlapped images was collected in each flight mission to cover the whole experimental crop-field. An important task prior to image analysis was the combination of all these individual and overlapped images by applying a process of mosaicking. The imagery had a 30% side-

lap and a 60% forward-lap to allow correct image mosaicking to generate a complete crop map in the whole study area. Agisoft PhotoScan Professional Edition (Agisoft LLC, St. Petersburg, Russia) was employed in this task. The mosaicking process had three principal steps. The first one was the image alignment, i.e., the software searches for common points in the images and matches them, as well as finding the position of the camera for each image and refining camera calibration parameters. The next step was to build the image geometry. Based on the estimated camera positions and images themselves a 3D polygon mesh, representing the overflown area, was built by PhotoScan software. Once the geometry was constructed, the individual images were projected over it for orthophoto generation. The resultant ortho-mosaicked image must be geometrically interoperable and must shows an accurate crop row matching between both sides of overlapped borderline images, both of which guarantee good performance of the subsequent image analysis.

4.4. Quantification of vegetation fraction

Six VIs and two VI combinations, based on RGB space, were tested for classifying green vegetation pixels in the mosaicked images and quantifying vegetation fraction.

- *Normalized Green-Red Difference Index* (Gitelson *et al*. 2002)

$$NGRDI = \frac{G-R}{G+R} \quad (1)$$

- *Excess Green* (Woebbecke *et al*. 1995)

$$ExG(2) = 2g - r - b \quad (2)$$

- *Color index of vegetation* (Kataoka *et al*. 2003)

$$CIVE = 0.441r - 0.881g + 18.78745 \quad (3)$$

- *Vegetativen* (Hague *et al*. 2006)

$$VEG = \frac{g}{r^a b^{(1-a)}} \text{ with a = 0.667 as in its reference} \quad (4)$$

- *Excess Green minus Excess Red* (Camargo Neto 2004)

$$ExGR = ExG - ExR = ExG - 1.4r - g \quad (5)$$

- *Woebbecke Index* (Woebbecke *et al*. 1995)

$$WI = \frac{g-b}{r-g} \quad (6)$$

- *Combination* (Guijarro *et al*. 2011)

$$COM = 0.25ExG + 0.3ExGR + 0.33CIVE + 0.12VEG \quad (7)$$

- *Combination 2* (Guerrero *et al*. 2012)

$$COM(2) = 0.36ExG + 0.47CIVE + 0.17VEG \quad (8)$$

The next normalization scheme was applied in some VIs:

$$r = \frac{R}{R+G+B}; g = \frac{G}{R+G+B}; b = \frac{B}{R+G+B} \quad (9)$$

These VIs were designed to accentuate the green component of the images, and VEG was also designed to cope with the variability of natural daylight illumination. The applications of the VIs were able to transform the images from the original RGB three-band space to a greyscale band. All the mosaicked images from the different dates and flight altitudes were transformed to greyscale images by the application of the above mentioned VIs. In the greyscale images generated by the VIs, pixels corresponding to vegetation zones in the field show intensity levels greater than the rest of the image pixels.

To perform image classification, the value of each greyscale image pixel was compared with a prefixed threshold; if the pixel value was higher than the threshold, then it was classified as vegetation. Once the image pixels were classified, the VF was determined as the percentage of pixels classified as vegetation per unit of ground surface:

$$\mathrm{VF} = \frac{\text{Pixels classified as vegetation (in a delimited area)}}{\text{total pixels (in a delimited area)}} \times 100 \quad (10)$$

The VF was calculated for 96 square frames of three different areas (16, 4 and 1 m^2) distributed regularly throughout the studied surface (Figure 2). The VF values for every frame were calculated using different thresholds (Table 1) in the greyscale images coming from the application of the studied VIs to all the mosaicked images from every date and flight altitude. The threshold ranges for every index were established to cover the lowest and highest VF values in the whole image. Once the threshold range was established for every VI, it was automatically divided to obtain 10 equidistant values within this range. Then, every one of these 10 values was tested in the determination of VF for 30 and 60 m flight altitude at any flight date.

Table 1. *Thresholds tested to determine the VF for 30 and 60 m flight altitude at any flight date according to the lowest and highest VF values in the mosaicked.*

Vegetation indices	Thresholds									
NGRDI	-0.08	-0.06	-0.05	-0.03	-0.01	00.01	00.03	00.05	00.06	00.08
ExG	0.03	0.05	0.08	0.11	0.14	0.16	0.19	0.22	0.25	0.27
CIVE	18.62	18.64	18.65	18.67	18.69	18.71	18.73	18.75	18.76	18.78
VEG	0.90	0.94	0.99	1.03	1.08	1.12	1.17	1.21	1.26	1.30
ExGR	-0.92	-0.90	-0.87	-0.84	-0.81	-0.79	-0.76	-0.73	-0.70	-0.68
COM	6.02	6.04	6.07	6.09	6.11	6.13	6.16	6.18	6.20	6.22
COM2	8.98	9.00	9.02	9.04	9.05	9.07	9.09	9.11	9.12	9.14
WI	-6.11	-4.38	-2.64	-0.90	0.83	2.57	4.30	6.04	7.78	9.51

4.5. Evaluation of VF mapping

For validation purposes, a flight at 10 m altitude was used to collect vertical pictures of the sampling frames. The UAV was programmed to fly continuously taking images every second to obtain several images for every frame, which allowed the choosing of the best one. The high proximity of these images to the frames made it possible to visualise individual plants. Therefore, the best image of every frame was used to extract the observed VF (OVF) data in every sampling point. The accuracy of the VF estimations was evaluated by comparing them with the observed VF values. The observed VF data were determined by using the index and threshold that better detected individual plants according to a visual interpretation (Figure 3). The following expression was calculated to evaluate the performance of the different indices and thresholds:

$$Accuracy(\%) = 100 - |OVF - VF)| \quad (11)$$

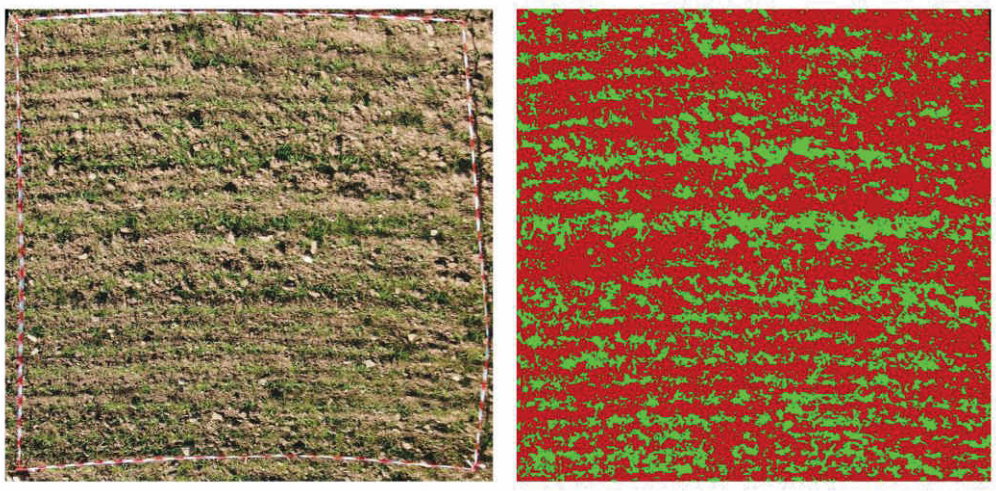

Figure 3. *Ten metre altitude frame image and the output of the image after the vegetation classification process.*

The application of equation (11) resulted in a high accuracy values. The following statistics from these values were calculated to study the VIs:

- Mean accuracy: calculated for every index as affected by the threshold, flight date, and altitude. It was used to determine the best threshold for every VI for a specific date and flight altitude. Once this threshold was selected, VIs could be compared based on their best operational conditions.
- Standard deviation (SD) of accuracy: calculated for the accuracy values achieved with the best threshold for every index as affected by the flight date and altitude. Every accuracy value was related with a specific frame, so it had coordinates on the field; therefore, the SD measurement of the dispersion from the mean had a spatial meaning in this study. High SD values indicated that the VI accuracy was not stable over the field, with areas in which the VF yielded good estimates and others in which it did not.
- Coefficient of variation (CV): calculated for the best mean accuracies of every VI along the six studied flight dates. It allowed the analysis of how the accuracy of a VI at a flight altitude varied over the time to select the VIs that achieved better classification results without being influenced by the flight date.

After the two best VIs were selected, their accuracy values for the best threshold at every date and flight altitude were distributed in a map using the coordinates of the frames from which they were calculated. Then, using the values at these points, density maps were generated to spatially represent the accuracy of the two VIs at every date and flight altitude. The observed and estimated VFs was also compared for these two VIs using a 1:1 line, which should have a correspondence of 1 in an ideal situation.

The study of the different thresholds and the accuracies achieved with their application to the images allowed the selection of the best VI. Additionally, to evaluate the feasibility of automatic thresholding, Otsu's method (Otsu 1979) was compared with the best VI from the best date of the experiment. This methodology was developed to be used on grey level histograms, so we tested it on the greyscale band generated by the application of the best VI in the RGB original image. In every validation frame, Otsu´s method automatically applied an optimal threshold based on minimizing combined intra-class variance. The results of the VF estimation in both cases, i.e., the best VI threshold and Otsu´s thresholding, were compared to determine if this methodology was applicable to quantify VF using UAV imagery.

JMP software (SAS, Cary, NC, USA) was employed to perform the data analysis. eCognition Developer 8 (Trimble GeoSpatial, Munich, Germany) was used to automate the VF quantification for

all the thresholds, flight altitudes and dates. The Otsu's thresholds were calculated using ImageJ 1.46r (Wayne Rasband, National Institutes of Health, USA).

5. RESULTS

The mean accuracy and the standard deviation at any flight date and altitude was determined using all the VIs with their corresponding 10 thresholds showed in Table 1. The threshold obtaining best results for every VI together to its accuracy and standard deviation at any flight date and altitude are shown in Table 2. At 30 m flight altitude, ExG reached the highest accuracy in the whole experiment on a concrete date (91.99% at 35 DAS); it also had the best mean accuracy for more dates (at 35, 43 and 60 DAS), and it showed the highest mean of accuracy over time (90.20%). At the 60 m flight altitude, Meyer achieved the highest mean accuracy for two dates (43 and 49 DAS), and VEG was also the best for two dates (68 and 75 DAS). The best mean accuracies over the time were reached by VEG (86.25%), closely followed by ExG (86.15%).

5.1. Classification accuracy of VF as affected by VI and spatial factor

Accuracy results were calculated for every georeferenced frame distributed on the field; therefore, the SD values were able to give spatial information about the consistency of VF mean classification accuracy across the experimental field. A low accuracy SD indicated a high spatial consistency of the VI for estimating VF. The lowest SD values were associated in several cases with the highest accuracy at each date and flight altitude, and in the other cases they were associated with the second or third highest accuracy. The ExG, WI and VEG indices showed the lowest SD at one specific date and flight altitude. The index with the best spatial consistency at 30 m and 60 m flight altitude was ExG (7.72 and 10.20, respectively), closely followed by VEG (7.75 and 10.22).

5.2. Classification accuracy of VF as affected by VI and temporal factors

The COM, COM2, ExG, ExGR, NGRDI and VEG indices showed similar accuracy values at all the studied dates; e.g., the ExG mean accuracy only fluctuated between 91.99% and 87.75%. Thus, temporal factors did not have a remarkable influence on the estimation of VF by these indices. However, the CIVE and Meyer accuracies were affected by time, with lower values on the last dates.

The analysis of CV evolution over time was used to determine which VIs showed lower variability over time. This is an important factor to be studied because it is better to use VIs that perform accurate VF quantification regardless of the flight date. The ExG and VEG were the indices with the lowest CVs over the time at the 30 and 60 m flight altitudes, with values of approximately 8.6% 11.8%, respectively.

Table 2. *Mean accuracy (A) and standard deviation (SD) of the accuracy for the best threshold for every index as affected by flight dates and altitudes (m).The mean, standard deviation and coefficient of variation of accuracy for every VI across time are also included.*

		Flight dates																									
		35 DAS				43 DAS				49 DAS				60 DAS				68 DAS				75 DAS						
Index	Flight altitude	A	±	SD	Th	A	±	SD	Th	A	±	SD	Th	A	±	SD	Th	A	±	SD	Th	A	±	SD	Th	Mean A	SD A	CV A (%)
CIVE	30	83.31	±	13.27	18.76	80.72	±	14.58	18.75	79.81	±	14.89	18.75	76.44	±	17.02	18.73	75.84	±	15.64	18.67	66.84	±	25.21	18.73	77.16	16.77	21.73
	60	80.31	±	14.51	18.76	75.96	±	15.88	18.76	76.31	±	17.14	18.75	72.57	±	18.12	18.73	69.38	±	16.28	18.62	62.74	±	25.90	18.73	72.88	17.97	24.66
COM	30	90.73	±	7.67	6.09	90.06	±	8.46	6.11	87.18	±	10.37	6.09	88.48	±	8.84	6.13	88.87	±	7.61	6.11	89.83	±	7.09	6.13	89.19	8.34	9.35
	60	86.32	±	9.92	6.09	84.59	±	10.43	6.11	83.18	±	13.77	6.09	81.71	±	14.16	6.13	85.67	±	10.66	6.13	84.39	±	10.93	6.11	84.31	11.64	13.81
COM2	30	88.88	±	7.72	9.04	90.33	±	8.17	9.04	85.20	±	11.13	9.02	88.47	±	7.44	9.07	90.52	±	7.31	9.05	89.42	±	8.24	9.05	88.80	8.34	9.39
	60	87.59	±	10.94	9.02	85.80	±	10.43	9.04	82.49	±	13.96	9.02	86.52	±	10.80	9.05	87.21	±	9.63	9.05	86.01	±	9.26	9.05	85.94	10.84	12.61
ExG	30	91.99	±	6.50	0.11	90.76	±	7.84	0.14	87.75	±	9.53	0.11	90.49	±	6.86	0.19	90.23	±	7.85	0.16	89.96	±	7.76	0.16	90.20	7.72	8.56
	60	87.19	±	11.67	0.08	85.49	±	12.30	0.11	83.93	±	10.94	0.11	86.91	±	9.07	0.16	87.81	±	8.00	0.14	85.55	±	9.21	0.16	86.15	10.20	11.84
ExGR	30	91.43	±	6.63	-0.81	90.03	±	8.48	-0.79	87.98	±	9.78	-0.81	87.18	±	9.76	-0.76	89.17	±	7.28	-0.79	88.76	±	8.48	-0.79	89.09	8.40	9.43
	60	84.85	±	12.72	-0.84	84.28	±	12.74	-0.81	84.48	±	12.89	-0.81	83.65	±	13.08	-0.73	86.62	±	9.33	-0.76	83.92	±	10.40	-0.79	84.63	11.86	14.01
WI	30	90.47	±	6.34	2.64	90.49	±	8.41	4.36	89.91	±	8.75	4.36	81.99	±	15.88	4.36	83.76	±	10.97	-6.11	77.76	±	22.07	4.36	85.73	12.07	14.08
	60	87.30	±	9.81	2.64	88.70	±	9.14	4.36	88.38	±	10.16	4.36	76.30	±	17.51	-2.67	83.76	±	12.32	-6.11	78.61	±	20.67	6.07	83.84	13.27	15.83
NGRDI	30	91.45	±	6.74	-0.03	90.01	±	8.21	-0.01	88.02	±	9.81	-0.03	87.66	±	9.32	0.01	90.03	±	7.24	-0.01	89.22	±	7.29	-0.01	89.40	8.10	9.06
	60	85.59	±	12.12	-0.05	84.69	±	12.70	-0.03	83.19	±	13.56	-0.03	82.68	±	12.26	0.05	82.66	±	9.31	-0.01	82.84	±	11.90	-0.03	83.61	11.97	14.32
VEG	30	91.81	±	6.51	1.12	87.91	±	8.57	1.21	87.33	±	9.68	1.12	89.84	±	7.91	1.21	90.31	±	6.82	1.17	90.67	±	6.99	1.21	89.65	7.75	8.64
	60	87.49	±	10.72	1.08	85.75	±	12.05	1.12	83.74	±	10.90	1.12	86.71	±	9.63	1.21	87.82	±	8.03	1.17	86.01	±	10.00	1.17	86.25	10.22	11.85

5.3. Classification accuracy of VF as affected by VI and the flight altitude

The mean accuracies at 30 m of CIVE, COM, COM2, ExG, ExGR, NGRDI and VEG were always higher than at the 60 m flight altitude. Only WI at 75 DAS reached a slightly better accuracy at the 60 m altitude. WI also showed the same accuracy at both flight altitudes at 68 DAS. On average, the accuracy of VF quantification was 3.95% higher at the 30 m altitude. The VI with the greatest accuracy variations associated with flight altitude was NGRDI, whereas the VI that was least affected by this parameter was WI.

5.4. Automatic thresholding by using Otsu´s method

Otsu's automatic thresholding methodology was applied to the ExG index for every one of the frames from the 30 m altitude flight at 35 DAS, which was the example in which the best accuracy was achieved. The application of this methodology led to obtaining one threshold by frame, with values ranging from 0.06 to 0.20 and a mean of 0.11. The use of its own threshold for VF quantification in every frame resulted in a mean accuracy of 91.19%, slightly lower than the one calculated using the best threshold from Table 1 (0.11) for ExG in all the frames (91.99%). The mean value of the VI in every frame which is an easy way to obtain a threshold (Burgos-Artizzu *et al*. 2011; Guijarro *et al*. 2011), was also tested for thresholding, however it led to an over-estimation of the VF (data not shown). The SD achieved with Otsu's method was 6.95, which indicated a spatial consistency similar to the one obtained using 0.11 as threshold in all the frames (6.50).

5.5. VF mapping from the best VIs

Considering the mean accuracy along all the temporal series, its coefficient of variation, and their spatial consistency, the best VIs were ExG and VEG. Therefore, they were studied more exhaustively. Maps of accuracy by date at the 30 m (Figure 4) and 60 m flight altitudes (Figure 5) were built and compared to the maps of the observed VF. The observed VF was also graphically compared with the estimated VF from the 30 and 60 m flights. Prior to the comments on these figures, some details must be clarified as follows:

1. The map size was not the same for all the dates because some images failed to be acquired at 10 m flight altitude, and consequently, there were some small areas in that were unfeasible to use to determine the observed VF.
2. The observed VF was lower on the last date than in the previous one, and this lower vegetation density was even visually apparent in the images. According to the field crop data recorded by the authors on the different flight dates, this could be due to the wheat and weed plants being at the beginning of the tillering growth stage, in which the wheat stems

become more vertical and show fewer surfaces in the aerial images (C. Fernández-Quintanilla, personal communication, May 16, 2013).

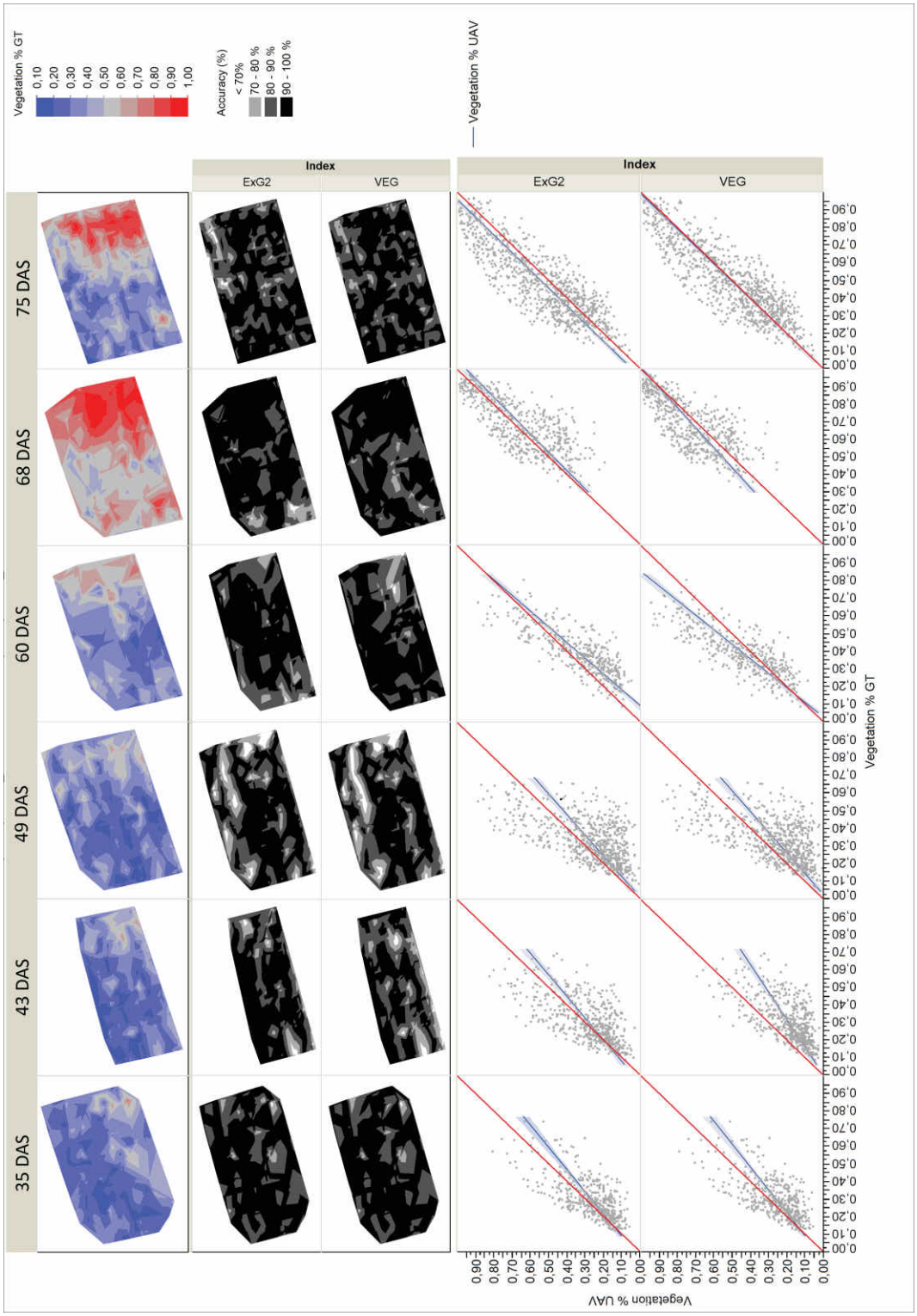

Figure 4. *Observed VF map. Accuracy maps for the best VIs, and graphics comparing the observed and estimated VFs at the 30 m flight altitude.*

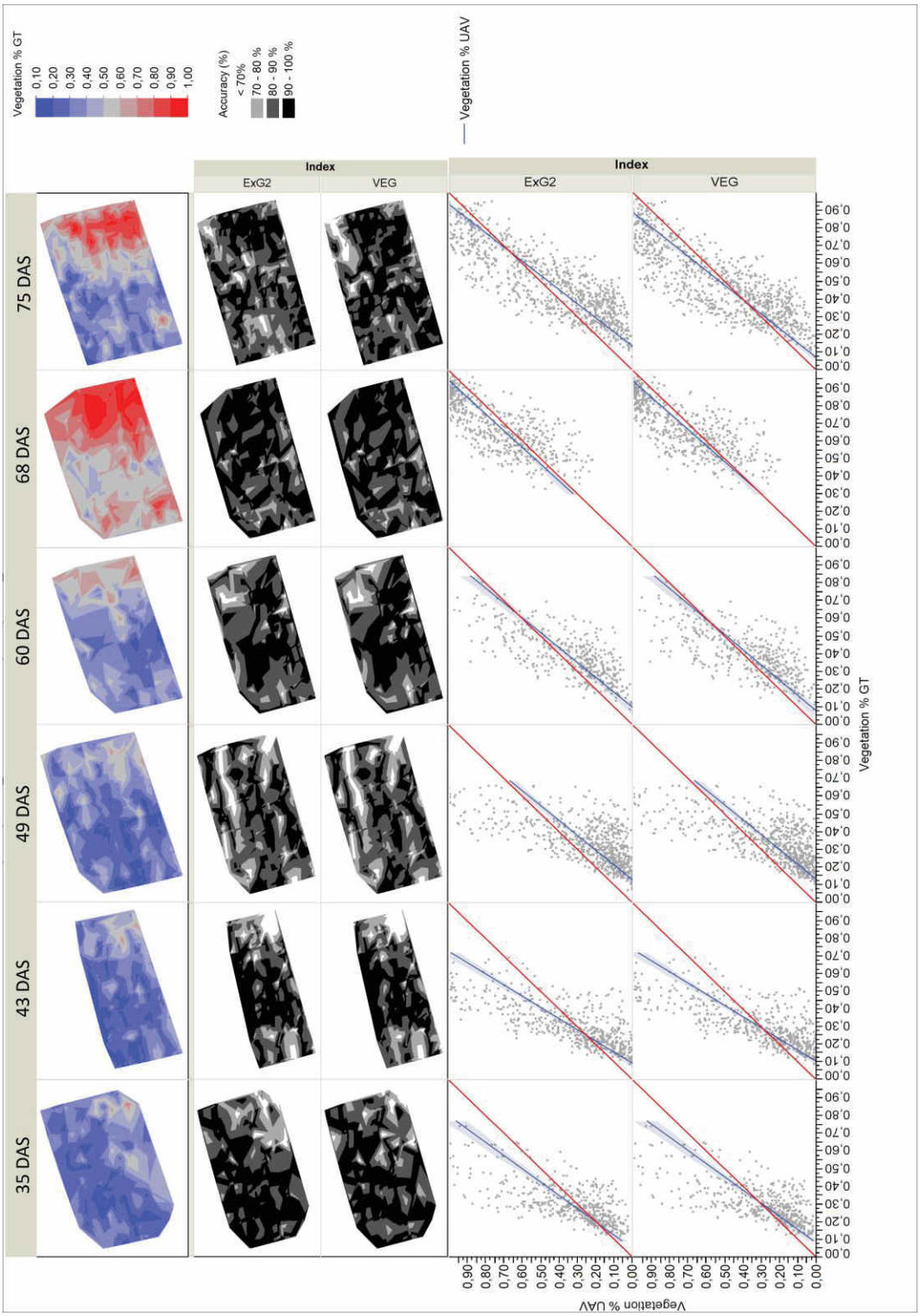

Figure 5. *Observed VF map. Accuracy maps for the best VIs, and graphics comparing the observed and estimated VFs at the 60 m flight altitude.*

Accuracy maps were almost identical for both VIs at every flight date. The mapping of accuracy revealed that there was a high proportion of the wheat field in which the accuracy was over 90%, indicating the suitability of the studied VIs for VF quantification. This proportion was lower in imagery acquired at the 60 m flight altitude, as suggested by the lower accuracy values shown in Table 2.

Zones with lower accuracy were located at the same places at both 30 and 60 m, but they were bigger at the higher altitude. Zones with lower accuracy were not consistent over time.

The graphical comparison of the observed and estimated VFs showed that most points were near the 1:1 line, which indicated a high correlation among them. On the first dates, the point cloud and the regression line did not cover the whole range of possible values because there were no frames with high VF values. At 68 DAS, as it was mentioned above, VF reached the highest values; therefore, there were no points in the graphic zone corresponding to lower VF values. The best fit between the regression line and the 1:1 line was reached at the three last dates at the 30 m flight altitude for ExG and VEG. At the 60 m flight altitude, the best fit was also reached at the three last dates for the two studied VIS.

6. DISCUSSION

The discrimination of vegetation in narrow crop row fields during the early growth stages, when the crop row width is 15 cm and the plant size is only of a few centimetres, requires the use of images with a ultra-high spatial resolution because at least four pixels are required to detect the smallest objects within an image (Hengl 2006). For this reason, distinguishing small seedlings has been commonly undertaken by analyzing images captured with cameras or sensors mounted in on-ground platforms (Burgos-Artizzu *et al*. 2010; Romeo *et al*. 2013). However, the use of remote images captured with UAVs flying at low altitudes offer a new opportunity that needs to be investigated in detail. This article shows the visible vegetation indices that best performed green vegetation discrimination in a wheat field tested on six different dates throughout the earliest stages of crop development and compared the results obtained in remote images captured at two different flight altitudes.

Although most VIs tested showed the ability to discriminate vegetation, two indices (ExG and VEG) had the highest classification accuracy independent of the image acquisition date. When mapping spatially variable features in precision agriculture, such as VF or vegetation vigour, good accuracy is needed. However, it is also required that this accuracy be homogenously distributed across the studied crop. Mapping these variables would be useless if the mapping accuracy differed from one zone to another. Therefore, the spatial consistency achieved for ExG and VEG makes them adequate for precision agriculture applications in which vegetation quantification is needed. Yu et al. (Yu *et al*. 2013) also reported that ExG was the VI with the best accuracy in their experiments in maize, closely followed by ExGR and VEG. The excellent fitting between the regression line and the 1:1 line in figures 4 and 5 for the three last dates indicates that there is a low probability of under or over-estimation of the vegetation fraction. The worse fitting achieved on the first dates could be due

to the lack of points in the graphic region corresponding to high VF values, which causes the accumulation of points in the opposite region of the graphic, while on the three last dates, there were points distributed all over the graphic.

From an agronomic point of view, temporal consistency evaluated by the CV of the accuracy is also of great importance because it allows overflying the crop just when the farmer wants to study the crop without loss in the accuracy of the VF quantification. For example, if the farmer's objective is to detect vegetation as a step prior to designing an early site-specific weed treatment, the crop images can be acquired a few days before the weed treatment is going to be applied.

Meyer and Neto (2008) reported that ExGR does not require a special threshold calculation in images acquired at 1 m above the ground. Their results showed that plant pixel values were all positive, and the remaining background pixels were all negative. However, for the UAV imagery studied in this work, different threshold values lower than zero (i.e., negative) were needed to classify vegetation pixels using ExGR. Those that involved a single threshold were not applicable in our work for every VI, but rather the different dates and flight altitudes analysed made it necessary to search for the best threshold in every case. Guijarro *et al*. (2011) and Burgos-Artizzu *et al*. (2011) working with on-ground imagery in maize crops stated that Otsu's thresholding method led to an under-estimation of vegetation in their image analysis. However, Otsu's thresholding method achieved a satisfactory accuracy for the results in our work with remote imagery. Considering the fact that different thresholds were needed for each VI and flight date, Otsu's method could be used to automate the threshold selection in future works where vegetation segmentation from UAV images is required.

Of relevant interest is the definition of the optimum pixel size needed according to the size of the plants to be discriminated. In remote sensing, the pixel size is directly proportional to the flight altitude. In our experiment, classification results were moderately affected by the flight altitude, with an average reduction of 3.95% in the classification results when flight altitudes increased from 30 m (1.14 cm/pixel) to 60 m (2.28 cm/pixel). When the spatial resolution is very high, the plants in the image are well delimited; however, when the spatial resolution is poorer, limits between plants and soil are fuzzy, and consequently, there is usually a higher proportion of pixels including information for both vegetation and bare soil. In our study, this mixed spectral information altered the VI values in those pixels affecting the accuracy of the VF detection. Excluding the pixels with mixed spectral information, the discrimination of pixels corresponding to bare soil or vegetation can be robustly performed because they have two different dominant spectral signatures, green for plants and red for soil (Guerrero *et al*. 2012). This spectral difference appears even in cases in which the leaf angle and small scale soil properties disrupt the homogeneity of these classes.

In a practical application of these VIs to VF quantification the selection of the flight altitude will depend on several factors, not only on the accuracy of the quantification. Therefore, the loss of about a 4% of accuracy could be assumed by the user if other important advantages are achieved by flying at 60 m instead of flying at 30 m altitude, as described before by Torres-Sánchez *et al*. (2013). For example, flying at 60 m allows the duplication of the area that can be overflown without problems related with the UAV's energy autonomy. This would reduce the number of images needed to cover the whole studied crop, making it possible to map the VF in a shorter time. If the purpose for VF mapping is ESSWM, the accuracy loss could be overcome by creating a buffer around the detected weeds, which will reduce the chance of missing isolated weeds.

The study of VF in wheat fields in the early season could be used for the detection and mapping of weeds for ESSWM. Crops do not cover the soil entirely in the first growth stages, so if there are regions with low and high VF at early season in a crop field, it can be assumed that the regions with a high percentage of vegetation are infested by weeds. In this stage, mapping weeds in wheat using remote sensing presents much greater difficulties than in the case of the late-stage season for three main reasons (López-Granados 2011): 1) weeds are generally distributed in small patches, which makes it necessary to work with remote images at very small pixel sizes, often on the order of centimetres (Society 1996); 2) grass weeds and monocotyledonous crops (e.g., *Avena* spp. or *Lolium* spp. in wheat) or broad-leaved weeds and many dicotyledonous crops (e.g., *Chenopodium* spp. in sunflower) generally have similar reflectance properties early in the season, which decreases the possibility of discriminating between vegetation classes using only spectral information; and 3) soil background reflectance may interfere with detection (Thorp and Tian 2004). The usual first step of the image processing is to separate plants (weeds and crop) from soil, and the second step is to discriminate between crop and weed plants (Torres-Sánchez *et al*. 2013). However, the difficulty of mapping early weeds in wheat fields (or other cereals sown in narrow crop rows) is related to the very small distance between crop rows (usually no greater than 15 cm) and the quick growth of these crops in the early growth stages, which cover the inter-row area in a few days, thus reducing the likelihood of weed detection.

Research about the evaluation of factors affecting the application of UAV platforms in weed science is still scarce. Some efforts are being made by the research community for the monitoring of crop growth or weed infestation in early stages using UAV images, although currently most of these investigations only show potential uses (Rasmussen *et al*. 2013) or are based on results with limited validation (Samseemoung *et al*. 2012). The influence of the spatial and spectral resolution of the UAV imagery in a multi-temporal study was evaluated in detail in our work. These factors were studied deeply under field conditions, and the results were evaluated with a complete validation set of 96

sampling frames in each of the six studied dates. Although sampling is a hard task in field conditions, it is absolutely needed for an objective evaluation of the results; otherwise the results can only be based on subjective interpretation. Moreover, investigations should also include all the operations needed to generate a whole georeferenced image of the studied field, including the mission planning and image mosaicking, because the advantage of UAV technology in comparison to other remote platforms is the ability to use mosaicked images to map large fields (Torres-Sánchez *et al*. 2013).

7. CONCLUSIONS

Visible spectral indices derived from imagery acquired from an UAV equipped with a low cost camera flying at low altitudes have shown the ability to discriminate vegetation in wheat fields in the early season. Among the tested indices, the two most successful were ExG and VEG, with ExG being the best for practical and farming applications due to its greater simplicity and its satisfactory mean accuracy and SD accuracy at 30 and 60 m flight altitudes for any image acquisition date. Therefore, the altitude and date to perform the flight depend on other parameters, such as the area to be flown over or the objective of the image acquisition.

Otsu's thresholding method can be applied to automatically determine the VI value that performs an adequate discrimination of vegetation. It achieves good accuracy results and allows the automation of the threshold selection, which is one of the key steps in vegetation discrimination through VIs.

The methodology presented herein could be used for mosaicking a range of small to large areas depending on the autonomy of the UAV. This advantage, together with the high temporal resolution and the ultra-high spatial resolution obtained within a range of 2.47 to 0.74 cm, would allow a greater extension of the detail in the information extracted from the images for weed patch detection, which is the final objective of the research described herein. An accurate VF quantification at very high spatial resolution, like that obtained in this study, can be useful in precision agriculture for different crop monitoring proposes. In the field of ESSWM, the VF maps could be linked to weed infestation, if it is assumed that a higher VF is related to the presence of weeds.

In conclusion, the most important achievement of this study was obtaining accurate VF georreferenced maps in wheat fields at the seedling stage with very high spatial resolution for further use in ESSWM using the ExG vegetation index obtained using an UAV and a low-cost camera. As stated in this paper, the flight altitude had very little effect on the accuracy of the performance of ExG, which is the most appropriate VI for mapping VF due to its high accuracy and its spatial and temporal consistency. The VF quantification through UAV images opens the door to further investigations, whose main objective should consist of the discrimination of the wheat row structure

for further identification of weed and crop plants, because the position of each plant relative to the crop rows might be the key feature used to distinguish between the weeds and crop plants. The reasoning behind this objective would be that once crop rows are mapped, if there is vegetation between them, this vegetation is most likely weed plants or weed patches, and thus, weeds could be discriminated and mapped.

8. ACKNOWLEDGMENTS

This research was partly financed by the TOAS Project (Marie Curie Program, ref.: FP7-PEOPLE-2011-CIG-293991, EU-7th Frame Program) and the RHEA project (NMP-CP-IP 245986-2, EU-7th Frame Program). Research of Dr. de Castro and Mr. Torres-Sánchez was financed by JAEPre and FPI Programs, respectively.

9. REFERENCES

Barati, S., Rayegani, B., Saati, M., Sharifi, A., & Nasri, M. (2011). Comparison the accuracies of different spectral indices for estimation of vegetation cover fraction in sparse vegetated areas. *The Egyptian Journal of Remote Sensing and Space Science*, *14*(1), 49–56. doi:10.1016/j.ejrs.2011.06.001

Bryson, M., Reid, A., Ramos, F., & Sukkarieh, S. (2010). Airborne vision-based mapping and classification of large farmland environments. *Journal of Field Robotics*, *27*(5), 632–655. doi:10.1002/rob.20343

Burgos-Artizzu, X. P., Ribeiro, A., Guijarro, M., & Pajares, G. (2011). Real-time image processing for crop/weed discrimination in maize fields. *Computers and Electronics in Agriculture*, *75*(2), 337–346. doi:10.1016/j.compag.2010.12.011

Burgos-Artizzu, X. P., Ribeiro, A., Tellaeche, A., Pajares, G., & Fernández-Quintanilla, C. (2010). Analysis of natural images processing for the extraction of agricultural elements. *Image and Vision Computing*, *28*(1), 138–149. doi:10.1016/j.imavis.2009.05.009

Camargo Neto, J. (2004). A combined statistical-soft computing approach for classification and mapping weed species in minimum-tillage systems. *ETD collection for University of Nebraska - Lincoln*, 1–170.

Castro, A. I. de, Jurado-Expósito, M., Peña-Barragán, J. M., & López-Granados, F. (2012). Airborne multi-spectral imagery for mapping cruciferous weeds in cereal and legume crops. *Precision Agriculture*, *13*(3), 302–321. doi:10.1007/s11119-011-9247-0

Castro, A. I. de, López-Granados, F., & Jurado-Expósito, M. (2013). Broad-scale cruciferous weed patch classification in winter wheat using QuickBird imagery for in-season site-specific control. *Precision Agriculture*, *14*(4), 392–413. doi:10.1007/s11119-013-9304-y

Delegido, J., Verrelst, J., Meza, C. M., Rivera, J. P., Alonso, L., & Moreno, J. (2013). A red-edge spectral index for remote sensing estimation of green LAI over agroecosystems. *European Journal of Agronomy*, *46*, 42–52. doi:10.1016/j.eja.2012.12.001

García Torres, L., & Fernández Quintanilla, C. (1991). *Fundamentos Sobre Malas Hierbas y Herbicídas*. Ministerio de Agricultura, Pesca y Alimentación, Servicio de Extensión Agraria.

Garcia-Ruiz, F., Sankaran, S., Maja, J. M., Lee, W. S., Rasmussen, J., & Ehsani, R. (2013). Comparison of two aerial imaging platforms for identification of Huanglongbing-infected citrus trees. *Computers and Electronics in Agriculture*, *91*, 106–115. doi:10.1016/j.compag.2012.12.002

Gitelson, A. A., Kaufman, Y. J., Stark, R., & Rundquist, D. (2002). Novel algorithms for remote estimation of vegetation fraction. *Remote Sensing of Environment*, *80*(1), 76–87. doi:10.1016/S0034-4257(01)00289-9

Guerrero, J. M., Pajares, G., Montalvo, M., Romeo, J., & Guijarro, M. (2012). Support Vector Machines for crop/weeds identification in maize fields. *Expert Systems with Applications*, *39*(12), 11149–11155. doi:10.1016/j.eswa.2012.03.040

Guijarro, M., Pajares, G., Riomoros, I., Herrera, P. J., Burgos-Artizzu, X. P., & Ribeiro, A. (2011). Automatic segmentation of relevant textures in agricultural images. *Computers and Electronics in Agriculture*, *75*(1), 75–83. doi:10.1016/j.compag.2010.09.013

Hague, T., Tillett, N. D., & Wheeler, H. (2006). Automated Crop and Weed Monitoring in Widely Spaced Cereals. *Precision Agriculture*, *7*(1), 21–32. doi:10.1007/s11119-005-6787-1

Hengl, T. (2006). Finding the right pixel size. *Computers & Geosciences*, *32*(9), 1283–1298. doi:10.1016/j.cageo.2005.11.008

Herwitz, S. ., Johnson, L. ., Dunagan, S. ., Higgins, R. ., Sullivan, D. ., Zheng, J., et al. (2004). Imaging from an unmanned aerial vehicle: agricultural surveillance and decision support. *Computers and Electronics in Agriculture*, *44*(1), 49–61. doi:10.1016/j.compag.2004.02.006

Hunt, Jr., E. R., Hively, W. D., Fujikawa, S. J., Linden, D. S., Daughtry, C. S. T., & McCarty, G. W. (2010). Acquisition of NIR-Green-Blue Digital Photographs from Unmanned Aircraft for Crop Monitoring. *Remote Sensing*, *2*(1), 290–305. doi:10.3390/rs2010290

Kataoka, T., Kaneko, T., Okamoto, H., & Hata, S. (2003). Crop growth estimation system using machine vision. In *2003 IEEE/ASME International Conference on Advanced Intelligent Mechatronics, 2003. AIM 2003. Proceedings* (Vol. 2, pp. b1079–b1083 vol.2). Presented at the 2003 IEEE/ASME International Conference on Advanced Intelligent Mechatronics, 2003. AIM 2003. Proceedings. doi:10.1109/AIM.2003.1225492

Laliberte, A., & Rango, A. (2006). Unmanned Aerial Vehicles (UAVs) for Rangeland Remote Sensing. Presented at the 3rd Annual Symposium research Insights in Semiarid Ecosystems. http://www.tucson.ars.ag.gov/rise/2006/Posters/LalibertePoster.pdf. Accessed 10 August 2012

López-Granados, F. (2011). Weed detection for site-specific weed management: mapping and real-time approaches. *Weed Research*, *51*(1), 1–11. doi:10.1111/j.1365-3180.2010.00829.x

Martín, M. P., Barreto, L., & Fernández-Quintanilla, C. (2011). Discrimination of sterile oat (Avena sterilis) in winter barley (Hordeum vulgare) using QuickBird satellite images. *Crop Protection*, *30*(10), 1363–1369. doi:10.1016/j.cropro.2011.06.008

Meyer, G. E., & Neto, J. C. (2008). Verification of color vegetation indices for automated crop imaging applications. *Computers and Electronics in Agriculture*, *63*(2), 282–293. doi:10.1016/j.compag.2008.03.009

Motohka, T., Nasahara, K. N., Oguma, H., & Tsuchida, S. (2010). Applicability of Green-Red Vegetation Index for Remote Sensing of Vegetation Phenology. *Remote Sensing*, *2*(10), 2369–2387. doi:10.3390/rs2102369

Otsu, N. (1979). A Threshold Selection Method from Gray-Level Histograms. *IEE Transactions on systems, man, and cybernetics*, *9*(1), 62–66.

Peña-Barragán, J. M., Ngugi, M. K., Plant, R. E., & Six, J. (2011). Object-based crop identification using multiple vegetation indices, textural features and crop phenology. *Remote Sensing of Environment*, *115*(6), 1301–1316. doi:10.1016/j.rse.2011.01.009

Rasmussen, J., Nielsen, J., Garcia-Ruiz, F., Christensen, S., & Streibig, J. C. (2013). Potential uses of small unmanned aircraft systems (UAS) in weed research. *Weed Research*, *53*(4), 242–248. doi:10.1111/wre.12026

Romeo, J., Pajares, G., Montalvo, M., Guerrero, J. M., Guijarro, M., & de la Cruz, J. M. (2013). A new Expert System for greenness identification in agricultural images. *Expert Systems with Applications*, *40*(6), 2275–2286. doi:10.1016/j.eswa.2012.10.033

Sakamoto, T., Shibayama, M., Kimura, A., & Takada, E. (2011). Assessment of digital camera-derived vegetation indices in quantitative monitoring of seasonal rice growth. *ISPRS Journal of Photogrammetry and Remote Sensing*, *66*(6), 872–882. doi:10.1016/j.isprsjprs.2011.08.005

Samseemoung, G., Soni, P., Jayasuriya, H. P. W., & Salokhe, V. M. (2012). Application of low altitude remote sensing (LARS) platform for monitoring crop growth and weed infestation in a soybean plantation. *Precision Agriculture*, *13*(6), 611–627. doi:10.1007/s11119-012-9271-8

Society, C. R. S. (1996). *26th International Symposium on Remote Sensing of Environment*. Canadian Aeronautic and Space Institute.

Thorp, K. R., & Tian, L. F. (2004). A Review on Remote Sensing of Weeds in Agriculture. *Precision Agriculture*, *5*(5), 477–508. doi:10.1007/s11119-004-5321-1

Torres-Sánchez, J., López-Granados, F., De Castro, A. I., & Peña-Barragán, J. M. (2013). Configuration and Specifications of an Unmanned Aerial Vehicle (UAV) for Early Site Specific Weed Management. *PLoS ONE*, *8*(3), e58210. doi:10.1371/journal.pone.0058210

Woebbecke, D. M., Meyer, G. E., Von Bargen, K., & Mortensen, D. A. (1995). Color indices for weed identification under various soil, residue, and lighting conditions. *Transactions of the ASAE*, *38*(1), 259–269.

Xiang, H., & Tian, L. (2011). Development of a low-cost agricultural remote sensing system based on an autonomous unmanned aerial vehicle (UAV). *Biosystems Engineering*, *108*(2), 174–190. doi:10.1016/j.biosystemseng.2010.11.010

Xiao, J., & Moody, A. (2005). A comparison of methods for estimating fractional green vegetation cover within a desert-to-upland transition zone in central New Mexico, USA. *Remote Sensing of Environment*, *98*(2–3), 237–250. doi:10.1016/j.rse.2005.07.011

Yang, C., Everitt, J. H., & Bradford, J. M. (2006). Comparison of QuickBird Satellite Imagery and Airborne Imagery for Mapping Grain Sorghum Yield Patterns. *Precision Agriculture*, *7*(1), 33–44. doi:10.1007/s11119-005-6788-0

Yu, Z., Cao, Z., Wu, X., Bai, X., Qin, Y., Zhuo, W., et al. (2013). Automatic image-based detection technology for two critical growth stages of maize: Emergence and three-leaf stage. *Agricultural and Forest Meteorology*, *174–175*, 65–84. doi:10.1016/j.agrformet.2013.02.011

CAPÍTULO 3

AN AUTOMATIC OBJECT-BASED METHOD FOR OPTIMAL THRESHOLDING IN UAV IMAGES: APPLICATION FOR VEGETATION DETECTION IN HERBACEOUS CROPS

An automatic object-based method for optimal thresholding in UAV images: Application for vegetation detection in herbaceous crops. *Computers and Electronics in Agriculture*, 114, 43–52. doi:10.1016/j.compag.2015.03.019

1. RESUMEN

En agricultura de precisión, la detección de la vegetación en cultivos herbáceos en fase temprana es un primer y crucial paso para afrontar objetivos como el conteo de plantas para la monitorización de la germinación, o para la detección de malas hierbas en el ámbito del manejo localizado de malas hierbas en fase temprana. La muy alta resolución espacial de las imágenes tomadas por vehículos aéreos no tripulados (UAV por sus siglas en inglés), y las potentes herramientas suministradas por el análisis de imagen orientado a objetos (OBIA por sus siglas en inglés) son la clave en la consecución de la detección de vegetación en cultivos herbáceos en fase temprana. El presente trabajo de investigación desarrolla un innovador algoritmo OBIA de cálculo de umbrales basado en el método de Otsu, y estudia como los resultados del algoritmo son influenciados por los diferentes parámetros de segmentación de la imagen (escala, forma y compacidad). Junto a la descripción general del procedimiento, éste fue aplicado a la detección de vegetación en imágenes remotamente capturadas por un UAV con dos sensores (una cámara convencional en el visible y una cámara multiespectral) sobre campos de tres cultivos herbáceos diferentes (maíz, girasol y trigo). Se analizó el funcionamiento del algoritmo OBIA para clasificar la vegetación usando umbrales automáticamente calculados para dos índices de vegetación: el ExG y el NDVI. El parámetro de escala de la segmentación afectó a los histogramas de los índices, lo que llevó a cambios en el cálculo del umbral óptimo para los índices de vegetación. Los otros parámetros involucrados en la segmentación (forma y compacidad) mostraron menor influencia en la precisión de la clasificación. Aumentar el tamaño de los objetos conllevó un descenso en el error en la clasificación hasta que se alcanzó un óptimo. Tras este valor óptimo, incrementar el tamaño de los objetos provocó una menor precisión en la clasificación.

2. ABSTRACT

In precision agriculture, detecting the vegetation in herbaceous crops in early season is a first and crucial step prior to addressing further objectives such as counting plants for germination monitoring, or detecting weeds for early season site specific weed management. The ultra-high resolution of UAV images, and the powerful tools provided by the Object Based Image Analysis (OBIA) are the key in achieving this objective. The present research work develops an innovative thresholding OBIA algorithm based on the Otsu's method, and studies how the results of this algorithm are affected by the different segmentation parameters (scale, shape and compactness). Along with the general description of the procedure, it was specifically applied for vegetation detection in remotely-sensed images captured with two sensors (a conventional visible camera and a multispectral camera) mounted on an unmanned aerial vehicle (UAV) and acquired over fields of

three different herbaceous crops (maize, sunflower and wheat). The tests analyzed the performance of the OBIA algorithm for classifying vegetation coverage as affected by different automatically selected thresholds calculated in the images of two vegetation indices: the Excess Green (ExG) and the Normalized Difference Vegetation Index (NDVI). The segmentation scale parameter affected the vegetation index histograms, which led to changes in the automatic estimation of the optimal threshold value for the vegetation indices. The other parameters involved in the segmentation procedure (i.e., shape and compactness) showed minor influence on the classification accuracy. Increasing the object size, the classification error diminished until an optimum was reached. After this optimal value, increasing object size produced bigger errors.

3. INTRODUCTION

In precision agriculture, detecting the vegetation in herbaceous crops in early season is a first and crucial step prior to addressing further objectives such as counting plants for germination monitoring, or detecting weeds for early season site specific weed management. Discrimination of the crop plants in their first stages of development needs images at very high spatial resolution, often in the order of mm or very few cm (Hengl 2006; López-Granados 2011). Also it is required that the images can be taken at the optimal moment for the desired purpose. The most suitable tool for accomplishing both requirements is the Unmanned Aerial Vehicle (UAV); UAVs flying at low altitudes (maximum altitude allowed in the Spanish law for UAVs is 120 m) allow acquiring images with very high spatial resolution (VHSR), and the low time required for launching an unmanned aerial mission makes it possible to take images just at the required moment. Furthermore, it has been demonstrated that vegetation indices (VI) calculated from UAV images are suitable for vegetation detection in herbaceous crops (Torres-Sánchez *et al*. 2014). VIs are the product of arithmetic operations performed with spectral information from the radiation reflected by the vegetation, and these operations enhance the spectral difference between classes.

VHSR images represent a challenge for classification because, unlike in lower resolution images, single pixels no longer capture the characteristics of the classification targets. Additionally, these images show higher intra-class spectral variability (Aplin 2006; Woodcock and Strahler 1987). For dealing with this spectral variability a new paradigm has emerged in recent years, the Object Based Image Analysis (OBIA) (Blaschke 2010). OBIA works with groups of homogeneous and contiguous pixels (called objects), which reduces the intra-class spectral variability caused by crown textures, gaps, and shadows. The basic idea of this process is to first group spatially adjacent pixels into spectrally homogeneous objects, and then conducting the classification using objects as the minimum processing units. Several studies (Addink *et al*. 2007; Drăguţ *et al*. 2010; Karl and Maurer

2010; Moffett and Gorelick 2013) have focused on the importance of segment size, and have noted its influence on classification accuracy. The influence of size is related to the spectral heterogeneity of the objects; higher object size causes an increase in internal heterogeneity of the objects because they include more pixels. Therefore, it is important to study how the selection of the parameters used for defining the segmentation process can affect vegetation detection in UAV images. As Hay et al. (Hay *et al*. 2005) pointed out, 'the real challenge is to define appropriate segmentation parameters (typically based on spectral homogeneity, size, or both) for the varying sized, shaped, and spatially distributed image-objects composing a scene, so that segments can be generated that satisfy user requirements.'

For achieving accurate and automatic vegetation detection, along with the correct segmentation parameters, it is necessary to find an automatic and efficient method to look for the VI threshold value that sets the breakpoint between vegetation and bare soil. There are several automatic methods for threshold calculation, among which Otsu's (Otsu 1979) method is one of the most utilized for agronomical issues (Guijarro *et al*. 2011; Meyer and Neto 2008). It assumes that the image contains two classes of pixels (bare soil and vegetation when considering crop scenarios) and then calculates the optimum threshold based on minimizing combined spread (intra-class variance). It has the advantages of being easy to compute, stable, and not dependent on other a priori information. Furthermore, automation of the thresholding by using Otsu's algorithm improves the transferability of the OBIA rule set to other images (Tiede *et al*. 2010) and it is useful to address the spatial variability of spectral values in VHSR images. However, despite the good results of the Otsu's method in per-pixel analysis, it has not been described and tested in an OBIA environment.

Taking into account the information and problems presented above, the objectives of the present study are to: 1) develop an automatic thresholding algorithm based on the Otsu´s method in an object-based framework, 2) study the influence of object size and other segmentation parameters in the classification outputs as affected by the type of image/camera/spatial resolution, and 3) evaluate the relationship between spectral thresholding and the object size in remote images with ultra-high spatial resolution. Finally, the resulting OBIA algorithm was tested for vegetation detection in UAV images acquired over three different crops in early season with two different sensors.

4. MATERIALS AND METHODS

4.1. Description of the automatic thresholding OBIA algorithm

The rule set for automatic thresholding was developed by using the Cognition network language of the software eCognition Developer 8.9. This language offers a multitude of options

related to OBIA (Hay and Castilla 2008). It supports programming tasks such as branching, looping, and the use of variables. A general scheme of the procedure is shown in the figure 1.

The first step in OBIA is the segmentation of the image. The image was segmented by using the multiresolution segmentation algorithm (MRSA) implemented in eCognition. MRSA is a bottom-up segmentation algorithm based on a pairwise region merging technique. It starts with one-pixel objects and merges them through an iterative process that minimizes the internal weighted heterogeneity of each object. In each iteration, objects are merged if the newly generated object does not exceed a heterogeneity threshold defined by the following algorithm settings: 1) scale parameter, 2) color/shape, and 3) smoothness/compactness. These factors can be controlled by the user:

- Scale parameter, which limits the heterogeneity of the final objects.
- Color/shape weights, which control how much the segmentation is based on image spectral (color) information *vs* object shape information.
- Smoothness/compactness weights, which control how much the object shape tends to be spatially compact vs spectrally homogeneous (smooth) but less compact.

Once the image is segmented, the value of the discriminant feature that is going to be thresholded is calculated and stored for each segment as an object variable. Then, the minimum value of this variable is searched and stored as a scene variable for subsequent use as the initial threshold to start the loop that leads to optimum threshold detection. Image objects with feature values higher than the initial threshold (all of them at the beginning of the loop) are classified as "foreground", and the remaining objects are labelled as "background". In the next step, the means of the feature for "foreground" and "background" objects are calculated and stored as scene variables, called "mean_f" and "mean_b", respectively. Then, the weight of each class in the image is calculated and stored as two other scene variables: Wf and Wb, for the "foreground" and "background" classes, respectively:

$$Wf = \frac{Number\ of\ foreground\ objects}{Total\ number\ of\ objects} \qquad (1)$$

$$Wb = \frac{Number\ of\ background\ objects}{Total\ number\ of\ objects} \qquad (2)$$

Once all of these variables are stored, and following the indications of Otsu's thresholding method (Otsu 1979), the between-class variance of the image (BCV) is calculated and stored as another scene variable called BCV:

$$BCV = Wf \times Wb \times (mean\_b - mean\_f)^2 \qquad (3)$$

When BCV is calculated for the initial threshold, the image objects are unclassified, and the initial threshold is incremented an amount named "increment". The "increment" parameter is user-configurable and its value will depend on the image histogram amplitude. All of the previous calculations are repeated for the new threshold, and its BCV is compared to that from the initial threshold. If the new BCV is higher than the previous one, its associated threshold is stored as "Opt threshold" and all the process is repeated. This "if-then" loop is stopped when all the possible values of the threshold are tested. The final threshold is the one that maximized the BCV, which had been already stored as "Opt threshold".

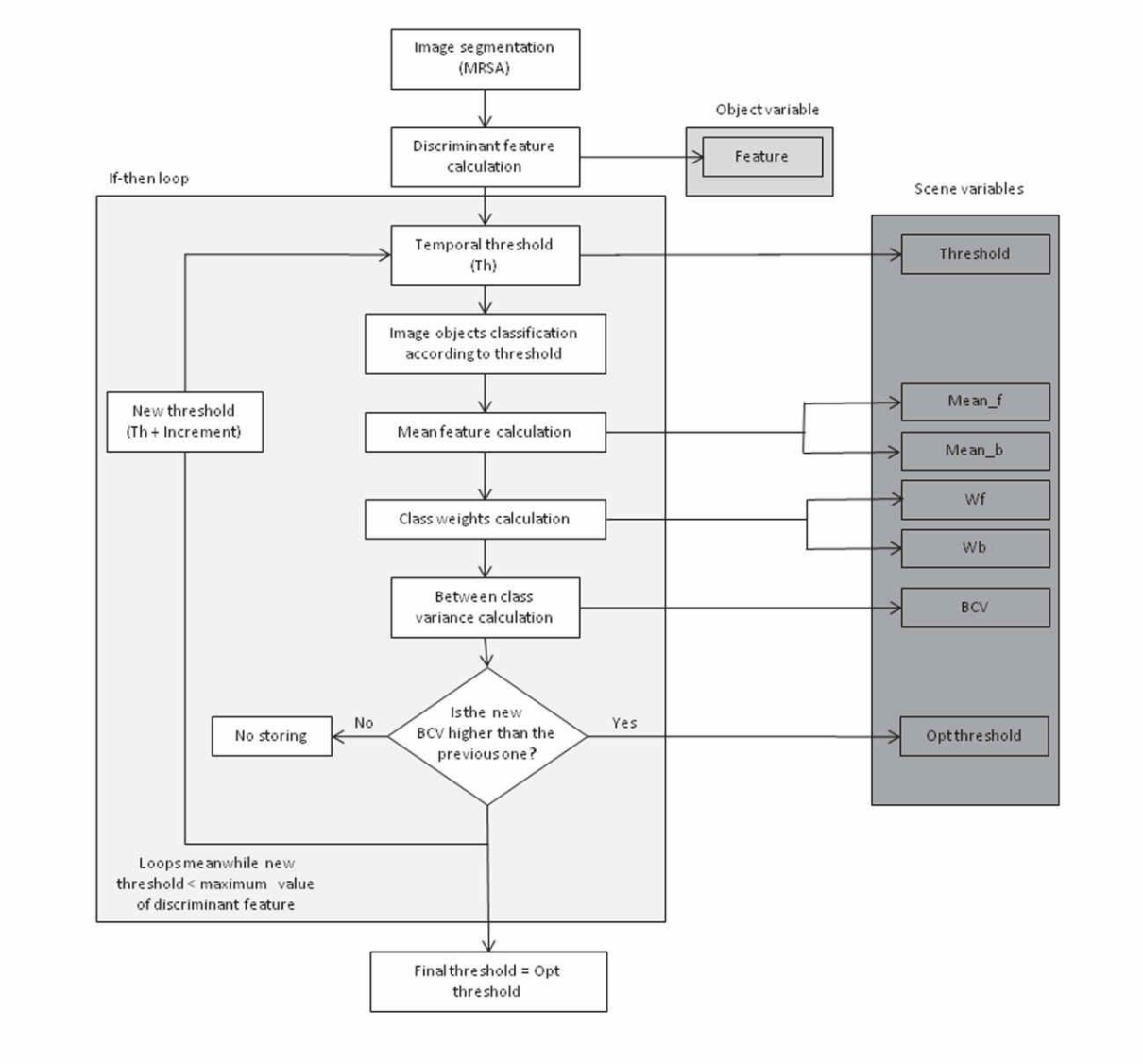

Figure 1. *Flowchart of the automatic thresholding method.*

4.2. Rule set application for vegetation detection

The rule set was applied to remotely-sensed images captured with two different sensors mounted on a UAV and acquired over fields of three different winter and summer herbaceous crops

(maize, sunflower and wheat). The plants were in their early growth stages that corresponds to the principal stage 1 (leaf development) of the "Biologische Bundesanstalt, Bundessortenamt und CHemische Industrie" (BBCH) extended scale (Meier 2001). Due to the differences on crop row separation (17 cm, 70 cm and 75 cm for wheat, sunflower and maize, respectively) and plant morphology (wheat and maize are monocotyledonous plants, and sunflower is a dicot), the images were very different between them, forming a complete image set to test the algorithm.

The remote images were acquired at 30 m flight altitude with two different sensors mounted separately in a quadrocopter UAV, model md4-1000 (microdrones GmbH, Siegen, Germany). The flight altitude and moment were in agreement with that used in Peña *et al*. (2013) for weed detection in a maize field. One of the used sensors was a conventional visible camera, model Olympus PEN E-PM1 (Olympus Corporation, Tokyo, Japan), which acquires 12-megapixel images in true Red-Green-Blue (RGB) colour with 8-bit radiometric resolution. The other sensor was a multispectral camera, model Tetracam mini-MCA-6 (Tetracam Inc., Chatsworth, CA, USA), composed of six individual digital channels arranged in a 2×3 array, configured to acquire images with 8-bit radiometric resolution. The camera has user configurable band pass filters (Andover Corporation, Salem, NH, USA) of 10-nm full-width at half maximum and centre wavelengths at B (450 nm), G (530 nm), R (670 and 700 nm), R edge (740 nm) and near-infrared (NIR, 780 nm). Both images were stored in TIFF format. Detailed information about the configuration of the UAV flights and specifications of the vehicle and the cameras can be found in Torres-Sánchez *et al*. (2013).

Variability in crops characteristics and in the spectral and spatial image resolutions allow us to affirm that the thresholding OBIA algorithm was tested in six different scenarios. The selected images covered an area of about 250 m^2 for each crop. These images were georeferenced by identifying ten ground control points and measuring their coordinates with a GPS receiver. These coordinates were then introduced into the images using ENVI software (ENVI 4.4., Research Systems Inc., Boulder, CO, USA). Due to the technical characteristics of each sensor, the images had different spatial resolutions; the pixel size was 1.14 cm for the conventional camera, and 1.62 cm for the multispectral camera.

In these real scenarios, different MRSA parameters values were studied in order to quantify their efficiency for discriminating vegetation objects. The assignment of these parameters is easily controlled by the configuration panel of the MRSA in eCognition software. All the image bands were assigned the same weight in the MRSA, whereas the segmentation parameters were evaluated in two consecutive phases in order to study their influence on the thresholding method. Firstly, the scale parameter was independently tested by fixing the shape parameter to 0.4 (thus giving a weight of 0.6 to color) and giving an equal weight to the compactness and smoothness parameters (i.e., a

value of 0.5 each one). The scale parameter is the most important setting for controlling object size and, according to (Moffett and Gorelick 2013), it affects more strongly the segmentation results in comparison to the minor impact of the remaining settings. In this first test, the scale values ranged from 2 to 40 in increments of 2 units; these values generated a set of segmentations including a big range of situations, from objects smaller than a crop plant, to objects including several plants and even bare soil. A value of 1, which equates to a pixel-oriented analysis, was also tested. Secondly, once the scale value that produced best classification accuracy was determined, shape/color and compactness/smoothness influence on classification was also studied by fixing the scale parameter to the best value obtained previously. In this second test, five values covering the whole range of possible values (0.1, 0.3, 0.5, 0.7 and 0.9) were assigned to each parameter of the MRSA algorithm, obtaining 25 new output segmentations.

Summarizing, twenty one different scale values were applied to the image dataset, which generated 126 output segmentations. Then, the thresholding method was tested on the Excess Green (ExG) images (visible-range camera) and on the Normalized Difference Vegetation Index (NDVI) images (multispectral camera) with the objective of separating between vegetation and bare-soil objects (Equations 4 and 5, respectively). Several previous studies have concluded that these vegetation indices accentuate vegetation in the remotely-sensed images (Guijarro *et al*. 2011; Peña *et al*. 2013; Torres-Sánchez *et al*. 2014). A threshold increment of 0.01 was used in each algorithm step due to the narrow range of the selected indices.

$$ExG = 2g - r - b; being\ g = \frac{G}{R+G+B}; r = \frac{R}{R+G+B}; b = \frac{B}{R+G+B} \quad (4)$$

$$NDVI = \frac{NIR-R}{NIR+R} \quad (5)$$

4.3. Image analysis

4.3.1. Influence of scale parameter on segmentation and thresholding rule set

The influence of the scale parameter on the segmentation output was quantified, and relationship between segmentation scale and averaged object size was plotted for each image. For the analyzed images, histograms of the vegetation index values in the segmented images were constructed for four different scale values in order to analyze how the size of the objects affects the distribution of the values of the spectral indices. Additionally, for studying the influence of the size of the objects in the automatic thresholding, a dot plot was made depicting the relationship between the scale and the threshold calculated by the rule set. All of the graphics and data analysis were performed using JMP software (SAS, Cary, NC, USA).

4.3.2. Evaluation of the OBIA algorithm for quantifying vegetation coverage

To evaluate the results of the discrimination between vegetation and bare soil attained by each combination of segmentation settings (see section 2.2), a systematic sampling procedure was conducted. In order to record real vegetation coverage, a vector shape file containing 30 square sampling frames, 1x1 m in size, and regularly distributed in every image was created using ArcGis software (ESRI, Redlands, CA, USA). The sampling area was representative of the vegetation observed in the experimental fields. Vegetation was manually delineated in all the sampling frames of the images in order to collect ground-truth data, *i.e.*, the real vegetation coverage.

The classification outputs were evaluated by calculating the difference between the percentage of the vegetation estimated by OBIA and the observed vegetation in the sampling frames (Equation 6). Values lower than 0 indicated under-estimation of the vegetation coverage and values higher than 0 indicated over-estimation. The classification error of the 30 frames was averaged for every segmented image.

$$Error(\%) = \frac{Estimated\ vegetation\ \% - Ground\ truth\ vegetation\ \%}{Ground\ truth\ vegetation\ \%} \times 100 \qquad (6)$$

In order to show the efficiency of the presented algorithm, required time for thresholding was measured for each one of the images, considering the scale parameter leading to the lower classification error in each case. These computations were done using a standard computer with 16 GB of RAM, an Intel Core i5 (Intel, Santa Clara, CA, USA) processor and a graphic card of 1 GB.

5. RESULTS AND DISCUSSION

5.1. Object size as affected by the segmentation scale parameter

Figures 2 and 3 show the numerical and graphical variation, respectively, of the object size according to different scale parameter values after the application of the MRSA segmentation procedure. Object size was directly related to the scale parameter in all the cases, showing a different degree of variation for each type of image and crop. As stated by Karl and Maurer (2010), the scale parameter in the MRSA is used to control the final size of the objects (Baatz and Schaepe 2000), and the use of coarser scales leads to the generation of larger objects. However, as noted by Moffet and Gorelick (2013) and Hay *et al*. (2005), it is not prescriptive of the final object size with independence of the image.

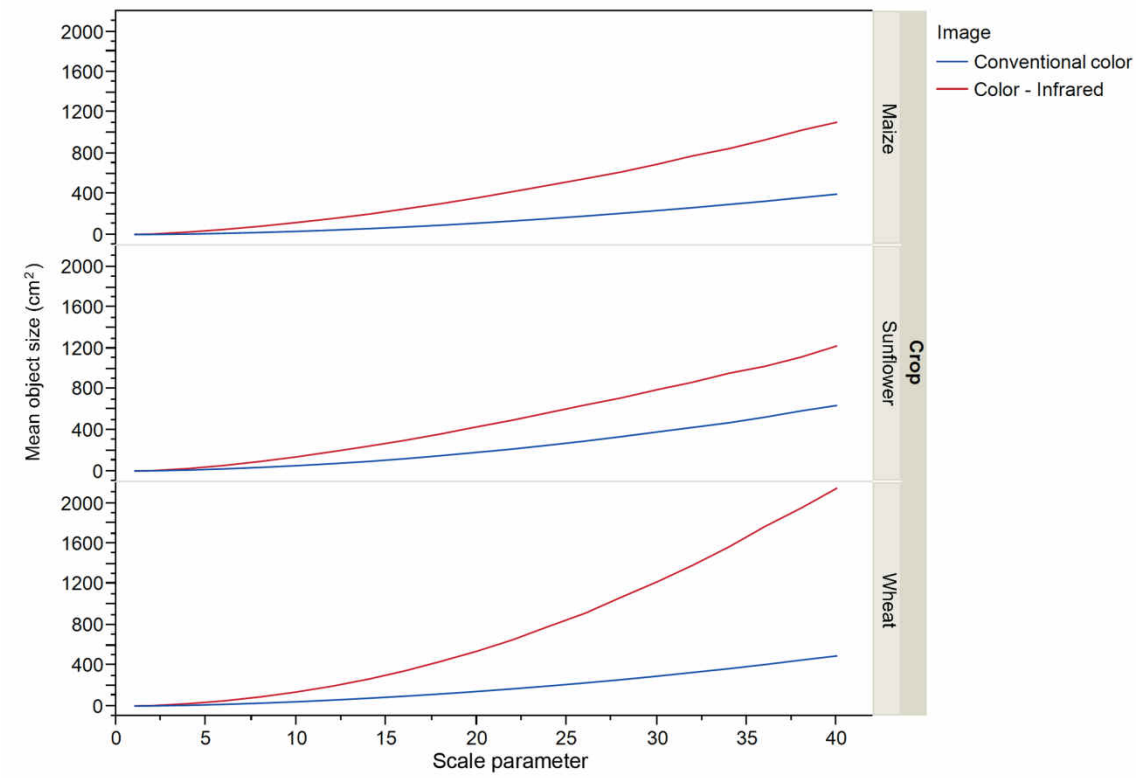

Figure 2. *Effect of the scale parameter on the size (cm^2) of the objects generated by the MRSA for the analyzed images.*

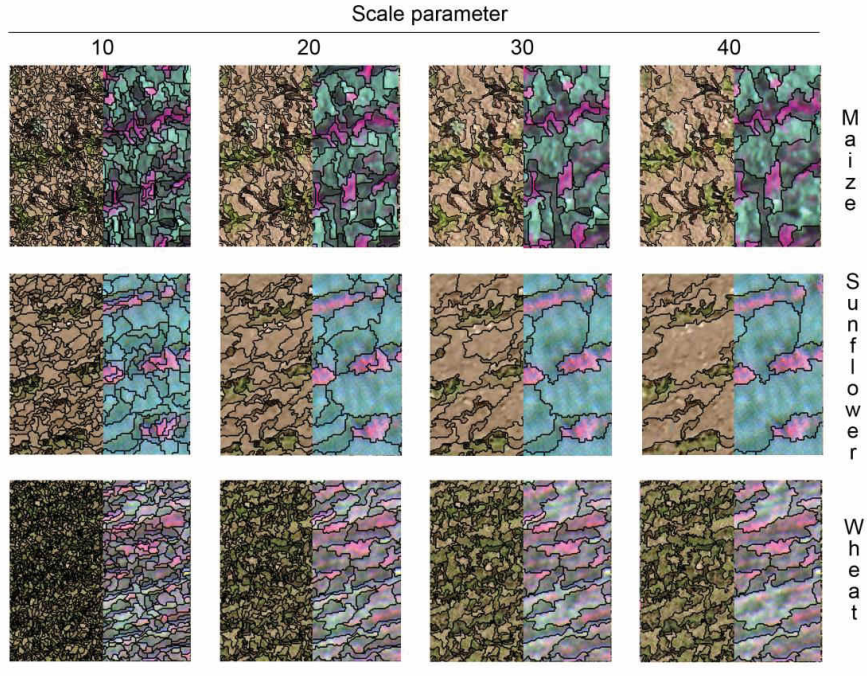

Figure 3. *Segmentation outputs with different values of the segmentation scale parameter as affected by type of image (conventional-color from the visible camera in the left and color-infrared from the multispectral camera in the right) and type of crop. As a measure reference, the distance between crop rows was 70 cm in sunflower, 75 cm in maize, and 17 cm in wheat.*

These differences among the images were due to the different spatial resolutions of both sensors, and to the intrinsic agronomic characteristics of each studied crop. In the conventional color images, the biggest object size ranged from 398 cm^2 in maize to 641 cm^2 in sunflower. The degree of variation was higher in the multispectral images, in which the biggest object size ranged from 1,105 cm^2 in maize to the 2,142 cm^2 in wheat. This higher size range was because the lower resolution of the multispectral camera is not enough for performing a good isolation of plants and bare soil, leading to the creation of a big amount of pixels with mixed spectral values of both classes. Therefore, the spectral homogeneity of the image was higher and the objects created by the MRSA, which takes the homogeneity into account with the scale parameter, were bigger. Consequently, the largest objects were generated in the multispectral image of wheat, where the small size of the plants and the low resolution of the sensor, lead to a higher homogeneity in the image.

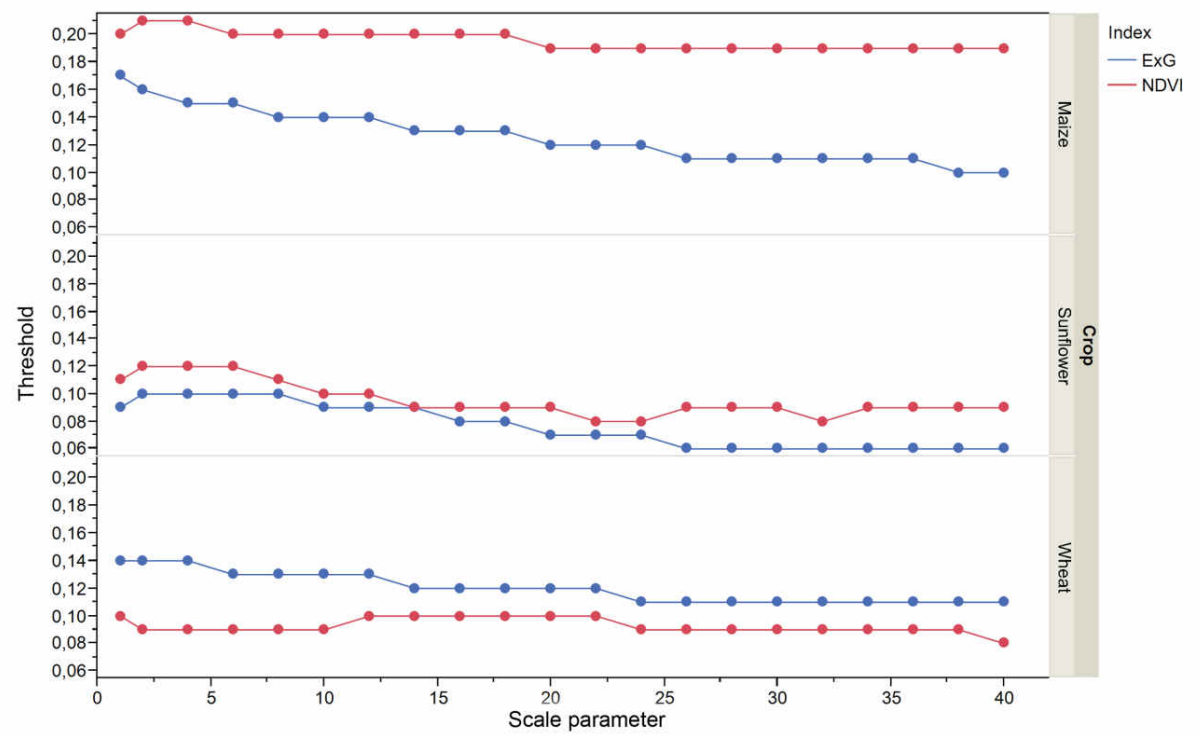

Figure 4. *Influence of the segmentation scale parameter on the threshold determined by the OBIA rule set for each vegetation index.*

5.2. Automatic threshold value as affected by the scale parameter

Figure 4 shows the influence of scale parameter on the threshold value calculated by the OBIA algorithm. In the three crops, the optimal thresholds established by the rule set for ExG slightly decreased when then scale parameter increased. This trend was more pronounced in maize (with ExG values between 0.17 and 0.10), followed by sunflower (0.10 – 0.06) and wheat (0.14 - 0.11). This downward trend might be caused by the fact that using low scale parameter values created small

vegetation objects, and the ones located at the centre of the plants usually have high vegetation index values, leading the thresholding method to select higher thresholds. When using higher scale parameter values, these vegetation objects are merged with the ones that are located at the plant borders and that have lower vegetation index values due to the mixture with bare soil objects. Consequently, the vegetation objects that cover complete plants have lower ExG values and the thresholding method selects lower thresholds.

In the case of the NDVI threshold values, a clear trend was not observed, and the values oscillated around a threshold. This difference could be due to the higher spectral separability between vegetation and bare soil achieved with NDVI.

5.3. Influence of the scale parameter on the vegetation index histograms

Figures 5 and 6 show the histograms of the values of the vegetation indices for the different segmented images. The histograms were calculated from the two sensors, but only those from the values of 10, 20, 30 and 40 along the scale are shown so as not to overwhelm the figures.

The range of the histograms showed a decreasing trend for both vegetation indices. This trend was stronger for the ExG values, as it can be viewed in Table 1. Histogram range reductions for ExG index were of 35%, 77% and 52% for maize, sunflower and wheat, respectively. For NDVI index, the range reductions were 19%, 17% and 27%, respectively. Narrowing of the ranges was probably for the same reason explaining the downward trend in ExG thresholds in relation to the scale parameter. This is because, when using lower scale parameter values, there are small objects that include pixels with extreme vegetation index values. However, when using higher scale parameter values, these small objects are integrated with larger ones, and the extreme values are smoothed because they are averaged with the other pixels inside the larger object. Consequently, at higher scales, extreme values disappear from the histogram and its range decreases. The lower degree of range reduction for the NDVI histograms could be related to the lower range of possible values that are allowed by its formula (Equation 5); while ExG can take values from -2 to 2, NDVI only takes values between -1 and 1.

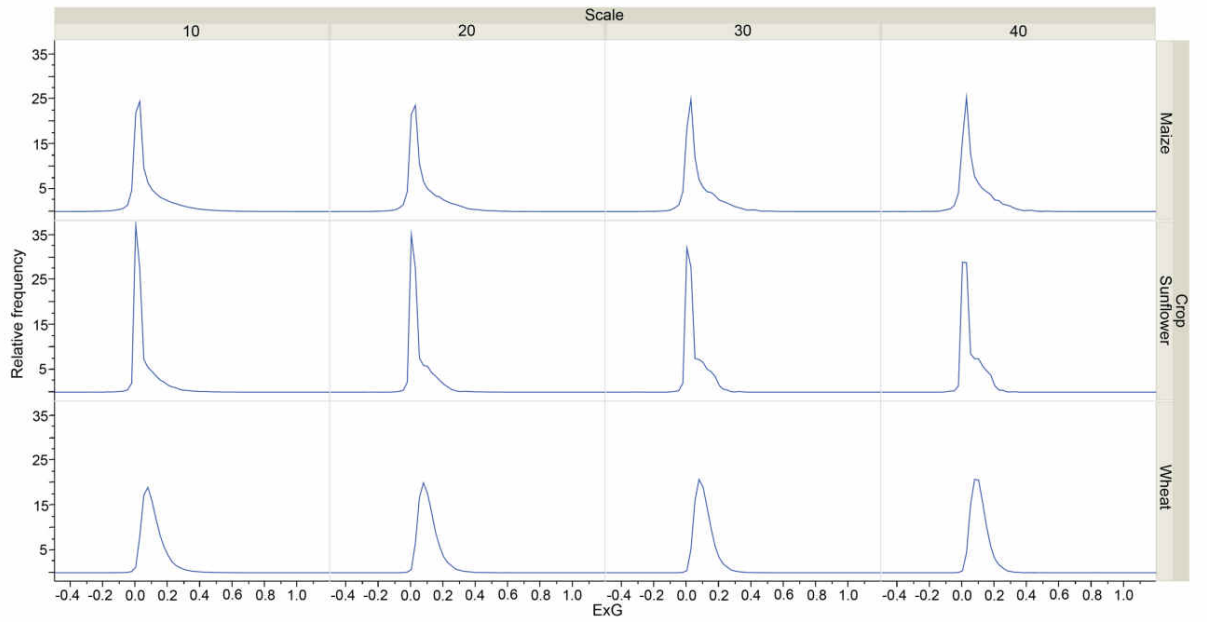

Figure 5. *Histograms of the values of the ExG index in the images segmented by different scale parameters from the conventional camera.*

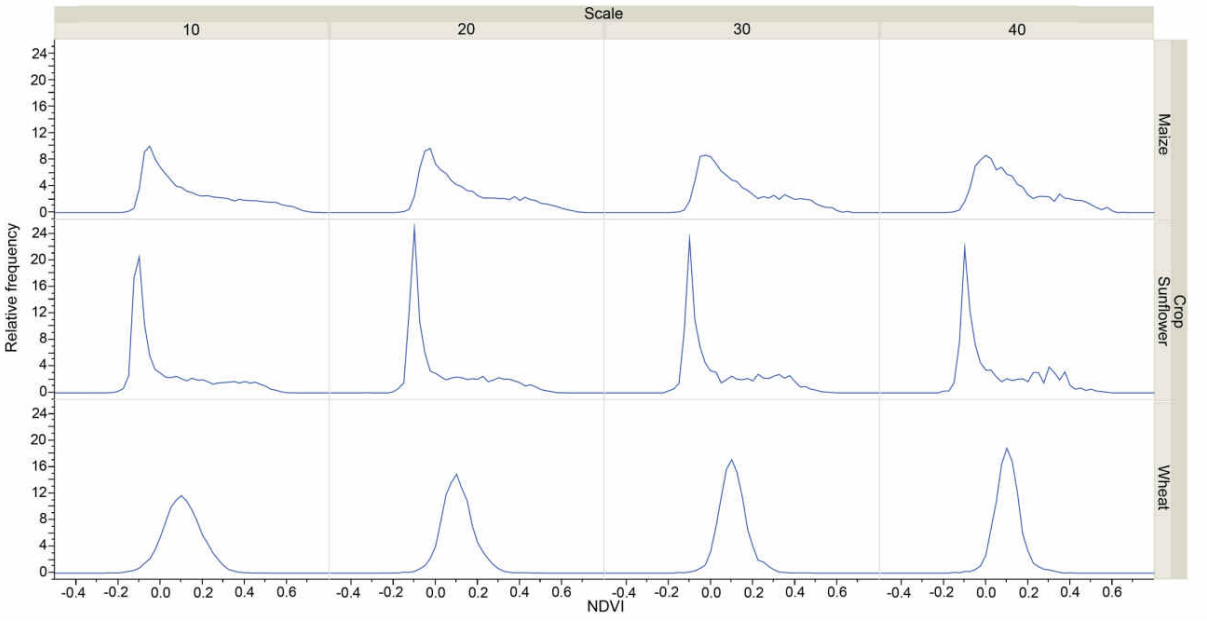

Figure 6. *Histograms of the values of the NDVI index in the images segmented by different scale parameters from the multispectral camera.*

Table 1. *Some descriptive statistics of the histograms (N: number of samples; Min: minimum; Max: Maximum).*

Crop	Index	Scale	N	Min	Max	Range
Maize	**ExG**	10	76 609	-1.000	1.206	2.206
		20	21 972	-1.000	0.839	1.839
		30	10 487	-1.000	0.638	1.638
		40	6 236	-0.807	0.638	1.444
	NDVI	10	20 836	-0.274	0.748	1.022
		20	6 879	-0.189	0.685	0.874
		30	3 594	-0.185	0.646	0.832
		40	2 252	-0.185	0.646	0.832
Sunflower	**ExG**	10	29 488	-0.897	0.887	1.783
		20	8 600	-0.897	0.571	1.468
		30	4 121	-0.330	0.348	0.678
		40	2 456	-0.109	0.302	0.412
	NDVI	10	9 466	-0.327	0.611	0.938
		20	3 053	-0.327	0.592	0.919
		30	1 661	-0.219	0.561	0.779
		40	1 079	-0.219	0.561	0.779
Wheat	**ExG**	10	106 462	-0.673	1.158	1.831
		20	32 072	-0.372	0.818	1.191
		30	15 682	-0.174	0.818	0.992
		40	9 336	-0.052	0.818	0.870
	NDVI	10	25 353	-0.271	0.477	0.748
		20	6 554	-0.261	0.477	0.738
		30	2 895	-0.159	0.453	0.613
		40	1 649	-0.159	0.390	0.549

Histogram shape was constant for the ExG values in all of the segmented images, except for sunflower whose shape histogram varied slightly. By contrast, the increases in the scale parameter changed the NDVI histograms from a unimodal distribution to a multimodal distribution for maize and sunflower, representing the two classes in the image: bare soil for the peak with the lower NDVI value and vegetation for the peak with the higher value. This hypothesis is reinforced because the threshold calculated by the algorithm in these images is located near the valley between the two peaks of the histogram corresponding to the two classes in the image. The shift in the histogram did not appear for wheat because the image objects covered vegetation and bare soil and therefore their spectral values were mixed for the studied scale parameter values. Hay *et al*. (2005) detected a similar trend in the analysis of aerial forest images. In their work, the histograms developed a multimodal distribution whose peaks corresponded to the dominant object classes in the image. As they stated, this type of histogram information is only available when using OBIA. The shift in histogram shape affected the NDVI values but not the ExG values. This could be due to the higher

spectral separability between the vegetation and bare soil that can be achieved using information from the NIR zone of the electromagnetic spectrum, in which live vegetation exhibits a very characteristic response. ExG histograms for sunflower did not reach a multimodal distribution, but it can be observed that they show a tail for the larger scale parameter values. Probably, this is due to the fact that sunflower plants (or group of plants) are more easily isolated from their environment because it is a dicot crop and has broad stalked leaves and more compact shape compared with monocots. That is, shape of sunflower plants is nearly similar to a circle, whereas maize plants have elongate stalkless leaves and present a shape similar to a star with peaks, so the ExG values are more aggregated in a closed area.

5.4. Vegetation detection

5.4.1. Classification accuracy as affected by segmentation scale

Differences in classification error with respect to object size, and consequently, to the scale parameter, for the three crops are presented in Figure 7. Object size influenced the quality of the classification in all cases. For ExG in all crops, small objects (i.e., small scale parameter values) led to an under-estimation of the vegetation. This under-estimation tended to diminish as the scale parameter increased, and the classification error was near zero for objects whose sizes were nearly the average size of the plants in the image. The best scale values for the conventional color image were 20 (96 cm^2), 18 (278 cm^2) and 4 (11 cm^2) for maize, sunflower and wheat, respectively (classification outputs for these values can be viewed in figure 8). Over-estimation of the vegetation occurred for the larger object sizes. Changes in the classification error with scale parameter value showed a similar trend to that described in other works (Addink *et al*. 2007; Karl *et al*. 2010; Kim *et al*. 2011); as the object size increased, the error decreased until an optimum was reached, after which increasing the object size resulted in greater errors. This is indicative of the existence of an optimum segmentation size related to classification quality. Kim *et al*. (2011) stated that the average size of image objects is similar to that of the targeted ground features in an optimal segmentation.

For the color-infrared image the best scale parameter values were 36 (331 cm^2), 12 (176 cm^2), and 1 (2 cm^2) for maize, sunflower and wheat, respectively (classification outputs for these values can be viewed in figure 8). There was not a clear trend relating object size and classification error for all the crops. This discrepancy with the results from the visible-range camera could be due to the lower spatial resolution of the multispectral camera, which would necessitate working with bigger objects. In maize the classification error diminished with the growing of the object size, reaching a value near to zero when the generated segments comprised larger vegetation areas, such as parts of crop rows or weed patches. The classification error was very low for all object sizes in sunflower, with optimal values close to a scale parameter value of 12 (176 cm^2); this is because the compactness of

the sunflower plants, and the homogeneity of the NDVI values inside them led in all cases to segmentations in which the resulting objects almost did not cover bare soil areas. In wheat, the lower classification error for the multispectral image was achieved for the scale parameter of 1, which is equal to a pixel based analysis; this is due to the small size of the wheat plants, whose pixels can be only isolated in the multispectral resolution with objects of one pixel size.

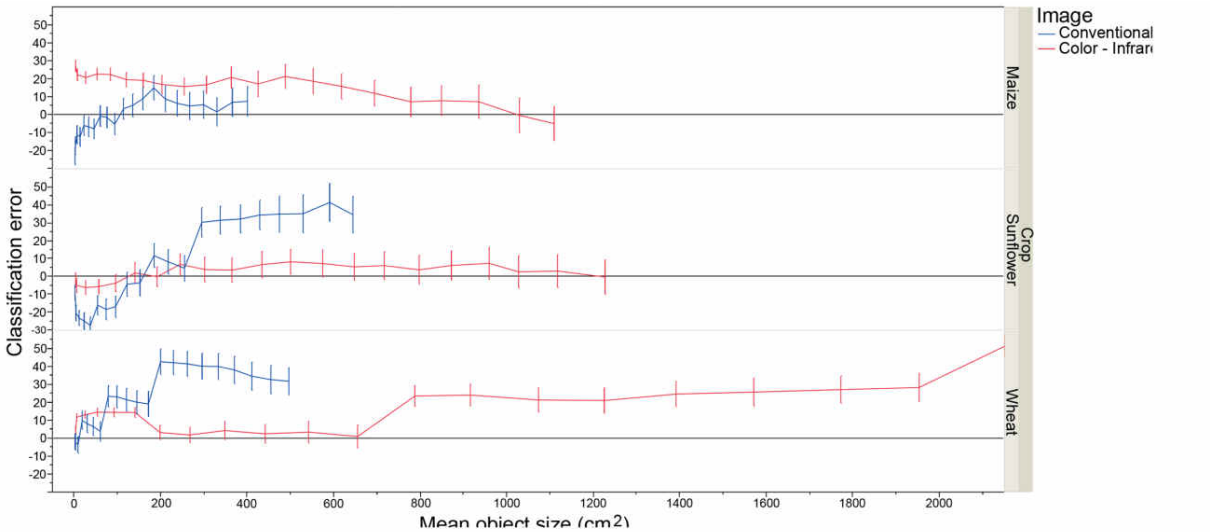

Figure 7. *Classification error (and its associated standard error) as affected by object size and type of image. 1) Conventional-color image from the visible camera, at 1.14 cm/pixel, and 2) color-infrared image from the multispectral camera, at 1.62 cm/pixel.*

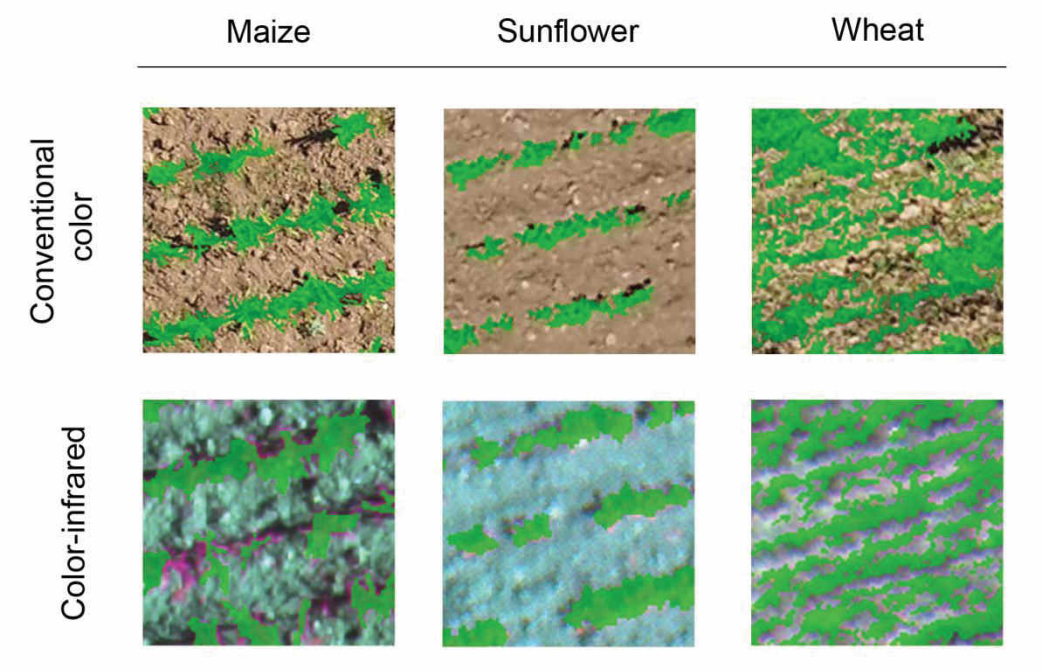

Figure 8. *Classification outputs for the best scale parameter for each crop and sensor.*

The time spent in thresholding each image for the scale parameter leading to the lower classification error was under one second in most cases, and in four of them was less than half

second (table 2). This processing speed makes the algorithm suitable for implementation in more complex classification algorithms needing vegetation detection as an intermediate step, such as the ones developed for weed detection in herbaceous crops in early season (Peña *et al*. 2013). The only exception for these low processing times was wheat in the color-infrared image, because the selected scale parameter generated small objects, leading the algorithm to consider a higher amount of objects in its looping process and, consequently, to consume more time in the thresholding operation.

Table 2. *Time spent by the thresholding algorithm in each crop. It was measured in each case for the scale parameter leading to the lower classification error.*

		Maize	Sunflower	Wheat
Conventional color	Scale parameter	20	18	4
	Thresholding time (s)	0.795	0.266	0.250
Color-infrared	Scale parameter	36	12	1
	Thresholding time (s)	0.14	0.171	33.665

5.4.2. Classification accuracy as affected by segmentation shape and compactness parameters

The best scale values for each crop and image, detailed in the previous section, were used to study the influence of shape and compactness parameters on classification accuracy. Figure 8 shows the classification error for the different combinations of values of shape and compactness. It can be seen that the errors were very similar for all the combinations. Bigger errors appeared only when the shape parameter was 0.9, especially for the color-infrared image in maize; this was because this value generated larger objects covering bare soil and vegetation, what affected their vegetation indices values because of the spectral values mixing and, consequently, led the thresholding algorithm to select an incorrect threshold. For the scale parameter studied, all the combinations of shape and compactness performed were able to delineate the plants. However, when the shape parameter was 0.9, there were objects covering bare soil and vegetation areas. These results confirm previous works from Moffett and Gorelick (2013), these authors stated that scale parameter affects more strongly the segmentation results in comparison to the minor relevance of shape and compactness.

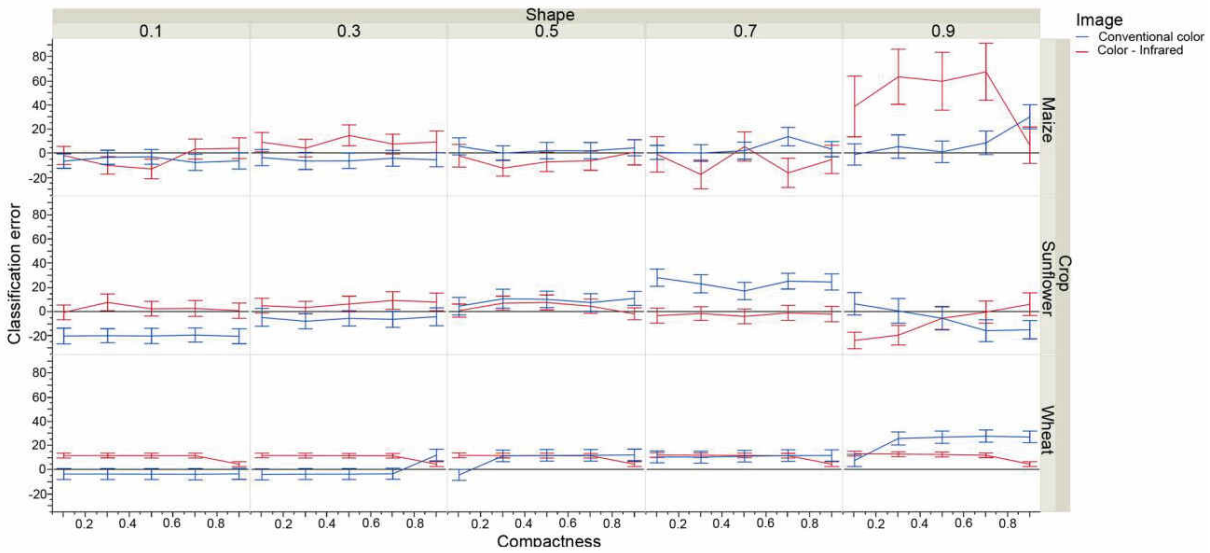

Figure 9. *Classification error (and its associated standard error) as affected by shape and compactness parameters and type of image.*

6. CONCLUSIONS

Automatic thresholding of spectral indices for vegetation classification in UAV images in an OBIA environment has been achieved by the development of an automatic and efficient algorithm. It has demonstrated its ability to automatically select a threshold from gray-level histograms independent of whether they were unimodal or multimodal histograms. Furthermore, it has the following advantages:

- The rule set stably and automatically selects a threshold, allowing unsupervised classification. This is essential for achieving complete automation of OBIA algorithms.
- It is a fast method (below one second in most cases) that does not require complicated calculations. It depends only on the mean and weight of the two classes used iteratively along the loop integrated in the rule set.
- The method does not depend on the classes included in the analyzed image. It can be used in a wide range of situations; the only adaptation needed is to change the discriminant feature and the "increment" parameter.
- Using this rule set in OBIA algorithms that have been developed for specific areas increases their transferability. This is because the elimination of absolute thresholds makes possible the application of the algorithms to images with different spectral values.

The influence of the scale parameter on the accuracy of the image classification outputs was demonstrated. It affected the histograms of the vegetation indices for the segmented images and it consequently led to changes in the threshold selected by the rule set, especially when working with

the ExG index. Increasing the object size, diminished the classification error until an optimum was reached, after which increasing the object size resulted in greater errors. Shape and compactness parameters of the MRSA showed little influence over the classification accuracy.

When tested with ultra-high resolution images taken from an UAV over crop fields, the rule set presented here achieved accurate vegetation classification results, with errors between 0 and 10%. Consequently, as part of a broader research program to generate early season site specific weed treatments, the algorithm is currently being used for vegetation detection in the development of a weed discrimination rule set in herbaceous crops.

7. ACKNOWLEDGMENTS

This research was partly financed by the TOAS Project (Marie Curie Program, ref.: FP7-PEOPLE-2011-CIG-293991, EU-7th Frame Program), and the AGL2011-30442-CO2-01 project (Spanish Ministry of Economy and Competition, FEDER Funds: Fondo Europeo de Desarrollo Regional). Research of Mr. Torres-Sánchez and Dr. Peña was financed by the FPI and Ramón y Cajal Programs (Spanish MINECO funds), respectively.

8. REFERENCES

Addink, E. A., de Jong, S. M., & Pebesma, E. J. (2007). The importance of scale in object-based mapping of vegetation parameters with hyperspectral imagery. *Photogrammetric Engineering and Remote Sensing*, *73*(8), 905–912.

Aplin, P. (2006). On scales and dynamics in observing the environment. *International Journal of Remote Sensing*, *27*(11), 2123–2140. doi:10.1080/01431160500396477

Baatz, M., & Schaepe, A. (2000). Multiresolution Segmentation: An Optimization Approach for High Quality Multi-Scale Image Segmentation (eCognition). http://www.ecognition.cc/download/baatz_schaepe.pdf. Accessed 18 April 2014

Blaschke, T. (2010). Object based image analysis for remote sensing. *ISPRS Journal of Photogrammetry and Remote Sensing*, *65*(1), 2–16. doi:10.1016/j.isprsjprs.2009.06.004

Drăguţ, L., Tiede, D., & Levick, S. R. (2010). ESP: a tool to estimate scale parameter for multiresolution image segmentation of remotely sensed data. *International Journal of Geographical Information Science*, *24*(6), 859–871. doi:10.1080/13658810903174803

Guijarro, M., Pajares, G., Riomoros, I., Herrera, P. J., Burgos-Artizzu, X. P., & Ribeiro, A. (2011). Automatic segmentation of relevant textures in agricultural images. *Computers and Electronics in Agriculture*, *75*(1), 75–83. doi:10.1016/j.compag.2010.09.013

Hay, G. J., & Castilla, G. (2008). Geographic Object-Based Image Analysis (GEOBIA): A new name for a new discipline. In T. Blaschke, S. Lang, & G. J. Hay (Eds.), *Object-Based Image Analysis* (pp. 75–89). Springer Berlin Heidelberg. http://link.springer.com/chapter/10.1007/978-3-540-77058-9_4. Accessed 18 July 2014

Hay, G. J., Castilla, G., Wulder, M. A., & Ruiz, J. R. (2005). An automated object-based approach for the multiscale image segmentation of forest scenes. *International Journal of Applied Earth Observation and Geoinformation*, *7*(4), 339–359. doi:10.1016/j.jag.2005.06.005

Hengl, T. (2006). Finding the right pixel size. *Computers & Geosciences*, *32*(9), 1283–1298. doi:10.1016/j.cageo.2005.11.008

Karl, J. W., Laliberte, A. S., & Rango, A. (2010). Spatial dependence of predictions from image segmentation: a methods to determine appropriate scales for producing land-management information. *Photogrammetry and Remote Sensing International Archives*.

Karl, J. W., & Maurer, B. A. (2010). Spatial dependence of predictions from image segmentation: A variogram-based method to determine appropriate scales for producing land-management information. *Ecological Informatics*, *5*(3), 194–202. doi:10.1016/j.ecoinf.2010.02.004

Kim, M., Warner, T. A., Madden, M., & Atkinson, D. S. (2011). Multi-scale GEOBIA with very high spatial resolution digital aerial imagery: scale, texture and image objects. *International Journal of Remote Sensing*, *32*(10), 2825–2850. doi:10.1080/01431161003745608

López-Granados, F. (2011). Weed detection for site-specific weed management: mapping and real-time approaches. *Weed Research*, *51*(1), 1–11. doi:10.1111/j.1365-3180.2010.00829.x

Meier, U. (2001). *BBCH Monograph: Growth stages for mono- and dicotyledonous plants.* Berlin: Blackwell Wiss.-Verlag. http://syntechresearch.hu/sites/default/files/publikaciok/bbch.pdf. Accessed 27 June 2013

Meyer, G. E., & Neto, J. C. (2008). Verification of color vegetation indices for automated crop imaging applications. *Computers and Electronics in Agriculture*, *63*(2), 282–293. doi:10.1016/j.compag.2008.03.009

Moffett, K. B., & Gorelick, S. M. (2013). Distinguishing wetland vegetation and channel features with object-based image segmentation. *International Journal of Remote Sensing*, *34*(4), 1332–1354. doi:10.1080/01431161.2012.718463

Otsu, N. (1979). A Threshold Selection Method from Gray-Level Histograms. *IEE Transactions on systems, man, and cybernetics*, *9*(1), 62–66.

Peña, J. M., Torres-Sánchez, J., de Castro, A. I., Kelly, M., & López-Granados, F. (2013). Weed Mapping in Early-Season Maize Fields Using Object-Based Analysis of Unmanned Aerial Vehicle (UAV) Images. *PLoS ONE*, *8*(10), e77151. doi:10.1371/journal.pone.0077151

Tiede, D., Lang, S., Hölbling, D., & Füreder, P. (2010). Transferability of OBIA rulesets for IDP camp analysis in Darfur. In *Proceedings of GEOBIA 2010—Geographic Object-Based Image Analysis.* Presented at the Geographic Object-Based Image Analysis, Ghent.

Torres-Sánchez, J., López-Granados, F., De Castro, A. I., & Peña-Barragán, J. M. (2013). Configuration and Specifications of an Unmanned Aerial Vehicle (UAV) for Early Site Specific Weed Management. *PLoS ONE*, *8*(3), e58210. doi:10.1371/journal.pone.0058210

Torres-Sánchez, J., Peña, J. M., de Castro, A. I., & López-Granados, F. (2014). Multi-temporal mapping of the vegetation fraction in early-season wheat fields using images from UAV. *Computers and Electronics in Agriculture*, *103*, 104–113. doi:10.1016/j.compag.2014.02.009

Woodcock, C. E., & Strahler, A. H. (1987). The factor of scale in remote sensing. *Remote Sensing of Environment*, *21*(3), 311–332. doi:10.1016/0034-4257(87)90015-0

CAPÍTULO 4

WEED MAPPING IN EARLY-SEASON MAIZE FIELDS USING OBJECT-BASED ANALYSIS OF UNMANNED AERIAL VEHICLE (UAV) IMAGES

Peña, J. M., Torres-Sánchez, J., de Castro, A. I., Kelly, M., & López-Granados, F. (2013). Weed Mapping in Early-Season Maize Fields Using Object-Based Analysis of Unmanned Aerial Vehicle (UAV) Images. *PLOS ONE*, 8(10), e77151. doi:10.1371/journal.pone.0077151.

1. RESUMEN

El uso de imágenes remotas capturadas usando vehículos aéreos no tripulados (UAV por sus siglas en inglés) tiene un gran potencial para el diseño de tratamientos localizados de malas hierbas en fase temprana, tarea que no había sido posible anteriormente con imágenes tomadas desde aviones o satélites. Con el objetivo de crear un mapa de malas hierbas en un campo experimental de maíz en España, se ha desarrollado un procedimiento de análisis de imagen orientado a objetos (OBIA por sus siglas en inglés) robusto y totalmente automático, para esto se ha utilizado una serie de imágenes tomadas con un sensor multiespectral de seis bandas (rango visible e infrarrojo) a bordo de un UAV. El procedimiento OBIA combina varias características contextuales, y jerárquicas basadas en objetos, y consta de tres fases consecutivas: 1) clasificación de las líneas de cultivo mediante la aplicación de una aproximación dinámica y auto-adaptativa de clasificación, 2) discriminación de cultivo y malas hierbas en base a su posición relativa con referencia a las líneas de cultivo, y 3) generación de un mapa de infestación de malas hierbas con una estructura de cuadrícula. La estimación de la cobertura de malas hierbas a partir del análisis de imagen produjo resultados satisfactorios. La relación entre densidades de malas hierbas estimadas y reales tuvo un coeficiente de correlación R2=0,89 y un error medio cuadrático de 0,02. Un mapa con tres categorías de cobertura de malas hierbas fue producido con una precisión general del 86%. En el campo experimental, el área libre de malas hierbas era de un 23%, y el área con baja cobertura de malas hierbas (<5%) fue del 47%, lo que implica un gran potencial para la reducción de la aplicación de herbicidas u otros métodos de control de malas hierbas. El procedimiento OBIA calcula múltiples datos y estadísticos derivados del resultado de la clasificación, lo que permite el cálculo de los requerimientos de herbicida y la estimación del coste de las operaciones de control de malas hierbas.

2. ABSTRACT

The use of remote imagery captured by unmanned aerial vehicles (UAV) has tremendous potential for designing detailed site-specific weed control treatments in early post-emergence, which have not possible previously with conventional airborne or satellite images. A robust and entirely automatic object-based image analysis (OBIA) procedure was developed on a series of UAV images using a six-band multispectral camera (visible and near-infrared range) with the ultimate objective of generating a weed map in an experimental maize field in Spain. The OBIA procedure combines several contextual, hierarchical and object-based features and consists of three consecutive phases: 1) classification of crop rows by application of a dynamic and auto-adaptive classification approach, 2) discrimination of crops and weeds on the basis of their relative positions with reference to the crop rows, and 3) generation of a weed infestation map in a grid structure. The estimation of weed

coverage from the image analysis yielded satisfactory results. The relationship of estimated versus observed weed densities had a coefficient of determination of r^2=0.89 and a root mean square error of 0.02. A map of three categories of weed coverage was produced with 86% of overall accuracy. In the experimental field, the area free of weeds was 23%, and the area with low weed coverage (<5% weeds) was 47%, which indicated a high potential for reducing herbicide application or other weed operations. The OBIA procedure computes multiple data and statistics derived from the classification outputs, which permits calculation of herbicide requirements and estimation of the overall cost of weed management operations in advance.

3. INTRODUCTION

Many agricultural crops require the use of herbicides as essential tools for maintaining the quality and quantity of crop production. Currently, the cost of herbicides accounts for approximately 40% of the cost of all the chemicals applied to agricultural land in Europe (ECPA 2010). Associated environmental and economic concerns have led to the creation of European legislation on the sustainable use of pesticides (Williams 2012). This legislation includes guidelines for the reduction in applications and the utilization of adequate doses based on the degree of weed infestation. Both components are integrated in the agronomical basis of the precision agriculture principles and especially of site-specific weed management (SSWM). This consists of the application of customized control treatments, mainly herbicides, only where weeds are located within the crop field in order to use herbicides and doses according to weed coverage (Srinivasan 2006). SSWM typically uses new technologies to collect and process spatial information on the crop field. Remote sensing technology can play a role here as an efficient and repeatable method to obtain crop field information related to weed infestation.

The analysis of remote images captured with aircraft and satellite platforms has resulted in numerous examples of weed mapping in late growth stages (de Castro *et al*. 2012; Koger *et al*. 2003; Peña-Barragán *et al*. 2007), although in many weed–crop systems, the optimal treatment time is early in the growth season when weeds and crops are in their seedling growth stages (López-Granados 2011). However, discriminating small seedlings with airborne and satellite imagery is problematic due to the insufficient spatial resolution of these images. This difficulty might be now overcome using the new generation of remote platforms known as unmanned aerial vehicles (UAV) or unmanned aerial systems (UAS). UAVs can operate at low altitudes and capture images at very high spatial resolutions (a few cm), which is not feasible with conventional remote platforms. Moreover, UAVs can work on demand with great flexibility at critical moments, depending on the agronomic goals involved. This is crucial for detecting small weed and crop plants at early stages in

the majority of fields. UAV technology has been adapted and utilized by diverse groups interested in agricultural investigation (Zhang and Kovacs 2012), and a few studies have reported the use of UAVs in assessing weed distribution or invasion of plants in rangeland monitoring (Göktoğan *et al*. 2010; Laliberte *et al*. 2010).

Along with spatial and temporal resolution requirements, spectral similarity between weed and crop plants, which occurs mainly in the early part of the growth season, makes discrimination between the two difficult (López-Granados 2011; Stafford 2000). This is an important limitation in the application of image analysis methods based on pixel information only. To address this limitation, a powerful procedure, such as object-based image analysis (OBIA) might be the only way to distinguish between weed and crop. The OBIA methodology first identifies spatially and spectrally homogenous units (objects) created by grouping adjacent pixels according to a procedure known as segmentation and next it combines spectral, contextual and morphological information to drastically improve image classification results (Blaschke 2010). In this process, the definition of the row structure formed by the crop is essential for further identification of plants (crop and weeds) because the position of each plant relative to the rows might be the key feature used to distinguish among the weeds and crop plants (Burgos-Artizzu *et al*. 2009).

In the context of SSWM, the ultimate objective of detecting weed patches is to generate efficient decision support system data that can be used with specific spraying machinery (Shaw 2005). For this purpose, several applications have been developed to delineate a restricted number of management zones based on crop status (Fridgen *et al*. 2004) or weed density thresholds in mature wheat fields (Gómez-Candón *et al*. 2012). However, the development of robust and automatic procedures for weed data acquisition, image analysis and delineation of weed cover zones is still challenging, even more so in early growth stages (López-Granados 2011). This research involves the whole process: acquisition of very-high-spatial-resolution remote images with a UAV, image analysis using object-based methods, and the ultimate objective of generating weed maps at early stages for in-season site-specific herbicide treatment. To achieve this objective, we developed an OBIA procedure consisting of three main phases: 1) automatic definition of crop rows within a maize field accomplished by combining spectral and contextual features in a customized looping rule set algorithm, 2) discrimination of weed seedlings and crop plants based on their relative positions, and 3) automatic generation of a weed coverage map in a grid framework adapted to the specification required by the herbicide spraying machinery.

4. MATERIALS AND METHODS

4.1. Study site

Remote images were taken on May 5th, 2011 on a maize field located in Arganda del Rey (Madrid, Spain, coordinates 40.320 N, 3.477 W, datum WGS84), just when post-emergence herbicide or other control techniques are recommended. The flights were authorized by a written agreement between the farm owners and our research group. The maize field was naturally infested with *Amaranthus blitoides* (broad-leaved weed) and *Sorghum halepense* (grass weed). The maize was at the stage of 4–6 leaves unfolded, and the weed plants were similar in size or in some cases smaller than the maize plants (Figure 1). Several visits to the field were conducted for monitoring of crop growth and weed emergence and finally to select the best moment to take the set of remote images. An experimental plot of 140x100 m was delimited within the crop field to perform the flights. The coordinates of each corner of the flight area were collected with a global positioning system (GPS) for use in planning the flight route.

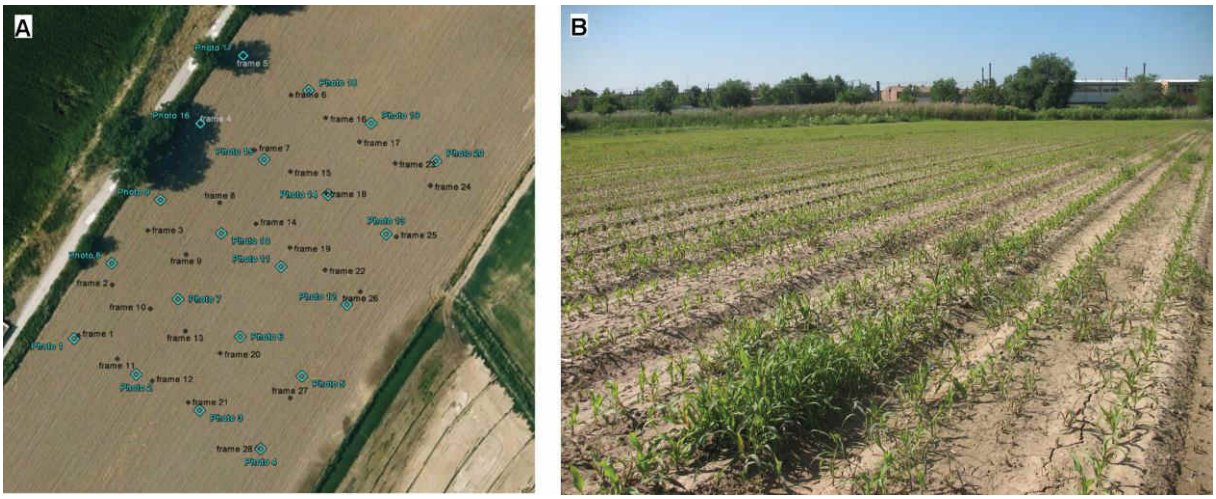

Figure 1. *Aerial view of the experimental field (a), showing the centers of the UAV aerial images in blue and the sampling points in black (see section 2.4), and in-field photograph of the study site (b), showing the maize rows and some patches of weed infestation.*

4.2. UAV flights and remote images

A model md4-1000 quadrocopter UAV (microdrones GmbH, Siegen, Germany) with vertical take-off and landing capabilities was used to collect the remote images (Figure 2a). This UAV can fly either by remote control or autonomously with the aid of its GPS receiver and its waypoint navigation system. It can carry any sensor that weighs less than 1.25 kg mounted under its belly. The images were collected with a Tetracam mini-MCA-6 camera (Tetracam Inc., Chatsworth, CA, USA), which is a lightweight (700 g) multispectral sensor with six individual digital channels arranged in a

2x3 array. Each channel has a focal length of 9.6 mm and a 1.3-megapixel (1,280 x 1,024 pixels) CMOS sensor that stores images on a compact flash card. The camera has user-configurable band-pass filters (Andover Corporation, Salem, NH, USA) of 10-nm full width at half-maximum and center wavelengths of 530, 550, 570 (the green region of the electromagnetic spectrum), 670 (the red region), 700 and 800 nm (the near-infrared region). The software PixelWrench2 was supplied with the camera to provide full camera control and image management, including correction of the vignette effect, alignment of RAW image sets and building of multi-band TIFs (Figure 2b), as explained in (Torres-Sánchez et al. 2013).

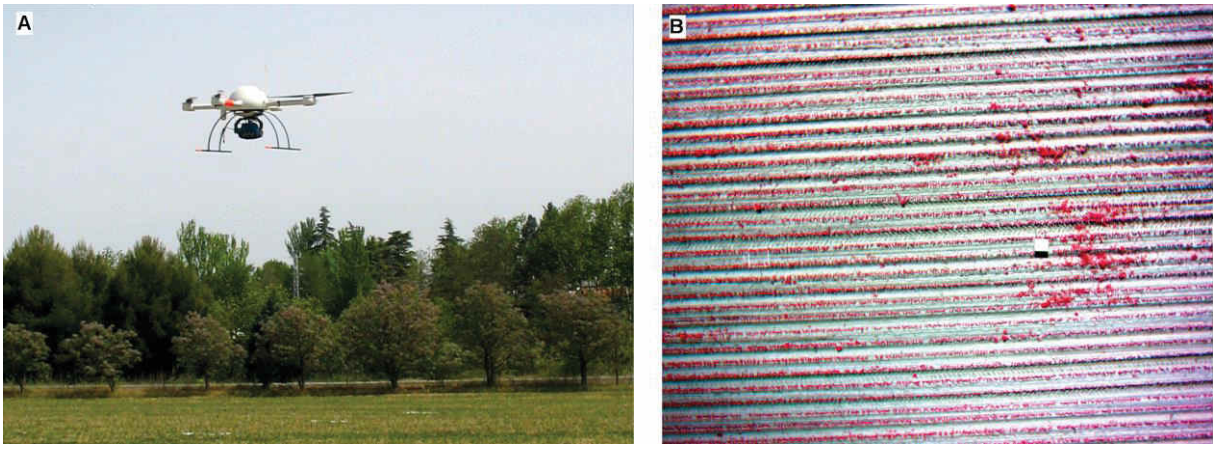

Figure 2. *Unmanned quadrotor-type aerial vehicle flying over the crop field (a), and aerial image (color–infrared composition) obtained by the UAV at an altitude of 30 m (b), showing the maize rows, some weed patches and the Spectralon® panel.*

The flight altitude was 30 m above ground level, yielding 20 images of 2-cm spatial resolution to cover the whole experimental field. During the UAV flights, a barium sulphate standard Spectralon® panel (Labsphere Inc., North Sutton, NH, USA) 1 x 1 m in size was placed in the middle of the field to calibrate the spectral data (Figure 2b). Digital images captured by each camera channel were spectrally corrected by applying an empirical linear relationship (Hunt, Jr. et al. 2010). Equation coefficients were derived by fitting the digital numbers of the MCA imagery located in the spectralon panel to the spectralon ground values.

4.3. Weed mapping by object-based image analysis (OBIA)

The spectral characteristics and general appearance of crop and weed plants are highly similar in the early season (López-Granados 2011; Stafford 2000) and are even more pronounced in remote images (Torres-Sánchez *et al*. 2013). Therefore, the effectiveness of weed discrimination might be increased by taking advantage of the relative position of every plant with reference to the crop row structure (Burgos-Artizzu *et al*. 2009). This information can be included in the classification procedure

using the OBIA methodology, allowing the combination of spectral, contextual and morphological information, among other features, of the objects created using a procedure known as segmentation (Peña-Barragán *et al*. 2011). The commercial software eCognition Developer 8 (Trimble GeoSpatial, Munich, Germany) was used to analyze the UAV images and develop an OBIA procedure. The rule set algorithm for weed mapping ran automatically and consisted of three consecutive phases: 1) classification of crop rows, 2) discrimination between crop plants and weeds based on their relative positions, and 3) generation of a weed infestation map in a grid structure. A flowchart of the process is shown in figure 3.

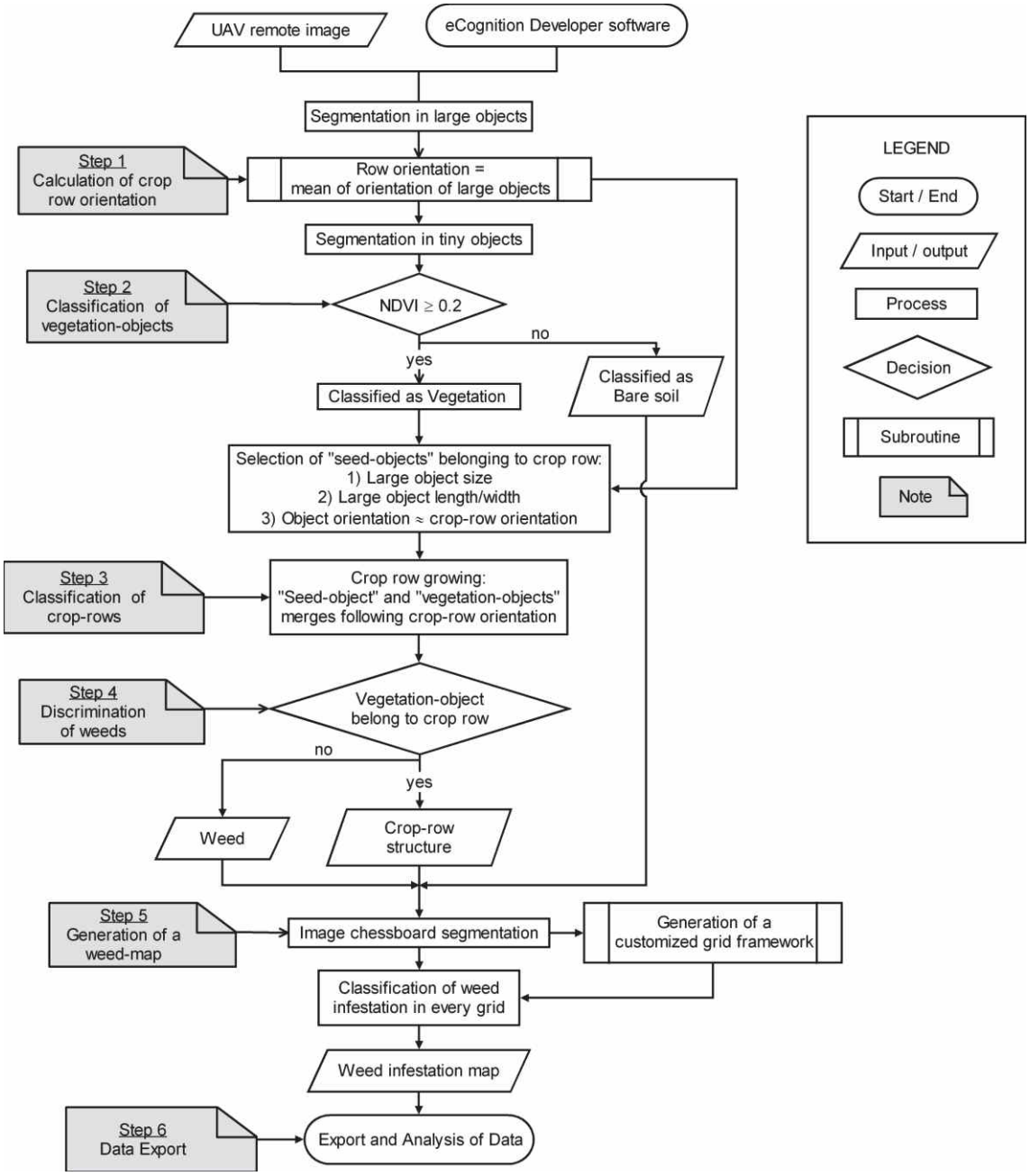

Figure 3. *Flowchart of the OBIA procedure for classification of crop rows and weeds and generation of a weed infestation map.*

4.3.1. Crop row classification

A dynamic and auto-adaptive classification approach was used to define the crop row structure, by mean of a combination of several object-based features that characterize a set of regular and quasi-equidistant lines of plants. In this process, the UAV images were segmented into homogeneous multi-pixel objects using the multiresolution algorithm (Baatz and Schaepe 2000). Segmentation is a bottom-up region-merging process in which the image is subdivided into homogeneous objects on the basis of several parameters (band weights, scale, color, shape, smoothness and compactness) defined by the operator. Two levels of segmentation were independently used throughout the procedure (Figure 4a): 1) a level at a scale of 140, to define the main orientation of the crop rows, and 2) a level at a scale of 10, to generate smaller objects for crop and weed discrimination. In both cases, the values of the other parameters involved in the segmentation were 0.9, 0.1, 0.5 and 0.5 for color, shape, smoothness and compactness, respectively.

After segmentation, the normalized difference vegetation index (NDVI; (Rouse *et al*. 1974)) was used to classify objects of vegetation (Figure 4b) as being those with NDVI values greater than 0.20. NDVI was selected as the best index for use in performing this classification, compared to other vegetation indices (Torres-Sánchez *et al*. 2013). A customized merging operation was then performed to create lengthwise vegetation objects, following the shape of a crop row. In this operation, two candidate vegetation objects were merged only if the length/width ratio of the target object increased after the merging. Next, the object that was largest in size and with orientation close to the row orientation was classified as a seed object belonging to a crop row. Lastly, the seed object grew in both directions, following the row orientation, and a looping merging process was performed until all the crop rows reached the limits of the parcel (Figure 4c). Every phase of the crop row classification process is described in detail in (Peña-Barragán *et al*. 2012).

4.3.2. Discrimination of crop and weeds

After classifying all the crop rows within an image, the algorithm generated a buffer zone along the longitudinal axis of each row by applying a chessboard segmentation process at an upper level of hierarchy. Two or more levels of segmentation form a hierarchical structure in the OBIA paradigm, in which super-objects belong to the upper level and include one or more sub-objects that belong to the lower level. In this case, the width of the buffer zone (upper hierarchical level) was defined by the average size of the vegetation objects in contact with the row structure. Next, the vegetation sub-objects located entirely below the buffer zone (lower hierarchical level) were classified as crop plants, and others were classified as weeds (Figure 4d). A more complex decision rule was made in the case of sub-objects located below the edge of the buffer zone. In this case, the sub-objects in

contact with or very close to other weeds were classified as weeds because aggregation among weed plants, i.e., weed patches, was generally observed (Heijting et al. 2007).

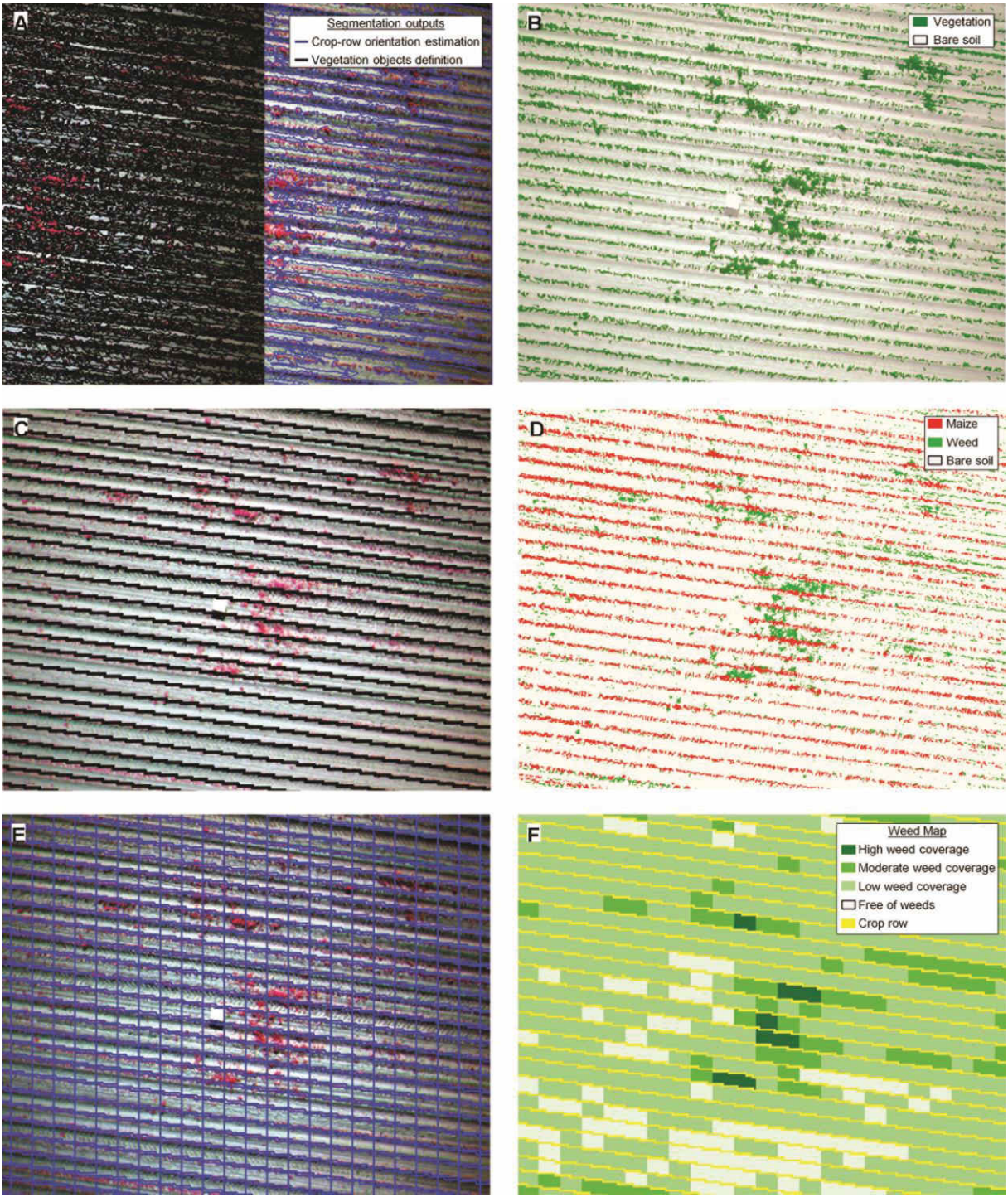

Figure 4. *Partial view of the outputs of the OBIA procedure at each step: a) segmentation outputs at scales of 140 (in blue) and 10 (in black), used to calculate row orientation and define vegetation objects, respectively; b) classification of objects of vegetation and bare soil ; c) definition of the crop row structure (in black); d) classified image with crop, weeds and bare soil; e) grid framework of the inter-row area; f) weed coverage map showing three levels of infestation (low, moderate and high), crop rows and weed-free zones.*

4.3.3. Weed coverage mapping

After weed–crop classification, the algorithm built a grid framework of the inter-row area by applying two consecutive processes: 1) copying the existing inter-row object level to an upper position, and 2) chessboard segmentation of this upper level and generation of grids of user-adjustable size (Figure 4e). For example, in this investigation, the grid length used was 1 m and the grid width used was the inter-row distance (0.7 m on average). Therefore, a new hierarchical structure was generated in the inter-row area between the grid super-objects (upper level) and the weed and bare-soil sub-objects (lower level). Next, an estimate of the weed coverage (% of weeds) was automatically calculated from the ratio of weed pixels to total pixels per grid (Burgos-Artizzu *et al*. 2009; Donald 2006). This calculation was based on the hierarchical relationship between grid super-objects and weed-infested sub-objects. Lastly, weed cover was also mapped on the basis of a number of user-adjustable categories defined by infestation thresholds. For example, in this investigation, the weed map identified both weed-free zones and weed-infested zones, which were categorized at three different levels of infestation, as follows: 1) low (<5% weed coverage), 2) moderate (5–20% weed coverage) and 3) high (>20% weed coverage) (Figure 4f). Both the grid dimensions and the number and thresholds of the weed infestation categories can be customized on the basis of cropping patterns and the specifications required by the herbicide spraying machinery.

4.4. The evaluation of the methodology

The rule set algorithm was created and configured using two of the aerial images and was tested using the rest of the images. To evaluate the results of the algorithm, a systematic on-ground sampling procedure was conducted during the UAV flight. The sampling consisted of placing 28 square white frames, 1x1 m in size, throughout the studied surface (Figure 5). The distribution of the samples was representative of the distribution of weed coverage levels in the experimental field. Weed mapping is considered a more complicated task in cases of low and moderate levels of weed infestation (greater confusion is possible due to the presence of bare soil) than in cases of high levels of weed infestation (at which bare soil has a minor influence) or weed-free zones (with no influence of weeds). For this reason, the sampling frames were primarily located in zones with low and moderate weed coverage levels rather than in weed-free zones or in zones with high or very high infestation levels.

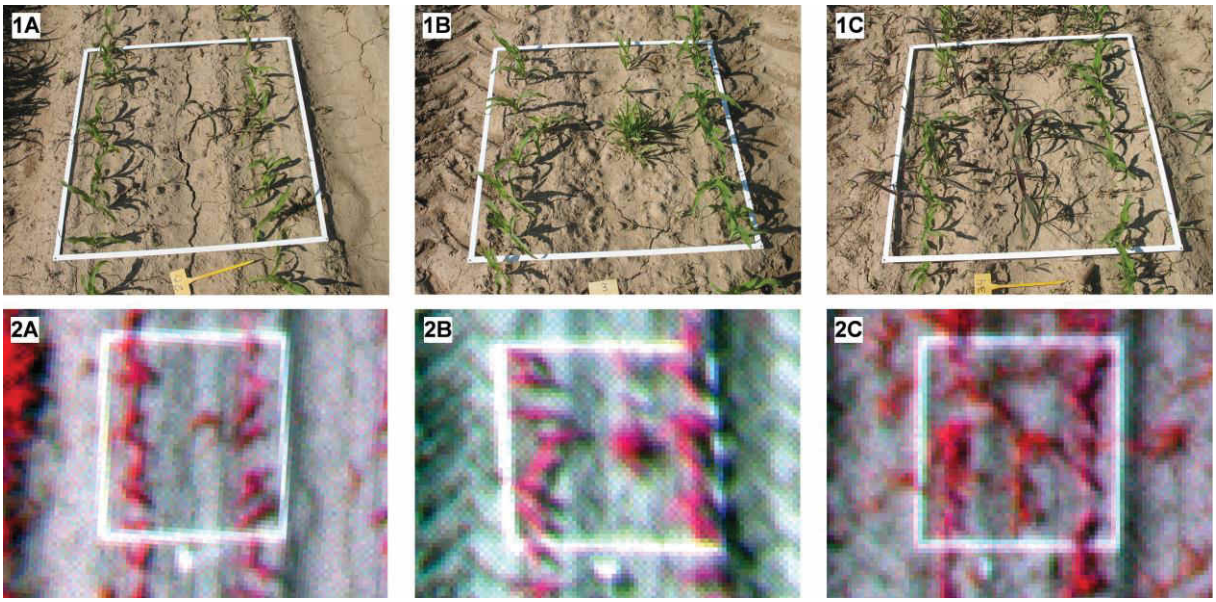

Figure 5. *On-ground photographs (1) and UAV images (2) of the 1x1-m frames used in the ground-truth sampling of three different categories of weed coverage: a) low, b) moderate, and c) high.*

Every frame was georeferenced with a GPS and photographed to compare on-ground weed infestation (observed weed coverage) with the outputs of the image classification process (estimated weed coverage). Weed coverage in the on-ground photographs was extracted through the application of a specific greenness index that accentuates the green color of the vegetation (Romeo *et al*. 2013). After a visual assessment of several indices, the excess green index (Torres-Sánchez *et al*. 2013; Woebbecke *et al*. 1995) was selected for use and applied to the photographs. Next, pixels with values greater than zero were classified as vegetation (weed and crop), and finally, weed pixels were isolated by manually masking crop row areas.

The fractions of weed area in the on-ground and aerial images were converted to percentages of the total area within every frame and were compared using a 1:1 line, which should have a correspondence of 1 in an ideal situation. This correspondence was evaluated by calculating the slope, the intercept and the coefficient of determination (R^2) of a linear regression model. The root mean square error (RMSE) was also calculated as an additional measure of the overall error of the estimations.

The accuracy of the classified images was also quantified by calculating the confusion matrix between weed mapping outputs and weed coverage in all the sampling frames grouped in the three categories (low, moderate and high weed densities) previously defined. The confusion matrix quantifies the overall accuracy (OA) of the classification, as well as its omission (OE) and commission (CE) errors in each category (Congalton 1991).

5. RESULTS AND DISCUSSION

5.1. Weed map information provided by the OBIA procedure

An advantage of the OBIA procedure, compared to traditional pixel-based methodologies, is its ability to compute multiple data and statistics derived from the image analysis and classification. Moreover, this information can be exported in several file formats, e.g., vector, image, ASCII, tables, etc. The algorithm developed in this study can compute and export information at several levels, depending on its position in the segmentation hierarchy, as described below.

5.1.1. Whole field: upper segmentation level

Global information for the crop field, including field dimensions, number of crop rows, crop row orientation, average crop row separation, weed-free area and total area of each weed coverage category, was computed at the upper segmentation level. A vector shapefile with the limits of the field and a georeferenced image file of the gridded weed map were also produced, as well as other image files of intermediate classification outputs, if required. The global data computed for the experimental field are given in table 1. The experimental field occupied 1.4 ha and had 142 crop rows approximately 140 m in length, separated from each other by 0.70 m on average. The area free of weeds was 23%, and the area with low weed coverage (<5% of weeds) was 47%, indicating a high potential for reducing herbicide applications or other weed operations in this field.

Table 1. *Global information on the whole experimental field computed according to the OBIA procedure at the upper segmentation level.*

Global Feature	Value
Field features	
Area (m^2)	14,000
Perimeter length (m)	480
Maximum length (m)	140
Minimum length (m)	100
Lat coordinate of the field center (°)	40.320 N
Lon coordinate of the field center (°)	3.477 W
Crop row features	
Number of rows (n)	142
Average row orientation (°)	32
Maximum row length (m)	140
Minimum row length (m)	140
Average distance between rows (m)	0.70
Weed map features	
Number of grid units (n)	19,880
Grid units free of weeds (n)	4,572
Grid units with weeds (n)	15,308
Area of grid units free of weeds (m^2,%)	3,258 (23%)
Area of grid units with weeds (m^2,%)	10,742 (77%)
Area with low weed coverage (<5%) (m^2,%)	6,618 (47%)
Area with moderate weed coverage (5-20%) (m^2,%)	3,230 (23%)
Area with high weed coverage (>20%) (m^2,%)	894 (7%)

5.1.2. Crop row structure: Intermediate segmentation level

Detailed information on each inter-row unit, including the identification number (automatically assigned), the geographic coordinates of the row extremes, the length and width, the percentage of area free of weeds, and the percentage of each category of weed coverage considered, was produced at the intermediate segmentation level. An example of crop row data computed for the experimental field is given in table 2. Among the rows indicated, weeds were found in 100% of the grid units of row 141, which had 10% weed infestation. In contrast, row 1 only had 3% weed infestation and 57% of its grid units were free of weeds.

Table 2. *Inter-row information for the experimental field computed by the OBIA procedure at the intermediate segmentation level.*

	Start		End		Size (m)		# Weed-infested grid units				
Row ID	Lat (40°N)	Lon (3°W)	Lat (40°N)	Lon (3°W)	Length	Width	Weed-free	Low (<5%)	Moderate (5–20%)	High (>20%)	Total
1	19´ 13.17″	28´ 38.93″	19´ 17.00″	28´ 35.72″	140	0.70	57	46	7	0	3
2	19´ 13.15″	28´ 38.90″	19´ 16.97″	28´ 35.69″	140	0.70	29	50	14	7	6
3	19´ 13.14″	28´ 38.86″	19´ 16.95″	28´ 35.65″	140	0.68	21	39	29	11	8
….	….	….	….	….	….	….	….	….	….	….	….
141	19´ 11.55″	28´ 35.29″	19´ 15.43″	28´ 32.03″	140	0.75	0	43	53	4	10
142	19´ 11.54″	28´ 35.26″	19´ 15.45″	28´ 32.06″	140	0.69	50	27	15	8	6

5.1.3. Weed infestation in grid units: lower segmentation level

Detailed information on each grid unit, including the identification number, geographic coordinates, dimensions, relative position within the crop row, distance to the start and the end of the crop row, weed coverage percentage and weed coverage category, was produced at the lower segmentation level. A list of the data computed in every grid unit of the experimental field is given in table 3. Among the grid units indicated, the highest weed coverage was measured in grid unit 3 (22%), located two meters from the beginning of row 1. In contrast, grid unit 1 was free of weeds.

The OBIA procedure generated a geo-referenced weed map that can be converted into a prescription herbicide application map and can then be transferred to machinery embedded with technologies for practical application of site-specific weed control strategies. The information provided in tables 1, 2 and 3 can be utilized by decision-making systems to calculate herbicide requirements or other weed operations in the field for the purposes of optimizing weeding machinery path planning and estimating the overall cost of weed management operations in advance (Pedersen et al. 2006). Moreover, multi-temporal analysis of abundance and distribution of weeds

within the same field is very helpful in studies of weed population dynamics and weed–crop interactions (e.g., crop yield losses).

Table 3. *Grid information for the experimental field computed by the OBIA procedure at the lower segmentation level.*

	Coordinates		Dimensions (m)		Position in row			Weed coverage	
Grid ID	**Lat (40°N)**	**Lon (3°W)**	**Length**	**Width**	**Row ID**	**Distance to start (m)**	**Distance to end (m)**	**% of Weeds**	**Weed category**
1	19´ 13.17"	28´ 38.93"	1	0.70	1	0	140	0	Weed-free
2	19´ 13.20"	28´ 38.90"	1	0.70	1	1	139	3	Low
3	19´ 13.23"	28´ 38.87"	1	0.70	1	2	138	22	High
….	….	….	….	….	….	….	….	….	….
19879	19´ 15.40"	28´ 32.05"	1	0.69	140	139	1	7	Moderate
19880	19´ 11.54"	28´ 35.26"	1	0.69	140	140	0	4	Low

5.2. The evaluation of the weed map

The algorithm developed in this study identified and counted the rows in the training images with 100% accuracy and only had minor errors in classifying short rows located in the corners of some testing images. The definition of the longitudinal edge of the crop rows was strongly affected by the presence of weed plants very close to or within the crop rows. The accuracy of the methodology was evaluated by comparing the estimation of weed coverage derived from the UAV image classification and the values observed in the on-ground sampling photographs (Figure 6). The relationship between the estimated and observed weed densities was highly satisfactory, with a coefficient of determination of R^2=0.89 and an RMSE=0.02, indicating good agreement in the three categories considered.

At low weed coverage, most values were located above the 1:1 line, indicating some degree of overestimation of the weed infestation. From an agronomical perspective, this pattern of results is not adverse because it reduces the chance of missing isolated weeds. That is, it takes into account the fact that farmers might choose to treat weed-free zones, rather than assume the risk of allowing weeds to go untreated (Gibson *et al*. 2004). In contrast, the OBIA procedure slightly underestimated weed infestation at moderate and high weed densities, which is less important if it is corrected in the design of the herbicide prescription maps (Gómez-Candón *et al*. 2011).

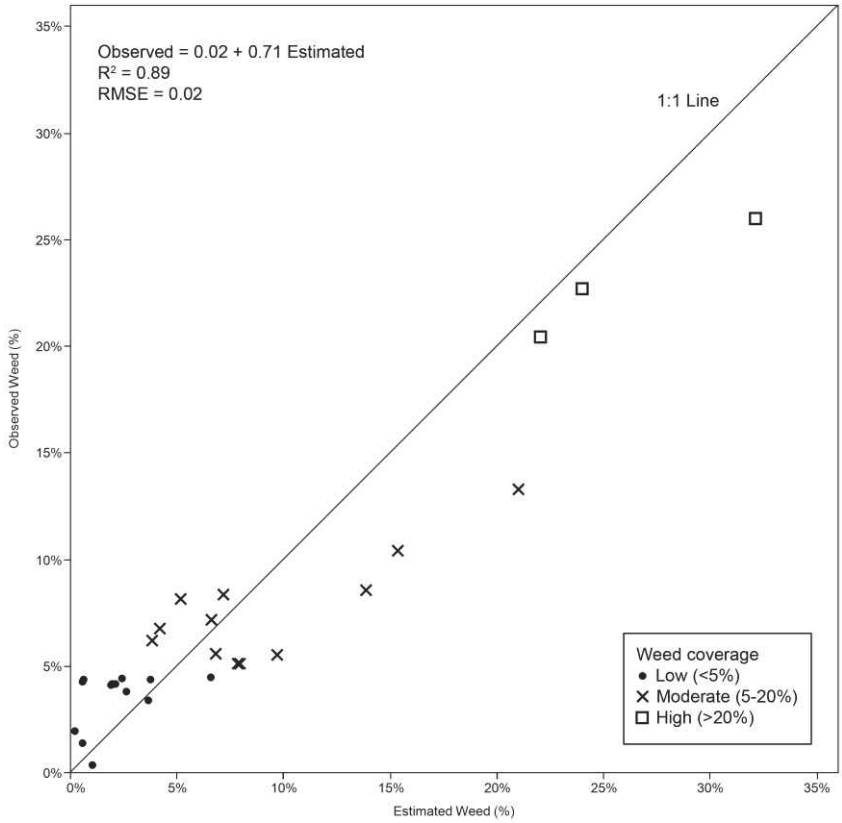

Figure 6. *Observed and estimated weed coverage (%) inside the sampling frames from on-ground photographs and UAV image analysis, respectively.*

The weed map, with weed infestation levels classified in three categories, was also evaluated using the confusion matrix shown in table 4. The matrix indicates an overall accuracy of 86% and a kappa index of 0.76. The classification was over grid units, not over pixels, so the OA was the percentage of frames correctly classified (the number correct frames as a percentage of the total number of sampling frames). Confusion between frames was minor and only occurred between consecutive categories. The matrix also indicates the omission and commission errors in each category. OE indicates the proportion of frames with an observed weed coverage that was misclassified as being of a different coverage, and CE indicates the proportion of frames classified with levels of weed coverage that really correspond to other levels of coverage. As previously mentioned, only errors of underestimation of the weed category are important from the perspective of weed control (López-Granados 2011), e.g., reporting 0% at low and high weed densities and reporting 17% of the frames at moderate weed coverage.

Table 4. *Classification matrix for three categories of weed coverage by comparing ground-truth weed sampling and the weed map derived from the UAV image classification.*

Ground-truth weed sampling	UAV weed map					
	Low (<5%)	Moderate (5–20%)	High (>20%)	Number of frames	Omission Error	Underestimation Error
Low (<5%)	**12**	1		13	8%	0%
Moderate (5–20%)	2	**9**	1	12	25%	17%
High (>20%)			**3**	3	0%	0%
Number of frames	14	10	4	28		
Commission Error	15%	10%	25%			
Correct classifications are shown in bold. Overall accuracy = 86%, Kappa index = 0.76						

6. CONCLUSIONS

An unmanned aerial vehicle and a six-band multispectral camera were used to collect remote images of a maize field in the early season for the purpose of generating weed maps for further early SSWM. A robust and automated OBIA procedure was developed for the automatic discrimination of crop rows and weeds in georeferenced and 2-cm spatial resolution remote images. The task was complex due to both the spectral properties and general appearance of weeds and crop plants are very similar in their early growth stages, and due to the difficulties created by variability and changing conditions in natural crop fields. The algorithm efficiently identified all the crop rows based on their linear pattern and on the contextual features of the vegetation objects that belong to the rows. Weed plants located in the inter-row area were then distinguished from crop plants on the basis of their relative positions with respect to the crop rows. Lastly, the weed cover percentages in three categories were determined to generate a weed map in a grid framework. The algorithm yielded very satisfactory results in most cases.

The OBIA procedure computes multiple data and statistics derived from the image analysis and the classification outputs that can be exported in image, vector and table file formats. The tables and weed map provided helpful information that can be used in decision-making systems to calculate herbicide requirements and estimate the overall cost of weed management operations.

The combination of ultra-high-spatial-resolution UAV remote images and the OBIA procedure developed in this study permits the generation of weed maps in early maize crops for use in planning the application of in-season weed control measures, which has not been possible previously with traditional airborne or satellite images. This technology can help in the implementation of the European legislation for the sustainable use of pesticides, which promotes reductions in herbicide applications and the utilization of doses appropriate to the levels of weed infestation present.

7. ACKNOWLEDGEMENTS

The authors thank Dr. María Teresa Gómez-Casero and Mr. Juan José Caballero Novella for their very useful help during the field work and Dr. José Dorado for granting permission for aerial images of the studied farm to be taken.

8. REFERENCES

Baatz, M., & Schaepe, A. (2000). Multiresolution Segmentation: An Optimization Approach for High Quality Multi-Scale Image Segmentation (eCognition). http://www.ecognition.cc/download/baatz_schaepe.pdf. Accessed 18 April 2014

Blaschke, T. (2010). Object based image analysis for remote sensing. *ISPRS Journal of Photogrammetry and Remote Sensing*, *65*(1), 2–16. doi:10.1016/j.isprsjprs.2009.06.004

Burgos-Artizzu, X. P., Ribeiro, A., Tellaeche, A., Pajares, G., & Fernández-Quintanilla, C. (2009). Improving weed pressure assessment using digital images from an experience-based reasoning approach. *Computers and Electronics in Agriculture*, *65*(2), 176–185. doi:10.1016/j.compag.2008.09.001

Castro, A. I. de, Jurado-Expósito, M., Peña-Barragán, J. M., & López-Granados, F. (2012). Airborne multi-spectral imagery for mapping cruciferous weeds in cereal and legume crops. *Precision Agriculture*, *13*(3), 302–321. doi:10.1007/s11119-011-9247-0

Congalton, R. G. (1991). A review of assessing the accuracy of classifications of remotely sensed data. *Remote Sensing of Environment*, *37*(1), 35–46. doi:10.1016/0034-4257(91)90048-B

Donald, W. W. (2006). Estimated corn yields using either weed cover or rated control after pre-emergence herbicides. *Weed Science*, *54*(2), 373–379.

ECPA. (2010). Industry statistics - ECPA total | European Crop Protection Association. http://www.ecpa.eu/information-page/industry-statistics-ecpa-total. Accessed 21 April 2014

Fridgen, J. J., Kitchen, N. R., Sudduth, K. A., Drummond, S. T., Wiebold, W. J., & Fraisse, C. W. (2004). Management Zone Analyst (MZA). *Agronomy Journal*, *96*(1), 100–108. doi:10.2134/agronj2004.1000

Gibson, K. D., Dirks, R., Medlin, C. R., & Johnston, L. (2004). Detection of Weed Species in Soybean Using Multispectral Digital Images. *Weed Technology*, *18*(3), 742–749. doi:10.1614/WT-03-170R1

Göktoğan, A., Sukkarieh, S., Bryson, M., Randle, J., Lupton, T., & Hung, C. (2010). A Rotary-wing Unmanned Air Vehicle for Aquatic Weed Surveillance and Management. *Journal of Intelligent & Robotic Systems*, *57*(1), 467–484. doi:10.1007/s10846-009-9371-5

Gómez-Candón, D., López-Granados, F., Caballero-Novella, J. J., García-Ferrer, A., Peña-Barragán, J. M., Jurado-Expósito, M., & García-Torres, L. (2011). Sectioning remote imagery for characterization of Avena sterilis infestations. Part B: Efficiency and economics of control. *Precision Agriculture*, *13*(3), 337–350. doi:10.1007/s11119-011-9250-5

Gómez-Candón, D., López-Granados, F., Caballero-Novella, J. J., García-Ferrer, A., Peña-Barragán, J. M., Jurado-Expósito, M., & García-Torres, L. (2012). Sectioning remote imagery for characterization of Avena sterilis infestations. Part A: Weed abundance. *Precision Agriculture*, *13*(3), 322–336. doi:10.1007/s11119-011-9249-y

Heijting, S., Van Der Werf, W., Stein, A., & Kropff, M. J. (2007). Are weed patches stable in location? Application of an explicitly two-dimensional methodology. *Weed Research*, *47*(5), 381–395. doi:10.1111/j.1365-3180.2007.00580.x

Hunt, Jr., E. R., Hively, W. D., Fujikawa, S. J., Linden, D. S., Daughtry, C. S. T., & McCarty, G. W. (2010). Acquisition of NIR-Green-Blue Digital Photographs from Unmanned Aircraft for Crop Monitoring. *Remote Sensing*, *2*(1), 290–305. doi:10.3390/rs2010290

Koger, C. H., Shaw, D. R., Watson, C. E., & Reddy, K. N. (2003). Detecting Late-Season Weed Infestations in Soybean (Glycine max). *Weed Technology*, *17*(4), 696–704. doi:10.1614/WT02-122

Laliberte, A. S., Herrick, J. E., Rango, A., & Winters, Craig. (2010). Acquisition, orthorectification, and classification of unmanned aerial vehicle (UAV) imagery for rangeland monitoring. *Photogrammetric Engineering and Remote Sensing*, *76*, 661–672.

López-Granados, F. (2011). Weed detection for site-specific weed management: mapping and real-time approaches. *Weed Research*, *51*(1), 1–11. doi:10.1111/j.1365-3180.2010.00829.x

Pedersen, S. M., Fountas, S., Have, H., & Blackmore, B. S. (2006). Agricultural robots—system analysis and economic feasibility. *Precision Agriculture*, *7*(4), 295–308. doi:10.1007/s11119-006-9014-9

Peña-Barragán, J. M., López-Granados, F., Jurado-Expósito, M., & García-Torres, L. (2007). Mapping Ridolfia segetum patches in sunflower crop using remote sensing. *Weed Research*, *47*(2), 164–172. doi:10.1111/j.1365-3180.2007.00553.x

Peña-Barragán, J. M., Ngugi, M. K., Plant, R. E., & Six, J. (2011). Object-based crop identification using multiple vegetation indices, textural features and crop phenology. *Remote Sensing of Environment*, *115*(6), 1301–1316. doi:10.1016/j.rse.2011.01.009

Peña-Barragán, Kelly, M., de Castro, & López-Granados. (2012). Object-based approach for crop row characterizatioin in UAV images for site-specific weed management. In *Proceedings of the 4th GEOBIA* (pp. 426–430). Presented at the International Conference on Geographic Object-Based Image Analysis, Rio de Janeiro, Brazil.

Romeo, J., Pajares, G., Montalvo, M., Guerrero, J. M., Guijarro, M., & de la Cruz, J. M. (2013). A new Expert System for greenness identification in agricultural images. *Expert Systems with Applications*, *40*(6), 2275–2286. doi:10.1016/j.eswa.2012.10.033

Rouse, J. W., Jr., Haas, R. H., Schell, J. A., & Deering, D. W. (1974). Monitoring Vegetation Systems in the Great Plains with Erts. *NASA Special Publication*, *351*, 309.

Shaw, D. R. (2005). Translation of remote sensing data into weed management decisions. *Weed Science*, *53*(2), 264–273. doi:10.1614/WS-04-072R1

Srinivasan, A. (2006). Precision Agriculture: an overview. In A. Srinivasan (Ed.), *Handbook of precision agriculture. Principles and applications.* (pp. 3–18). New York: Food Products Press. The Haworth Press.

Stafford, J. V. (2000). Implementing Precision Agriculture in the 21st Century. *Journal of Agricultural Engineering Research*, *76*(3), 267–275. doi:10.1006/jaer.2000.0577

Torres-Sánchez, J., López-Granados, F., De Castro, A. I., & Peña-Barragán, J. M. (2013). Configuration and Specifications of an Unmanned Aerial Vehicle (UAV) for Early Site Specific Weed Management. *PLoS ONE*, *8*(3), e58210. doi:10.1371/journal.pone.0058210

Williams, J. C. (2012). New EU pesticide legislation–the view of a manufacturer. In *The Dundee Conference. Crop Protection in Northern Britain, 2012, Dundee, UK, 28-29 February 2012* (pp. 7–14). The Association for Crop Protection in Northern Britain. http://www.sipr.ac.uk/CPNB/Index_and_Proceedings_2012.pdf#page=16. Accessed 5 September 2016

Woebbecke, D. M., Meyer, G. E., Von Bargen, K., & Mortensen, D. A. (1995). Color indices for weed identification under various soil, residue, and lighting conditions. *Transactions of the ASAE*, *38*(1), 259–269.

Zhang, C., & Kovacs, J. M. (2012). The application of small unmanned aerial systems for precision agriculture: a review. *Precision Agriculture*, *13*(6), 693–712. doi:10.1007/s11119-012-9274-5

CAPÍTULO 5

QUANTIFYING EFFICACY AND LIMITS OF UNMANNED AERIAL VEHICLE (UAV) TECHNOLOGY FOR WEED SEEDLING DETECTION AS AFFECTED BY SENSOR RESOLUTION

Peña, J. M., Torres-Sánchez, J., Serrano-Pérez, A., de Castro, A. I., & López-Granados, F. (2015). Quantifying Efficacy and Limits of Unmanned Aerial Vehicle (UAV) Technology for Weed Seedling Detection as Affected by Sensor Resolution. *Sensors*, 15(3), 5609–5626. doi:10.3390/s150305609.

1. RESUMEN

Para optimizar la aplicación de herbicidas en cultivos se necesitan mapas de malas hierbas obtenidos de forma precisa y en el momento requerido. En este contexto, la presente investigación cuantificó la eficacia y limitaciones de imágenes remotas tomadas con un UAV para la detección temprana de malas hierbas en estado de plántula. La capacidad para discriminar malas hierbas fue significativamente afectada por la resolución espectral (tipo de cámara), espacial (altura de vuelo) y temporal (fecha del estudio) de las imágenes. Las imágenes en color-infrarrojo tomadas a 40 m de altura y 50 días tras la siembra (fecha 2), cuando las plantas tenían 5-6 hojas verdaderas, dieron lugar a la mayor precisión en la detección de malas hierbas (91%). A esta altura de vuelo, las imágenes tomadas antes de la fecha 2 tuvieron resultados ligeramente mejores que las tomadas después. Sin embargo, esta tendencia cambió en las imágenes en rango visible tomadas a 60 o más metros de altura, las cuales arrojaron resultados notablemente mejores en la fecha 3 (57 días tras la siembra) gracias al mayor tamaño de las plantas. Nuestros resultados mostraron los requerimientos en cuanto a resolución espectral y espacial necesarios para generar un mapa de malas hierbas en fase temprana, así como el mejor momento para la toma de las imágenes con un UAV, con el objetivo último de aplicar estrategias de control localizado de malas hierbas.

2. ABSTRACT

In order to optimize the application of herbicides in weed-crop systems, accurate and timely weed maps of the crop-field are required. In this context, this investigation quantified the efficacy and limitations of remote images collected with an unmanned aerial vehicle (UAV) for early detection of weed seedlings. The ability to discriminate weeds was significantly affected by the imagery spectral (type of camera), spatial (flight altitude) and temporal (the date of the study) resolutions. The colour-infrared images captured at 40 m and 50 days after sowing (date 2), when plants had 5–6 true leaves, had the highest weed detection accuracy (up to 91%). At this flight altitude, the images captured before date 2 had slightly better results than the images captured later. However, this trend changed in the visible-light images captured at 60 m and higher, which had notably better results on date 3 (57 days after sowing) because of the larger size of the weed plants. Our results showed the requirements on spectral and spatial resolutions needed to generate a suitable weed map early in the growing season, as well as the best moment for the UAV image acquisition, with the ultimate objective of applying site-specific weed management operations.

3. INTRODUCTION

Sunflower is the most important annual oilseed crop in southern Europe and the Black Sea area, with over 5 M·ha grown annually (FAO 2014). Spain has 0.8 M·ha of sunflowers (MAGRAMA 2014). The patchy distribution of weeds in sunflower fields has already been demonstrated using on-ground sampling (M. Jurado-Expósito et al. 2009; Montserrat Jurado-Expósito et al. 2003) and remote imagery from piloted aircraft (Peña-Barragán et al. 2007). Although the distribution of weeds is patchy, herbicides are usually broadcast over entire fields, even onto the weed-free areas. To overcome this problem, site-specific weed management (SSWM) is used to spray an adapted herbicide treatment only on weed patches and/or to adjust different herbicide applications according to weed species composition, e.g., herbicide resistant, broadleaved or grass weeds. Thus, one of the crucial components for SSWM is accurate and timely weed maps, which must be generated to design the corresponding site-specific herbicide applications (Shaw 2005). With the SSWM approach, the hope is to also reduce herbicide use.

This strategy fits well with European concerns on herbicide use (Horizon 2020, European Commission, Societal Challenge 2: Sustainable Food Security. SFS-3-2014: Practical solutions for native and alien pests—including weeds—affecting crops) and has prompted the European Union to enact restrictive legislation (Regulation EC No. 1107/2009 and Directive 2009/128/EC). The legislation requires action to achieve the sustainable use of pesticides and to promote the use of the most advanced and latest technologies. Of the advanced technologies in weed research today, one of the most promising and innovative is the use of Unmanned Aerial Vehicles (UAVs or drones) equipped with a perception system for mapping weeds. The maps generated from the remote images captured with the UAV can be used for the further design of appropriate site-specific control measures.

Compared with other remote platforms such as satellites or piloted aircrafts, UAVs can operate at low altitudes (e.g., <120 m), even on cloudy days, and can provide an ultra-high spatial resolution (e.g., pixels < 3 cm) image of the entire crop field. Configurations and specifications for an UAV to map weeds for early site-specific weed management have been reported by (Torres-Sánchez *et al*. 2013). The UAV can be programmed on demand and it can fly with great flexibility and collect remote imagery of crops at critical times in the growing season, thereby improving the farmer's decision-making process (Lelong *et al*. 2008). The total availability is fundamental for UAVs to perform a multi-temporal study in early weed detection and to determine the best time for taking the imagery needed to design post-emergence herbicide control strategies, just when the crop and weeds have similar appearance and spectral characteristics (López-Granados 2011; Torres-Sánchez, Peña, *et al*. 2014). With the high spatial and temporal resolution requirements and the spectral

similarity between weed and crop seedlings, remote-sensed discrimination of early-season crop and weeds remains a challenge in weed research.

According to (Yu *et al*. 2006), one of the inherent problems with increasing the spatial resolution of remote images is that single pixels no longer capture the characteristics of classification targets. This produces an increase in intra-class spectral variability and, subsequently, a reduction in statistical separability among classes with conventional pixel-based classification methods, which can involve a reduction in classification performance and accuracy in comparison with coarser resolution images. Object-based image analysis (OBIA) is a powerful procedure and a fine alternative to the pixel-based methods (Blaschke 2010). The OBIA approach first identifies spatially and spectrally homogenous units (objects) created by grouping adjacent pixels according to a procedure known as segmentation. It then develops automated and auto-adaptive classification methods by using the objects as the minimum information units and combining their spectral, contextual (position, orientation), morphological and hierarchical information. This methodology has been used successfully for segmenting and classifying a QuickBird satellite image as the first step in isolating wheat fields from other soil uses for further detection of cruciferous weed patches at a late growth stage (de Castro *et al*. 2013). Recently, Peña *et al*. (2013) translated the OBIA strategy to early-season weed discrimination in maize by using UAV imagery and a three-step automatic classification approach: (1) image segmentation into multi-pixel regions that define plants (crop and weeds) and soil background objects; (2) discrimination of vegetation objects based on spectral information; and (3) classification of crop and weed plants based on the position of each plant relative to the crop rows. This OBIA strategy produced maps of three weed coverage categories, and (Peña *et al*. 2013) concluded that an accurate definition of the crop-row structure was essential for the subsequent discrimination between crop and weeds.

Another crucial point for improving the discrimination of weeds in ultra-high spatial resolution images would be to enhance the differences among vegetation and non-vegetation (mostly bare soil) objects by using vegetation indices as well as to determine the optimal threshold value that sets the breakpoint between both general classes (Montalvo *et al*. 2013). One of the automatic methods for threshold calculation is Otsu's (Otsu 1979), which is commonly applied to binary classification (in our case, bare soil and vegetation) and calculates the optimum threshold based on minimising combined spread (intra-class variance). A recent evaluation of the performance of Otsu's threshold method in UAV images (Torres-Sánchez *et al*. 2015) considered two different vegetation indices as well as the influence of image resolution and objects size (*i.e.*, segmentation scale), and concluded that these parameters are critical to accurately characterise the spectral threshold for a precise classification of vegetation (crop and weeds) and non-vegetation objects.

Accounting for the factors introduced previously, the objectives of this work were as follows: (1) to determine the optimum configuration of the UAV flight for the altitude, the date of flight (*i.e.*, crop and weed phenological stage) and the type of sensor (visible-light *vs.* visible-light + near-infrared multispectral cameras); (2) to determine the best sensor for enhancing vegetation (crop and weed) and bare soil class discrimination as affected by the vegetation index applied; and (3) to design and evaluate an OBIA procedure for crop and weed patch detection. Limitations and opportunities of using higher flight altitudes were also analysed for each sensor, aiming to optimise the image acquisition and classification processes.

4. EXPERIMENTAL SECTION

4.1. Study Site

The multi-temporal study was carried out in a sunflower field situated at the public farm Alameda del Obispo, in Córdoba (southern Spain, coordinates 37,856N, 4806W, datum WGS84). The sunflower crop was sown on 15 April 2014, at 6 kg·ha−1 in rows 0.70 m apart, and emergence of the sunflower plants began 15 days after sowing (DAS). An area of approximately 0.5 ha, with flat ground (average slope <1%) and naturally infested by broadleaved weeds such as Chenopodium album L. and Convolvulus arvensis L, was studied in detail. Weed and crop plants were in the principal stage 1 (leaf development) from the BBCH extended scale (Meier 2001) during the study and grew from four true leaves (code 14–16) in the beginning of the experiment to eight true leaves (code 18) at the end.

4.2. UAV Flights: Camera, Altitudes and Dates

The remote images were acquired with two different cameras mounted separately in a quadrocopter UAV, model md4-1000 (microdrones GmbH, Siegen, Germany, Figure 1A): (1) a conventional still visible-light camera, model Olympus PEN E-PM1 (Olympus Corporation, Tokyo, Japan), which acquired 12-megapixel images in true Red-Green-Blue (RGB) colour with 8-bit radiometric resolution; and (2) a multispectral camera, model Tetracam mini-MCA-6 (Tetracam Inc., Chatsworth, CA, USA), which acquired 1.3-megapixel images composed of six individual digital channels arranged in a 2 × 3 array that can acquire images with either 8-bit or 10-bit radiometric resolution (Figure 1B). This camera has user configurable band pass filters (Andover Corporation, Salem, NH, USA) of 10-nm full-width at half maximum and centre wavelengths at B (450 nm), G (530 nm), R (670 and 700 nm), R edge (740 nm) and near-infrared (NIR, 780 nm).

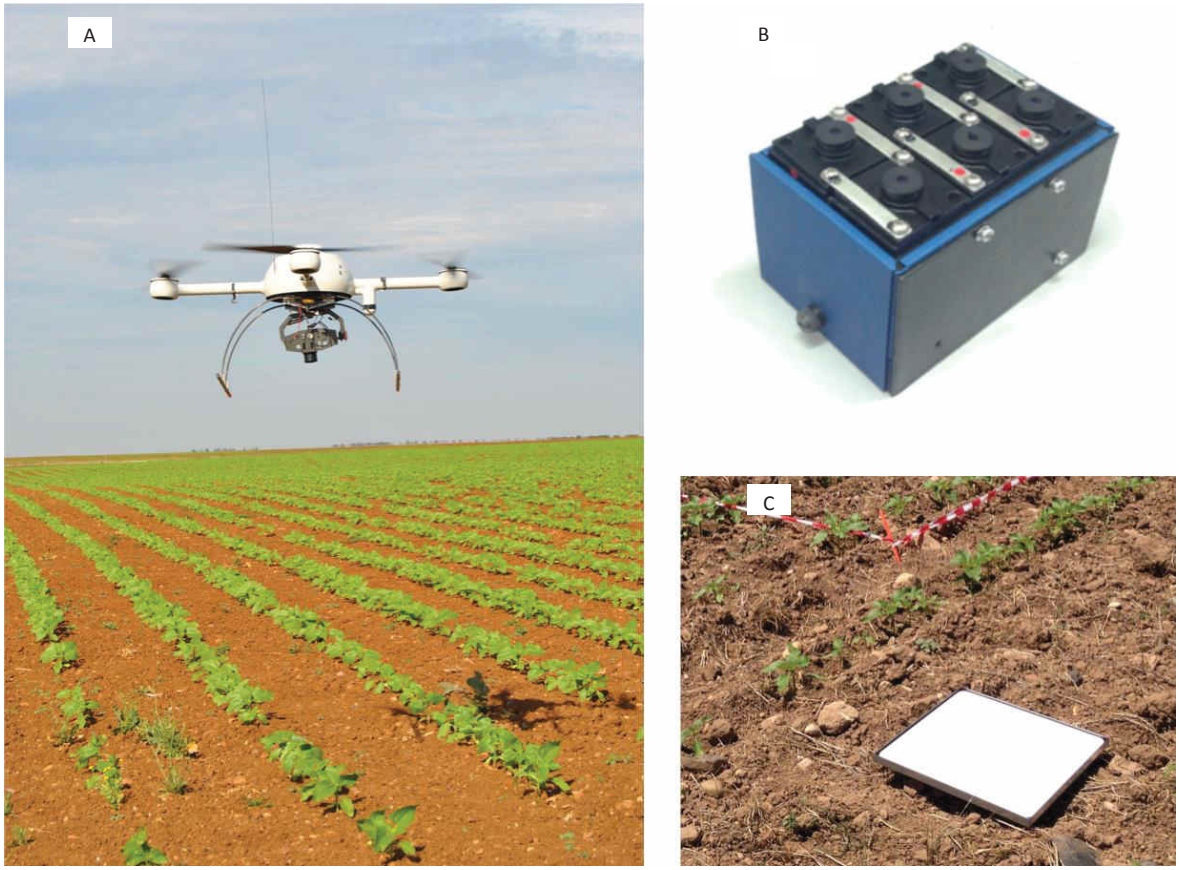

Figure 1. *(A) Unmanned aerial vehicle (UAV), model microdrone MD4-1000, with the visible-light camera attached, flying over the sunflower crop in the early season; (B) TetraCam Multispectral camera; and (C) Spectralon® panel placed in the middle of the field to calibrate the spectral data.*

Detailed information on the configuration of the UAV flights and specifications of the vehicle and the cameras can be found in (Torres-Sánchez *et al*. 2013). A set of aerial images was collected at intervals of 6-7 days on 29 May (date 1, 44 DAS), 4 June (date 2, 50 DAS) and 11 June (date 3, 57 DAS) to quantify multi-temporal discrimination of weeds and crop at the different growth stages described previously (Figure 2). On each date, flights for each camera were conducted at four different altitudes: 40, 60, 80 and 100 m. Each flight route was programmed into the UAV software so that the vehicle ascended vertically above a fixed point in the sunflower field. Once the UAV achieved each programmed altitude, a unique image was captured as the vehicle stopped. In total, twenty four images were taken and analysed, which were geo-referenced by identifying a set of ground target points located in the field by using a GPS and attributing their coordinates to the remote images by using the ENVI software (ENVI 4.4., Research Systems Inc., Boulder, CO, USA).

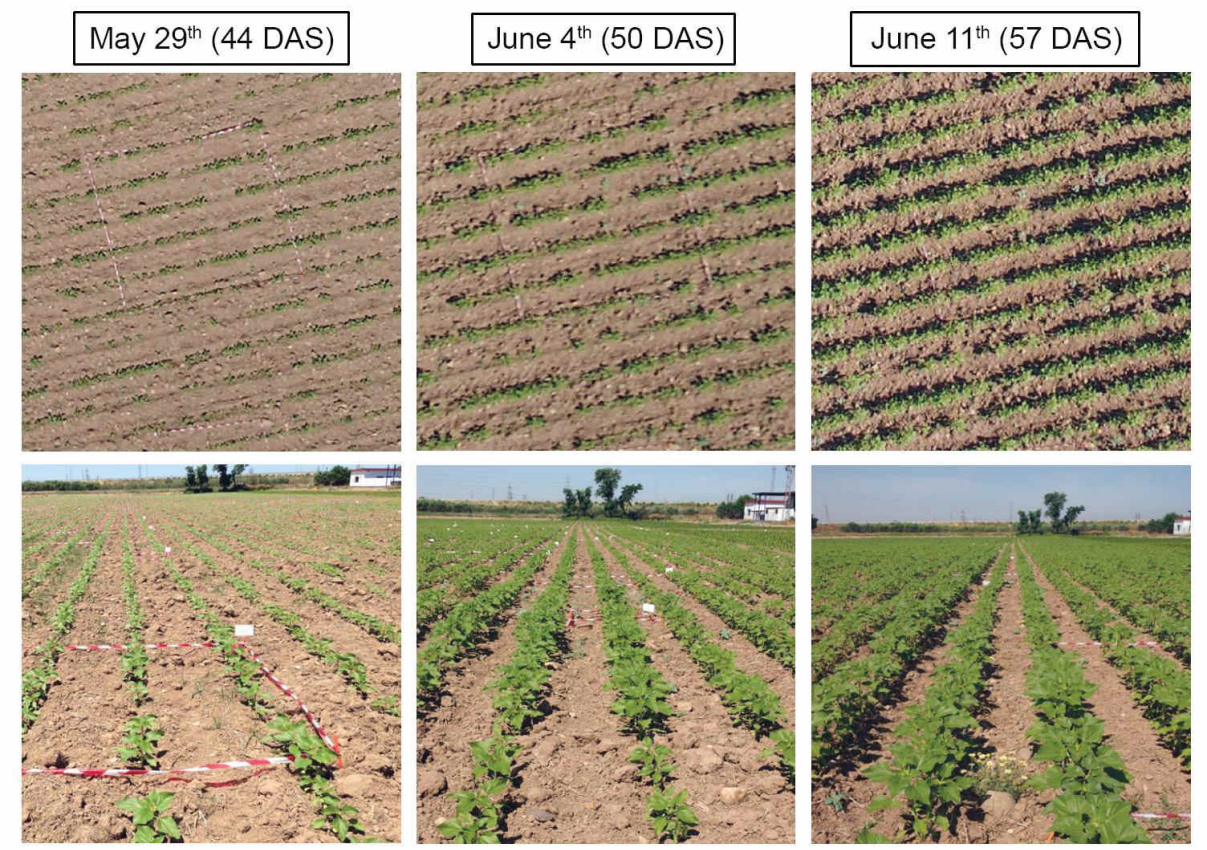

Figure 2. *UAV images collected over the sunflower field at 40 m on three different dates in the early season (top) and associated on-ground photograph (bottom).*

In the course of the UAV flights, a barium sulphate standard Spectralon® panel (Labsphere Inc., North Sutton, NH, USA) of 0.45 × 0.45 m (Figure 1C) was placed in the middle of the field to correct the image data for the effects of shifting light conditions (e.g., due to changes in solar elevation or clouds) over time (several flight missions in three different dates). Digital images were spectrally corrected by applying an empirical linear relationship in which the equation coefficients were derived by fitting the digital numbers of the image pixels located in the Spectralon panel to the Spectralon ground values (Hunt, Jr. *et al*. 2010). The images taken with the visible-light camera were used directly after downloading to the computer, but images taken with the multispectral camera required preprocessing. This camera takes the images of each channel in raw format and stores them separately on six individual CF cards embedded in the camera. Therefore, an alignment process was needed to group the six single images into a multi-band image. The Tetracam PixelWrench 2 software (Tetracam Inc.) supplied with the multispectral camera was used to perform the alignment process.

4.3. OBIA Algorithm

The OBIA procedure designed for the weed mapping tasks was developed using the commercial software eCognition Developer 8.9 (Trimble GeoSpatial, Munich, Germany). It was based on the weed mapping algorithm fully described in our previous work conducted in early-season

maize fields (Peña *et al*. 2013; Peña-Barragán *et al*. 2012). However, the procedure presented here is original and includes improvements and variations related to the special characteristics of sunflower crops.

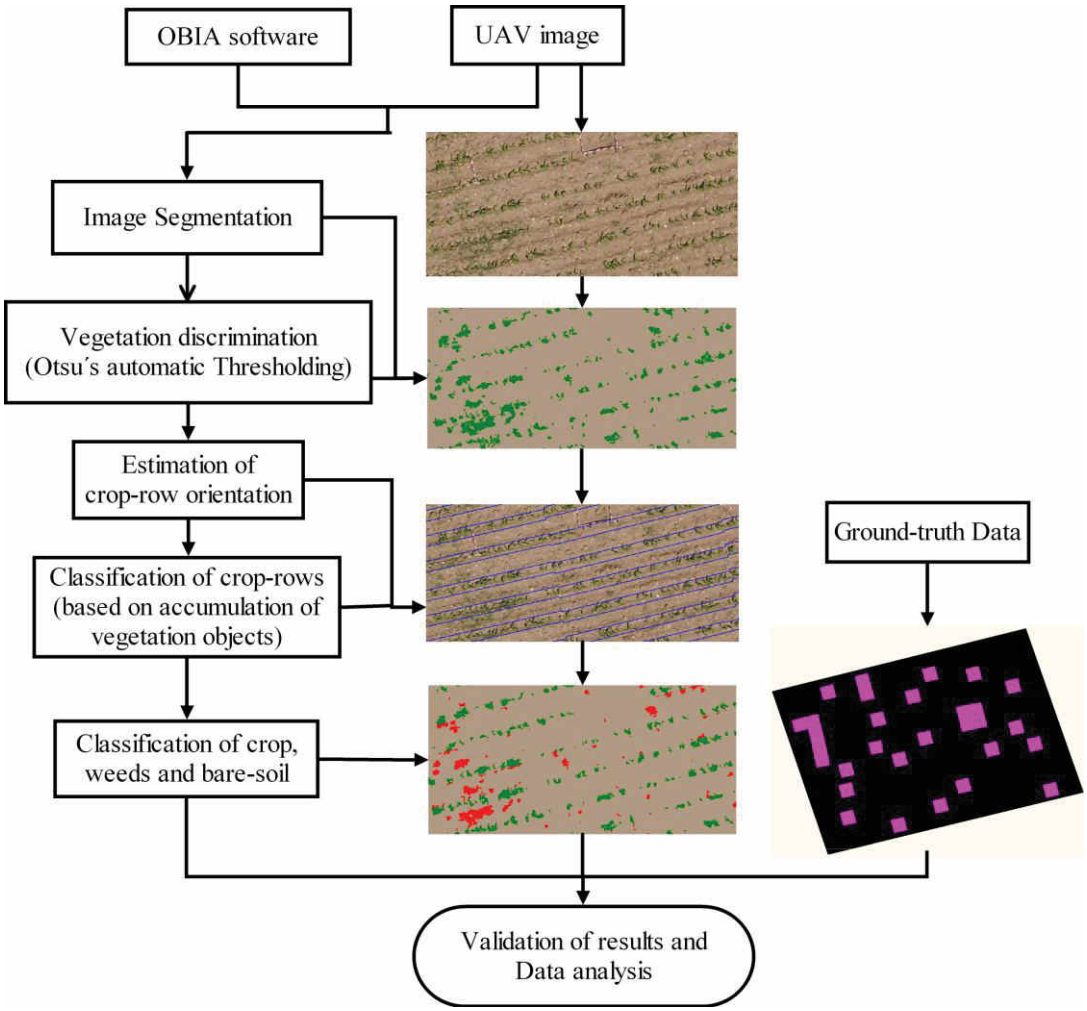

Figure 3. *Flowchart of the OBIA procedure applied for crop-row classification and weed detection.*

The OBIA algorithm combined object-based features such as spectral values, position, orientation and hierarchical relationships among analysis levels; the algorithm recognised that the plants growing on the surface between crop rows were weed plants. Therefore, the algorithm was programmed to accurately detect the crop rows by the application of a dynamic and auto-adaptive classification process, and then classified the vegetation objects outside the crop rows as weeds. The flowchart of the detailed image analysis can be examined in (Peña *et al*. 2013); in this paper, only the main variations and upgrades are emphasised. The entire process is automatic and is composed of a sequence of routines described as follows (Figure 3):

(a). Field segmentation in sub-plots: The algorithm segmented the UAV images into small plots of a customised size to address the spatial and spectral variability of the crop field. In our case, sub-plots of 5 × 5 m were selected and sequentially analysed.

(b). Sub-plots segmentation in objects: The image sub-plots were sub-segmented using the multi-resolution algorithm implemented in eCognition to create multi-pixel objects representing the elements of the fields, *i.e.*, crop and weed plants (vegetation objects) and soil background (bare soil objects). Segmentation is a bottom-up region-merging process based on band weights and on five parameters (scale, colour, shape, smoothness and compactness) defined by the operator. After visually testing several segmentation outputs, the selected values were 10, 0.9, 0.1, 0.5 and 0.5 for scale, colour, shape, smoothness and compactness, respectively. Within the range of spatial resolutions (a few centimetres) studied in this investigation, this segmentation setting was adequate for all the studied scenarios. However, this issue merits further investigation aiming to optimize the segmentation setting as affected by the crop pattern (e.g., crop row separation) and image spatial resolution (Torres-Sánchez *et al*. 2015). The resulting objects contained new contextual and morphological information (e.g., orientation, position, size, shape, and others) that were used in the next phases of the classification process.

(c). Vegetation objects discrimination: After segmentation, the first step in the classification process was to discriminate the vegetation objects from the bare soil objects. Two spectral indices were used: (1) the Excess Green index (ExG, Equation (1)) for the visible-light camera (Tellaeche *et al*. 2008; Woebbecke *et al*. 1995); and (2) the Normalised Difference Vegetation Index (NDVI, Equation (2)) for the multispectral camera (Rouse *et al*. 1973). The indices were calculated as follows:

$$ExG = 2g - r - b;\ r = \frac{R}{R+G+B}\ g = \frac{G}{R+G+B}\ b = \frac{B}{R+G+B} \quad 1)$$

$$NDVI = \frac{NIR - R}{NIR + R} \quad 2)$$

These indices enhance spectral differences of vegetation objects against the non-vegetation ones as previously reported by (Jorge Torres-Sánchez et al. 2013), while minimizing solar radiance and soil background effects (Jackson and Huete 1991). The determination of the optimum ExG and NDVI values for vegetation discrimination in the UAV images was conducted by an automatic and iterative threshold approach following the method of Otsu (Otsu 1979) and implemented in eCognition according to (Torres-Sánchez *et al*. 2015):

(d). Crop-row classification: Once the vegetation objects were discriminated, the crop-row structure was classified by following three steps: (1) estimation of the crop-row orientation; (2) image gridding based on stripes following the crop-row orientation; and (3)

crop-row classification. First, crop-row orientation was determined by an iterative process in which the image was repeatedly segmented in stripes with different angles (from 0° to 180°, with 1° of increase ratio), with the selected orientation the one in which the stripes showed a higher percentage of vegetation objects. Next, a new segmentation level (*i.e.*, upper level) was created above the previous multi-resolution one (*i.e.*, lower level) in which the image was segmented to create a mesh of stripes with the same direction as the selected crop-row orientation angle. Finally, the stripe in the upper segmentation level with the higher percentage of vegetation objects in the lower segmentation level were classified as crop rows, following the criteria described in (Guerrero *et al*. 2013). In this process, after a stripe was classified as a crop-row, the separation distance between rows (0.7 m in sunflower) was used to mask the neighbouring stripes within this distance, which avoided classifying areas with high weed infestation as crop rows.

(e). Weed and crop discrimination: Once the crop-rows were classified, the remaining stripes were classified as crop-row buffer (strings in contact with the crop rows) and non-crop area in the upper segmentation level. Next, the hierarchical relationship between the upper and the lower segmentation levels was used to execute the discrimination of crop and weeds. The vegetation objects (in the lower segmentation level) that were located either under the crop rows or under the non-crop area (in the upper segmentation level) were classified either as sunflower or as weeds, respectively. The remaining vegetation objects located under the buffer area were classified following a criterion of minimum spectral distance, *i.e.*, an unclassified vegetation object was assigned to the sunflower or weed class depending on its higher degree of spectral similarity to its surrounding sunflower or weed objects, respectively.

(f). Weed coverage assessment: A vector file containing 30 geo-referenced sampling frames, 1 × 1 m in size, was overlapped in the classified image to calculate the relative area corresponding to each class, *i.e.*, sunflower, weeds and bare soil, in every frame. Weed coverage was determined as the percentage of pixels classified as weed per unit of ground surface. Information derived from these frames was used for validation purposes, as explained in the next section.

4.4. Evaluation of OBIA Algorithm Performance

The performance of the OBIA algorithm in each case study (each camera, flight altitude and date) was evaluated by visually comparing the results obtained for crop-row identification and weed discrimination with real data observed in 30 ground-truth 1 × 1 m^2 sampling frames in the field.

These sampling areas were regularly distributed in the study area and were representative of the weed infestation observed in the field and included a number of sampling frames free of weeds. Ground-truth observations were derived from vertical remote images collected with a UAV flight at 10 m. For this purpose, the UAV equipped with the visible-light camera was programmed to fly continuously taking overlapped images every second (80% forward-lap and 30% side-lap). The set of UAV images were mosaicked using Agisoft Photoscan Professional Edition (Agisoft LLC, St. Petersburg, Russia) software following the protocol described in (Gómez-Candón *et al*. 2014; Torres-Sánchez *et al*. 2013). Because of the low flight altitude, the mosaicked image had 0.38 cm/pixel of spatial resolution, which made it possible to visually identify the individual plants in every reference frame and thus conduct a manual classification of the ground-truth data for crop plants, weeds and bare-soil (Figure 4). By comparing observed data and classification outputs in each case study, the OBIA algorithm was evaluated by quantifying the number of correct frames, *i.e.*, those sampling frames in which all the weed plants were correctly attributed to weed objects (Figure 4-1-C). There is no 4-1, please confirm Alternatively, incorrect frames (e.g., crop plants classified as weed objects, weed plants classified as bare soil objects, *etc.*) were also labelled as three different types: (1) underestimated, *i.e.*, weed-infested frames in which some weed plants were detected but other weed plants remained undetected by the OBIA algorithm (Figure 4-2-C); (2) false negative, *i.e.*, weed-infested frames in which no weeds were detected (Figure 4-3-C); and (3) false positive, *i.e.*, frames in which weeds were overestimated (e.g., crop plants or bare soil elements classified as weed objects) (Figure 4-4-C).

5. RESULTS AND DISCUSSION

5.1. Image Spatial Resolution and Covered Area As Affected by Flight Altitude

The image spatial resolution captured by each camera and the area covered by each individual image at different UAV flight altitudes are shown in Table 1. The visible-light and the multispectral cameras captured images with pixel sizes ranging from 1.52 cm to 3.81 cm and from 2.16 cm to 5.41 cm at flight altitudes of 40 and 100 m, respectively (Figure 5), as determined by a proportional relationship between sensor resolution and flight altitude. The ultra-high spatial resolution of the sensors is one of the crucial features for weed mapping early in the season when crop and weeds are at a young phenological stage (e.g., four true leaves).

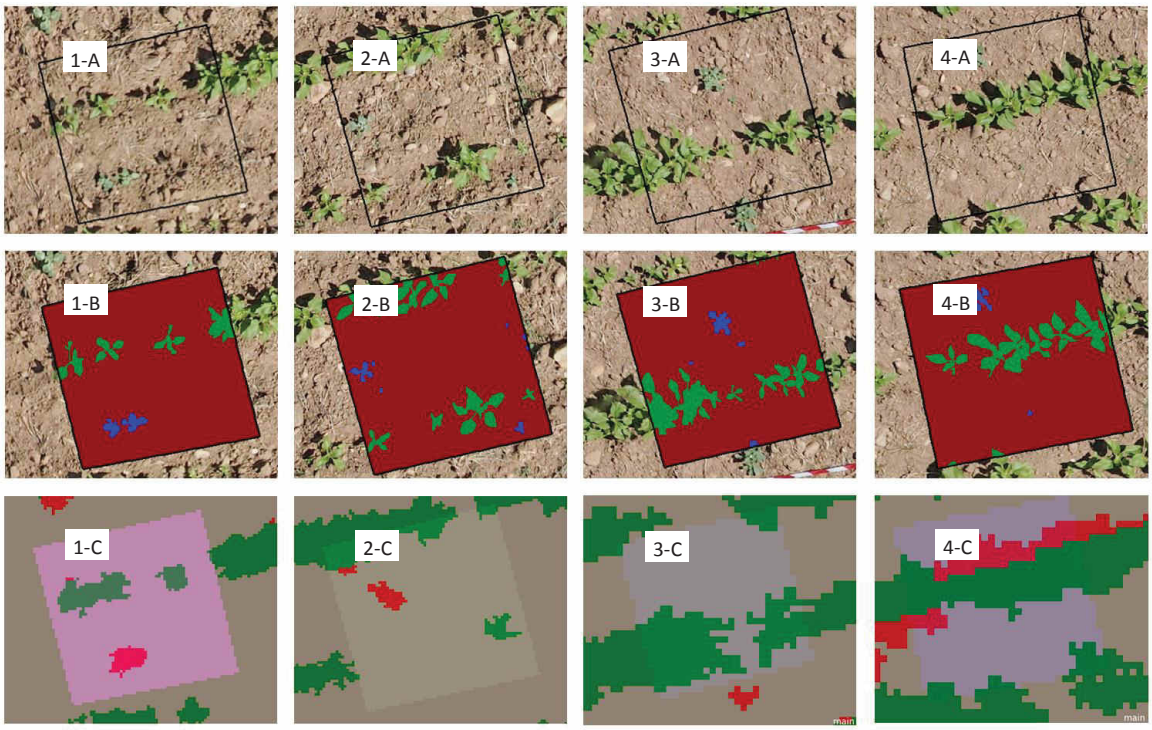

Figure 4. *Examples of four sampling frames showing: (1) correct classification; (2) underestimation of weeds; (3) false negative errors (i.e., no detection of weeds); and (4) false positive errors (i.e., overestimation of weeds) in three scenarios: (A) On-ground photographs; (B) manual classification of observed data; and (C) image classification performed by the OBIA algorithm. Clearer original image*

Table 1. *Image spatial resolution (pixel size) and area covered as affected by flight altitude and type of camera.*

Flight Altitude	Pixel Size (cm)		Covered Area (ha)	
	Visible-Light Camera	Multispectral Camera	Visible-Light Camera	Multispectral Camera
40 m	1.52	2.16	0.28	0.06
60 m	2.28	3.27	0.63	0.14
80 m	3.04	4.33	1.13	0.25
100 m	3.81	5.41	1.77	0.38

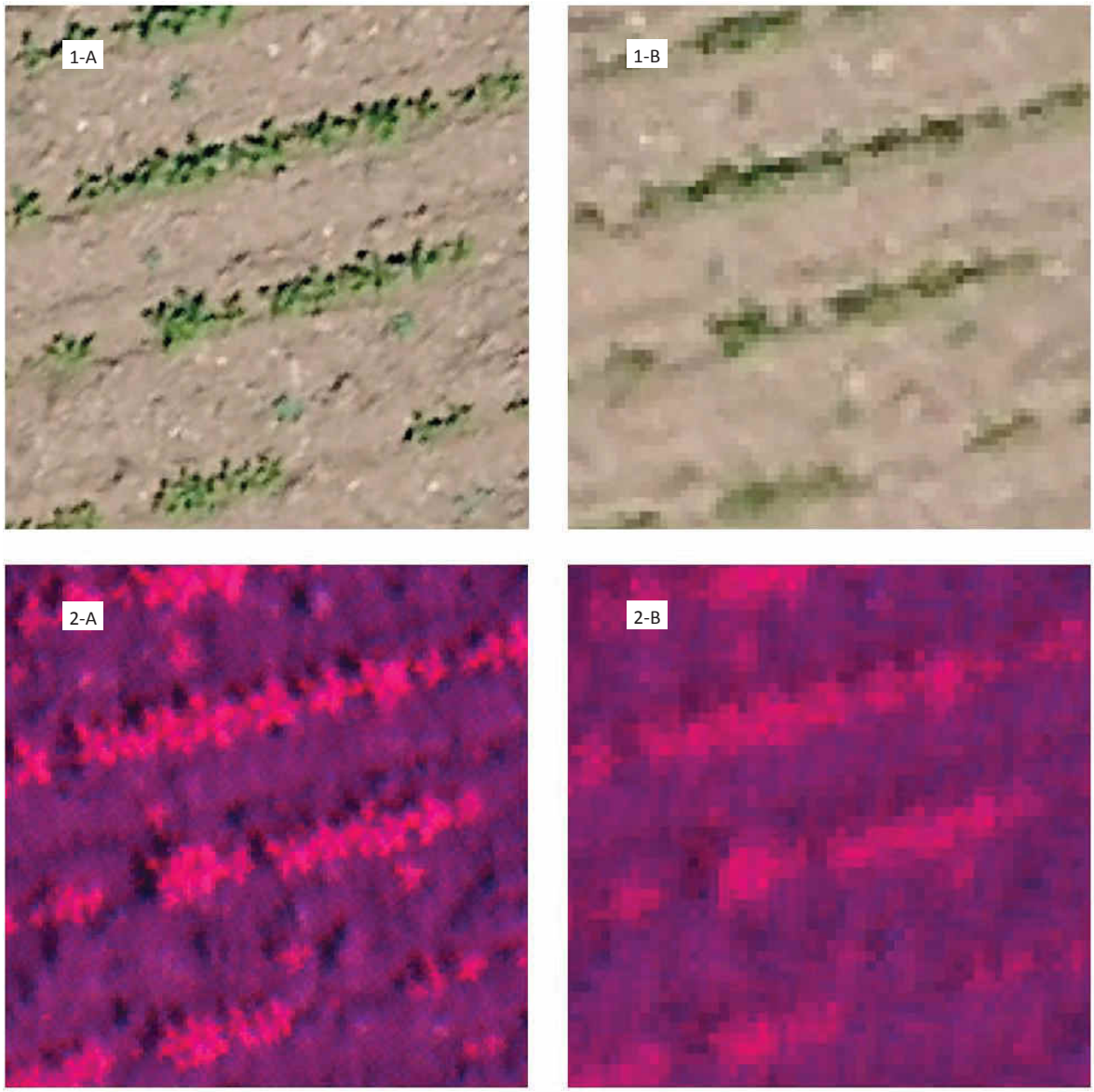

Figure 5. *Details of the image spatial resolution captured by the visible-light camera and the multispectral camera at: (A) 40 m altitude; and (B) 100 m altitude.*

In general, at least four pixels are required to detect the smallest objects within an image (Hengl 2006). Accordingly, if the discrimination of individual weed plants is the objective, the pixel size should be approximately 1–4 cm, which corresponds to flight altitudes of 40 to 100 m for the visible-light camera and altitudes of 40 to 60 m for the multispectral camera. However, if the objective is weed patch detection, the pixel size of remote images could be 5 cm or even greater, which corresponds to a flight altitude of 100 m or higher for both cameras. One of the most relevant parameters was the area overlap because of its strong implications for the configuration of the optimum flight mission. This parameter is directly related to the flight altitude and the type of camera. At the flight altitudes in this study, each remote image captured with the visible-light camera covered approximately 4.6 times more surface area than the multispectral camera, e.g., increasing from 0.06 ha to 0.28 ha at 40 m and from 0.38 to 1.77 ha at 100 m, respectively (Figure 6).

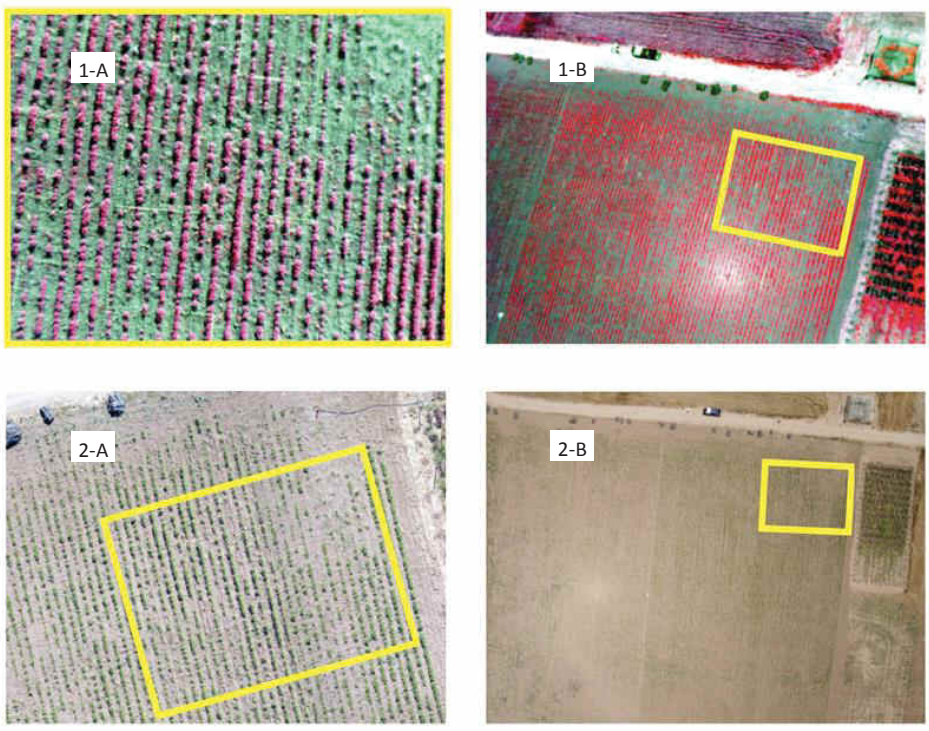

Figure 6. *Individual UAV images collected with the multispectral (1) and the visible-light (2) cameras at: 40 m (A); and 100 m (B) altitude. The yellow squares serve to compare the area covered by the images from each camera at both flight altitudes. The sunlight effect (light spot) observed in 1-B and 2-B were minimized after applying vegetation indices (see Section 4.3).*

The differences in pixel size and covered area were because of the technical specifications of each camera, since the camera focal length affects both parameters, whereas the camera sensor size only affects the image's pixel size. Accordingly, when the user defines the flight program, it is necessary to balance the flight project to keep the image spatial and spectral quality steady, as the area covered is considered. Two main conditions must accounted for: (1) to provide remote images with a fine enough spatial and spectral resolution to guarantee weed discrimination at early growth stages; and (2) to cover as much surface area as possible to optimise the operation length of the UAV flight.

5.2. Accuracy Assessment on Classification of Crop-Rows

The OBIA algorithm identified and counted the number of sunflower rows with 100% accuracy in all the images, independent of the camera type, date or flight altitude (Figure 7). This demonstrated the efficiency and robustness of the procedure developed for crop-row classification in which the stripes with the higher percentage of vegetation objects were selected as seeds for crop-row identification. This has strong implications for the success of the next steps in the OBIA procedure designed for weed discrimination, which should be focused on minimising potential errors in detecting the vegetation objects (weeds) located in the area between the sunflower rows.

Table 2. *Accuracy assessment of weed detection as affected by camera (vegetation index), date (phenological stage) and flight altitude. In columns, percentage of ground-truth frames correctly and incorrectly classified (see Section 2.4 and Figure 4).*

Flight date (Phenological Stage)	Weed Presence	Flight Altitude (m)	Camera (Vegetation Index)							
			Visible-Light (ExG)				Multispectral (NDVI)			
			Correct (%)	Under-Estimated (%)	False – (%)	False + (%)	Correct (%)	Under-estimated (%)	False – (%)	False + (%)
Date 1–44 DAS (4 true leaves)	Weed	40	71	5	14	10	71	10	19	-
		60	43	10	43	4	62	10	28	-
		80	29	10	48	13	57	10	33	-
		100	19	10	24	47	43	14	29	14
	No weed	40	100	-	-	-	100	-	-	-
		60	100	-	-	-	100	-	-	-
		80	44	-	-	56	100	-	-	-
		100	33	-	-	67	100	-	-	-
Date 2–50 DAS (5–6 true leaves)	Weed	40	77	5	14	4	91	9	-	-
		60	64	18	14	4	62	19	19	-
		80	45	14	27	14	55	9	36	-
		100	45	5	9	41	50	14	27	9
	No weed	40	88	-	-	12	100	-	-	-
		60	88	-	-	12	100	-	-	-
		80	63	-	-	37	100	-	-	-
		100	37	-	-	63	88	-	-	12
Date 3–57 DAS (7–8 true leaves)	Weed	40	68	14	18	-	60	7	33	-
		60	68	14	18	-	50	9	36	5
		80	50	-	14	36	41	9	36	14
		100	27	-	41	32	41	-	45	14
	No weed	40	88	-	-	12	100	-	-	-
		60	100	-	-	-	88	-	-	12
		80	63	-	-	37	88	-	-	12
		100	63	-	-	37	100	-	-	-

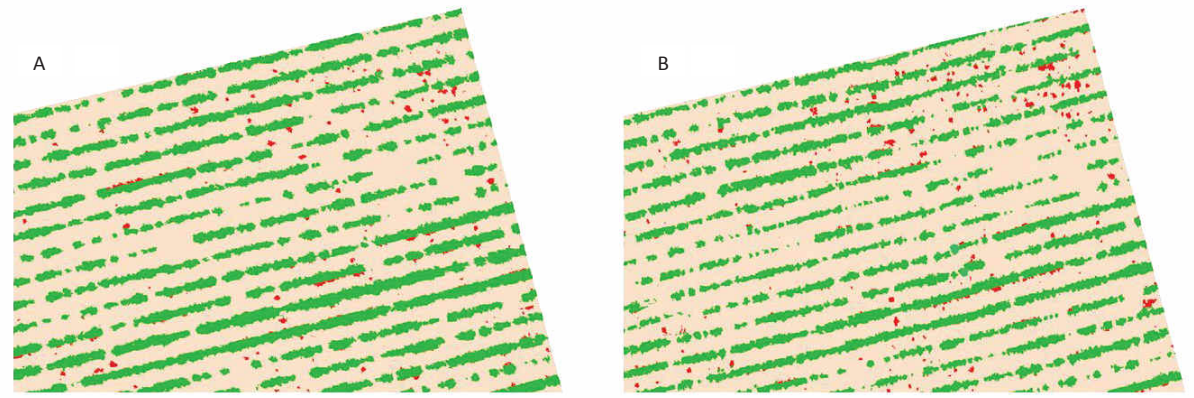

Figure 7. *Image classified in weeds (red), sunflower crop rows (green) and bare soil (brown) using an UAV flying at 40 m altitude with: (A) visible-light camera (ExG index); and (B) multispectral camera (NDVI index).*

5.3. Weed Discrimination As Affected by Camera, Date and Flight Altitude

Accuracy assessment on weed discrimination attained from analyses of the UAV images captured by each camera on each flight (four flight altitudes and three flight dates) is shown in Table 2. A ground-truth frame was classified as correct if all the weed plants within the frame were correctly attributed to weed objects. Otherwise, the frame was labelled as either underestimated, false negative or false positive according to the error observed (see Section 2.4). On the first date (44 DAS, when crop and weed were at the four true leaf phenological stage), 71% classification accuracy for both cameras was obtained for discrimination of weeds at the lowest altitude (40 m). However, at higher flight altitudes, the multispectral camera had higher accuracy (from 62% at 60 m to 43% at 100 m) than the visible-light camera (43% and 19%, respectively). From the analysis of the errors, most errors at 40, 60 and 80 m were attributed to false-negative errors, *i.e.*, misclassification was produced by non-detection of weeds (Figure 4-3-C) keep consistent with that labelled in Figure 4 or, of minor importance, because of the underestimation of weed coverage (Figure 4-2-C). At 100 m, the trend was maintained in images captured with the multispectral camera but not with the images captured by the visible-light camera because, in the latter case, most of the errors were due to false positives (47%), which was attributed to classification of sunflowers as weeds (Figure 4-4-C). This source of error gains importance at higher altitudes because of the spectral mixture between sunflowers and bare soil elements that occurred in the edges of the crop-rows. Because of a loss of spatial resolution, spectral information of the row edge pixels is a mix of sunflower (high ExG and NDVI values) and bare soil (low ExG and NDVI values) spectral response, which is similar to the weed spectral response in some cases (mainly in the visible-light images) and, as a result, it causes over-classification of weeds in the crop-row edges. On the first date, the algorithm for weed detection performed better for imagery captured with the multispectral camera at any of the flight altitudes even with its lower spatial resolution, compared with the visible-light imagery. This indicated that the near-

infrared spectral information used by the multispectral camera is more suitable for this task and compensated for its lower spatial resolution (Table 1). From an agronomic point of view, the false positive errors (overestimation of weeds) are more acceptable than false negative errors (non-detection of weeds) for generating the weed maps in practice, assuming that farmers would choose to treat weed-free areas rather than risk allowing weeds to go untreated (Gibson *et al*. 2004). However, both cameras were fully effective (100% accuracy) at 40 and 60 m in the classification of the weed-free areas, which drastically reduced the potential impact of an overestimation of the weeds at the field scale. The accuracy was maintained by the images captured at 80 and 100 m with the multispectral camera but not with the visible-light images (44% and 33% accuracy, respectively).

On the second date (50 DAS, when crop and weeds were at the five-six true leaf phenological stage), the weed detection procedure found higher classification accuracy for both cameras, resulting in 77% and 91% of correct weed-infested frames at 40 m for the visible-light and the multispectral cameras, respectively. Similar to results from the previous date, the classification accuracy decreased in all the images with increasing altitude. The majority of errors were attributed to no-detection (false negative) and underestimation of weeds, although the highest value was the false positive error (41%) from the visible-light images captured at 100 m because of incorrect classification of the crop-row edges as weeds (Figure 4-4-C). In the weed-free frames, the images captured with the multispectral camera were 100% accurate at 40, 60 and 80 m, although the OBIA algorithm slightly decreased its accuracy to 88% at 100. In the visible-light images, the results followed the trend of the first date, although the images had lower accuracy at 40 and 60 m (88%) and higher accuracy at 80 m (63%) and 100 m (37%) in comparison with the previous date. As an example, the weed maps generated on the second date from the images captured by both sensors at 40 m (best scenario) are shown in the Figure 7. Weed coverage was found to be 1.25% of the field area with the NDVI images (multispectral camera) and 0.98% with the ExG images (visible-light camera).

On the third date (57 DAS, when crop and weeds were at the seven-eight true leaf phenological stage), lower accuracy of weed detection was found, in general, than on the previous dates for the majority of the images and flight altitudes analysed, with the exception of the visible-light images captured at 60 and 80 m. For example, the accuracy of weed detection in the images captured at 40 m was 3% and 9% lower with the visible-light camera (ExG images) and 11% and 31% lower with the multispectral camera (NDVI images) in comparison with the results from date 1 and 2, respectively. On this date (57 DAS), the highest percentage of errors was mainly from non-detection of weeds (false negative) in both types of images, although primarily in the images captured with the multispectral camera. Although the weed plants were bigger on this date and their discrimination supposedly easier, weeds were masked by sunflower shadows, which increased the degree of weed

misclassification. False positive errors were also an important source of confusion in the visible-light images captured at 80 and 100 m, occurring in 36% and 32% of the weed-infested frames, respectively, and in 37% of the weed-free frames at both altitudes. As on the previous dates, performance of the OBIA algorithm in the weed-free zones was very satisfactory with the multispectral camera at any altitude and with the visible-light camera at 40 and 60 m.

After the importance of efficient classification of crop-rows, spectral information derived from ExG (in the visible-light images) and NDVI (in the images captured with the multispectral camera) indices could initially be considered the primary factor affecting weed identification. However, image spatial resolution (or, equally, flight altitude) and the date of the study (*i.e.*, crop and weed phenological stage) were also key factors in the accuracy of the classification, mainly in the weed-infested zones (Table 2). According to the results obtained for the weed-infested frames using UAV images captured at 40 m with either of the cameras, the best time for weed detection in early-season sunflower fields was approximately 52 days after sowing (date 2). At this altitude, our results showed that the images captured before this date were more suitable for weed detection than the images captured later in the growing season. However, the best time for weed detection differed for each type of image at higher flight altitudes. If the visible-light camera was used at 60 or 80 m, the best results were obtained for date 3 (57 DAS) because this camera was ineffective on the earliest dates due to the small size of the weed plants and some degree of confusion between their bright leaves and the bare background soil. This problem was minor with the multispectral camera because of the near-infrared information provided in these images, and the results were slightly better on date 1 (44 DAS) than on date 3 at 60, 80 and 100 m.

Considering both weed-infested and weed-free zones, the accuracy obtained with the multispectral camera (by using NDVI images) was 14%, 18% and 5% higher than the accuracy achieved with the visible-light camera (by using ExG images) on dates 1, 2 and 3, respectively. These results have relevant implications for choosing the most appropriate camera because the visible-light camera is a low-cost sensor, whereas the multispectral camera is a costly sensor. Moreover, the visible-light camera generates higher spatial resolution imagery, and its images cover a larger area of study in comparison with the multispectral camera. The errors observed in the ExG images were mainly due to false negative (*i.e.*, no-detection of weeds); the NDVI images detected weed plants in a higher number of frames, but weed coverage was underestimated in some cases. The latter errors could be more acceptable to the farmers because they usually prefer a conservative option and avoid leaving weed patches untreated. Importantly, the OBIA algorithm successfully detected 100% of the crop rows and almost all the weed-free frames in the majority of the cases. This result is essential for providing accurate information to the decision-making system and to help the farmers select, with

near 100% confidence, the weed-free areas where the site-specific weed control equipment does not need to go. This is very relevant not only for reducing herbicide applications but for optimising energy (fuel) and field operating time and expense.

6. CONCLUSIONS

Until now, obtaining weed infestation maps early in the growing season has been a great challenge because of the reduced size of the weed and crop plants and their spectral similarity at an early phenological stage. This challenge has been overcome in this investigation by the combined use of an Unmanned Aerial Vehicle (UAV), remote images captured with cameras at visible and near-infrared spectral ranges, and application of object-based image analysis (OBIA) techniques. With both cameras, the highest accuracy in weed detection was achieved with the images captured at 40 m on date 2 (50 days after sowing, DAS) when weeds and sunflower plants had 5-6 true leaves (code 15-16, BBCH scale). On this date, up to 91% accuracy was attained with the images captured by the multispectral camera. At 40 m, the images captured sooner (date 1) reported slightly better results than the images captured later (date 3). However, from 60 m altitude and higher, the images captured with the visible-light camera reported notably better results on date 3 because of the larger size of the weed plants and less confusion distinguishing between crop-row edges and weeds. The source of errors was different for each scenario studied. In general, the errors in the weed-infested zones were mostly attributed to no-detection or underestimation of weeds, whereas the errors in the weed-free zones were due to the wrong classification of the crop-row edges as weeds. This latter type of error was more accentuated in the images captured at higher altitudes due to their lower spatial resolution that blurred spectral detection.

Extrapolating our results to practical use for farmers and prior to performing an UAV flight operation, it is recommended that several factors be considered: (1) camera characteristics and price; (2) area covered by each flight; (3) degree of accuracy needed; and (4) agronomic objective. Therefore, the information reported in this article might be very useful for commercial companies that offer UAV services to farmers or to farmers who own their UAV and must decide on the type of camera (*i.e.*, spatial and spectral sensor resolution) to be used and the optimal flight altitude needed to generate a suitable weed map of the sunflower field early in the season to apply site-specific weed management operations.

7. ACKNOWLEDGMENTS

This research was partly financed by the TOAS European Project (FP7-PEOPLE-2011-CIG-293991) and the Recupera 2020 Project (Spanish MINECO and EU-FEDER Funds). Research of Peña,

Torres-Sánchez and de Castro was financed by the Ramon y Cajal (Spanish MINECO), the FPI (Spanish MINECO) and the JAE-predoc (Spanish CSIC-FEDER funds) Programs, respectively.

8. REFERENCES

Blaschke, T. (2010). Object based image analysis for remote sensing. *ISPRS Journal of Photogrammetry and Remote Sensing*, *65*(1), 2–16. doi:10.1016/j.isprsjprs.2009.06.004

de Castro, A. I., López Granados, F., & Jurado-Expósito, M. (2013). Broad-scale cruciferous weed patch classification in winter wheat using QuickBird imagery for in-season site-specific control - Springer. *Precision Agriculture*, *14*(4), 392–413. Accessed 30 August 2013

FAO. (2014). FAOSTAT. http://faostat3.fao.org/faostat-gateway/go/to/home/E. Accessed 18 June 2014

Gibson, K. D., Dirks, R., Medlin, C. S., & Johnston, L. (2004). Detection of weed species in soybean using multispectral digital images. *Weed Technology*, *18*(3), 742–749. doi:10.1614/WT-03-170R1

Gómez-Candón, D., Castro, A. I. D., & López-Granados, F. (2014). Assessing the accuracy of mosaics from unmanned aerial vehicle (UAV) imagery for precision agriculture purposes in wheat. *Precision Agriculture*, *15*(1), 44–56. doi:10.1007/s11119-013-9335-4

Guerrero, J. M., Guijarro, M., Montalvo, M., Romeo, J., Emmi, L., Ribeiro, A., & Pajares, G. (2013). Automatic expert system based on images for accuracy crop row detection in maize fields. *Expert Systems with Applications*, *40*(2), 656–664. doi:10.1016/j.eswa.2012.07.073

Hengl, T. (2006). Finding the right pixel size. *Computers & Geosciences*, *32*(9), 1283–1298. doi:10.1016/j.cageo.2005.11.008

Hunt, Jr., E. R., Hively, W. D., Fujikawa, S. J., Linden, D. S., Daughtry, C. S. T., & McCarty, G. W. (2010). Acquisition of NIR-Green-Blue Digital Photographs from Unmanned Aircraft for Crop Monitoring. *Remote Sensing*, *2*(1), 290–305. doi:10.3390/rs2010290

Jackson, R. D., & Huete, A. R. (1991). Interpreting vegetation indices. *Preventive Veterinary Medicine*, *11*, 185–200.

Jurado-Expósito, M., López-Granados, F., García-Torres, L., García-Ferrer, A., Sánchez de la Orden, M., & Atenciano, S. (2003). Multi-species weed spatial variability and site-specific management maps in cultivated sunflower. *Weed Science*, *51*(3), 319–328. doi:10.1614/0043-1745(2003)051[0319:MWSVAS]2.0.CO;2

Jurado-Expósito, M., López-Granados, F., Peña-Barragán, J. M., & García-Torres, L. (2009). A digital elevation model to aid geostatistical mapping of weeds in sunflower crops. *Agronomy for Sustainable Development*, *29*, 391–400. doi:10.1051/agro:2008045

Lelong, C. C. D., Burger, P., Jubelin, G., Roux, B., Labbé, S., & Baret, F. (2008). Assessment of Unmanned Aerial Vehicles Imagery for Quantitative Monitoring of Wheat Crop in Small Plots. *Sensors*, *8*(5), 3557–3585. doi:10.3390/s8053557

López-Granados, F. (2011). Weed detection for site-specific weed management: mapping and real-time approaches. *Weed Research*, *51*(1), 1–11. doi:10.1111/j.1365-3180.2010.00829.x

MAGRAMA. (2014). Annual agrarian statistics. http://www.magrama.gob.es/es/estadistica/temas/default.aspx. Accessed 18 April 2014

Meier, U. (2001). *Growth stages of mono- and dicotyledonous plants. BBCH Monograph*. Federal Biological Research Centre for Agriculture and Forestry. http://www.bba.de/veroeff/bbch/bbcheng.pdf

Montalvo, M., Guerrero, J. M., Romeo, J., Emmi, L., Guijarro, M., & Pajares, G. (2013). Automatic expert system for weeds/crops identification in images from maize fields. *Expert Systems with Applications*, *40*(1), 75–82. doi:10.1016/j.eswa.2012.07.034

Otsu, N. (1979). A Threshold Selection Method from Gray-Level Histograms. *IEE Transactions on systems, man, and cybernetics*, *9*(1), 62–66.

Peña, J. M., Torres-Sánchez, J., de Castro, A. I., Kelly, M., & López-Granados, F. (2013). Weed Mapping in Early-Season Maize Fields Using Object-Based Analysis of Unmanned Aerial Vehicle (UAV) Images. *PLoS ONE*, *8*(10), e77151. doi:10.1371/journal.pone.0077151

Peña-Barragán, J. M., López-Granados, F., Jurado-Expósito, M., & García-Torres, L. (2007). Mapping Ridolfia segetum patches in sunflower crop using remote sensing. *Weed Research*, *47*(2), 164–172. doi:10.1111/j.1365-3180.2007.00553.x

Peña-Barragán, Kelly, M., de Castro, & López-Granados. (2012). Object-based approach for crop row characterizatioin in UAV images for site-specific weed management. In *Proceedings of the 4th GEOBIA* (pp. 426–430). Presented at the International Conference on Geographic Object-Based Image Analysis, Rio de Janeiro, Brazil.

Rouse, J. W., Haas, R. H., Schell, J. A., & Deering, D. W. (1973). Monitoring vegetation systems in the Great Plains with ERTS, NASA SP-351 (Vol. 1, pp. 309–317). Presented at the Third ERTS Symposium, Washington, DC, USA: NASA Sp-351 I.

Shaw, D. R. (2005). Translation of remote sensing data into weed management decisions. *Weed Science*, *53*(2), 264–273. doi:10.1614/WS-04-072R1

Tellaeche, A., BurgosArtizzu, X. P., Pajares, G., Ribeiro, A., & Fernández-Quintanilla, C. (2008). A new vision-based approach to differential spraying in precision agriculture. *Computers and Electronics in Agriculture*, *60*(2), 144–155. doi:10.1016/j.compag.2007.07.008

Torres-Sánchez, J., López-Granados, F., De Castro, A. I., & Peña-Barragán, J. M. (2013). Configuration and Specifications of an Unmanned Aerial Vehicle (UAV) for Early Site Specific Weed Management. *PLoS ONE*, *8*(3), e58210. doi:10.1371/journal.pone.0058210

Torres-Sánchez, J., López-Granados, F., & Peña, J. M. (2015). An automatic object-based method for optimal thresholding in UAV images: application for vegetation detection in herbaceous crops. *Computers and Electronics in Agriculture*, 114, 43–52. doi:10.1016/j.compag.2015.03.019.

Torres-Sánchez, J., Peña, J. M., de Castro, A. I., & López-Granados, F. (2014). Multi-temporal mapping of the vegetation fraction in early-season wheat fields using images from UAV. *Computers and Electronics in Agriculture*, *103*, 104–113. doi:10.1016/j.compag.2014.02.009

Woebbecke, D. M., Meyer, G. E., Von Bargen, K., & Mortensen, D. A. (1995). Color indices for weed identification under various soil, residue, and lighting conditions. *Transactions of the American Society of Agricultural Engineers*, *38*(1), 259–269. Accessed 5 July 2011

Yu, Q., Gong, P., Clinton, N., Biging, G., kelly, M., & Schirokauer, D. (2006). Object-based detailed vegetation classification with airborne high spatial resolution remote sensing imagery. *Photogrammetric Engineering & Remote Sensing*, *72*(7), 799–811.

CAPÍTULO 6

EARLY SEASON WEED MAPPING IN SUNFLOWER USING UAV TECHNOLOGY: VARIABILITY OF HERBICIDE TREATMENT MAPS AGAINST WEED THRESHOLDS

López-Granados, F., Torres-Sánchez, J., Serrano-Pérez, A., Castro, A. I. de, Mesas-Carrascosa, F.-J., & Peña, J.-M. (2015). Early season weed mapping in sunflower using UAV technology: variability of herbicide treatment maps against weed thresholds. *Precision Agriculture*, 17(2), 183–199. doi:10.1007/s11119-015-9415-8

1. RESUMEN

El control localizado de malas hierbas es definido como la aplicación adaptada de tratamientos de control sólo donde se encuentran las malas hierbas, usando el herbicida adecuado a la emergencia de malas hierbas. El objetivo de este estudio fue la generación de mapas de infestación de plántulas de malas hierbas en dos campos de girasol median el análisis de imágenes aéreas solapadas del espectro visible e infrarrojo cercano tomadas por un UAV a 30 y 60 m de altura. Las principales tareas se centraron en la configuración y evaluación del UAV y sus sensores para la toma de imágenes y el mosaicado, así como en el desarrollo de un procedimiento automático y robusto de análisis de imagen para la cartografía de plántulas de malas hierbas con el objetivo de diseñar un programa de control localizado de malas hierbas. La estrategia de control se basó en siete umbrales de tratamiento con incrementos del 2,5%, desde un umbral del 0% (el herbicida debe ser aplicado en cuanto haya presencia de malas hierbas) hasta el 15% (se aplica si la cobertura de malas hierbas es mayor del 15%). Como un primer paso del análisis de imagen, las hileras de girasol fueron correctamente alineadas en el orto-mosaico, lo que permitió un análisis de imagen preciso usando OBIA. El algoritmo OBIA desarrollado para la cartografía de malas hierbas en fase temprana con imágenes mosaicadas clasificó las hileras de girasol con un 100% de precisión en ambos campos, a todas las alturas de vuelo y con los dos sensores, indicando la robustez del algoritmo. En cuanto a la discriminación de malas hierbas, altas precisiones fueron observadas usando la cámara multiespectral a cualquier altura de vuelo, con la precisión más alta (casi 100%) siendo registrada para el umbral de tratamiento del 15%, aunque se obtuvieron resultados satisfactorios para los umbrales del 2,5% y 5%, con precisiones mayores del 85% para ambos campos. Las menores precisiones (entre el 50 y 60%) fueron conseguidas con la cámara visible a todas las alturas y para el umbral del 0%. Los ahorros en herbicida fueron relevantes en ambos campos, aunque fueron mayores en el campo 2 debido a su menor infestación. Estos ahorros variaron de acuerdo a los diferentes escenarios estudiados. Por ejemplo, en el campo 2 a 30 m de altura y usando la cámara multiespectral, un rango del 23-3% del campo podría ser tratado para umbrales del 0 al 15%. El procedimiento OBIA calculó múltiples datos que permitieron la estimación de las necesidades de herbicida para un control localizado y a tiempo de las plántulas de malas hierbas.

2. ABSTRACT

Site-specific weed management is defined as the application of customised control treatments only where weeds are located within the crop-field by using adequate herbicide according to weed emergence. The aim of the study was to generate georeferenced weed seedling infestation maps in two sunflower fields by analysing overlapping aerial images of the visible and near-infrared spectrum

(using visible or multi-spectral cameras) collected by an unmanned aerial vehicle (UAV) flying at 30 and 60 m altitudes. The main tasks focused on the configuration and evaluation of the UAV and its sensors for image acquisition and ortho-mosaicking, as well as the development of an automatic and robust image analysis procedure for weed seedling mapping used to design a site-specific weed management program. The control strategy was based on seven weed thresholds with 2.5 steps of increasing ratio from 0% (herbicide must be applied just when there is presence or absence of weed) to 15% (herbicide applied when weed coverage > 15%). As a first step of the imagery analysis, sunflower rows were correctly matched to the ortho-mosaicked imagery, which allowed accurate image analysis using object-based image analysis (OBIA methods). The OBIA algorithm developed for weed seedling mapping with ortho-mosaicked imagery successfully classified the sunflower-rows with 100% accuracy in both fields for all flight altitudes and camera types, indicating the computational and analytical robustness of OBIA. Regarding weed discrimination, high accuracies were observed using the multi-spectral camera at any flight altitude, with the highest (approximately 100%) being those recorded for the 15% weed threshold, although satisfactory results from 2.5% and 5% thresholds were also observed, with accuracies higher than 85% for both field 1 and field 2. The lowest accuracies (ranging from 50 to 60%) were achieved with the visible camera at all flight altitudes and 0% weed threshold. Herbicide savings were relevant in both fields, although they were higher in field 2 due to less weed infestation. These herbicide savings varied according to the different scenarios studied. For example, in field 2 and at 30 m flight altitude and using the multi-spectral camera, a range of 23 to 3% of the field (i.e., 77 and 97% of area) could be treated for 0 to 15% weed thresholds. The OBIA procedure computed multiple data which permitted calculation of herbicide requirements for timely and site-specific post-emergence weed seedling management.

3. INTRODUCTION

Efficient and timely post-emergence weed control is a critical task in crop production because inappropriate weed management tends to reduce yield and increase the negative impacts on the environment. Inappropriate weed management is often related to incorrect herbicide use resulting from three main problems. The first is applying herbicides when weeds are not in the suitable phenological stage (generally when weeds have 4-6 true leaves, although this depends on specific weed species or group of species), the second is applying herbicides without considering any weed threshold (i.e., the weed infestation level above which a treatment is required (Swanton *et al*. 1999)), the third is broadcasting herbicides over the entire field, even when weed-free areas are present due to the usual weed patchy distribution (Jurado-Expósito *et al*. 2003, Jurado-Expósito *et al*. 2005). The first problem is usually addressed using the expert knowledge of farmers. The other two problems can be overcome by developing site-specific weed management (SSWM) strategies according to

weed thresholds (Longchamps *et al*. 2014). These strategies may consist of both a single herbicide treatment to weed patches where a unique group of weeds is present (for example either grass or broadleaved weeds), or use of several herbicides according to the presence of different weed species or group composition, such as grass, broadleaved weeds or a specific problematic weed such as *Orobanche*-broomrape, which can be a serious problem in sunflower production (García-Torres *et al*. 1994; Molinero-Ruiz *et al*. 2014). Sunflower (*Helianthus annuus* L.) is the most important annual oilseed crop in southern Europe and the Black Sea region, with over 5 M ha grown annually (FAO 2015), of which 0.8 M ha are in Spain (MAGRAMA 2014). Weed control operations (either chemical or physical) using large agricultural machinery account for a significant proportion of production costs, create various agronomic problems (soil compaction and erosion) and represent a risk for environmental pollution. In this context, there is a demand for developing a timely, post-emergence, site-specific management program in order to reduce the issues associated with current weed control practices in sunflower and to comply with the European legislation and concerns (Regulation EC No 1107/2009; Directive 2009/128/EC; Horizon2020).

To achieve these goals, it is necessary to generate the weed cover maps, which allow the translation of the spatial distribution of the weed infestation into site-specific herbicide treatment maps. As reported earlier, one of the main variables considered in the weed control decision process in sunflower is weed threshold, which is based on weed density or level of infestation (Castro-Tendero and García-Torres 1995; Carranza *et al*. 1995). If these weed cover or weed infestation maps are built using a grid design, a weed threshold can be derived, which is the percentage of weed cover in every grid, above which a treatment is required. This threshold could be the baseline to generate the herbicide treatment maps. Remote sensing, together with proximal sensing, are now two of the principal sources of data to monitor weeds in a cost effective way. There are previous studies that have investigated weed detection and mapping in crops at late growth stages, e.g., flowering, using imagery from piloted airborne or satellite able to register visible and near-infrared information (Gutiérrez-Peña *et al*. 2008; de Castro *et al*. 2012; de Castro *et al*. 2013). However, the images from these platforms have limited ability to detect weeds at the seedling stage due to their low spatial resolution. Other remote platforms, on the other hand, can generate the high spatial resolution imagery (pixel size ≤ 0.05 m) needed to map weeds at very early phenological stages, which can then be used to develop efficient post-emergence controls. Recent research emphasises the suitability of unmanned aerial vehicles (UAV) for this purpose (López-Granados 2011; Zhang and Kovacs 2012). A key component of a UAV is the versatility of the configuration of onboard sensors, flight altitude, flight planning, etc. The required parameters and their implications for the potential use of UAV in early weed detection have been reported by Torres-Sánchez *et al*. (2013). The main advantages of using UAV is that they can carry (even simultaneously) different sensors to record reflected energy at

diverse spectral ranges according to each detection objective, fly at different altitudes to adjust the desired high spatial resolution and be programmed on demand at critical stages of crop growth. This is crucial when detecting weeds in crops for early post-emergence SSWM when crops and weeds are at the same early phenological stage and they show spectral and visual similarities.

As a result of collecting images with a very high spatial resolution, UAV images taken at low altitude cannot cover the entire study area. This causes the need to take a sequence of a percentage of forward (lateral) and side (longitudinal) overlapped imagery, which acquire a number of images per hectare depending on the flight altitude. These individual images must then be stitched together and ortho-rectified to create an accurately geo-referenced ortho-mosaicked image of the entire plot for further analysis and classification. Image mosaicking is a well-known task for integrating spatial data to assess and monitor disasters (Li *et al*. 2011), map archaeological sites (Lambers *et al*. 2007) or conduct high quality cadastral and urban planning (Haarbrink and Eisenbeiss 2008) using local invariant features or ground control points to perform the aero-triangulation. However, the splicing image used to generate an ortho-image (also named ortho-mosaicked image) of herbaceous crops at early stages of phenological development presents serious difficulties due to the high repetitive pattern of these fields. In a recent work, our research group discussed a detailed procedure to produce accurate ortho-imagery with spatial resolutions from 0.0074 to 0.0247 m and representing the entire area of wheat fields (rows 0.15 m apart) by using UAV flying at low altitudes (Gómez-Candón *et al*. 2014). This work concluded that one of the crucial parameters for generating ortho-mosaicked imagery when mapping row crop environments is crop row alignment on both sides of the overlapped images. This issue was addressed and crop line continuity was preserved because overall spatial errors less than twice the spatial resolution were obtained. This methodology was very useful in the development of the objectives herein presented.

One of the intrinsic problems when processing very high spectral resolution imagery is that individual pixels do not capture the distinctiveness of the targets investigated, which generates a high intra-class spectral variability and, consequently, resulting in difficulties to achieve statistical separation. Segmentation is the process of dividing a digital image into multiple regions according to the proposed objective. For example, to discriminate weeds in a crop using UAV imagery, the segmentation would consist of multi-pixel regions defined by crop, weeds and bare soil. That is, throughout the segmentation, spatially adjacent and spectrally homogeneous pixels would be grouped to create units named objects that contain more information than individual pixels, allowing for a more meaningful interpretation. This is the main idea behind the steps of the OBIA (object-based-image-analysis) procedure: 1) to automatically segment an image into objects, 2) to combine their spectral, contextual, morphological and hierarchical information, and 3) to classify the image by

using them as the minimum information units (Blaschke, 2010). Peña *et al*. (2013) developed an OBIA algorithm using single UAV imagery (not ortho-mosaicked imagery) for early detection of weeds in maize

As previously described, UAV ortho-mosaics are becoming an important tool for the development of site-specific weed prescription strategies because they can offer information on the entire study area and can detect small plants (crop and weeds) at early growth stages, which are not detected using other kinds of remote platforms with coarse spatial resolution (like satellite or conventional aerial platforms with which objects smaller than 0.20 m cannot be detected). Considering that highly accurate mosaics have been obtained working in wheat fields (Gómez-Candón *et al*. 2014), generation of ortho-mosaicked imagery for sunflower fields with 0.70 m row spacing seems to be a reasonable starting point for developing an early SSWM program, in which the relative location of weeds in proximity to the crop rows is a hypothesis for discriminating and mapping weed cover. Thus, the objectives of this work were to: 1) assess the optimal planning of UAV flights with respect to flight altitude and sensor type (visible *vs* visible+Near-infrared cameras) for generating accurate ortho-imagery, 2) design and evaluate an OBIA procedure for mapping bare soil, crop-rows, weed-patches and weed-free zones using the ortho-mosaicked imagery, and 3) simulate several field-based scenarios according to different weed thresholds to evaluate the sections of the sunflower fields that should be and not be managed with herbicide.

4. MATERIALS AND METHODS

4.1. Sites

The study sites were two commercial sunflower fields with flat ground (average slope <1%) situated at Monclova Farm, in Seville province (southern Spain, central co-ordinates datum WGS84: 37.528N and 5.315W for field 1, and 37.524N, 5.318W for field 2). The sunflower crops were sown on March 25th, 2013, at 6 kg ha^{-1} in rows 0.70 m apart, and emergence of the sunflower plants started 15 days after sowing. The sunflower fields had an area of approximately 1 ha each, and were naturally infested by the broadleaved weeds *Amaranthus blitoides S. Wats* (pigweed), *Sinapis arvensis* L. (mustard) and *Convolvulus arvensis* L. (bindweed), as well as *Chenopodium album* L. (lambsquarters) in field 2. All these weed species can be controlled by the same type of herbicide. Weed and crop plants were in the principal stage 1 (leaf development, four-six true leaves, codes 14-16) from the BBCH (Biologische Bundesanstalt, Bundessortenamt und CHemische Industrie) extended scale (Meier 2001).

4.2. UAV flights: cameras and altitudes

The co-ordinates of each corner of the experimental fields were collected with GPS for planning the flight route. Then, each flight route was programmed into the UAV software to allow the UAV to attain every programmed altitude and required degree of image overlap. This imagery was collected with two different cameras mounted separately in a quadrocopter UAV, model md4-1000 (microdrones GmbH, Siegen, Germany, Fig. 1) on May 7th 2013 at two different altitudes: 30 and 60 m. A sequence of 30% side-lap and 60% forward-lap imagery was collected to cover the entire area of the experimental sunflower fields corresponding to each flight mission cameras and altitudes (Fig. 2). One of the cameras used was a low-cost digital visible camera, model Olympus PEN E-PM1 (Olympus Corporation, Tokyo, Japan), which acquires 12-megapixel images in true Red-Green-Blue (RGB) colour with 8-bit radiometric resolution. The other sensor was a multi-spectral camera, model Tetracam mini-MCA-6 (Tetracam Inc., Chatsworth, CA, USA), which acquires 1.3-megapixel images composed of six individual digital channels arranged in a 2×3 array that can acquire images with either 8-bit or 10-bit radiometric resolution. This camera has user configurable band pass filters (Andover Corporation, Salem, NH, USA) of 10-nm full-width at half maximum and centre wavelengths in the B (450 nm), G (530 nm), R (670 and 700 nm), R edge (740 nm) and near-infrared (NIR, 780 nm) spectral regions. Detailed information about the configuration of the UAV flights and specifications of the vehicle and the cameras can be found in Torres-Sánchez *et al*. (2013). The images taken with the visible camera were used directly after downloading to the computer, but those taken with the multi-spectral camera required pre-processing. This multi-spectral sensor acquires images in each channel in raw format and stores them separately on six individual CF cards embedded in the camera. Therefore, an alignment process was needed to group, in a single file, the six images taken at each waypoint. The Tetracam PixelWrench 2 software (Tetracam Inc., Chatsworth, CA, USA) supplied with the multi-spectral camera was used to perform the alignment process.

In the course of the UAV flights, a barium sulphate standard spectralon® panel (Labsphere Inc., North Sutton, NH, USA) of 1 x 1 m dimension was also placed in the middle of the fields to calibrate the spectral data (Fig. 3). Digital images captured in each camera spectral channel were spectrally corrected by applying an empirical linear relationship (Hunt, Jr. et al. 2010). Equation coefficients were derived by fitting digital numbers of the multi-spectral images located in the spectralon panel to the spectralon ground values.

Figure 1. *Microdrone MD4-1000 with the multispectral camera (6 channels) embedded flying over one the sunflower experimental fields.*

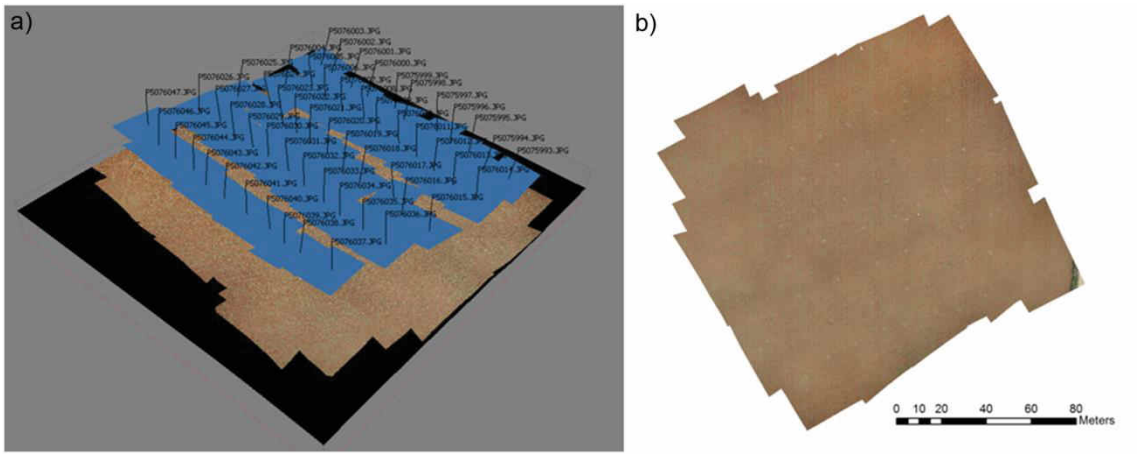

Figure. 2. *a) Screen shot of the set of overlapped images taken with UAV flying at 30 m altitude equipped with the still visible camera in Field 1 (1 ha surface); b) Resulting orthomosaicked imagery.*

Figure 3. *a) Partial view of the ortho-mosaicked imagery at 30 m altitude (sunflower field 2), showing the sunflower rows, the spectralon (white square placed between two sunflower rows at the bottom-left), some patches of weed infestation and some of the 49 1x1 m square frame; b) Detail of vector file created for every 1 m x 1 m square frames (yellow); c) Detail the vector file created for the sunflower crop (green) and weed (violet) classes in one the 49 square frames.*

4.3. Image mosaicking

Image mosaicking is an important task prior to image analysis and consists of the combination of the sequence of overlapped imagery by applying a process of mosaicking using Agisoft PhotoScan Professional Edition (Agisoft LLC, St. Petersburg, Russia). On the day of the UAV flights, a systematic on-ground sampling procedure was conducted, which consisted of placing 49 1x1 m sampling areas, or frames, regularly distributed throughout the two experimental fields according to a representative distribution of weed infestation in the experimental fields (Fig. 3). All the frames were georeferenced and, of the 49 frames, 12 were utilised as artificial terrestrial targets in order to perform the imagery ortho-rectification and mosaicking process. All of the 49 frames were also employed later in the validation of the OBIA procedure for the weed discrimination, as explained in the evaluation of the OBIA algorithm performance section. The mosaicking process had three principal steps for each field: 1) image alignment, i.e., the software searches for common points in the images and matches them, in addition to finding the position of the camera for each image and refining camera calibration parameters, 2) construction of image geometry based on the estimated camera positions and images themselves to produce a 3D polygon mesh representing the overflow areas was built by PhotoScan, and 3) projection of individual images once the geometry was built for ortho-photo generation. The resultant ortho-mosaicked images must show a high-quality landscape metric and an accurate

sunflower row matching between consecutive images in order to guarantee good performance of the subsequent segmentation and classification analyses.

4.4. OBIA algorithm

The OBIA procedure designed for the weed mapping objectives was developed using the commercial software eCognition Developer 8.9 (Trimble GeoSpatial, Munich, Germany). This OBIA procedure was based on an algorithm for weed mapping in early-season maize fields fully described in previous work by our research group (Peña *et al*. 2013), though that work was conducted using single imagery, whereas the procedure presented herein includes some relevant variations and upgrades related to the unique characteristics of sunflower crops. The OBIA algorithm combined object-based features such as spectral values, position, orientation and hierarchical relationships among analysis levels. The algorithm was based on the position of crop and weed plants relative to the crop rows, that is, every plant not located on the crop line was considered a weed. Therefore, the algorithm was programmed to accurately recognise and detect the crop rows by the application of a dynamic and auto-adaptive classification process, and then classified the vegetation objects outside the rows as weeds. The detailed image analysis workflow is described by Peña *et al*. (2013) and only the variations and improvements are described in the following steps:

a) Field segmentation in to sub-parcels: ortho-mosaicked images taken with every camera and flight altitude were segmented into small parcels whose size is user-configurable and, in this case, was 5×5 m. Every sub-parcel was analysed individually to address the spatial and spectral variability of the crop.

b) Sub-parcel segmentation in to objects: the sub-parcel images were sub-segmented using a multi-resolution algorithm to create homogeneous multi-pixel objects corresponding to two classes: vegetation (crop and weeds) and non-vegetation (bare soil) objects. Since these objects come from the merger of spectrally and spatially homogeneous pixels, they contain new information that was used in the next phases of the OBIA procedure. In this study, this new information corresponded to 1, 10, 0.6, 0.4, 0.5, 0.5 for band weights, scale, color, shape, smoothness and compactness, respectively.

c) Vegetation objects discrimination: once the sub-parcels were segmented, the vegetation (crop and weeds) objects were discriminated from the bare soil objects. Two spectral indices were used: Excess Green (ExG, Woebbecke *et al*. 1995; equation 1) for the visible camera, and NDVI (Rouse et al. 1973; equation 2) for the multi-spectral camera because both indices enhance spectral differences of vegetation objects against the non-vegetation objects in UAV images, as previously reported by Torres-Sánchez *et al*. (2014). The determination of the optimal ExG and NDVI values for

vegetation discrimination was conducted by an adaptation to eCognition of an iterative automatic thresholding by using Otsu's method (Otsu 1979) adapted to UAV imagery for detection of three herbaceous crops, including sunflower (Torres-Sánchez *et al*. 2015).

$$ExG = 2g - r - b; \quad r = \frac{R}{R+G+B} \quad g = \frac{G}{R+G+B} \quad b = \frac{B}{R+G+B} \quad (1)$$

$$NDVI = \frac{NIR-R}{NIR+R} \quad (2)$$

d) Sunflower crop-line detection: after classifying vegetation and bare soil objects, those corresponding to vegetation were merged to determine the crop-row structure. Crop row orientation was determined by an iterative process in which the image was successively segmented in stripes with different angles (from 0 to 180º, with 1º of increasing ratio). This segmentation in stripes was performed in a new level above the one with the classified vegetation in order to not lose this information. Finally, the crop orientation was selected according to which stripes showed a higher percentage of vegetation objects in the lower level. After a stripe was classified as a sunflower crop-line, the separation distance between rows (0.70 m) was used to mask the adjacent stripes with this distance in order to avoid classifying areas with potential high weed infestation as crop rows.

e) Weed-patches and weed-free maps: once the crop-rows were classified, the remaining stripes were classified as crop-row buffers (linear segments in contact with the crop rows) and non-crop areas in the upper segmentation level. Next, the hierarchical relationship between the upper and the lower segmentation levels was used to discriminate crop from weeds. The vegetation objects (in the lower segmentation level) that were located either under the crop rows or under the non-crop area (in the upper segmentation level) were classified either as sunflower or as weeds, respectively. The remaining vegetation objects located under the buffer area were classified following a criterion of minimum spectral distance, i.e., an unclassified vegetation object was assigned to the sunflower or the weed class depending on a higher degree of spectral similarity of their ExG and NDVI values to their surrounding sunflower or weed objects for the visible and the multi-spectral images, respectively.

f) Site-specific treatment maps: after mapping weed-patches and weed-free areas, the algorithm built a grid framework at an upper level and applied a chessboard segmentation to generate grids of user-configurable size. For example, in this investigation and according to the usual characteristics of sunflower and weed-control machinery, the grid size was 0.5 x 0.5 m. Therefore, a new hierarchical structure was generated between the grid super-objects at the upper level and the sub-objects classified as sunflower, weeds or bare soil at the lower level. Next, the site-specific treatment maps were created according to the weed coverage maps estimated previously.

g) Maps at several weed thresholds: the weed coverage was mapped by identifying both weed-free and weed-infested zones on the basis of seven thresholds with intervals of 2.5 from 0% (herbicide post-emergence treatment must be applied just when there is presence or absence of weed) to 15% (herbicide must be applied whether weed coverage > 15%) with an increase 2.5% per threshold level. That is, seven herbicide treatment maps resulting from a given threshold value were studied for every flight altitude and camera. Both the grid dimensions and the number and thresholds of the weed infestation can be customised according to other cropping patterns and the specifications required by the herbicide spraying machinery.

4.5. Evaluation of OBIA algorithm performance

For validation purposes, the ortho-mosaicked visible imagery collected at 30 m altitude was used in both fields to quantify classification accuracy because this image had a high spatial resolution which allowed the visual identification of weeds in each of the 49 sampling frames. That is, ground reference observations were derived from the vertical remote images collected at 30 m altitude. In addition, each sampling frame was georeferenced with a DGPS and was photographed to help to visually identify the individual or group of weeds and create Figure 3c to compare the on-ground weed infestation (observed weed density) with the outputs from image classification (estimated weed density). Therefore, two vector shape files were created, one of them containing the 49 1 x1 m^2 sampling areas (Fig. 3b) and the other one including the crop and weeds existing in every frame (Fig. 3c) by using Quantum GIS software (QGIS, GNU General Public License). These vector files were then introduced in to the eCognition software to obtain the percentage of surface area occupied by the three classes, i.e., sunflower, weeds and bare soil, in every square frame in order to generate the reference data. Afterwards, the first vector file was overlapped with the classified image obtained by the OBIA algorithm to calculate the relative area corresponding to each class in every frame. The accuracy of the classified images was quantified by calculating the error matrix between weed coverage mapping outputs and the field reference data in all sampling frames grouped by the weed threshold (0 to 15% weed coverage) previously defined. The confusion matrix quantified the overall accuracy (OA) of the classification in each threshold (Congalton, 1991).

5. RESULTS AND DISCUSSION

5.1. Spatial resolution and area covered by ortho-mosaicked imagery

The visible and multi-spectral cameras collected images with pixel sizes ranging from 0.0114 to 0.0162 m and from 0.0228 to 0.0327 m at flight altitudes of 30 and 60 m, respectively, as determined by a proportional relationship between imagery spatial resolution and flight altitude (Table 1).

Furthermore, slight changes in flight altitude during the flight are critical for low altitude image acquisition because these variations can cause important differences in the ortho-image spatial resolution. Weeds can be present in the field as small or large patches, so the spatial resolution of the image must be considered accordingly (Figure 4). If the objective is the detection of small weed patches, the pixel size could be 0.01 – 0.03 m which corresponds to flight altitudes of 30 and 60 m for the visible camera and 30 m for the multi-spectral camera. However, when a weed patch is larger, the UAV images could have a pixel size larger than 0.03 m, which corresponds to 60 m flight altitude in the multi-spectral camera.

Table 1. *Image spatial resolution, flight length and number of images per hectare as affected by flight altitude and type of camera.*

Camera	Flight altitude (m)	Flight length (m:s)	# Images	Pixel size (m)
Visible (RGB*)	30	11:56	42	0.0114
	60	5:41	12	0.0228
Multispectral (RGB+NIR*)	30	28:00	117	0.0162
	60	11:14	35	0.0327

*RGB: Red, Blue Green, Near-Infrared

The number of images and the flight length needed to cover the entire study area increased from 42 to 117 images and from 12 to 28 minutes for the visible and the multi-spectral camera, respectively, at 30 m altitude. A similar trend was observed at 60 m altitude. The different spatial resolutions and area covered for the visible and multi-spectral cameras at the same flight altitude resulted from differences in the technical specifications of each camera; i.e., the camera's focal length and sensor size affect the extent of area covered for a given sensor, and the pixel size of the sensor (measured in µm) determines the relationship between flight altitude and spatial resolution for a given sensor. Therefore, a decrease in the flying altitude reduces the area covered by each single image, which results in an increase in both the sequence of images and the complexity of the image mosaicking procedure to obtain an ortho-image covering the entire study area. Considering these relationships between flight characteristics and camera types, the first decision to make when the user defines the flight program is which combination of flight altitude and camera type is ideal to keep the image spatial and spectral quality consistent to ensure weed detection and minimise the operating time, given potential UAV battery limitations. These considerations need to be addressed to design prescription control maps because early SSWM requires high accuracy geo-referencing in agreement to the details of the crop, weeds and soil background classes when both kind of plants are at very similar phenological stages and a repeating crop pattern is present.

5.2. Classification of sunflower crop rows

Sunflower crop rows were detected and mapped with 100% accuracy in the ortho-mosaics, at all flight altitudes and camera types, using the OBIA algorithm (Fig. 4). This was due not only to the performance of this procedure but also to the high matching of crop-line continuity of ortho-imagery during the mosaicking process. If mosaics were not accurate enough, crop rows would appear broken, incorrectly geo-referenced and consequently, moved, which would affect further OBIA classification. This algorithm was upgraded to incorporate the special characteristics of sunflower crops and now includes relevant variations to previous versions, e.g., imagery was mosaicked to study the whole fields to optimise the image analysis, and weed thresholds were considered in the construction of site-specific treatment maps. Other authors have mosaicked imagery from other row crops such as corn, although the objective was to determine the effect of topography on the rate of cross-pollination (Haarbrink and Eisenbeiss 2008). However, they found that obtaining an accurate ortho-image was difficult, but they did not need to map crop rows. Therefore, one of the critical results of the work reported here was the robustness of both the mosaicking and OBIA methods developed for crop-row classification and mapping. This is relevant for the successful detection of the vegetation objects referred to weeds placed in the inter-row areas.

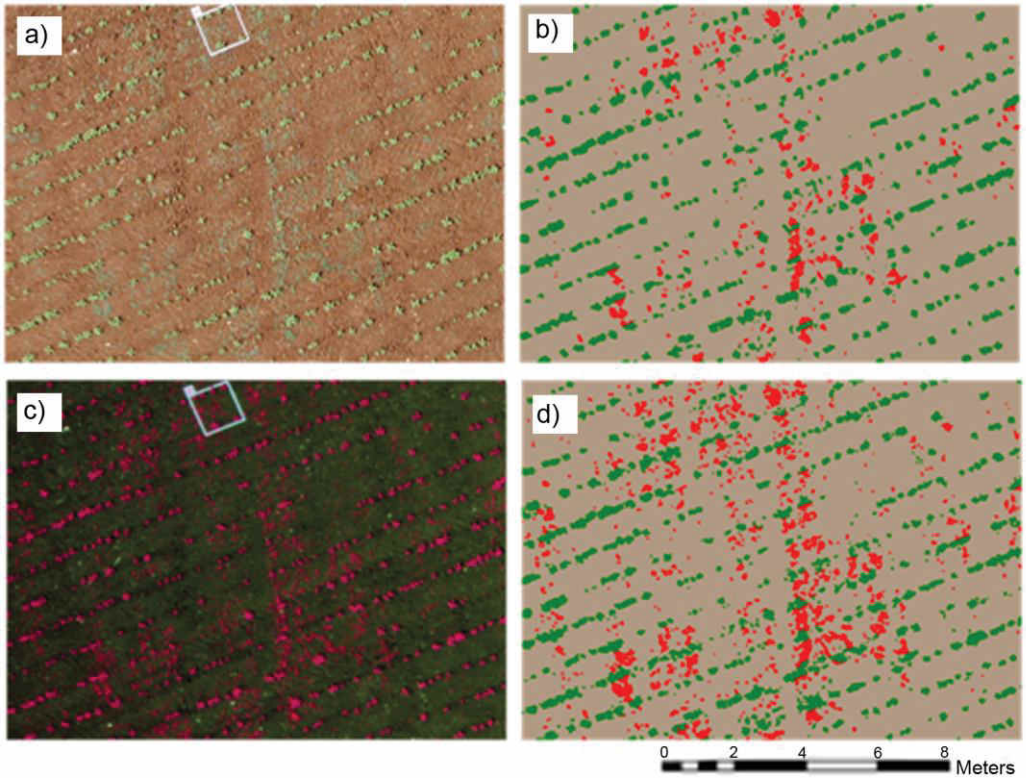

Fig. 4. *a) Illustration (14 m x 8 m) of the ortho-mosaicked image taken with the still visible camera at 30 m altitude, and b) corresponding weed seedling map using OBIA (green: sunflower rows; red: weeds; grey: bare soil); c) Illustration of the ortho-mosaicked image taken with the multispectral camera at 30 m altitude, and d) Corresponding weed seedling map using OBIA.*

5.3. Effect of cameras and flight altitudes on mapping of weed-patches and weed-free areas

The accuracy of weed-patch discrimination, as affected by flight altitude and camera using seven threshold values, are shown in Figure 5 for both sunflower fields. The classification was over grid units, not over pixels, therefore the accuracy was the percentage of frames correctly classified, i.e., the number of correct frames as a percentage of the total number of sampling frames. The threshold corresponding to zero means that the OBIA algorithm detects simply the presence or absence of weeds, that is, a percentage of weeds greater than zero was detected in the inter-row area, and consequently, all these weeds must be treated. A threshold of 15% means that at least 15% of the inter-row area of every frame was infested; if a lower weed infestation is detected and mapped, no treatment should be applied.

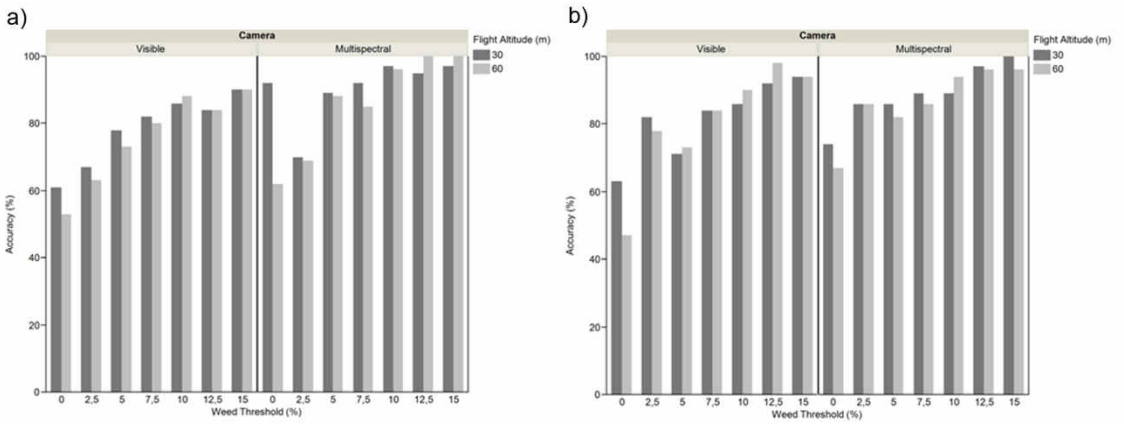

Figure 5. *Accuracy (%) of weed maps according to seven weed thresholds for the images collected with the still visible and multispectral cameras collected at 30 m and 60 m altitude for (a) Field 1, (b) Field 2).*

Both sunflower fields showed similar results and trends. Higher accuracies were observed with the multi-spectral camera at both flight altitudes, the highest (approximately 100%) was recorded for 15% threshold, although satisfactory results from 2.5% and 5% thresholds were also obtained with accuracies higher than 85% for fields 2 and 1, respectively. The lowest accuracies (ranging from 50 to 60%) were achieved with the visible camera at any flight altitude and 0% of threshold value although, according to Thomlinson *et al*. (1999) who standardised the overall accuracy of 85% for minimum established values, acceptable accuracies were also recorded from a 7.5% threshold for both fields. Best accuracies were achieved for the higher thresholds because, normally, they imply the presence of larger weed patches which are more easily detected by the OBIA algorithm. When analysing frames with only 2.5% weed infestation, the most common situation is that the weed patches are very small, and consequently, they are more difficult to discriminate. Analysing the flight altitude, accuracies for the images taken with the visible camera at 60 m were higher than at 30 m for 10% weed threshold for field 1 and 12.5% in field 2. A similar trend was observed with the multi-spectral camera. Therefore, a higher altitude corresponds to higher accuracies for high weed thresholds in

both fields. This indicated that, in a sunflower field with a high weed infestation, the UAV could be programmed to fly at 60 m altitude and perform better than at 30 m, because the weed map would have a satisfactory accuracy, while requiring fewer images per ha, thus improving both the flight time and the mosaicking process.

Traditionally, ExG and NDVI indices have been widely used in mapping vegetation (190,000 and 330,000 results in Google for "remote sensing" plus "Excess Green", and "NDVI", respectively; accessed August 2015), however, they were quite limited for mapping crop-rows and weeds using pixel-based-image-analysis in the preliminary image analyses (data not shown). This is because reflectance data are sensitive to canopy cover, and spectral data from crop and weed plants at early phenological stage are rather similar and difficult to discern. The OBIA procedure developed has the ability to build objects using several criteria of homogeneity, in addition to spatially accurate information (e.g., position, orientation, hierarchical relationships among image analysis levels). Figure 6 displays several illustrative examples of early, site-specific, post-emergence grid maps for different scenarios at 30 m flight altitude, using both visible and multi-spectral cameras. They also contain four thresholds and the spatial distributions of treated and untreated grids. For a wider weed threshold, a lower weed-patch area was observed, and vice versa, consequently, the threshold value has a direct effect on the percentage of the field to be treated (Figure 7). The herbicide savings obtained were relevant for both cameras and altitudes in both fields, although they were higher in field 2 due to the lower degree of weed infestation. The percentage of treated area was calculated to be higher when using the multi-spectral camera because the weed patches were better discriminated and the maps generated were more accurate than those from the visible camera.

That is, some weed patches present in the field were not correctly classified with imagery from the visible camera, and as a result, no treatment was indicated. For example, using the multi-spectral camera at 30 m altitude, a range of 3% to 23% of the field (i.e., 77% and 97% of untreated area) could be treated for weed thresholds from 0 to 15%, corresponding to accuracies ranging from 74% to 100% for field 2. On the other hand, using the visible camera at 30 m, a range of 3 to 9% of the field (i.e., 92% and 97% of untreated area) could be treated for weed thresholds from 0 to 15%, corresponding to accuracies from 63 to 94% for field 1. As Figure 6 shows, there are some parts of the fields where there were clearly weed-free zones and where site-specific weed control equipment was not needed, allowing not only the potential reduction of herbicide applications but also the optimisation of fuel, field operating time and cost. Currently, accurate site-specific equipment for farmers to implement site-specific weed management is available. In addition, collaborative efforts have been conducted to develop autonomous and robotic tractors carrying different implements for site-specific control of weeds and other pests using a high-level decision-making system. This system

was designed to accurately manage the type of herbicide or dose level for other pesticides according to a prescription map (Pérez-Ruiz et al. 2015).

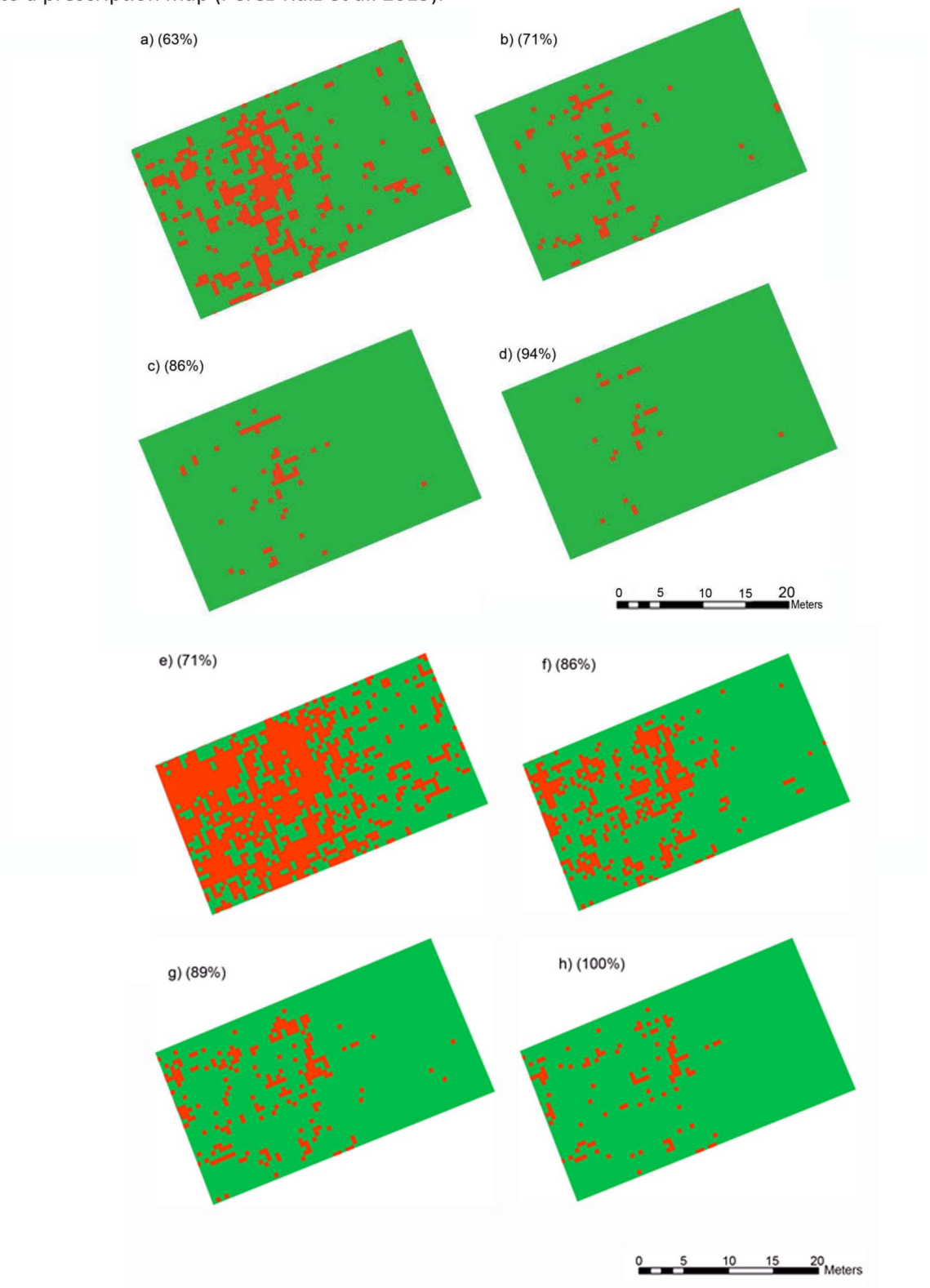

Figure 6. *Several examples of maps showing the herbicide application area ( ) obtained for 30 m altitude, and using still visible camera (four upper figures) and multispectral camera (four bottom figures) for Field 2 corresponding to four weed thresholds: a) & e) 0% ; b) & f) 5%; c) & g) 10%; d) & h) 15%. The accuracy of every weed map is showed in parenthesis.*

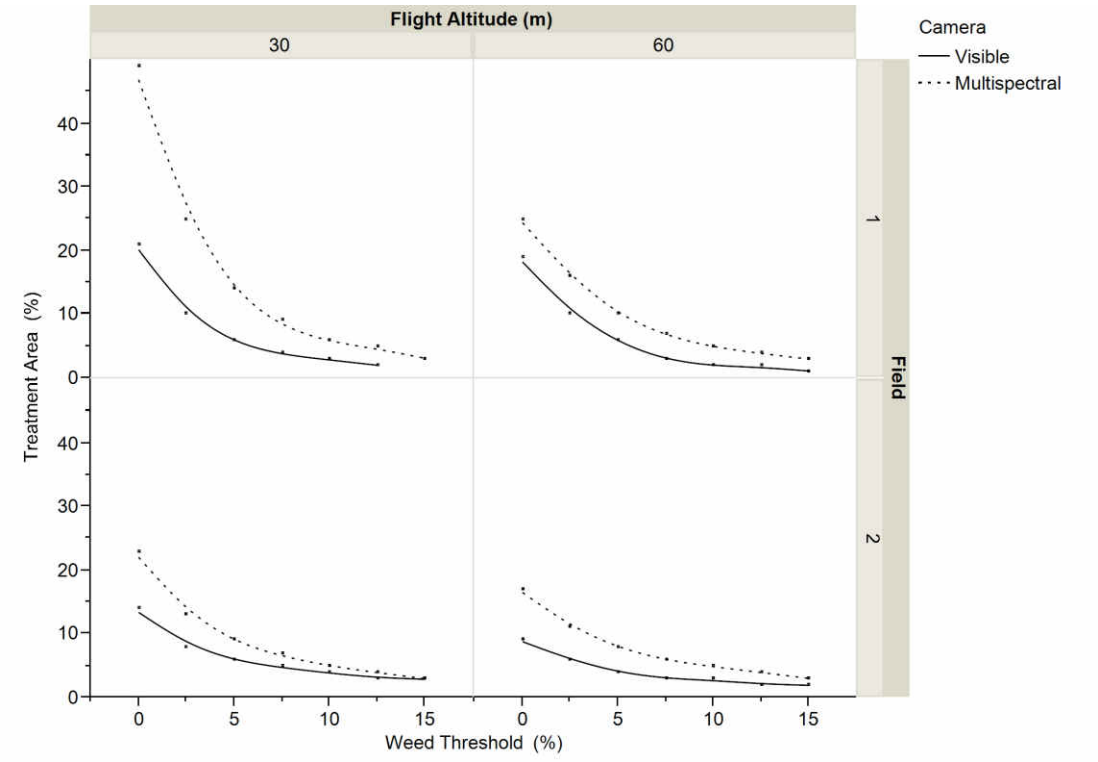

Figure 7. *Percentage of field surface requiring weed control in both sunflower fields based on seven weed thresholds according by flight altitudes and cameras.*

The spatial structure was also different in both fields, i.e., the weeds were distributed in patches across all of field 1, but were more localised in a part of field 2. The extent of the weed-infested area and its spatial distribution, as well as the adoption of weed thresholds, are crucial for the design and implementation of early SSWM. In addition, Gibson *et al*. (2004) stated that farmers would choose to treat weed-free areas rather than assume the risk of allowing weeds to go untreated, and Czapar *et al*. (1997) reported several reasons to consider the use of thresholds, such as crop competition, harvesting problems, weed seed production and seed bank replenishment, time required to survey fields or even general field appearance. Analysing this latter work, the time spent to explore fields was perceived to be a limitation for the acceptance of weed thresholds by 6% of growers, while 26% of dealers and 39% of farm managers also identified it as a restraint. This could be overcome by using the technology presented here based on a UAV since the time spent to acquire 1 ha of sunflower area was less than half an hour for any of the flight altitudes and cameras (Table 1). Of course, the processing time for image analysis would have to also be considered, although once the algorithm is developed, this time would be minimal for successive use in as many sunflower fields as required. Field appearance was identified by 75 % of the dealers and 36% of growers as an important limitation. This can be relevant if weeds of medium to large size are present in the sunflower fields, as was the case in this study. Pigweed and lambsquarters are considered large weeds, while mustard and bindweed are medium weeds according to the SEMAGI expert system

developed for weed management in sunflower (Castro-Tendero and García-Torres 1995). The authors evaluated herbicide selection according to potential yield reduction from multi-species weed infestations by assigning three size categories (small, medium and large) to weeds and relating the percentage of sunflower losses to weed density and weed biomass. They concluded that the subjective evaluation of farmers for weed infestation assessment usually considers the size of the weed for herbicide decisions and this is in agreement with the results reported by Czapar *et al*. (1997). Using SEMAGI and geostatistical tools, Jurado-Expósito *et al*. (2003) reported the usefulness of weed infestation maps for identifying the area exceeding the economic threshold to plan site-specific spraying strategies; they obtained 61% herbicide reduction. Therefore, the site-specific treatment maps considering the different thresholds shown in Figure 6 could help farmers to decide on early SSWM operations without forgetting the subjective evaluation of their fields as an important component of their decision making. For example, according to the previously mentioned limitations found by land owners, it seems unlikely that they would choose the 15% threshold keeping treated approximately 5% of both fields (Figure 6) and untreated most of the fields, particularly when these areas subjectively would appear highly infested due to large size of weeds such as lambsquarters or pigweeds.

Current investigations are focusing on improving the OBIA algorithm when a number of specific field conditions, such as curved crop rows, are present in the fields.

6. CONCLUSIONS

Because the spatial structure of patchy distribution of weeds allows mapping of infested and un-infested areas, the objectives were to detect patches of weeds at early phenological stages using UAV imagery and to design a timely and efficient weed control program based on site-specific herbicide treatments according to weed cover. A UAV equipped with RGB or multi-spectral cameras flying at 30 and 60 m altitude was used to acquire a set of overlapped images. The spatial resolution of the image, area covered by each image and flight timing were very sensitive to the flight altitude. At a lower altitude using the visible camera, the UAV captured slightly finer spatial resolution imagery than at the same altitude using the multi-spectral camera. However, the number of images needed to cover the entire field at 30 m altitude with the visible camera was much lower than for the multi-spectral camera, showing that it may be a limiting factor due to potential UAV energy limitations. The overlapped images were ortho-mosaicked to generate imagery at very-high spatial resolutions (pixels ranging from 0.0114 to 0.0327 m). An accurate and automated OBIA procedure was developed to detect and map bare soil, crop-rows and weeds. Accurate site-specific herbicide treatment maps were created according to different factors: flight altitudes, camera types and weed

thresholds, and then relevant herbicide savings were calculated. This information can help to balance spatial resolution, which depends on flying altitude and type of camera with decision-making to calculate herbicide requirements and plan the overall weed management operations.

7. ACKNOWLEDGMENTS

This research was partially financed by the RECUPERA 2020 Project (Agreement CSIC-Spanish MINECO and EU-FEDER funds). Research of Mr. Torres-Sánchez and Dr. de Castro was financed by the FPI and the JAE-predoc (CSIC-FEDER) Programs, respectively.

8. REFERENCES

Blaschke, T. (2010). Object based image analysis for remote sensing. *ISPRS Journal of Photogrammetry and Remote Sensing, 65*, 2–16.

Carranza, P., Saavedra, M. & Gacría-Torres, L. (1995). *Ridolfia segetum* Moris. competition with sunflower (*Helianthus annuus* L.). *Weed Research*, *35*, 369-375.

Castro-Tendero, A. J. & García-Torres, L. (1995). SEMAGI—an expert system for weed control decision making in sunflowers. *Crop Protection, 14*, 543–548.

Congalton, R. G. (1991). A review of assessing the accuracy of classifications of remotely sensed data. *Remote Sensing of Environment, 37*, 35-46

Czapar, G. F., Curry, M. P., & Wax, L. M. (1997). Grower acceptance of economic thresholds for weed management in Illinois. *Weed Technology, 11*, 828–831.

De Castro, A. I., Jurado-Expósito, M., Peña-Barragán, J. M. & López-Granados, F. (2012). Airborne multi-spectral imagery for mapping cruciferous weeds in cereal and legume crops. *Precision Agriculture, 13,* 302–321.

De Castro, A. I., López-Granados, F., Peña-Barragán, J. M. & Jurado-Expósito, M. (2013). Broad-scale cruciferous weed patches classification in winter wheat using QuickBird imagery for in-season site-specific control. *Precision Agriculture, 14,* 392-417.

FAO (2015). http://faostat3.fao.org/faostat-gateway/go/to/home/E. Accessed 16 June 2014

García-Torres, L., López-Granados, F. & Castejón-Muñoz, M. (1994). Preemergence herbicides for the control of broomrape (*Orobanche cernua* Loefl.) in sunflower (*Helianthus annuus* L.). *Weed Research, 34*, 395-402.

Gibson, K. D., Dirks, R., Medlin, C. R. & Johnston, L. (2004). Detection of weed species in soybean using multispectral digital images. *Weed Technology, 18,* 742–749.

Gómez-Candón, D., De Castro, A. I. & López-Granados, F. (2014). Assessing the accuracy of mosaics from unmanned aerial vehicle (UAV) imagery for precision agriculture purposes. *Precision Agriculture, 15,* 44-56.

Gutiérrez-Peña, P. A., López-Granados, F., Peña-Barragán, J. M., Jurado-Expósito, M., Gómez-Casero, M. T., & Hervás-Martínez, C. (2008). Mapping sunflower yield as affected by *Ridolfia segetum* patches and elevation by applying Evolutionary Product Unit Neural Networks to remote sensed data. *Computers and Electronics in Agriculture, 60*, 122-132.

Haarbrink, R. B. & Eisenbeiss. H. (2008). Accurate DSM production from unmanned helicopter systems. *The International Archives of the Photogrammetry, Remote Sensing and Spatial Information Sciences*. Vol. XXXVII. Part B1. Beijing 2008, (pp 1259-1264).

Horizon (2020) http://ec.europa.eu/programmes/horizon2020/ Accessed 16 June 2015.

Hunt, Jr., E. R., Hively, W. D., Fujikawa, S. J., Linden, D. S., Daughtry, C. S. T. & McCarty, G. W. (2010). Acquisition of NIR-green-blue digital photographs from unmanned aircraft for crop monitoring. *Remote Sensing, 2,* 290–305.

Jurado-Expósito, M., López-Granados, F., García-Torres, L., García-Ferrer, A., Sánchez de la Orden, M. & Atenciano, S. (2003). Multi-species weed spatial variability and site-specific management maps in cultivated sunflower. *Weed Science, 51*, 319-328.

Jurado-Expósito, M., López-Granados, F., González-Andújar, J. L. & García-Torres, L. (2005). Characterizing population rate of *Convolvulus arvensis* in wheat-sunflower no-tillage systems. *Crop Science, 45*, 2106-2112.

Lambers, K., Eisenbeiss, H., Sauerbier, M., Kupferschmidt, D.,Gaisecker, Th., Sotoodeh, S., et al. (2007). Combining photogrammetry and laser scanning for the recording andmodelling of the late intermediate period site of Pinchango Alto, Palpa, Peru. *Journal of Archaeological Science, 34,* 1702-1712.

Li, Ch-ch., Zhang, G-S., Lei, T-J. & Gong, A-D. (2011). Quick image-processing method of UAV without control points data in earthquake disaster area. *Transactions Nonferrous Metals Society of China, 21*, s523-s528.

Longchamps, L., Panneton, B., Simard, M. J. & Leroux, G. D. (2014). An Imagery-based weed cover threshold established using expert knowledge. *Weed Science, 62,* 177-185.

López-Granados, F. (2011). Weed detection for site-specific weed management: mapping and real-time approaches. *Weed Research, 51,* 1–11.

MAGRAMA (2015). Ministerio Agricultura, Alimentación y Medioambiente http://www.magrama.gob.es/es/estadistica/temas/default.aspx. Accessed 16 June 2015 (in Spanish).

Meier, U. (2001). *Growth stages of mono- and dicotyledonous plants. BB Monograph*. Federal Biological Research Centre for Agriculture and Forestry. Available at: http://www.jki.bund.de/fileadmin/dam_uploads/_veroeff/bbch/BBCH-Skala_englisch.pdf. Accessed 16 June 2015.

Molinero-Ruiz, L., García-Carneros, A. B., Collado-Romero, M., Rarancius, S., Domínguez, J. & Melero-Vara, J. (2014). Pathogenic and molecular diversity in highly virulent populations of the parasitic weed *Orobanche cumana* (sunflower broomrape) from Europe. *Weed Research, 54,* 87-98.

Otsu, N. (1979). A Threshold Selection Method from Gray-Level Histograms. *IEEE, Man, and Cybernetics Society*, *9*, 62–66.

Peña, J. M., Torres-Sánchez, J., de Castro, A. I., Kelly, M. & López-Granados, F. (2013). Weed mapping in early-season maize fields using object-based analysis of unmanned aerial vehicle (UAV) images. *PLOS ONE, 8,* e77151

Pérez-Ruiz, M., Gonzalez-de-Santos, P., Ribeiro, A., Fernandez-Quintanilla, C., Peruzzi, A., Vieri, M., et al. (2015). Highlights and preliminary results for autonomous crop protection. *Computers and Electronics in Agriculture, 110*, 150-161

Rouse, J. W., Haas, R. H., Schell, J. A. & Deering, D. W. (1973). Monitoring vegetation systems in the Great Plains with ERTS. In: *Proceedings of the Earth Resources Technology Satellite Symposium* NASA SP-351, (Vol 1, pp. 309−317). Washington, DC.

Swanton, C. J., Weaver, S., Cowan, P., Van Acker, R., Deen ,W. & Shreshta, A. (1999). Weed thresholds: theory and applicability. *Journal of Crop Production, 2,* 9-29.

Thomlinson, J. R., Bolstad, P. V. & Cohen, W. B. (1999). Coordinating methodologies for scaling landcover classification from site-specific to global: steps toward validating global maps products. *Remote Sensing of Environment, 70*, 16–28.

Torres-Sánchez, J., López-Granados, F., de Castro, A. I. & Peña-Barragán, J. M. (2013). Configuration and specifications of an unmanned aerial vehicle (UAV) for early site specific weed management. *PLOS ONE, 8*, e58210

Torres-Sánchez, J., Peña-Barragán, J. M., de Castro, A. I. & López-Granados, F. (2014) Multi-temporal mapping of the vegetation fraction in early-season wheat fields using images from UAV. *Computers and Electronics in Agriculture, 103,* 104–113.

Torres-Sánchez J., López-Granados, F. & Peña-Barragán, J. M. (2015). An automatic object-based method for optimal thresholding in UAV images: Application for vegetation detection in herbaceous *Computers and Electronics in Agriculture, 114*, 43–52.

Woebbecke, D. M., Meyer, G. E., Von Bargen, K. & Mortensen, D. A. (1995). Color Indices for Weed Identification Under Various Soil, Residue, and Lighting Conditions. *Transactions of the ASAE, 38,* 259-269.28.

Zhang, C. & Kovacs, J. (2012). The application of small unmanned aerial systems for precision agriculture: a review. *Precision Agriculture 13,* 693–712.

CAPÍTULO 7

HIGH-THROUGHPUT 3-D MONITORING OF AGRICULTURAL-TREE PLANTATIONS WITH UNMANNED AERIAL VEHICLE (UAV) TECHNOLOGY

Torres-Sánchez, J., López-Granados, F., Serrano, N., Arquero, O., & Peña, J. M. (2015). High-Throughput 3-D Monitoring of Agricultural-Tree Plantations with Unmanned Aerial Vehicle (UAV) Technology. *PLOS ONE*, 10(6), e0130479. doi:10.1371/journal.pone.0130479

1. RESUMEN

Las características geométricas de los árboles cultivados como el área de copa proyectada, la altura y el volumen de la copa, proporcionan información muy útil sobre el estado de la plantación y la producción del cultivo. Sin embargo, la estimación de estas variables suele ser hecha de manera tradicional tras un duro y exhaustivo trabajo de campo, y aplicando ecuaciones que tratan a los árboles como figuras geométricas, lo que produce resultados inconsistentes. Como alternativa, este trabajo presenta un procedimiento innovador para calcular las características tridimensionales de árboles individuales y en seto aplicando dos fases consecutivas: 1) generación de modelos digitales de superficies con vehículos aéreos no tripulados, y 2) uso de técnicas de análisis de imagen orientado a objetos. Nuestro procedimiento produjo resultados satisfactorios tanto en plantaciones de árboles individuales como en seto, llegando a un 97% de precisión en la cuantificación del área de copa proyectada y mínimas desviaciones en las estimaciones de la altura y el volumen en comparación con las mediciones en campo. Los mapas generados por el procedimiento podrían ser interesados para comprender las relaciones entre el crecimiento de los árboles y factores relacionados con el terreno, o para optimizar las operaciones de manejo del cultivo en el contexto de la agricultura de precisión con relevantes implicaciones agro-medioambientales.

2. ABSTRACT

The geometric features of agricultural trees such as canopy area, tree height and crown volume provide useful information about plantation status and crop production. However, these variables are mostly estimated after a time-consuming and hard field work and applying equations that treat the trees as geometric solids, which produce inconsistent results. As an alternative, this work presents an innovative procedure for computing the 3-dimensional geometric features of individual trees and tree-rows by applying two consecutive phases: 1) generation of Digital Surface Models with Unmanned Aerial Vehicle (UAV) technology and 2) use of object-based image analysis techniques. Our UAV-based procedure produced successful results both in single-tree and in tree-row plantations, reporting up to 97% accuracy on area quantification and minimal deviations compared to in-field estimations of tree heights and crown volumes. The maps generated could be used to understand the linkages between tree grown and field-related factors or to optimize crop management operations in the context of precision agriculture with relevant agro-environmental implications.

3. INTRODUCTION

The geometric measurements of the agricultural trees, such as tree height and crown volume, serve to monitor crop status and dynamic, to analyse tree production capacity and to optimise a number of agronomic tasks, such as water use, nutrient application, pruning operations and pest management. Conventionally, the main tree dimensions are measured by hand after an intensive field work and next the crown volume is estimated with equations that treat the trees as regular polygons or by applying empiric models (West 2009). However, collecting this data at the field scale is very time-consuming and generally produces uncertain results because of the lack of fit of the real tree to the geometric models or to the great variability in orchards that can affect the suitability of models based on in-field measurements. Among the technological alternatives, the Light Detection And Ranging (LiDAR) laser scanners and the stereo vision systems by using terrestrial or remote-sensed measurements are currently the most relevant (Rosell and Sanz 2012). However, these techniques have also their own limitations in real tree orchards. On the one hand, although the terrestrial devices are very precise to measure tree architecture (Fernández-Sarría *et al*. 2013; Moorthy *et al*. 2011; Rovira-Más *et al*. 2008), they are inefficient in large spatial extents and are difficult to use in hard-to-reach field areas. On the other hand, remote-sensed data collected with piloted aircrafts and satellites do not often fulfil the technical requirements (e.g., sufficient spatial resolution or number of stereoscopic pairs) needed to detect the 3-dimensional (3-D) characteristics of agricultural trees in most cases (Rosell and Sanz 2012).

In recent years, a new aerial platform has joined the traditional ones: the Unmanned Aerial Vehicles (UAV) or drones (Luo *et al*. 2014; Marris 2013). Several investigations (Zhang and Kovacs 2012) have demonstrated the advantages of the UAVs in comparison to airborne or satellite missions regarding its low cost and greater flexibility in flight scheduling (Torres-Sánchez *et al*. 2014), which make UAV technology a proper tool for farmers and researchers to monitor crops at the field scale (Anderson 2014). In addition, the UAV can automatically flight at low altitudes and with large overlaps, which permit the acquisition of ultra-high spatial resolution images (in the range of a very few centimetres) and the generation of the Digital Surface Model (DSM) using automatic photo-reconstruction methods that are based on the "Structure from Motion" approach for 3-D reconstruction. As a consequence, recent investigations have focused on the generation of DSM with UAVs (Nex and Remondino 2014) and its interpretation over agricultural areas (Bendig *et al*. 2014; Díaz-Varela *et al*. 2015; Zarco-Tejada *et al*. 2014).

However, in order to take full advantage of this technology, another primary step involves the implementation of robust and automatic image analysis procedures capable of retrieving useful

information from the images. To reach a high level of automation and adaptability, we propose the application of object-based image analysis (OBIA) techniques. OBIA overcomes some limitations of pixel-based methods by grouping adjacent pixels with homogenous spectral values after a segmentation process and by using the created "objects" as the basic elements of analysis (Blaschke *et al*. 2014). Next, OBIA combines spectral, topological, and contextual information of these objects to address complicated classification issues. This technique has been successfully applied in UAV images both in agriculture (Diaz-Varela *et al*. 2014; Peña *et al*. 2013), grassland (Laliberte and Rango 2011) and urban (Qin 2014) scenarios.

In this article, we report an innovative procedure for a high-throughput and detailed 3-D monitoring of agricultural tree plantations by combining UAV technology and advanced OBIA methodology. After the DSM generation with UAV images, this procedure automatically classifies every tree in the field and computes its position, canopy projected area, tree height and crown volume. For training and testing purposes, we used olive plantations as model systems and selected several sites with a variable degree of tree shapes and dimensions, both in conventional single-tree and in row-structured plantation systems. Efficacy of the procedure was assessed by comparing UAV-based measurements and in-field estimations. In addition, effects of spectral and spatial resolutions on the entire process were evaluated in each type of plantation by performing different flight missions in which two flight altitudes and two sensors (a conventional low-cost visible-light camera and a 6-band multispectral color-infrared camera) were separately tested. Finally, time required by each stage of the full process was weighted according to the flight mission performed.

4. MATERIALS AND METHODS

The full procedure consisted on three main phases (Fig. 1): 1) the acquisition of very high spatial resolution remote images with an unmanned aerial platform, 2) the generation of orthomosaics and DSMs by applying close-range photogrammetry methods, and 3) the application of advanced object-based algorithms to analyse the images and to retrieve the position and the geometric features of each tree or tree-row in the whole field. Next, each stage is described in detail.

4.1. Description of the UAV and the sensors

The UAV used in this investigation was a quadrocopter with vertical take-off and landing (VTOL), model MD4-1000 (microdrones GmbH, Siegen, Germany) (Fig. 2a). This UAV is equipped with four brushless motors powered by a battery and it can be manually operated by radio control (1000 m control range) or it can fly autonomously with the aid of its Global Position System (GPS) receiver

and its waypoint navigation system. The VTOL system makes the UAV independent on a runway, which allows the use of the UAV in a wide range of different situations, e.g., even on steep olive orchards.

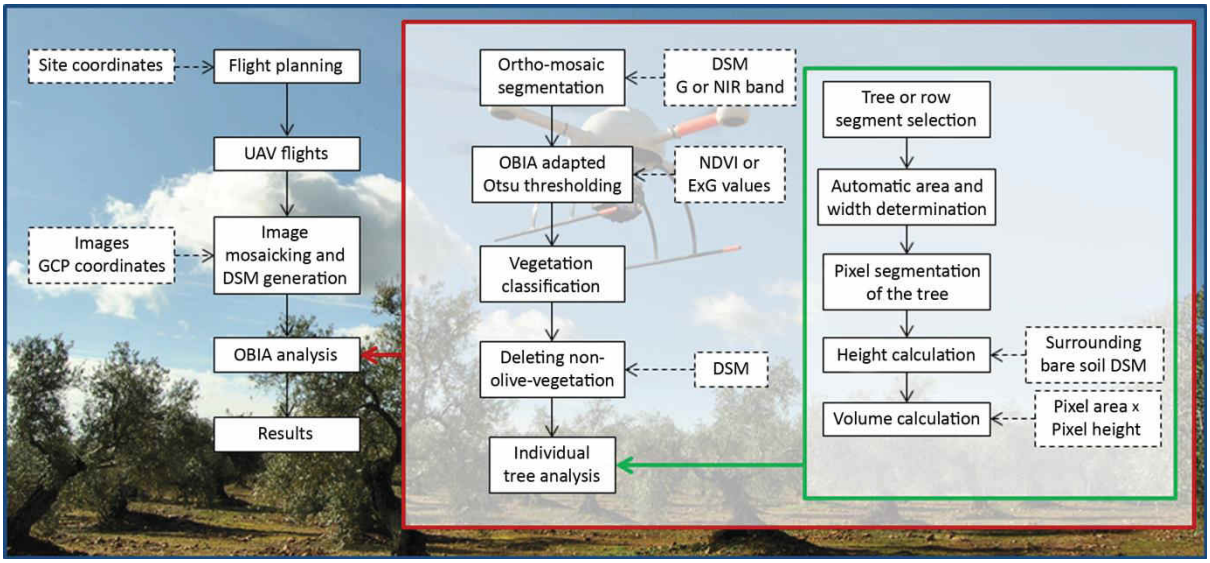

Figure 1. *Flowchart of the entire procedure for 3-D monitoring of agricultural tree plantations by combining UAV technology and object-based image analysis. (Abbreviations: 3-D (three dimensional); GPS (Global Position System); UAV (Unmanned Aerial Vehicle); GCP (Ground Control Point); DSM (Digital Surface Model); G (Green band); NIR (Near Infra-Red band); OBIA (Object-Based Image Analysis).*

Two sensors were separately tested: 1) a still point-and-shoot visible-light camera, model Olympus PEN E-PM1 (Olympus Corporation, Tokyo, Japan) (Fig. 2b), and 2) a six-band multispectral camera, model Tetracam mini-MCA-6 (Tetracam Inc., Chatsworth, CA, USA) (Fig. 2c). On the one hand, the visible-light camera produces 12.2 megapixel format (4,032 x 3,024 pixels) images in true colour (Red, R; Green, G; and Blue, B, bands) with 8-bit radiometric resolution, which are stored in a secure digital SD-card. It is equipped with a 14-42 mm zoom lens, although it was fixed at 14 mm focal length for these works. The camera's sensor size is 17.3 x 13.0 mm and the pixel size is 0.0043 mm. These parameters are needed to calculate the image resolution on the ground or, i.e., the ground sample distance (GSD) as affected by the flight altitude (equation 1). On the other hand, the multispectral camera is a lightweight (700 g) sensor composed of six individual digital channels arranged in a 2x3 array. Its sensor size is 6.66 x 5.32 mm and the pixel size is 0.0052 mm. Each channel has a focal length of 9.6 mm and a 1.3 megapixel (1,280 x 1,024 pixels) CMOS sensor that stores the images on a compact flash CF-card. The images were acquired with 8-bit radiometric resolution. The camera has user configurable band pass filters (Andover Corporation, Salem, NH, USA) of 10-nm full-width at half-maximum and centre wavelengths at B (450 nm), G (530 nm), R (670

and 700 nm), R edge (740 nm) and near-infrared (NIR, 780 nm). More details about the sensors and UAV configuration can be consulted in (Torres-Sánchez *et al*. 2013).

$$\mathrm{GSD} = \frac{\text{Sensor Pixel Size} \times \text{Flight Altitude}}{\text{Focal Length}} \qquad (1)$$

Figure 2. *The quadrocopter UAV, model md4-1000, taking off in one of the studied fields (a) and the sensors used in this investigation: the visible-light camera (b) and the multispectral camera (c).*

4.2. Study sites and UAV flight missions

We used olive plantations as model systems to develop and evaluate our procedure and selected four different sites with a variable degree of tree shapes and dimensions, as well as with two different plantation patterns: two fields with a traditional single-tree distribution (Fig. 3a,c) and two fields with the trees in rows (Fig. 3b,d). The fields were identified by four different letters to facilitate the reading of the article, as follows: field A: located in the public research farm "Alameda del Obispo" in Cordoba, field B: a private farm located in Adamuz (Cordoba province), field C: a private farm located in Pedro Abad (Cordoba province), and field D: a private farm located in Villacarrillo (Jaen province).

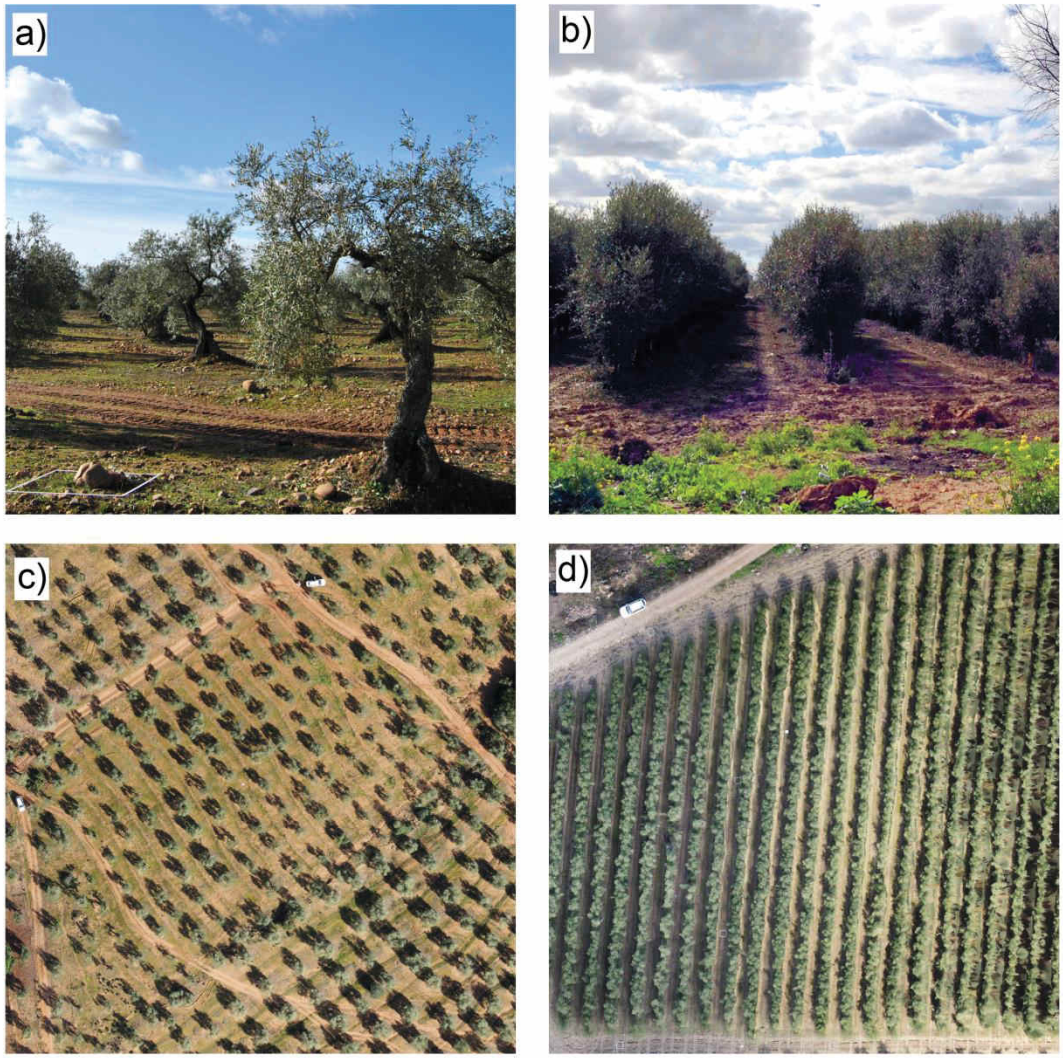

Figure 3. *On-ground (top) and aerial (down) views of two plantations studied in this investigation with single-tree (a, c) and tree-row (b, d) patterns, respectively.*

Different flight missions with the two sensors mounted independently in the UAV were performed in every field (Table 1). In the private farms, the flights were authorized by a written agreement between the farm owners and our research group. On the one hand, the UAV route was configured with the visible-light camera to continuously take photos at an interval of 1 second, which resulted to a forward lap of 90% at least. In this case, the UAV flied in line with a side lap of 60%. With the multispectral camera, the UAV route was programmed to stop in every acquisition point due to camera technical limitations for continuum shooting (slower processing speed). In this case, the images were taken with a side lap and a forward lap of 60%. In all flight missions, the image overlapping was high enough to apply the 3-D reconstruction procedure in the next stage. According to these flight configurations, the visible-light camera can cover roughly 10 ha and 20 ha and the

multispectral camera roughly 3 ha and 6 ha, at 50 and 100 m altitude, respectively, in each regular 30-minutes flight.

Table 1. *Description of the tree plantations and of the flight operations performed in each field.*

Tree plantation			Flight operation[2]		
Field ID	**Location[1]**	**Plantation pattern (tree spacing)**	**Flight date**	**Sensor**	**Flight altitude (m)**
A	Cordoba (37.855N, 4.806W)	Single-trees (7x7 m)	21st Aug, 2013	Visible-light	50, 100
				Multispectral	50
B	Adamuz (37.992N, 4.505W)	Single-trees (8x8 m)	21st Feb, 2014	Visible-light	50,100
				Multispectral	50,100
C	Pedro Abad (37.960N, 4.466W)	Tree-rows (3.75x1.3 m)	21st Feb, 2014	Visible-light	50,100
				Multispectral	50,100
D	Villacarrillo (38.113N, 3.163W)	Tree-rows (8x4 m)	12th May, 2014	Visible-light	50,100
				Multispectral	100

[1] Lat/Lon coordinate system; Datum WGS84.

[2] Multispectral images of the field "B" at 100 m altitude and of the field "D" at 50 m altitude were not taken due to technical problems.

The acquired images had different spatial resolutions according to the technical characteristics of the sensor and to the flight altitude as follows (equation 1): 1) the visible camera flying at 50- and 100-m altitudes produced RGB images with a GSD of 1.53 and 3.06 cm, respectively; and 2) the multispectral camera flying at 50- and 100-m altitudes produced multispectral images with a GSD of 2.71 and 5.42 cm, respectively. These experiments aimed to assess the influence of spatial and spectral resolution on the accuracy of the DSM generation and on the performance of the OBIA tasks (see sections 2.3 and 2.4, respectively). The flight routes fulfilled the requirements that were established by the Spanish National Agency of Aerial Security for maximum flight altitude allowed for UAVs, which is currently fixed at 120 m (MPR 2014).

4.3. Generation of the ortho-mosaics and of the Digital Surface Models (DSM)

Mosaicking and DSM generation were performed using the Agisoft PhotoScan Professional Edition software (Agisoft LLC, St. Petersburg, Russia). The mosaicking process was fully automatic with the exception of the manual localisation of a few ground control points that were taken in each field. The entire automatic process involves three principal stages: 1) aligning images, 2) building field geometry, and 3) ortho-photo generation. First, the camera position for each image and the common points in the images were located and matched, which refined the camera calibration parameters. Next, the DSM was built based on the estimated camera positions and the images themselves. This second stage needs high computational resources and it usually takes a long time in

the case of using many high-resolution images. Finally, the separated images were projected over the DSM, and the ortho-mosaic was generated. The DSM is a 3-dimensional polygon mesh that represents the overflown area and reflects the irregular geometry of the ground and the tree crowns. The DSMs were joined to the ortho-mosaics as Tiff files, which produced a 4-band multi-layer file from the visible-light camera (RGB bands and the DSM) and a 7-band multi-layer file from the multispectral sensor (6 bands and the DSM). A more detailed explanation of the PhotoScan functioning is given in (Dandois and Ellis 2013).

4.4. Object-based image analysis (OBIA) procedure

The multi-layer files that were generated in the previous stage were analysed with an original OBIA algorithm that was developed with the eCognition Developer 9 software (Trimble GeoSpatial, Munich, Germany). This algorithm is auto-adaptive to any remote image with independence of the plantation pattern and it can be apply with minimum user interference. The algorithm is composed of a number of rules that are grouped in four consecutive main phases (Fig. 4):

1) Image segmentation: The image was segmented into objects using the multiresolution segmentation algorithm (Baatz and Schäpe 2000) (Fig. 4a). For a better delineation of the trees, the layers in which the trees were more prominent, i.e., the DSM layer and either the Green band from the visible-light images or the NIR band from the multispectral image, were weighted to 1, and the remaining layers were weighted to 0. The scale parameter varied in the function of the sensor and the spatial resolution, and the remaining segmentation parameters were 0.6, 0.4, 0.5 and 0.05 for colour, shape, smoothness and compactness, respectively (Fig. 4b).

2) Image classification: The classification task took advantage of the capacity of certain vegetation indices to enhance the discrimination of vegetation targets. In this investigation, the Excess Green index (ExG, equation 2, (Woebbecke *et al*. 1995)) for the visible-light images and the Normalised Difference Vegetation Index (NDVI, equation 3, (Rouse *et al*. 1973)) for the multispectral images were calculated. Then, a threshold for vegetation discrimination was established using Otsu´s automatic thresholding method (Otsu 1979) as adapted to the OBIA framework (Torres-Sánchez *et al*. 2015). After the application of the threshold to the vegetation indices values, vegetation was isolated from bare soil (Fig. 4c). Next, the herbaceous vegetation surrounding the trees was isolated considering the DSM layer and applying the criterion of vegetation with low height compared to surrounding soil (Fig. 4d). The vegetation pixel height was derived from the relative difference of the DSM values between the pixels of each individual vegetation object and the pixels of the bare soil surrounding each object. In this step, only the bare soil pixels that were very close to each

vegetation object were specifically selected as the baseline for height calculation, eliminating potential errors due to the terrain slope (Fig. 4e).

$$ExG = 2g - r - b; \text{being } g = \frac{G}{(R+G+B)}; r = \frac{R}{(R+G+B)}; b = \frac{B}{(R+G+B)} \quad (2)$$

$$NDVI = \frac{(NIR - R)}{(NIR + R)} \quad (3)$$

3) Computing and mapping of the 3-D features (canopy width, length and projected area, tree height and crown volume) of each individual tree or tree-row: The vegetation objects that were classified as trees in the previous stage were merged to compound each individual tree or tree-row. This merging operation was performed in a new level created over the original segmentation. Therefore, a hierarchical segmentation structure was generated, in which the merged objects (trees or tree-rows) were in the upper level and the segmented objects were in the bottom level. At this point, the geometric features such as width, length and projected area of the tree canopy and the tree height were automatically calculated by applying a looping process in which each tree or tree-row was individually identified and analysed. Next, the crown volume was calculated by integrating the volume of all of the individual pixels (bottom level) that were positioned below each tree or tree-rwo (upper level) in the hierarchical structure. In this operation, the height and area of every tree pixel were multiplied to obtain the pixel volume, and the tree volume was subsequently derived by adding the volume of all of the pixels below each olive tree or tree-row. This step was performed at the pixel level, which permitted dealing with the irregular shape of every tree or tree-row and consequently avoiding the errors that are usually produced in empirical estimations due to inexact comparisons of the trees or tree-rows to regular solids.

4) Delivery of the map outputs: After computing the tree geometrical features, the OBIA procedure automatically exported such information as vector (e.g., shapefile format) and table (e.g., excel or ASCII format) files for further analysis and applications.

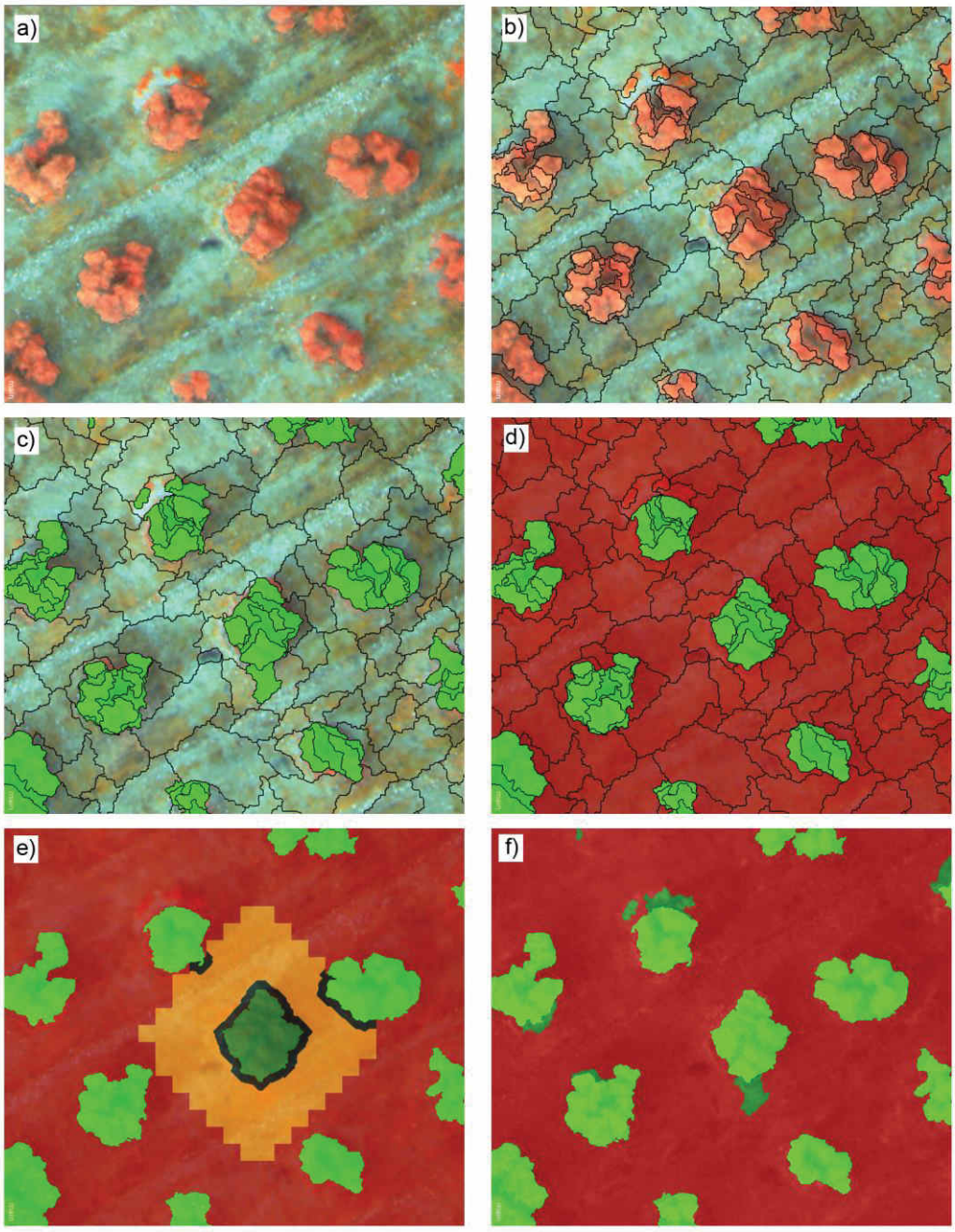

Figure 4. *Partial views of each phase of the OBIA procedure developed to classify agricultural-tree plantations: a) Mosaicked image composed of the spectral information (in this example, multispectral bands) and the DSM data, b) segmentation output, c) classification of the vegetation objects (in green color), d) removal of the herbaceous vegetation, e) identification of the bare-soil area (in orange color), which is used as the base line to calculate the height of the neighbouring vegetation objects (in dark green color), and f) classification of the trees (in bright green color), herbaceous vegetation (in dark green color) and bare soil (in red color) based on the spectral information and the vegetation height.*

4.5. Training and validation of the methodology

This investigation was conducted following a training/validation procedure. The training stage was performed in the field A and the field C as representative of single-tree and tree-row plantations, respectively, and consisted of testing the flight configuration and image acquisition. This stage also involved visual tests of image quality and evaluation of the aptitude of the mosaicked images and their associated DSMs to build the tree structures and to retrieve their geometric features. In addition, we also developed the OBIA algorithms in the training fields. Next, the validation procedure was performed in the field B and the field D as representative of single-tree and tree-row plantations, respectively. Three geometric features, namely the projected area of the canopy, tree height and crown volume, were evaluated by comparing the UAV-estimated values and the on-ground values observed in the validation fields.

In the case of the projected area, the observed values were derived by manually delineating the shape of all of the trees or tree-rows over the mosaicked images that were generated in each flight route. Then, the classification outputs that were generated by the OBIA algorithms were overlapped with the manual classifications to compute the area of coincidence for each tree or tree-row and to calculate the overall classification accuracy in each scenario (equation 4).

$$\text{Overall Classification Accuracy}\,(\%) = 100 \times \left(\frac{\text{Area correctly classified}}{\text{Total area}} \right) \quad (4)$$

In the case of height and volume quantification, 24 trees in the field B and 30 trees in the field D were selected for validation. All of the trees were georeferenced with a GPS device to locate their position in the mosaicked images. In addition, the tree height and canopy diameter were manually measured with a ruler, and the crown volume was estimated assuming an ellipsoid form and applying a validated method (equation 5) for olive tree geometric measurements (Pastor 2005). However, the crown volumes were not calculated in the field D because its row structure impeded the identification of tree edges in the longitudinal axis.

$$\text{Crown volume}\,(\text{m}^3) = \frac{\pi}{6} \times \left(\frac{(\text{Canopy length axis}) + (\text{Canopy width axis})}{2} \right)^2 \times (\text{Tree height}) \quad (5)$$

The efficacy of the entire procedure (mosaicked images, DSM layer and OBIA algorithms) to measure the tree height and crown volume of individual trees was assessed by comparing the UAV-estimated values and on-ground values that were observed in the 54 validation trees. Then, the overall accuracy and its associated average error (equation 6) that were attained in each scenario (two validation fields and several flight altitudes), as well as the root mean square error (RMSE) and

correlation coefficient that were derived from the regression fit, were calculated to quantify the influence of each factor on monitoring each studied tree variable.

$$\text{Average Feature Error} = \frac{\sum_{i=0}^{n} \left| (\text{UAV} - \text{measured Feature}_i) - (\text{Field} - \text{observed Feature}_i) \right|}{\text{Number of trees}} \quad (6)$$

5. RESULTS AND DISCUSSION

5.1. Quality of ortho-mosaic and DSM generation

The figs 5a and 5b show the 3-D representation generated in two fields with single-tree and tree-row systems, respectively. Each image was composed of two products: the ortho-mosaic and its associated DSM. Both plantations were modelled in 3-D with high accuracy, showing the irregular shape of the trees and of the tree-rows including typical crown gaps and branch distribution, which allowed computing tree volume regarding the real crown shape. The ortho-mosaics were successfully created in all the studied scenarios (four fields, two sensors and two flight altitudes), with the exception of the images that were collected with the multispectral sensor over the tree-row plantations. However, the quality of the DSMs was variable as affected by the sensor type and the tree plantation system (Table 2). With the independence of the flight altitude, the DSMs were satisfactorily generated in both single-tree plantations (field A and field B) with the multispectral sensor and in both tree-row plantations (field C and field D) with the visible-light camera. In fact, more than 96% of the trees in the single-tree fields and the 100% of the rows in the tree-row fields were correctly modelled, and only some mixing effects were observed after the image analysis process in the DSMs that were generated with the visible-light images that were captured at a 100-m altitude. In contrast, the DSM generation procedure partially failed with the visible-light images collected in the single-tree fields (mainly in the field B). In these cases, the 3-D structure of some of the trees was not built and, consequently, the mosaicked images showed some blurry areas. On the one hand, we observed that the procedure for 3-D reconstruction with the visible-light images was more problematic in the trees with a low canopy density. As a consequence, we hypothesized that the low colour contrast between some trees and their surrounding bare soil area was the reason of the errors in the generation of the DSM in the separated-tree cropping system scenarios. In fact, greater errors were obtained in the field B, where the colour of many trees was similar to that of bare soil, than in the field A, where a greater contrast between the trees and the bare soil was observed. On the other hand, the multispectral sensor totally failed in both row-tree plantations due to certain difficulties of the 3-D reconstruction software to find common points during the image alignment process. We attributed these errors to insufficient spatial resolution of this sensor in

order to match similar points in overlapped images taken over homogeneous targets, as we also observed in additional investigations on herbaceous crops.

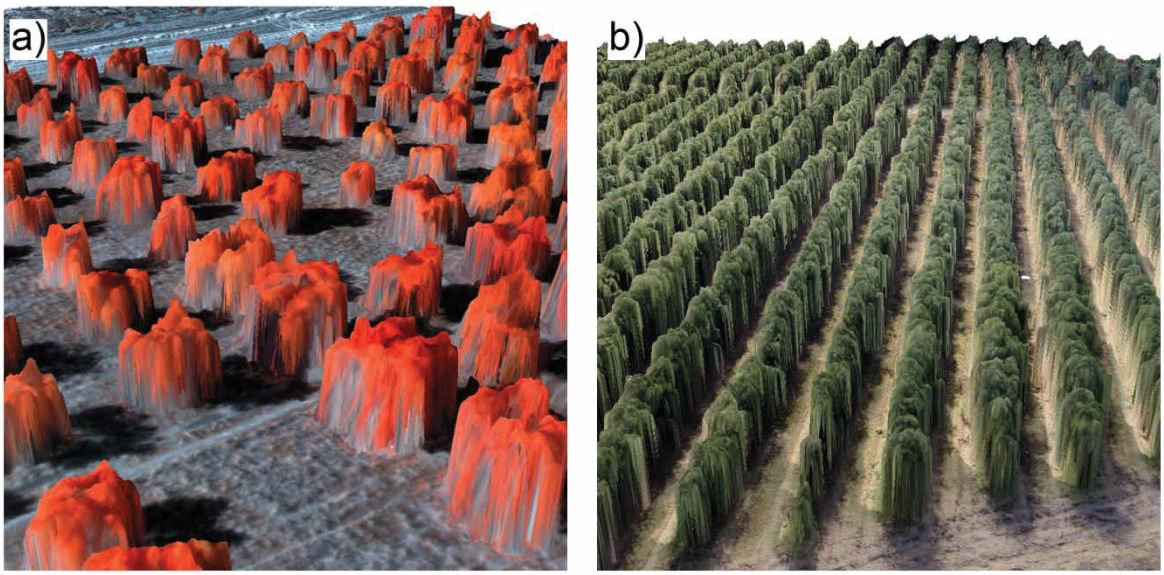

Figure 5. *3-D representation of a single-tree plantation generated with a multispectral sensor (a) and of a tree-row plantation generated with a visible-light camera (b).*

Table 2. *Number and percentage of trees or tree-rows correctly reconstructed during the DSM generation procedure as affected by the sensor type and the flight altitude in each of the studied fields.*

				Trees or tree-rows correctly reconstructed	
Field ID	**Plantation pattern**	**Sensor**	**Fligh altitude (m)**	**Number**	**%**
A	Single-trees	Visible-light	50	65	73
			100	86	97
		Multispectral	50	89	100
B	Single-trees	Visible-light	50	27	20
			100	74	55
		Multispectral	50	135	100
			100	130	96
C	Tree-rows	Visible-light	50	9	100
			100	9	100
		Multispectral	50	0	0
			100	0	0
D	Tree-rows	Visible-light	50	10	100
			100	10	100
		Multispectral	50	10	100

5.2. Classification accuracy as affected by the flight altitude

After building the 3-D models of the four studied fields, we applied our original OBIA procedure in order to classify the remote images (Fig. 6) and to measure the geometric features of each individual tree or tree-row, whichever applies. Our OBIA procedure was designed to auto-adapt, with minimum user intervention, to any agricultural tree plantation with a similar crop patterns (e.g., citrus groves, vineyards or *Prunus* orchards). The algorithms were submitted to a training/validation procedure, in which the images collected in the fields A and C were used for creating and training the OBIA algorithm and the images collected in the fields B and D were used to validate the results (section 2.5). The classification procedure achieved an overall accuracy of approximately 95% or even higher in the most cases (Table 3). With the independence of the sensor used and the field studied, minor differences in the classification accuracy were observed for different flight altitudes. The visible-light and the multispectral sensors captured images with pixel sizes ranging from 1.5 cm to 3.1 cm and from 2.7 cm to 5.4 cm at the studied flight altitudes, respectively. The high spatial resolution imagery that was generated by both sensors, even at a 100-m flight altitude, permitted the correct identification of the tree canopy, which produced a successful classification in every case. Generally, at least four pixels are required to detect the smallest objects within an image (Hengl 2006). Accordingly, the sensors that were used in this investigation were adequate for analysing individual tree or tree-row structures with a minimum dimension of approximately 10x10 cm or even smaller if the flight altitude was lower than 100 m. Therefore, these results recommend collecting the UAV remote images at the highest altitude allowed by the aviation regulations (in Spain, 120 m maximum (MPR 2014)) in order to capture the maximum ground area in each image and to consequently optimise the flight mission length and image ortho-mosaicking process.

Table 3. *Overall accuracy attained by the OBIA algorithm in the classification stage.*

Field ID	Plantation pattern	Sensor	Flight Altitude (m)	Overall Accuracy (%)
A	Single-trees	Multispectral	50	97.4
B	Single-trees	Multispectral	50	96.9
			100	94.5
C	Tree-rows	Visible-light	50	93.1
			100	86.8
D	Tree-rows	Visible-light	50	96.4
			100	95.7

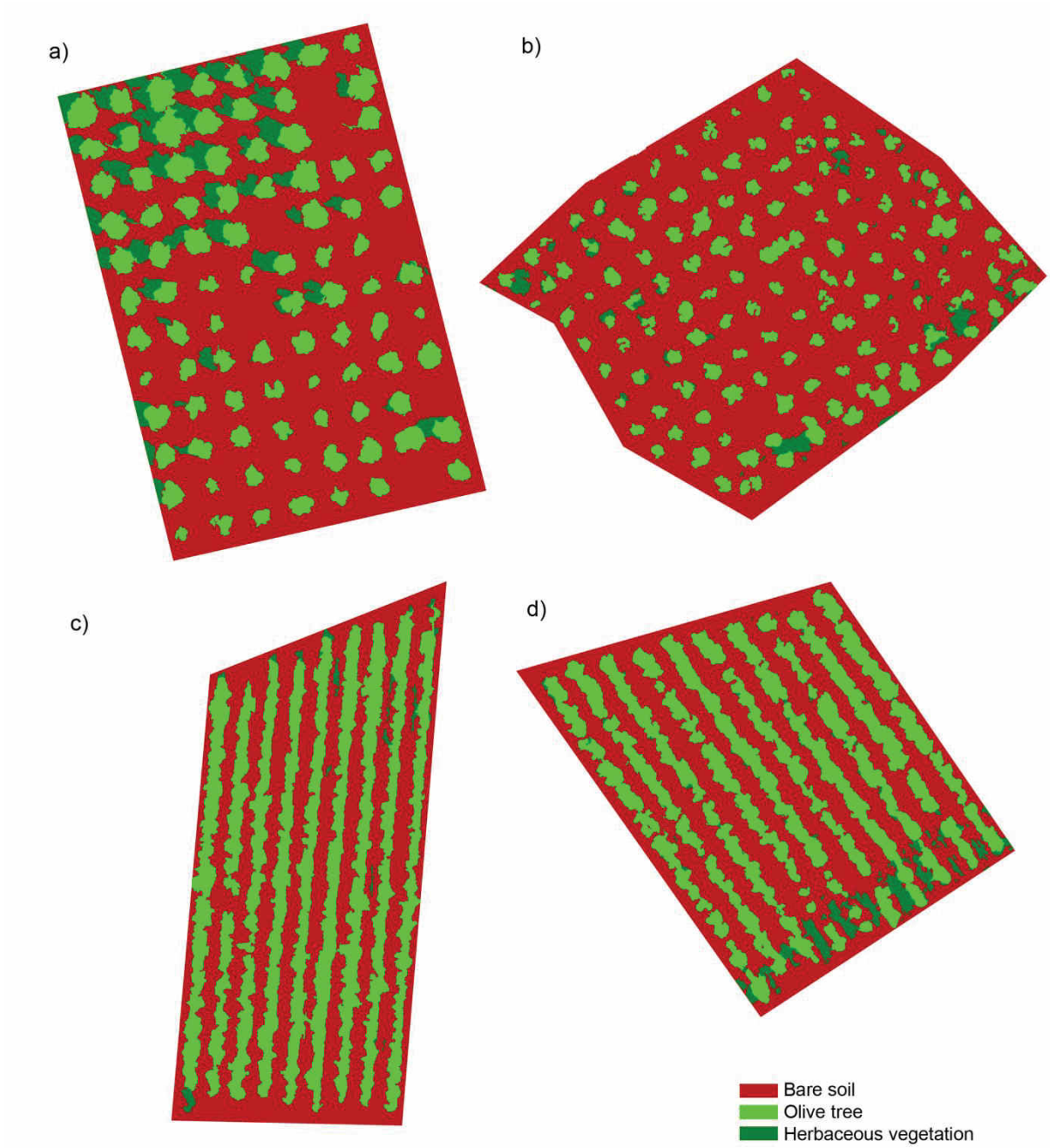

Figure 6. *Classification outputs generated by the OBIA algorithm developed in this investigation. Our innovative algorithm automatically classified individual trees (a, b) or tree-rows (c, d), herbaceous vegetation and bare soil areas and, simultaneously, computed the geometric features (projected canopy area, tree height and crown volume) of each individual tree or tree-row in the whole plantation.*

5.3. Quantification of the tree geometric features (canopy area, tree height and crown volume)

5.3.1. Canopy area

The relation between canopy projected area classified by the OBIA procedure and the observed values at the 50-m-altitude images was close to the 1:1 line (R^2=0.94, RMSE=1.44 m^2), although it tended to a subtle underestimation of the trees or groups of nearby trees larger than 20

m^2 (Fig. 7). With the 100-m-altitude images, this relationship was also close to the 1:1 line, but the correlation coefficient (R^2=0.90) and the RMSE (2.14 m^2) was slightly worse than at the ones reported at 50-m-altitude. The canopy areas of all the trees were estimated with minimum errors in the images at both flight altitudes, which demonstrated algorithm robustness. In fact, the tree canopy edges were automatically defined with high precision even in zones with surrounding herbaceous vegetation, where discriminating vegetation types is a complicate task due to their similar spectral responses. In this case, tree classification was facilitated by incorporating the DSM information (i.e., pixel height) as an input layer in the segmentation procedure and, afterwards, by using an automatic height-based thresholding method for identifying the tree canopy edges.

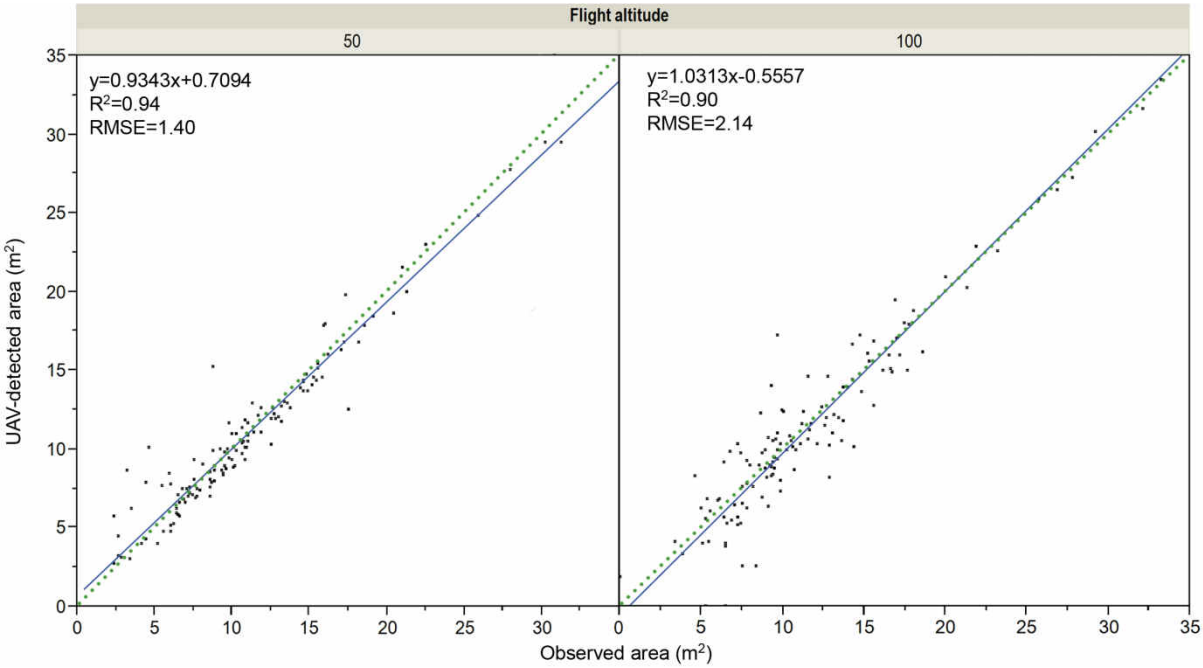

Figure 7. *Classified vs. observed tree projected area after applying the OBIA algorithm in the remote images collected at 50 m (left) and 100 m (right) of flight altitude over the field B. The solid line is the fitted linear function and the dotted line is the 1:1 line.*

5.3.2. Tree height

Tree height was estimated with unprecedented accuracy, reporting averaged errors in the range of 0.17-0.18 m from the images captured with the visible-light camera and of 0.22-0.53 m from the images captured with the multi-spectral camera (Table 4). Previous investigations with a similar image-based UAV technology reported RMSE values on tree height estimations in the range of 0.33-0.39 m (Zarco-Tejada *et al*. 2014) and of 0.44-0.59 m (Kattenborn *et al*. 2014) in olive-tree and palm-tree plantations, respectively. An essential difference with these investigations refers to the image analysis technique used to compute the tree parameters in each case. We implemented an OBIA algorithm instead of the pixel-based filtering algorithms applied in (Kattenborn *et al*. 2014;

Zarco-Tejada *et al*. 2014). OBIA has various advantages for analysing high-resolution images where the pixels can be aggregated to create new elements (e.g., trees) with an evident spatial pattern. Here, the OBIA algorithm identified all the trees in the plantation with very high accuracy (table 3) and treated each of the trees as an individual object. This tree-by-tree procedure can exactly select the local maxima (in the tree apex) and minima (in the surrounding on-ground base-line) extreme pixels that are used by the OBIA algorithm to calculate the height of each individual tree. By comparing the on-ground observed and the UAV-measured height values, the coefficient of determination was 0.90 and 0.84 for the UAV-images captured at 50-m and 100-m flight altitudes, respectively (Fig. 8). The regression line was very close to the 1:1 line with the results derived from the images captured at 50-m flight altitude, although some under-estimation was obtained from the 100-m-altitude images, particularly in the case of trees shorter than 4 m height. In general, the UAV-based estimations of the tree heights only deviated a few centimetres from the on-ground measurements. However, these deviations were greater in the shortest trees and using the highest flight altitude, which likely denotes a positive relationship between both variables. For this application, these errors are tolerable but, if required, vertical estimations could be improved by reducing the flight altitude according to tree heights, although further investigation is needed to determine the optimal flight configuration for image-based 3-D photo-reconstruction.

Table 4. *Tree height quantification errors (average and standard deviation) accounted in the validation fields.*

				Tree height quantification error		
Field ID	**Plantation pattern**	**Sensor**	**Flight Altitude (m)**	**Averaged**		**Standard deviation**
B	Single-trees	Multispectral	50	0.22 m	(6.32 %)	3.41
			100	0.53 m	(15.55 %)	8.12
D	Tree-rows	Visible-light	50	0.18 m	(3.75 %)	3.06
			100	0.17 m	(3.54 %)	3.16

5.3.3. Crown volume

A precise measurement of tree projected area and tree height was crucial for modelling tree crowns and consequently for computing tree volume in the next phase. The relationship between the UAV-based and the on-ground-based volume estimations of the individual trees is shown in the fig 9. The coefficient of determination was 0.65 and 0.63 with the 50- and the 100-m-altitude images, respectively. In this case, the differences between both variables do not denote real errors of the UAV-based measurements because the on-ground-based values were derived by applying the conventional geometric equation that considers the trees as ellipsoid forms (West 2009), which can produce inexact on-ground estimations. On the contrary, the 3-D products derived in this

investigation reconstruct the irregular shape of the tree crown, which hypothetically allows better estimations of tree volume than those ones derived from on-ground measurements. In any case, similar magnitudes were observed between both approaches with independence of the flight altitude considered; i.e., the trees that were identified as bigger on the ground were also quantified as trees with larger volumes by the UAV-based procedure and vice versa (Fig. 10).

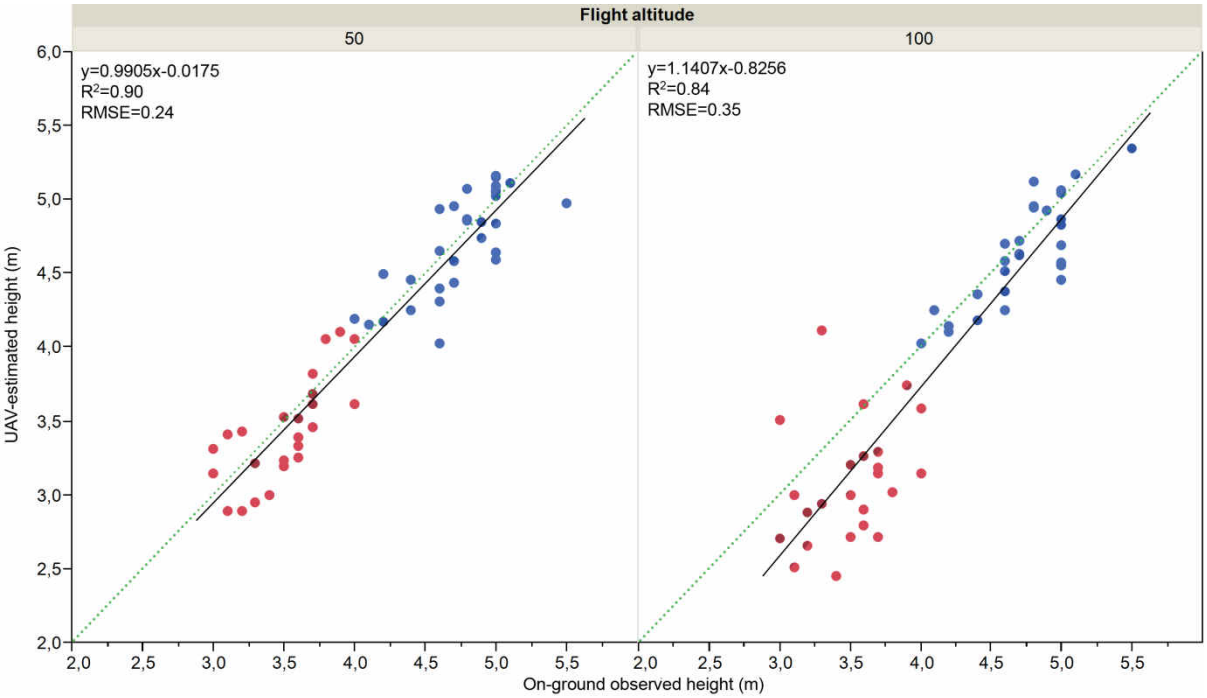

Figure 8. *Comparison between on-ground observed and UAV-estimated tree height values measured from the images captured at 50 m (left) and 100 m (right) of flight altitude, respectively. The results in the tree-row plantations (blue dots) were obtained with the visible-light camera and in the single-tree plantations (red dots) with the multispectral sensor. The solid line is the fitted linear function and the dotted line is the 1:1 line.*

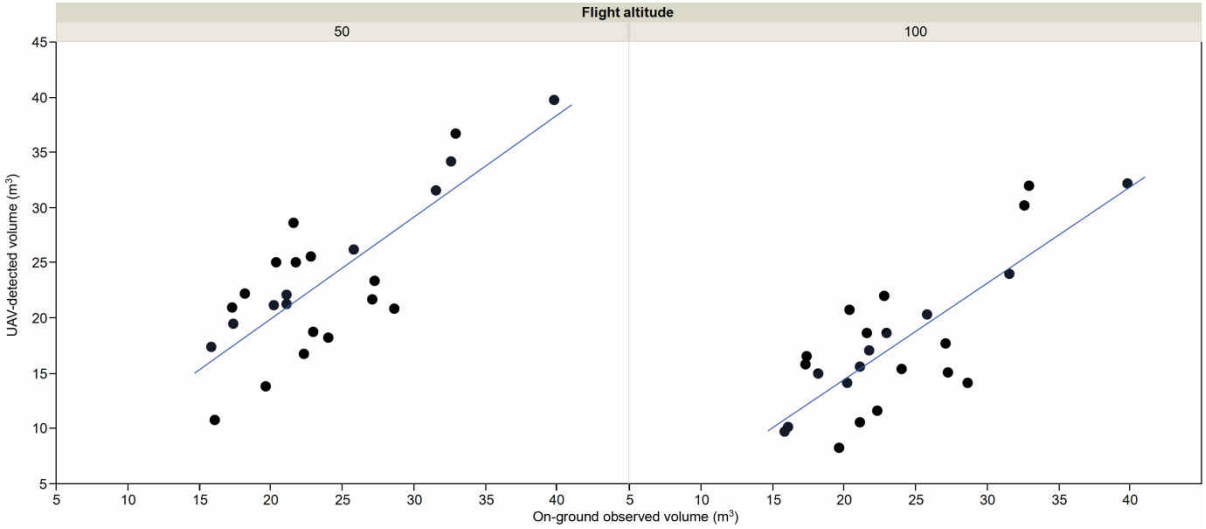

Figure 9. *Comparison between on-ground-based volume estimations and UAV-based tree volume values computed from the UAV-images captured at 50 m (left) and 100 m (right) of flight altitude, respectively. The UAV-based values were calculated by integrating the volume of all the pixels within each image-object*

corresponding to each individual tree, which permitted dealing with the irregular shape of every tree and consequently avoiding the errors due to inexact comparisons of the trees to regular solids. The UAV-based values were compared to on-ground estimations, which were calculated after manually measuring tree canopy diameter and tree height with a ruler and then applying the ellipsoidal geometric model.

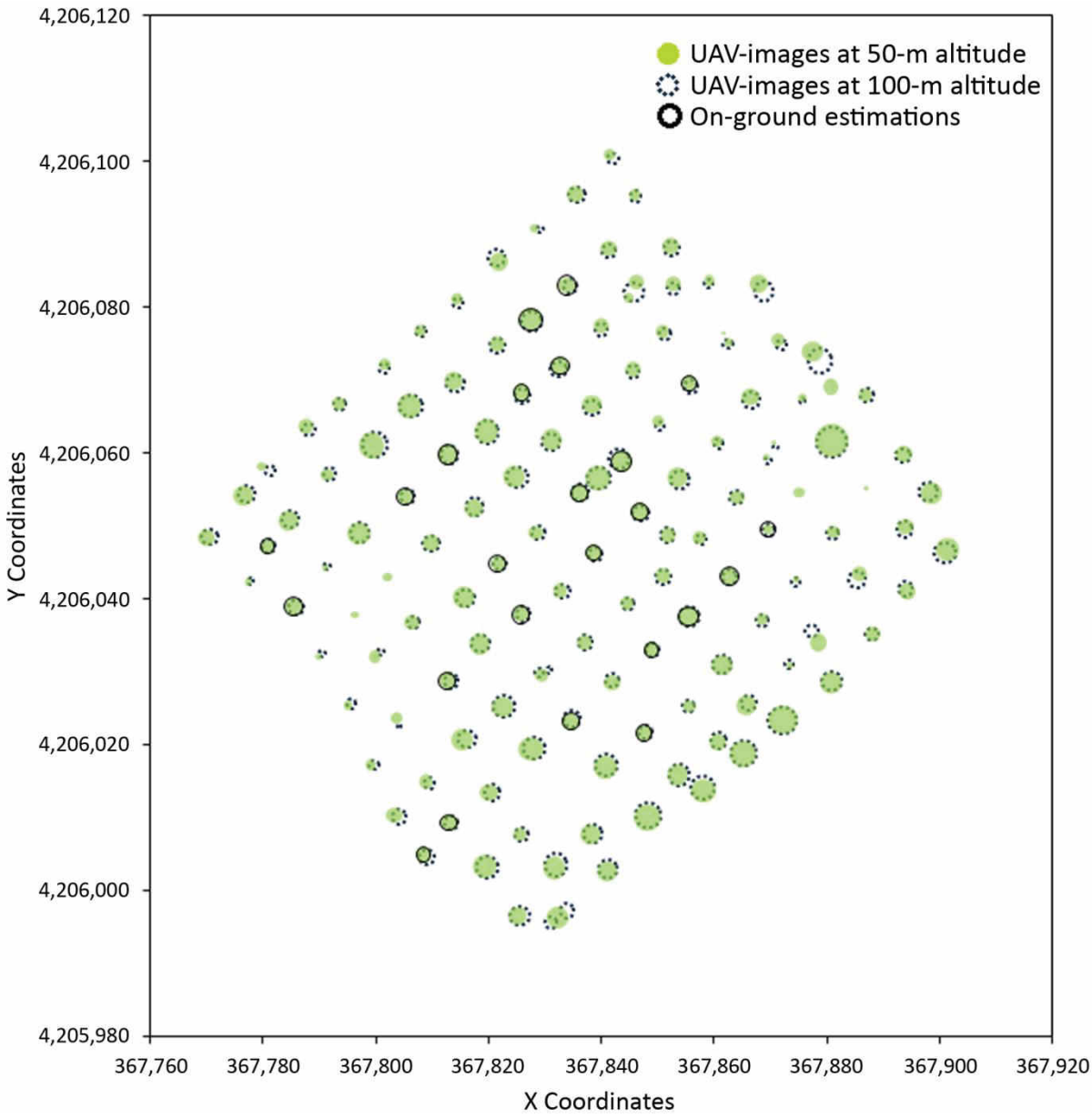

Figure 10. *Spatial position and crown volume computed in the validation field B by using UAV-images captured at 50 m (green circles) and at 100 m (dotted circles) of flight altitude with the multispectral sensor and their relative comparison to the on-ground estimations of the validation trees (solid circles).*

5.4. Detailed map information provided by the OBIA algorithm

After extracting the geometric features of every individual tree or tree-row in the entire plantations, an additional advantage of the OBIA procedure was its capacity to automatically compute such information at different levels and export accurate data as vector (e.g., shapefile

format) and table (e.g., excel or ASCII format) files. On the one hand, global information at the field level includes field dimensions, the number of trees, averaged tree spacing and tree statistical data (e.g., medium and standard deviation of tree heights and crown volumes). On the other hand, spatial data at the tree or tree-row level includes the central coordinates, dimensions of the main length and width axes, canopy projected area, tree height and crown volume (Table 5). This spatial information allows creating maps of each one of the geometric features studied (Fig. 10), which show the heterogeneity of the whole plantation and the zones in the field with different tree growth.

Table 5. *A sample of the output data file computed at the tree level. Accurate spatial data of each individual tree was automatically computed by the OBIA procedure in a field with 135 trees. In this case, the remote images were taken at 50 m flight altitude with a multispectral sensor.*

Tree ID	Position[1]		Geometric features				
	X	Y	Length axis (m)	Width axis (m)	Projected area (m^2)	Height (m)	Volume (m3)
1	367,769	4,206,048	4.78	4.00	13.21	3.85	21.84
2	367,774	4,206,048	5.15	4.72	12.98	1.67	11.66
3	367,777	4,206,042	2.51	1.59	2.57	3.25	5.47
…	…	…	…	…	…	…	…
135	367,784	4,206,050	4.59	4.34	12.91	3.49	33.21

[1] UTM coordinate system (zone 30N); Datum WGS84.

5.5. Time consumption

Considering the entire workflow from flight operation to features extraction, the required time to monitor one hectare of field surface varied from several minutes to a few hours depending on the sensor used and the number of the remote images collected by the UAV (Table 6). Most percentage of time was dedicated to image mosaicking and analysis, which is mainly affected by image spatial resolution. For this reason, time needed to process the visible-light images (4,032 x 3,024 pixels) was pretty longer in comparison to multispectral images (1,280 x 1,024 pixels). However, processing time was registered using a standard computer (16 GB of RAM, Intel core i5 processor and graphic card of 1 GB), so a drastic reduction of this time is possible with a more powerful computer.

Table 6. *Averaged time per surface hectare consumed by each step of the UAV-based workflow as affected by the type of sensor and flight altitude.*

			Time (h:min)/ha			
Sensor	**Flight altitude (m)**	**# images/ha**	**Flight operation[1]**	**Image mosaicking**	**OBIA analysis**	**Total**
Multispectral	50	60	0:13	0:25	0:09	0:47
	100	10	0:07	0:02	0:04	0:13
Visible-light	50	70	0:05	4:00	1:10	4:15
	100	20	0:03	0:40	0:25	1:08

[1] With the visible-light camera, the UAV route was configured to continuously take photos with an interval of 3 seconds, flying in lines at 3 m/s with a side lap of 60%. With the multispectral camera, the UAV route was programmed to stop in every acquisition point. The multispectral images were taken with 60% side and forward overlaps.

Accordingly, an agreement between result accuracy and operation length is needed in order to select the sensor and the optimum flight configuration. In our investigation, results obtained at 50 m altitude were around 10-20% better than the ones obtained at 100 m altitude, although image processing was around four times longer at 50 m altitude. From a practical point view, the 100-m-altitude images are recommended in order to increase the ground area covered in each flight and, consequently, to reduce both the mission length and size of the image set. However, the potential precision expected from each flight altitude should also be considered according to the project quality requirements.

6. CONCLUSIONS

This investigation has shown the capacity of UAV technology to efficiently produce 3-D geometrical data of hundreds of agricultural trees at the field level. In combination with an innovative object-based image analysis algorithm, we computed the canopy area, tree height and crown volume of the trees in a timely and accurate manner, which offers a very valuable alternative to hard and inefficient field work. After comparing a set of remote images collected with both a visible-light camera and a multispectral sensor, we concluded that the upper one is better recommended for fields with a tree-row plantation pattern and the latter one for single-tree plantations. We also observed minimum differences between the results obtained with the images collected at 50-m and at 100-m of flight altitude, concluding that the taller altitude should be generally selected in order to reduce the time needed to collect and to process the images.

The georeferenced information provided by our procedure allows creating maps of orchard heterogeneity and, consequently, observing zones with different tree sizes. These maps are critical

to understand the linkages between tree grown and field-related factors (soil properties, weed infestations, etc.) or to study the mutual relationship between nearby trees, which can help to detect problems associated to soil or crop deficiencies or to diagnostic tree pathologies. In addition, these maps allow adopting a strategy for site-specific management of homogenous zones based on filed field or tree spatial variability in the context of precision agriculture (Zhang and Kovacs 2012), which could increase farmer net economic returns by economising on inputs (fertiliser, pesticide, water, etc) and field operations (pesticide application, irrigation, harvesting, pruning, etc).

Particularly in this context, there is a demand for developing a timely site-specific program to reduce the issues that are associated with current pest control practices in crops and to comply with the European legislation and concerns for the Sustainable Use of Pesticides (Regulation EC No 1107/2009; Directive 2009/128/EC). These regulations include such key elements as reductions in applications using an adequate amount of pesticides according to the specific requirements. Our investigation offers a reliable tool for an accurate and high-throughput monitoring of the spatial variability of agricultural-tree fields under two different plantation patterns, including tree height and crown volume of all the trees in the whole plantation, which could be used to save agricultural inputs and to optimize crop management operations with relevant agro-environmental implications.

7. ACKNOWLEDGEMENTS

The authors thank Irene Borra-Serrano and Angélica Serrano-Pérez for their very useful help during field works.

8. REFERENCES

Anderson, C. (2014, April 23). Cheap Drones Give Farmers a New Way to Improve Crop Yields. *MIT Technology Review*. http://www.technologyreview.com/featuredstory/526491/agricultural-drones/. Accessed 25 January 2015

Baatz, M., & Schäpe, A. (2000). Angewandte Geographische Informationsverarbeitung XII (Vol. XII, pp. 12–23). Presented at the Beiträge zum AGIT Symposium, Salzburg (Austria): J. Strbl (Ed.). Karlruhe, Herbert Wichmann Verlag.

Bendig, J., Bolten, A., Bennertz, S., Broscheit, J., Eichfuss, S., & Bareth, G. (2014). Estimating Biomass of Barley Using Crop Surface Models (CSMs) Derived from UAV-Based RGB Imaging. *Remote Sensing*, *6*(11), 10395–10412. doi:10.3390/rs61110395

Blaschke, T., Hay, G. J., Kelly, M., Lang, S., Hofmann, P., Addink, E., et al. (2014). Geographic Object-Based Image Analysis – Towards a new paradigm. *ISPRS Journal of Photogrammetry and Remote Sensing*, *87*, 180–191. doi:10.1016/j.isprsjprs.2013.09.014

Dandois, J. P., & Ellis, E. C. (2013). High spatial resolution three-dimensional mapping of vegetation spectral dynamics using computer vision. *Remote Sensing of Environment*, *136*, 259–276. doi:10.1016/j.rse.2013.04.005

Díaz-Varela, R. A., de la Rosa, R., León, L., & Zarco-Tejada, P. J. (2015). High-Resolution Airborne UAV Imagery to Assess Olive Tree Crown Parameters Using 3D Photo Reconstruction: Application in Breeding Trials. *Remote Sensing*, *7*(4), 4213–4232. doi:10.3390/rs70404213

Diaz-Varela, R. A., Zarco-Tejada, P. J., Angileri, V., & Loudjani, P. (2014). Automatic identification of agricultural terraces through object-oriented analysis of very high resolution DSMs and multispectral imagery obtained from an unmanned aerial vehicle. *Journal of Environmental Management*, *134*, 117–126. doi:10.1016/j.jenvman.2014.01.006

Fernández-Sarría, A., Martínez, L., Velázquez-Martí, B., Sajdak, M., Estornell, J., & Recio, J. A. (2013). Different methodologies for calculating crown volumes of Platanus hispanica trees using terrestrial laser scanner and a comparison with classical dendrometric measurements. *Computers and Electronics in Agriculture*, *90*, 176–185. doi:10.1016/j.compag.2012.09.017

Hengl, T. (2006). Finding the right pixel size. *Computers & Geosciences*, *32*(9), 1283–1298. doi:10.1016/j.cageo.2005.11.008

Kattenborn, T., Sperlich, M., Bataua, K., & Koch, B. (2014). Automatic single palm tree detection in plantations using UAV-based photogrammetric point clouds. In *The International Archives of the Photogrammetry, Remote Sensing and Spatial Information Sciences* (Vol. XL–3, pp. 139–144). Presented at the ISPRS Technical Commission III Symposium, Zurich, Switzerland. doi:10.5194/isprsarchives-XL-3-139-2014

Laliberte, A., & Rango, A. (2011). Image processing and classification procedures for analysis of sub-decimeter imagery acquired with an unmanned aircraft over arid rangelands. *GIScience and Remote Sensing*, *48*(1), 4–23. Accessed 1 October 2012

Luo, C., Li, X., & Dai, Q. (2014). Biology's drones: New and improved. *Science*, *344*(6190), 1351–1351. doi:10.1126/science.344.6190.1351-b

Marris, E. (2013). Drones in science: Fly, and bring me data. *Nature*, *498*(7453), 156–158. doi:10.1038/498156a

Moorthy, I., Miller, J. R., Berni, J. A. J., Zarco-Tejada, P., Hu, B., & Chen, J. (2011). Field characterization of olive (Olea europaea L.) tree crown architecture using terrestrial laser scanning data. *Agricultural and Forest Meteorology*, *151*(2), 204–214. doi:10.1016/j.agrformet.2010.10.005

MPR. (2014). *Real Decreto-ley 8/2014, de 4 de julio, de aprobación de medidas urgentes para el crecimiento, la competitividad y la eficiencia (in Spanish)*. Madrid, Spain: Spanish Ministry of the Presidency, Official Bulletin (BOE). https://www.boe.es/diario_boe/txt.php?id=BOE-A-2014-7064. Accessed 25 January 2015

Nex, F., & Remondino, F. (2014). UAV for 3D mapping applications: a review. *Applied Geomatics*, *6*(1), 1–15. doi:10.1007/s12518-013-0120-x

Otsu, N. (1979). A Threshold Selection Method from Gray-Level Histograms. *IEEE Transactions on Systems, Man and Cybernetics*, *9*(1), 62–66. doi:10.1109/TSMC.1979.4310076

Pastor, M. (Ed.). (2005). *Cultivo del olivo con riego localizado : diseño y manejo del cultivo y las instalaciones, programación de riegos y fertirrigación*. Mundi Prensa Libros S.A. http://dialnet.unirioja.es/servlet/libro?codigo=8551. Accessed 27 August 2014

Peña, J. M., Torres-Sánchez, J., de Castro, A. I., Kelly, M., & López-Granados, F. (2013). Weed Mapping in Early-Season Maize Fields Using Object-Based Analysis of Unmanned Aerial Vehicle (UAV) Images. *PLoS ONE*, *8*(10), e77151. doi:10.1371/journal.pone.0077151

Qin, R. (2014). An Object-Based Hierarchical Method for Change Detection Using Unmanned Aerial Vehicle Images. *Remote Sensing*, *6*(9), 7911–7932. doi:10.3390/rs6097911

Rosell, J. R., & Sanz, R. (2012). A review of methods and applications of the geometric characterization of tree crops in agricultural activities. *Computers and Electronics in Agriculture*, *81*, 124–141. doi:10.1016/j.compag.2011.09.007

Rouse, J. W., Haas, R. H., Schell, J. A., & Deering, D. W. (1973). Monitoring vegetation systems in the Great Plains with ERTS. In S. C. Freden, E. P. Mercanti, & M. A. Becker

(Eds.), *Volume I: Technical Presentations* (Vol. 1, pp. 309–317). Presented at the Third Earth Resources Technology Satellite-1 Symposium, Washington, DC, USA: NASA, Sp-351 I.

Rovira-Más, F., Zhang, Q., & Reid, J. F. (2008). Stereo vision three-dimensional terrain maps for precision agriculture. *Computers and Electronics in Agriculture*, *60*(2), 133–143. doi:10.1016/j.compag.2007.07.007

Torres-Sánchez, J., López-Granados, F., De Castro, A. I., & Peña-Barragán, J. M. (2013). Configuration and Specifications of an Unmanned Aerial Vehicle (UAV) for Early Site Specific Weed Management. *PLoS ONE*, *8*(3), e58210. doi:10.1371/journal.pone.0058210

Torres-Sánchez, J., López-Granados, F., & Peña, J. M. (2015). An automatic object-based method for optimal thresholding in UAV images: Application for vegetation detection in herbaceous crops. *Computers and Electronics in Agriculture*, *114*, 43–52. doi:10.1016/j.compag.2015.03.019

Torres-Sánchez, J., Peña, J. M., de Castro, A. I., & López-Granados, F. (2014). Multi-temporal mapping of the vegetation fraction in early-season wheat fields using images from UAV. *Computers and Electronics in Agriculture*, *103*, 104–113. doi:10.1016/j.compag.2014.02.009

West, P. W. (2009). *Tree and forest measurements* (2nd ed.). Berlin, Germany: Springer-Verlag.

Woebbecke, D. M., Meyer, G. E., Von Bargen, K., & Mortensen, D. A. (1995). Color indices for weed identification under various soil, residue, and lighting conditions. *Transactions of the American Society of Agricultural Engineers*, *38*(1), 259–269. Accessed 5 July 2011

Zarco-Tejada, P. J., Diaz-Varela, R., Angileri, V., & Loudjani, P. (2014). Tree height quantification using very high resolution imagery acquired from an unmanned aerial vehicle (UAV) and automatic 3D photo-reconstruction methods. *European Journal of Agronomy*, *55*, 89–99. doi:10.1016/j.eja.2014.01.004

Zhang, C., & Kovacs, J. M. (2012). The application of small unmanned aerial systems for precision agriculture: a review. *Precision Agriculture*, *13*(6), 693–712. doi:10.1007/s11119-012-9274-5

CAPÍTULO 8

3-D VINEYARD MONITORING WITH UAV IMAGES AND A NOVEL OBIA PROCEDURE FOR PRECISION VITICULTURE APPLICATIONS

Torres-Sánchez, J., López-Granados, F., Jiménez-Brenes, F.M., Borra-Serrano, I., de Castro, A.I., Peña, J.M. (2016). 3-D vineyard monitoring with UAV images and a novel OBIA procedure for precision viticulture applications. Enviado a *Computers and Electronics in Agriculture*

1. RESUMEN

La estructura tridimensional de los viñedos puede ser reconstruida mediante la aplicación de la fotogrametría a imágenes aéreas tomadas con UAV. Esta información tridimensional es muy valiosa para la implementación de estrategias de viticultura de precisión, como por ejemplo, el diseño de tratamientos localizados adaptados a la detección de las cepas y marras, o el ajuste de las aplicaciones de fitosanitarios de acuerdo al tamaño de la cepa, entre otros. Sin embargo, el procesamiento de la gran cantidad de datos sobre el cultivo presentes en las imágenes y modelos tridimensionales de las viñas es actualmente un cuello de botella de esta tecnología. Para resolver esta limitación, se ha desarrollado un novedoso y robusto algoritmo de OBIA para la caracterización y monitorización 3D de viñedos. El procedimiento OBIA es totalmente automático, es auto-adaptativo a diferentes situaciones en el campo y puede calcular información del cultivo exportable en formato de tabla, vectorial o ráster. Los resultados obtenidos en tres campos de ensayo en dos fechas demostraron una gran precisión en la clasificación de las cepas, de en torno al 90-95%, así como pequeños errores en la estimación de la altura de la viña (RMSE de 0,18 m de media). Además, el algoritmo puede calcular la posición, área proyectada y volumen de cada cepa en el viñedo, lo que aumenta el potencial de esta tecnología para las aplicaciones de control localizado.

2. ABSTRACT

The three-dimensional (3D) structure of vineyard fields can be generated by combining aerial images collected with Unmanned Aerial Vehicle (UAV) technology and photo-reconstructed digital surface models (DSMs). This 3D information is very valuable for the implementation of precision viticulture strategies, e.g., designing site-specific treatments adapted to grapevines and gap detection or the adjustment of phytosanitary applications according to canopy size and height, among others. However, processing the large amount of detailed crop data embedded in the UAV images and the DSMs is currently a bottleneck of this technology. To solve this limitation, a novel and robust object-based image analysis (OBIA) procedure was developed for vineyard field monitoring and 3D grapevine characterization. The OBIA procedure is fully automatic, is auto-adaptive to different crop-field conditions and can compute explicit crop information both in table, vector (shape-file) and raster (map) formats, as follows: 1) grapevines and row gap classification, and 2) grapevine dimensions. The results obtained in three testing fields on two different dates showed high accuracy in the classification of grapevine area and row gaps at approximately 90% and 95%, as well as minor errors in grapevine height estimates (RMSE of 0.18 m, on average). In addition, the customized algorithms included in the OBIA procedure computed the position, projected area and

volume of every grapevine in the field, which increased the potential of this UAV-based technology as a tool for site-specific crop management applications.

3. INTRODUCTION

Vineyard yield and grape quality depends on several field-related factors and changing weather conditions. Studying the influence and spatial distribution of these factors allows grape growers to improve vineyard management according to quality and productivity parameters (Bramley and Hamilton 2004). In this context, precision viticulture (PV) has arisen in recent years as a new approach in grape production. PV is based in assessing intra- and inter- crop-field spatial variability and implementing site-specific crop management systems (Arnó Satorra *et al*. 2009). The ultimate objective is to optimize crop production and profitability through a reduction in production inputs (e.g., pesticides, fertilizers, machinery, fuel, water, etc.) and, consequently, diminish potential damage to the environment due to the over-application of inputs (Schieffer and Dillon 2014; Tey and Brindal 2012). To design site-specific management strategies, georeferenced information of the grapevine canopy structure and its variability at the field scale are required as fundamental input data. As an alternative to time-consuming on-ground methods traditionally used to collect crop data, remote sensing offers the possibility of a rapid assessment of large vineyard areas (A. Hall *et al*. 2002; Johnson *et al*. 2003). Among the remote sensing platforms, Unmanned Aerial Vehicles (UAVs) stand out because of their unprecedented high spatial and temporal resolutions, which are essential for the accurate and timely monitoring of the crop. At present, UAVs are widely used for a wide range of purposes in viticulture, such as the assessment of water status (Baluja *et al*. 2012), characterization of the vine canopy (Ballesteros *et al*. 2015; Mathews and Jensen 2013), or to study the spatial variability of yield and berry composition (Rey-Caramés *et al*. 2015). UAVs are able to fly at low altitudes with high image overlap, which permits the generation of Digital Surface Models (DSMs) using photo-reconstruction techniques and artificial vision (Nex and Remondino 2013). The UAV-based DSMs have recently been used in agricultural applications, e.g., for the three-dimensional (3D) characterization of herbaceous and woody crops with the aim of monitoring crop conditions and growth (Bendig *et al*. 2014; Burgos *et al*. 2015; Torres-Sánchez *et al*. 2015).

Processing the large amount of detailed crop data embedded in the UAV images and the DSMs to extract useful information requires the implementation of robust and automatic image analysis procedures. In the last few years, object-based image analysis (OBIA) has reached high levels of automation and adaptability to ultra-high spatial resolution images and, in comparison with conventional pixel-based methods, proposes better solutions to the problem of pixel heterogeneity (Blaschke *et al*. 2014). The first step in OBIA is image segmentation, which consists of creating

"objects" by grouping adjacent pixels with homogenous spectral values. Next, OBIA combines the spectral, topological and contextual information of these objects to address complicated classification issues. Successful examples of OBIA applications include agricultural (Peña *et al*. 2013), grassland (Laliberte and Rango 2011) and forest scenarios (Hellesen and Matikainen 2013).

In this investigation, a novel OBIA procedure, composed of a rule-set of customized algorithms, was developed for the monitoring of vineyard fields with the main objective of automatically characterizing the 3D structure of the grapevines. This 3D information was previously generated by combining aerial images collected with an UAV equipped with a low-cost camera and photo-reconstructed digital surface models (DSMs). Specific objectives included the following: 1) automatic classification of grapevines and row gaps, even in fields with inter-row vegetation (cover-crop, weeds or grass), which has been reported in previous studies as a complex scenario due to the spectral similarity of different vegetation types observed in the field (Baluja *et al*. 2012), and 2) automatic estimation of grapevines position (geographic coordinates) and dimensions (projected area, height, and volume). This output information is very valuable to for the application of precision viticulture strategies, e.g., designing site-specific treatments adapted to grapevine structure and the detection of row gaps or adjusting phytosanitary applications according to canopy size and height, which can contribute to notable savings in products and tasks (Llorens *et al*. 2010).

4. MATERIALS & METHODS

4.1. Study fields and UAV flights

The experiment was carried out in three different commercial vineyards located in the province of Lleida, Northeastern Spain (Table 1). The private company Raimat, owner of the fields, authorized this investigation and gave permission for the UAV flights. All the fields were vertically shoot-positioned with the rows separated by 3 m, and had inter-row green vegetation (Fig. 1a).

Table 1. *Main characteristics of the study fields. Coordinates are in the WGS84, UTM zone 31N reference system.*

Field	Grape variety	Studied Area (m^2)	Central Coordinates (X, Y)
9	Merlot	4,925	291,009 E; 4,613,392 N
24	Albariño	4,415	291,303 E; 4,614,055 N
111	Chardonnay	2,035	290,910 E; 4,616,282 N

The remote images were acquired with a low-cost commercial off-the-shelf camera, model Olympus PEN E-PM1 (Olympus Corporation, Tokyo, Japan) mounted in a quadcopter model MD4-

1000 (microdrones GmhH, Siegen, Germany) (Fig 1b). The camera weighs 0.38 kg and is equipped with a 14–42 mm zoom lens, although it was fixed to a 14 mm focal length for this study. The camera's sensor size is 17.3 x 13.0 mm and the pixel size is 0.0043 mm. The camera takes 12.2 megapixel (4,032 x 3,024 pixels) images in true color (Red, R; Green, G; and Blue, B, bands) with 8-bit radiometric resolution, which are stored in a secure digital SD-card in JPEG format. The UAV can be manually operated by radio control (1,000 m control range) or it can execute user-defined flight routes autonomously using its autopilot in combination with its Global Navigation Satellite System (GNSS) receiver. The UAV is battery powered and can load any sensor weighing up to 1.25 kg.

Figure 1. *Images of the studied fields: a) green inter-row covers in Field 111 on July; b) the unmanned aerial vehicle taking off over Field 9; c) and d) comparative of the condition of the vines in Field 24 on July and September.*

Two flights were performed in each field, on 29th July 2015 and on 16th September 2015, corresponding to different crop stages. In July, the grapevine canopy was fully developed, while in September, the grapes had been machine-harvested, and consequently, the grapevine canopy was less dense (Fig.1c and 1d). The diversity of the fields and the different dates made possible the analysis of a wide range of situations to ensure the robustness of the OBIA procedure. All of the flights were performed at a 30 m flight altitude, with a resulting ground sampling distance of 1 cm. The flight route was designed with a forward lap of 93% and a side lap of 60%, which was high

enough to achieve the 3D reconstruction of woody crops according to previous investigations (Torres-Sánchez *et al*. 2015).

4.2. DSM and orthomosaic generation

DSM and orthomosaic generation was done using the Agisoft PhotoScan Professional Edition software (Agisoft LLC, St. Petersburg, Russia) version 1.2.4 build 1874. The mosaicking process was fully automatic, with the exception of the manual localization of 5 ground control points taken with a GPS device in the corners and in the center of each field for georeferencing the DSM and orthomosaic. The whole automatic process involves three principal stages: 1) aligning images, 2) building field geometry, and 3) ortho-photo generation. First, the camera position for each image and common points in the images were located and matched, which facilitated the refinement of camera calibration parameters. Next, the DSM was built based on the estimated camera positions and the images themselves. Finally, the individual images were projected over the DSM, and the orthomosaic was generated. The DSMs were saved in greyscale tiff format. More details about the Photoscan functioning are given in (Dandois and Ellis 2013). Information about the processing parameters of the software can be observed in Table 1.

***Table 2**. Processing parameters of the DSM and orthomosaic generation processes in Agisoft Photoscan*

PROCESSING PARAMETER	VALUE
Alignment parameters	
Accuracy	High
Pair preselection	Disabled
Dense point cloud	
Quality	High
Depth filtering	Mild
DEM	
Coordinate system	WGS84 / UTM zone 31 N
Source data	Dense cloud
Orthomosaic	
Blending mode	Mosaic

4.3. OBIA algorithm

The OBIA algorithm for the detection and characterization of grapevine rows (Fig. 2) was developed with the eCognition Developer 9 software (Trimble GeoSpatial, Munich, Germany). It does not need any user intervention and can be divided into three major steps: 1) grapevine classification, in which the grapevines are detected with the DSM using their differences in height with reference to

the soil; 2) row gap detection, in which the row segments in the absence of grapevines are classified as “gaps”; and 3) morphological characterization of every grapevine segment. The DSM in geoTIFF format was used to perform the three steps, while the orthomosaics were only used to validate the classification results.

1. Vine classification: the DSM is segmented in a grid of squares with 0.5-m sides. This size was selected in relation to the vine row width, which is approximately 0.7 m. All of the squares with a standard deviation of the values in the DSM below 0.15, i.e., squares with a low variability in their altitude, are classified as soil squares. The remaining squares are classified as “vine candidates”. One by one, the squares classified as “vine candidates” are segmented in pixel size, and the mean difference of altitude between these pixels and the neighboring soil squares is calculated. If the difference is higher than the minimum vine altitude (0.8 m in these fields), the pixel is classified as “vine”. Analyzing each “vine candidate” separately allows only the surrounding soil altitude to be taken into account, which prevents a comparison of the vine height with the average soil altitude, which could result in mistakes in vineyards grown in fields with slope. After the processing of all of the “vine candidate” squares, the vines in the field are classified. This process is quick due to the simplicity of the calculations, and the presence of cover in the inter-row areas does not interfere with the vine classification because it is based on height detection and not on vegetation indices thresholding.
2. Gap detection in vine rows: once all of the vines are classified, their orientation is used to rotate the image. By doing this, the image shows the rows horizontally, which eases the following processes. The first one is the creation of an upper level of analysis, which is segmented in horizontal rows with a width of 0.5 m. Then, the algorithm looks for the row with the highest percentage of vine in the lower level. This row and its neighbors are classified as a “vine row”, and the rows sharing a border with these ones are classified as “no vine rows” to simplify the search for vine rows in the following steps of the algorithm. These steps are repeated in a loop until all of the rows are classified as “vine row” or “no vine row”. For detecting the gaps in the vine rows, they are segmented and the objects without vines in the lower analysis level are classified as “gap”. The “gap” objects are copied to the lower level, and the upper level is deleted. After all of these processes, the vines and the gaps in the vine rows are classified.
3. Vine segments characterization: the vine rows were segmented into 2-m-long objects, and a lower level representing the vine divided in pixels was created. At this point, the geometric features such as width, length and projected area of the vine canopy and the vine height were automatically calculated by applying a looping process in which each vine segment was

individually identified and analyzed. Next, the crown volume was calculated by integrating the volume of all of the individual pixels (bottom level) that were positioned below each vine segment (upper level) in the hierarchical structure. In this operation, the height and area of every vine pixel were multiplied to obtain the pixel volume, and the vine volume was subsequently derived by adding the volume of all of the pixels below each vine segment. This step was performed at the pixel level, which permitted dealing with the irregular shapes of the vines. This process was very similar to the last step of the algorithm developed for olive characterization in (Torres-Sánchez et al. 2015).

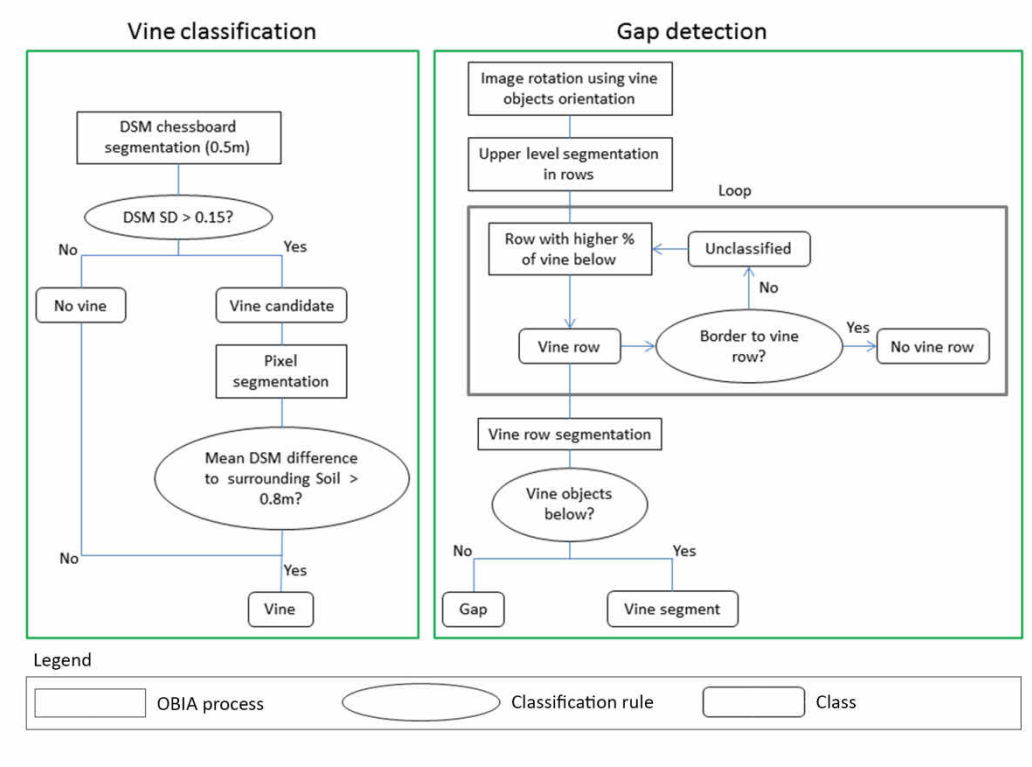

Figure 2. *Explicative diagram of the automatic OBIA algorithms. Abbreviations used: DSM (digital surface model), SD (standard deviation)*

4.4. Validation

4.4.1. Grapevine classification and gap detection

Manual classification of the orthomosaics was done over 20 squares of 2 × 2 m located on a grid basis over the study fields (Fig. 3a and b), the points were marked on the field using an artificial target for locating them more easily on the orthomosaics. The squares were designed with the same orientation as the vine rows using ArcGis 10.0 (ESRI, Redlands, CA, USA) shapefiles. The manual editing tools of eCognition were used for the manual classification of vine and soil in the 20 squares. This classification was compared with the output of the automatic classification algorithm, and confusion matrices were constructed using the results of the comparison. Cohen's Kappa index (Eq.

1) and overall accuracy (OA) (Eq. 2) were computed for the confusion matrix resulting from the comparison.

$$1) \qquad kappa = \frac{p_o - p_c}{1 - p_c}$$

$$p_o = actual\ proportion\ of\ agreement$$

$$p_c = proportion\ of\ chance\ agreement$$

$$2) \qquad OA = \frac{True\ positive + True\ negative}{Total}$$

The automatically generated maps with the classification of vines and gaps were overlaid with the orthomosaics to validate the gap detection section of the algorithm. The lengths of correctly classified gaps, non-detected gaps, and vines classified as gaps were measured using ArcGIS 10.0.

4.4.2. Grapevine height

In every field and on every date, the grapevine height was measured using a ruler (Fig. 3c) on both sides of the points located in the field for classification validation, resulting in 40 validation data in every field and on every date. The measured height of the vines was compared to the height detected by the OBIA algorithm in the validation points. The R^2 and root mean square error (RMSE) of this comparison were calculated using JMP software (SAS, Cary, NC, USA).

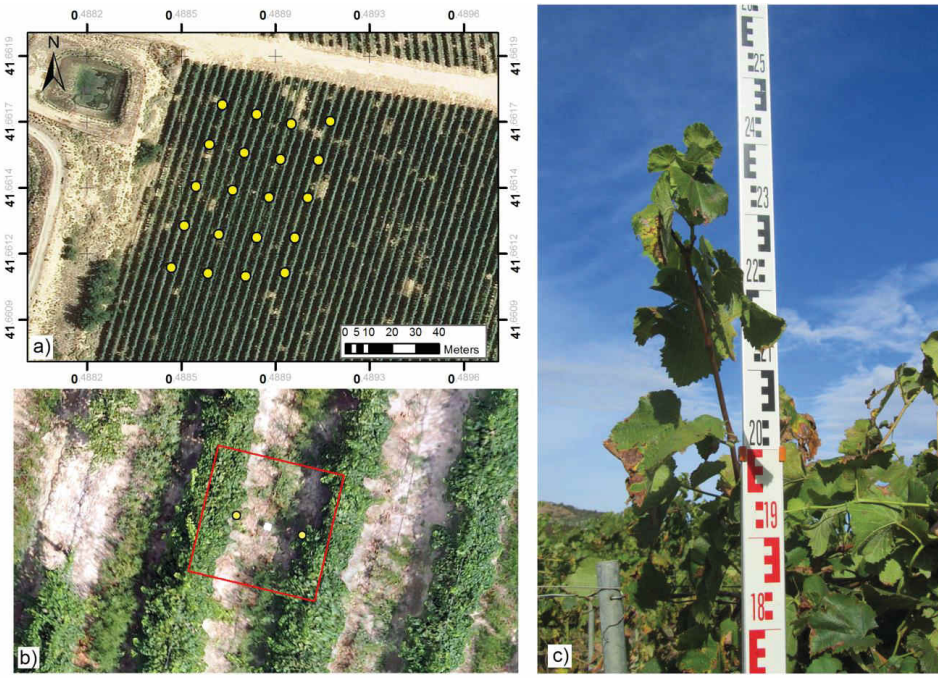

Figure 3. *Experimental set for validating the vine height detection results: a) point grid in Field 9 on July; b) one of the vector squares used for classification validation (the yellow points indicate the positions of height measurements); c) measurement of the vine height.*

5. RESULTS AND DISCUSSION

5.1. Vine classification

Vine classification based on height differences (Fig. 4c and d) provided by the DSM achieved high levels of accuracy, being 93.61% (Table 3) the lower OA value reached among all of the studied fields. In the six cases analyzed, the kappa index values were over 0.7, and they were very near to 0.9 in Fields 9 and 24 on both studied dates (Table 3), which demonstrates a good classification accuracy taking into account that kappa values range from -1 to 1. The accuracy was higher in Fields 9 and 24 because they had more vigorous and developed vine canopies. On the other hand, the vines in Field 111 were smaller and less vigorous, which resulted in a poorer 3D reconstruction, and, consequently, in a lower performance of the DSM based OBIA algorithm. The low and irregular growth of vines in Field 111 led the property to uproot the entire parcel in the winter of 2015-2016. Therefore, the lower kappa values could be from the fact that the existence of very thin branches with few leaves made the 3D modelling of the crop more difficult. The contrast between the kappa values in Field 111 and the high OA values reached in both dates is because the vine covered only a small proportion of the image; consequently, the high percent of soil in the image ensure a high OA value, even if the algorithm did not detect the vine accurately.

Table 3. *Kappa index values for the vine classification in the three fields on both study dates.*

Field	Date	Overall accuracy (%)	kappa
9	July	95.54	0.91
	September	95.41	0.89
24	July	95.19	0.87
	September	95.98	0.85
111	July	93.61	0.78
	September	96.07	0.73

Vine classification accuracy is important in itself because of its applicability to vine monitoring purposes. However, it is also important because it can be used as a beginning step for information extraction of the vine with the same sensor or using other sensors. When using thermal sensors to assess the vineyard water status, a good vine classification is required for extracting thermal data corresponding only to the vine canopy (Baluja *et al*. 2012). Baluja *et al*. tried to use NDVI thresholding techniques for pure canopy pixel extraction, but it led to problems with the inclusion of soil pixels or with large losses of information. Thresholding methods for vine classification can cause problems due to shadows and to inter-row cover crops. Determining an optimal threshold is a compromise between retaining non-vine NDVI values and losing vine NDVI values. It is very difficult to achieve an optimal balance and, consequently, thresholding on its own is not suitable for vine row classification

(Smit et al. 2010). Finally, Baluja et al. used a watershed algorithm available in GRASS GIS (Metz *et al*. 2010) that improved the classification (data not shown numerically in their work) although they mention that it also caused soil inclusion in the vine classification. Because the vine classification approach presented in this work is based on 3D reconstruction rather than on vegetation index thresholding, less than 6.5% (data not shown) of the soil was classified as vine, and the green cover in the inter-row did not interfere in the vine classification. Consequently, it could be used to mask soil pixels in thermal imagery for the assessment of the vineyard water status. Another important aspect of the proposed methodology is that it does not need any user intervention, while other approaches need of manual touch-up for removing non-vine objects (Mathews 2014) or need manually delineated regions of interest to ensure their vigor information belongs only to the vine (Matese *et al*. 2015) and it was not influenced by the spectral information of the green cover (Fig. 1a and 4a) growing in the inter-row areas.

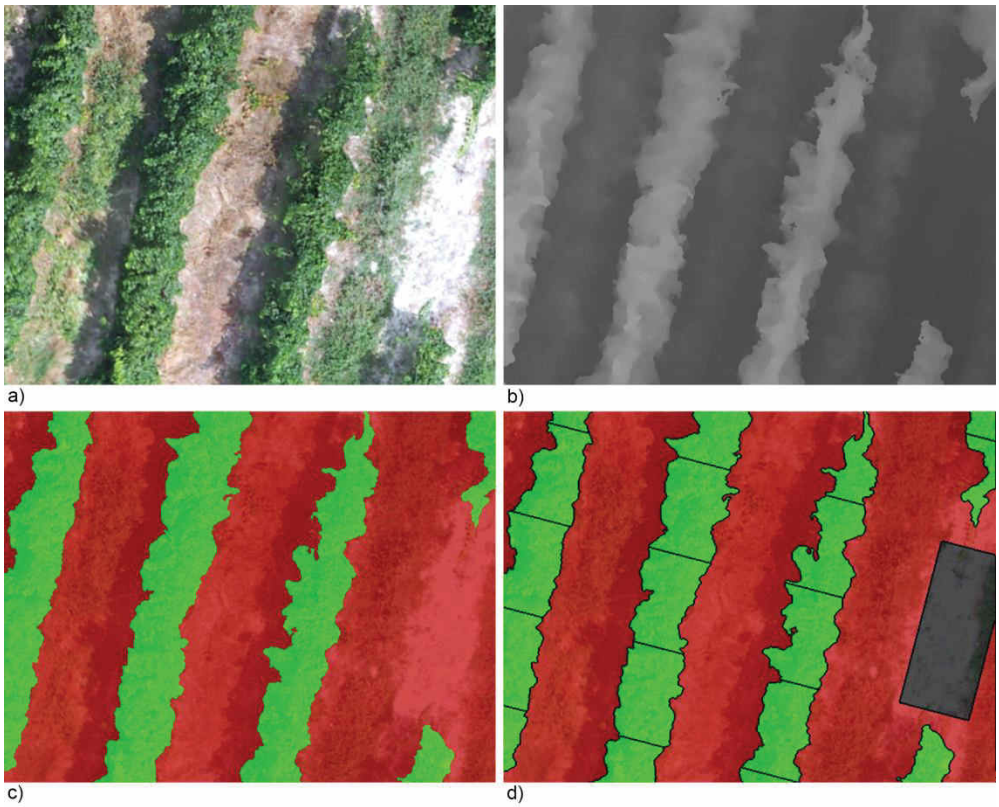

Figure 4. *Different results of the workflow over the same area of Field 9 on July: a) orthomosaic; b) digital surface model; c) vine classification output; d) gap detection and vine segments ready for its characterization.*

5.2. Vine gaps detection

All of the gaps were detected in the three fields and on both dates, with only the exception of Field 9 in September, and even in this case, more than 95% of the gaps' length was detected (Table 4). False positive rates were very low in Fields 9, 24 and 111 in July, but on the second date for Field

111 the algorithm detected about 50% more gaps than actually existed. This result is in agreement with the lower kappa achieved in the vine classification in the same case, and it is also related to the less correct 3D reconstruction due to the bad condition of the crop. The results in Field 111 in July were better because the vine canopy in September was affected by the harvest machinery and, consequently, was in worse condition. In any case, the vineyard health was so bad even in July that the property uprooted the field a few months later.

The lower accuracy in gap detection and vine classification in Field 111 in September contrasts with the low RMSE achieved in the height detection (Fig. 6). This is because the validation of height detection was done by measuring the height of the top area of the vines in the field, and the 3D reconstruction software was able to detect these singular points. However, in Field 111 in September, it had problems with the reconstruction of the lower parts of the vine due to the presence of a weak canopy with sparse leaves. Consequently, the algorithm was able to accurately detect the vine height but achieved worse results in vine classification and gap detection, which where the parts of the algorithm where the whole vine geometry should be correctly generated.

Table 4. *Results of the gap detection in vine rows. Percentages were calculated over the total length of gaps in the field.*

Field	Date	True positive (%)	False positive (%)	False negative (%)
9	July	100.00	1.12	0.00
	September	96.79	0	3.21
24	July	100.00	1.03	0.00
	September	100.00	5.98	0.00
111	July	100.00	0.00	0.00
	September	100.00	46.81	0.00

5.3. Vine height quantification

The OBIA algorithm accurately extracted the plant height from the vineyard DSM, only one of the field measurements was omitted because the algorithm did not detect the vine in it. An R^2 of 0.89 was achieved in the correlation of the measured height with the detected height for the combination of all fields and dates (Fig. 5). The RMSE of this correlation was 0.18 m, very near to the one achieved in the detection of tree height in (Torres-Sánchez *et al*. 2015). When analyzing the data by field and date (Fig. 6), it can be seen that the RMSE was lower in all cases, with the exception of Field 24 in July, and in four cases, it was equal to or lower than 0.12 m. The low errors in height detection are similar to the one achieved in (Burgos *et al*. 2015), where, although there was not an exhaustive height detection validation, the difference between the average detected height and the

topping height measured in the field was 0.13 m. Burgos et al. used a flight plan with a crossing lines pattern, which implies needing more time for flying a vineyard, and, consequently, reducing the maximum area that could be analyzed due to the limited UAV autonomy. Another difference with the present work is that they needed to generate a digital terrain model to study the crop height while the use of OBIA in the present work allowed omitting this step in the analysis workflow.

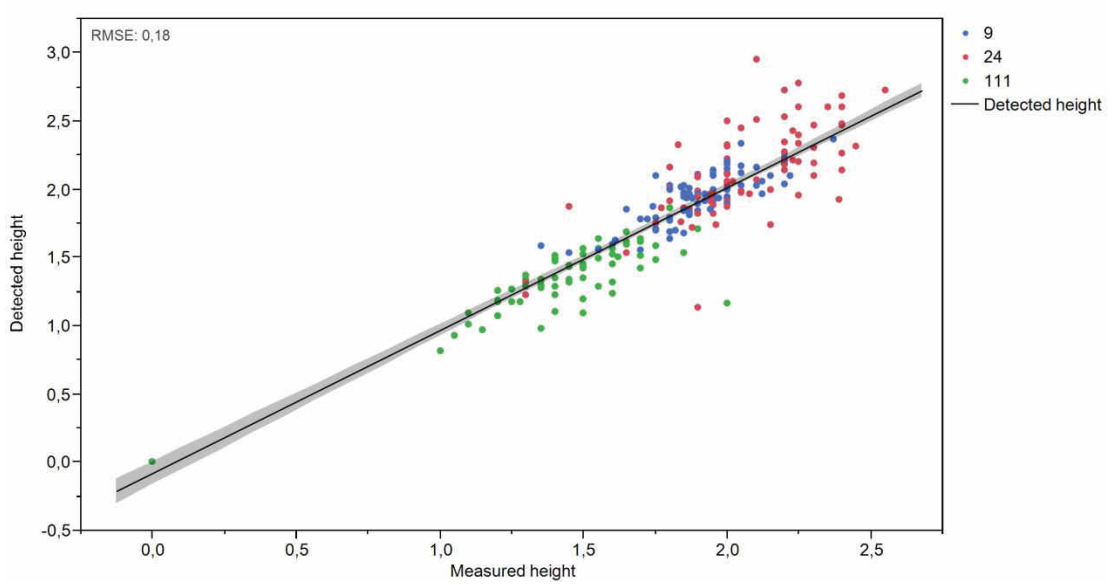

Figure 5. *Graphical comparison of measured vs. detected vine height. Different colors in the points indicate the different fields. The results of July and September are shown together.*

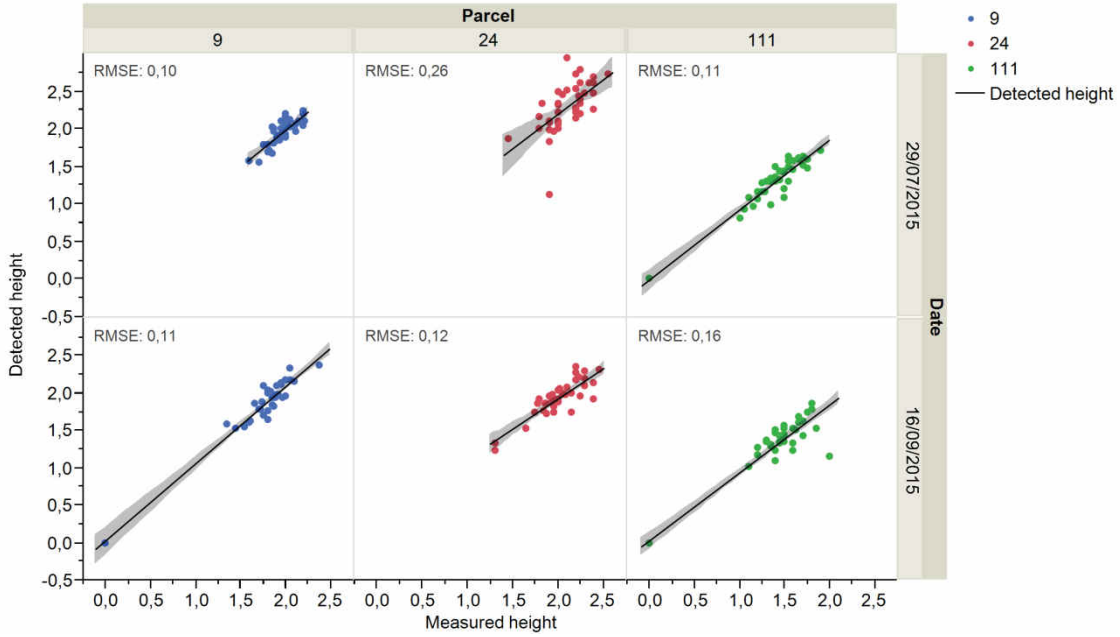

Figure 6. *Graphical comparison of measured vs. detected vine height divided by field and date. Different colors in the points indicate the different fields.*

5.4. Volume mapping

The workflow presented herein allows for growth monitoring of the vineyard during the entire growing cycle through the detection of the vineyard area and height, and the localization of gaps in the vine rows. The combination of accurate vine detection with good detection of vine height and its variability allows the calculation of the vine canopy volume (Fig. 7). All of these variables can be mapped in different moments of the year, which allows the identification of areas inside the vineyard that could have a problem and, consequently, need site-specific management (Andrew Hall et al. 2010). This information can also be exported as table files (e.g., Excel or ASCII format) (Table 5) for its use in variable-rate sprayers, a technique that has allowed savings of up to 58% of the application volume (Llorens et al. 2010), which represents an important reduction in pollution and operation costs.

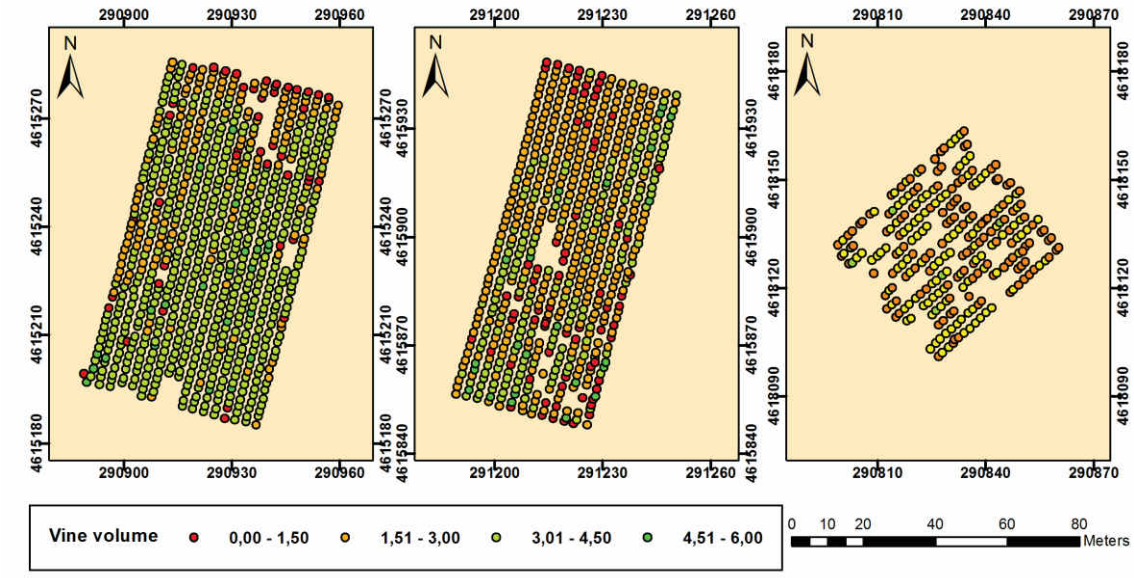

Figure 7. *Volume maps of the three fields on July. From left to right: Field 9, Field 24, and Field 111. Coordinates are in the WGS84, UTM zone 31N reference system.*

Table 5. *A sample of the output data file for vine segments of field 9 in September.*

X Center	Y Center	Length (m)	Width (m)	Area (m^2)	Vine max height (m)	Vine mean height (m)	Vine volume (m3)
290909.63	4615191.17	1.36	0.48	0.51	2.02	1.49	0.76
290909.85	4615192.23	2.06	1.41	1.93	2.13	1.33	2.56
…	…	…	…	…	…	…	…
290910.55	4615194.39	2.05	1.21	1.32	2.22	1.53	2.02
290918.60	4615225.30	2.06	1.74	2.35	2.22	1.72	4.05
290919.09	4615227.23	2.14	1.65	2.15	2.18	1.54	3.31
290919.60	4615229.19	2.03	1.37	1.46	2.00	1.41	2.06
290920.12	4615231.14	2.19	1.63	2.13	2.00	1.40	2.99

6. CONCLUSIONS

Three commercial vineyards were modelled in 3D on two different dates using images acquired with a low-cost camera onboard a UAV. A robust and automatic OBIA algorithm was developed for the 3D characterization of the vine parcels, including vine classification, height estimation and gap detection. Vine classification was based on the height variation in the DSMs because green-cover growing in the inter-rows could have led to misclassification due to the similarity in the spectral values of the cover and the vine canopy. The algorithm accurately detected the vine area, height, and the existence of gaps in most cases.

The combination of ultra-high-spatial resolution DSMs and the OBIA algorithm developed in this paper has been shown to be a valuable tool for the accurate characterization of the vines. The OBIA procedure computes multiple data that can be exported in image, vector and table format to be used as inputs in the design of variable rate treatments for precision viticulture. Furthermore, the classification of the vine can be used as a mask over thermal or multispectral imagery of the vineyards to isolate pixels corresponding to the vine canopy, which would allow for the extraction of more accurate information by avoiding the spectral mixing of the different soil uses.

7. ACKNOWLEDGMENTS

The authors thank RAIMAT S.A. for allowing developing the field work and UAV flights in its vineyards. This research was funded by the AGL2014-52465-C4-4R project (Spanish Ministry of Economy and Competition, FEDER Funds: Fondo Europeo de Desarrollo Regional). Research of Mr. Torres-Sánchez and Dr. Peña was financed by the FPI (BES-2012-052424) and Ramón y Cajal (RYC-2013-14874) Programs (Spanish MINECO funds), respectively.

8. REFERENCES

Arnó Satorra, J., Martínez Casasnovas, J. A., Ribes Dasi, M., & Rosell Polo, J. R. (2009). Review. Precision viticulture. Research topics, challenges and opportunities in site-specific vineyard management. http://repositori.udl.cat/handle/10459.1/41557. Accessed 30 September 2015

Ballesteros, R., Ortega, J. F., Hernández, D., & Moreno, M. Á. (2015). Characterization of Vitis vinifera L. Canopy Using Unmanned Aerial Vehicle-Based Remote Sensing and Photogrammetry Techniques. *American Journal of Enology and Viticulture*, ajev.2014.14070. doi:10.5344/ajev.2014.14070

Baluja, J., Diago, M. P., Balda, P., Zorer, R., Meggio, F., Morales, F., & Tardaguila, J. (2012). Assessment of vineyard water status variability by thermal and multispectral imagery using

an unmanned aerial vehicle (UAV). *Irrigation Science*, *30*(6), 511–522. doi:10.1007/s00271-012-0382-9

Bendig, J., Bolten, A., Bennertz, S., Broscheit, J., Eichfuss, S., & Bareth, G. (2014). Estimating Biomass of Barley Using Crop Surface Models (CSMs) Derived from UAV-Based RGB Imaging. *Remote Sensing*, *6*(11), 10395–10412. doi:10.3390/rs61110395

Blaschke, T., Hay, G. J., Kelly, M., Lang, S., Hofmann, P., Addink, E., et al. (2014). Geographic Object-Based Image Analysis – Towards a new paradigm. *ISPRS Journal of Photogrammetry and Remote Sensing*, *87*, 180–191. doi:10.1016/j.isprsjprs.2013.09.014

Bramley, R. g. v., & Hamilton, R. p. (2004). Understanding variability in winegrape production systems. *Australian Journal of Grape and Wine Research*, *10*(1), 32–45. doi:10.1111/j.1755-0238.2004.tb00006.x

Burgos, S., Mota, M., Noll, D., & Cannelle, B. (2015). Use of Very High-Resolution Airborne Images to Analyse 3d Canopy Architecture of a Vineyard. *The International Archives of Photogrammetry, Remote Sensing and Spatial Information Sciences*, *40*(3), 399.

Dandois, J. P., & Ellis, E. C. (2013). High spatial resolution three-dimensional mapping of vegetation spectral dynamics using computer vision. *Remote Sensing of Environment*, *136*, 259–276. doi:10.1016/j.rse.2013.04.005

Hall, A., Lamb, D. w., Holzapfel, B., & Louis, J. (2002). Optical remote sensing applications in viticulture - a review. *Australian Journal of Grape and Wine Research*, *8*(1), 36–47. doi:10.1111/j.1755-0238.2002.tb00209.x

Hall, A., Lamb, D. W., Holzapfel, B. P., & Louis, J. P. (2010). Within-season temporal variation in correlations between vineyard canopy and winegrape composition and yield. *Precision Agriculture*, *12*(1), 103–117. doi:10.1007/s11119-010-9159-4

Hellesen, T., & Matikainen, L. (2013). An Object-Based Approach for Mapping Shrub and Tree Cover on Grassland Habitats by Use of LiDAR and CIR Orthoimages. *Remote Sensing*, *5*(2), 558–583. doi:10.3390/rs5020558

Johnson, L. F., Roczen, D. E., Youkhana, S. K., Nemani, R. R., & Bosch, D. F. (2003). Mapping vineyard leaf area with multispectral satellite imagery. *Computers and Electronics in Agriculture*, *38*(1), 33–44. doi:10.1016/S0168-1699(02)00106-0

Laliberte, A., & Rango, A. (2011). Image Processing and Classification Procedures for Analysis of Sub-decimeter Imagery Acquired with an Unmanned Aircraft over Arid Rangelands. *GIScience & Remote Sensing*, *48*(1), 4–23. doi:10.2747/1548-1603.48.1.4

Llorens, J., Gil, E., Llop, J., & Escolà, A. (2010). Variable rate dosing in precision viticulture: Use of electronic devices to improve application efficiency. *Crop Protection*, *29*(3), 239–248. doi:10.1016/j.cropro.2009.12.022

Matese, A., Toscano, P., Di Gennaro, S. F., Genesio, L., Vaccari, F. P., Primicerio, J., et al. (2015). Intercomparison of UAV, Aircraft and Satellite Remote Sensing Platforms for Precision Viticulture. *Remote Sensing*, *7*(3), 2971–2990. doi:10.3390/rs70302971

Mathews, A. J. (2014). Object-based spatiotemporal analysis of vine canopy vigor using an inexpensive unmanned aerial vehicle remote sensing system. *Journal of Applied Remote Sensing*, *8*(1), 085199. doi:10.1117/1.JRS.8.085199

Mathews, A. J., & Jensen, J. L. R. (2013). Visualizing and Quantifying Vineyard Canopy LAI Using an Unmanned Aerial Vehicle (UAV) Collected High Density Structure from Motion Point Cloud. *Remote Sensing*, *5*(5), 2164–2183. doi:10.3390/rs5052164

Metz, M., Mitasova, H., & Harmon, R. S. (2010). Accurate stream extraction from large, radar-based elevation models. *Hydrology and Earth System Sciences Discussions*, *7*(3), 3213–3235. doi:10.5194/hessd-7-3213-2010

Nex, F., & Remondino, F. (2013). UAV for 3D mapping applications: a review. *Applied Geomatics*, *6*(1), 1–15. doi:10.1007/s12518-013-0120-x

Peña, J. M., Torres-Sánchez, J., de Castro, A. I., Kelly, M., & López-Granados, F. (2013). Weed Mapping in Early-Season Maize Fields Using Object-Based Analysis of Unmanned Aerial Vehicle (UAV) Images. *PLoS ONE*, *8*(10), e77151. doi:10.1371/journal.pone.0077151

Rey-Caramés, C., Diago, M. P., Martín, M. P., Lobo, A., & Tardaguila, J. (2015). Using RPAS Multi-Spectral Imagery to Characterise Vigour, Leaf Development, Yield Components and Berry Composition Variability within a Vineyard. *Remote Sensing*, *7*(11), 14458–14481. doi:10.3390/rs71114458

Schieffer, J., & Dillon, C. (2014). The economic and environmental impacts of precision agriculture and interactions with agro-environmental policy. *Precision Agriculture*, *16*(1), 46–61. doi:10.1007/s11119-014-9382-5

Smit, J. L., Sithole, G., & Strever, A. E. (2010). Vine signal extraction : an application of remote sensing in precision viticulture. Presented at the Article, SASEV. doi:http://scholar.sun.ac.za/handle/10019.1/8420

Tey, Y. S., & Brindal, M. (2012). Factors influencing the adoption of precision agricultural technologies: a review for policy implications. *Precision Agriculture*, *13*(6), 713–730. doi:10.1007/s11119-012-9273-6

Torres-Sánchez, J., López-Granados, F., Serrano, N., Arquero, O., & Peña, J. M. (2015). High-Throughput 3-D Monitoring of Agricultural-Tree Plantations with Unmanned Aerial Vehicle (UAV) Technology. *PLoS ONE*, *10*(6), e0130479. doi:10.1371/journal.pone.0130479

CAPÍTULO 9

CONCLUSIONES

El objetivo general de la presente Tesis Doctoral ha sido el desarrollo de metodologías automatizadas y robustas para la cartografía de malas hierbas en cultivos herbáceos en fase temprana y la monitorización tridimensional de cultivos leñosos, con el fin último de contribuir a la implementación de estrategias de técnicas de aplicación variable en el ámbito de la agricultura de precisión que permitan un uso sostenible de los productos fitosanitarios.

Este objetivo global se ha desarrollado a través de los siguientes objetivos específicos:

6. Estudiar la configuración y las especificaciones técnicas de un UAV y de los sensores embarcados para su aplicación en la detección temprana de malas hierbas y contribuir a la generación de mapas para diseñar un programa de control dirigido únicamente a dichas emergencias.
7. Evaluar los índices espectrales en el rango visible existentes en la literatura científica para su aplicación en la discriminación de suelo desnudo y vegetación (malas hierbas y cultivo) en imágenes tomadas con un UAV sobre cultivos de trigo en fase temprana.
8. Implementar en un entorno OBIA un método de cálculo automático de umbrales para la detección de vegetación (cultivo y malas hierbas) en imágenes procedentes de UAV tomadas en cultivos herbáceos (maíz, trigo y girasol) en fase temprana.
9. Desarrollar una metodología OBIA automática y robusta para la discriminación de malas hierbas en cultivos herbáceos en fase temprana, así como evaluar la influencia sobre su funcionamiento de distintos parámetros relacionados con la programación de los vuelos y la adquisición de imágenes UAV.
10. Desarrollar una metodología OBIA automática y robusta para la caracterización tridimensional de cultivos leñosos (olivar y viña) mediante imágenes y MDS generados a partir de imágenes procedentes de un UAV.

De los trabajos desarrollados para alcanzar los objetivos específicos marcados en esta Tesis Doctoral se han podido obtener las siguientes **conclusiones**:

1. La tecnología UAV es capaz de proporcionar imágenes con la resolución espacial y temporal necesarias para la detección de malas hierbas en fase temprana. La resolución espacial de las imágenes, el área cubierta por cada una y el tiempo de vuelo necesario para abarcar una parcela completa varían en función de las especificaciones del sensor, el porcentaje de solape (transversal y longitudinal) y la altura de vuelo. La resolución espacial óptima debe ser definida de acuerdo al objetivo planteado. Para discriminar plantas individuales de malas hierbas, sería recomendable un píxel menor de 4 cm, lo que con los sensores utilizados en esta Tesis correspondió a altitudes de vuelo por debajo de 100 m. Si el objetivo es la detección de rodales de malas hierbas, el UAV puede volar más alto y generar píxeles de

menor resolución. Además de la altitud de vuelo y el sensor utilizado, es necesario considerar el porcentaje de solape y la duración de las baterías del UAV ya que el número de imágenes necesarias para cubrir una parcela completa a baja altura y con elevados porcentajes de solape requiere más tiempo y ello puede ocasionar problemas relacionados con la autonomía del UAV en el diseño de rutas de vuelo.

2. Las diferencias espectrales en imágenes tomadas con un UAV entre malas hierbas, cultivo y suelo desnudo fueron significativas para los índices NGRDI y ExG, sobre todo en vuelos a 30 m de altitud. Sin embargo, a mayor altitud las malas hierbas y plantas de cultivo en fases tempranas de crecimiento presentan valores espectrales similares. La estrategia que podría mejorar su clasificación sería mediante el uso de técnicas OBIA que añadan al análisis de las imágenes información contextual a la espectral.
3. Los índices de vegetación calculados a partir de una serie multitemporal de imágenes tomadas con un sensor en rango visible (RGB) de bajo coste a bordo de un UAV permiten discriminar vegetación (cultivo y malas hierbas) en campos de trigo en fase temprana. Entre los índices evaluados, los resultados más satisfactorios fueron obtenidos con ExG y VEG, siendo ExG el más preciso para aplicaciones prácticas en agricultura debido a su mayor simplicidad y su mejor ajuste en vuelos realizados a 30 y 60 m de altitud en todas las fechas de toma de imágenes evaluadas. Por tanto, la altitud y la fecha de vuelo deben ser evaluados y fijados según los objetivos de la toma de imágenes.
4. Es posible la umbralización automática de índices espectrales para la clasificación de vegetación (cultivo y malas hierbas) mediante el desarrollo de un algoritmo automático y eficiente que adapta el método de Otsu a un entorno OBIA. Se ha demostrado la habilidad del algoritmo para seleccionar un umbral de un histograma de niveles de gris con independencia de que este sea unimodal o bimodal. Además, el uso de este procedimiento en un entorno OBIA aumenta su transferibilidad al eliminar la necesidad de calcular los umbrales óptimos para cada área de manera manual.
5. Se ha desarrollado un procedimiento OBIA robusto y automático para la discriminación de malas hierbas en imágenes tomadas por UAV sobre cultivos herbáceos en fase temprana. Las malas hierbas son identificadas en base a su posición relativa respecto a las líneas de cultivo. El algoritmo diseñado calcula parámetros estadísticos derivados del análisis de la imagen y puede ser exportado en diversos formatos, lo que permite su implementación en programas de SSWM para el diseño de mapas de tratamientos herbicidas.
6. En campos de girasol y estudiando un conjunto de imágenes multitemporales, la mayor precisión en la detección de malas hierbas fue obtenida mediante imágenes capturadas a 40 m de altitud 50 días después de la siembra, cuando el cultivo y las malas hierbas tienen 5-6

hojas verdaderas (código 15-15 en la escala BBCH). En esta fecha, se obtuvo una precisión del 91% con un sensor multiespectral (RGB+NIR). En vuelos a 40 m de altitud, las imágenes capturadas en la fecha anterior mostraron una precisión ligeramente mayor que las tomadas con posterioridad. Sin embargo, a altitudes superiores a los 60m, las imágenes generadas con el sensor en rango visible (RGB) dieron mejores resultados en la tercera fecha debido al mayor tamaño de las malas hierbas. Con el fin de ofrecer una aplicación práctica al usuario interesado, se realizan una serie de recomendaciones para que antes de iniciar trabajos de detección de malas hierbas con UAV se consideren varios factores: 1) características y precio del sensor; 2) área cubierta en cada vuelo; 3) grado de precisión necesario; 4) objetivo agronómico.

7. La combinación de imágenes UAV de muy alta resolución espacial con el procedimiento OBIA desarrollado permite la generación de mapas de malas hierbas en cultivos herbáceos en fase temprana. Estos mapas de emergencias permiten diseñar mapas de tratamientos localizados de herbicidas que se pueden adaptar a cada cultivo y a diferentes tamaños de distancia entre los pulverizadores de los equipos de tratamiento, lo cual no había sido posible previamente. El procedimiento OBIA permite calcular información del cultivo exportable en los formatos de tabla, vectorial o ráster. Esta tecnología ha demostrado la posibilidad de ahorros medios herbicidas cercanos 70%, pudiendo ayudar en la implementación de las legislaciones europea y española para el uso sostenible de fitosanitarios, una de cuyas finalidades consiste en promover la reducción de las aplicaciones de herbicidas.

8. Se ha demostrado la capacidad de la tecnología UAV para generar eficientemente datos tridimensionales de centenares de árboles en cultivos leñosos. En la investigación realizada en esta Tesis Doctoral se eligió el cultivo del olivar por su relevancia en la Cuenca Mediterránea y se abordó en parcelas gestionadas tanto de manera intensiva (en seto) como tradicional. Mediante el innovador algoritmo OBIA desarrollado, se ha podido llegar a un 97% de precisión en la cuantificación del área de copa proyectada y a mínimas desviaciones en las estimaciones de la altura y el volumen, ofreciendo una valiosa alternativa a las mediciones en campo. La información georreferencia generada por el procedimiento OBIA permite crear mapas que reflejan la variabilidad del cultivo, pudiendo ser utilizados para el diseño de tratamientos fitosanitarios con tecnología variable que ayuden a reducir la cantidad de producto aplicado a su parte aérea y en consonancia con las legislaciones europea y española vigentes. El procedimiento OBIA permite calcular información del cultivo exportable en los formatos de tabla, vectorial o ráster. Además, permite estudiar las relaciones entre el crecimiento de los árboles y otros factores como propiedades del suelo, la topografía del

terreno, infestaciones de malas hierbas o árboles afectados por algún insecto-plaga, hongo u otro tipo de estrés.

9. Se ha desarrollado un novedoso y robusto algoritmo de OBIA para la caracterización y monitorización 3D de viñedos. La clasificación de la viña se basó en la variación de alturas en los MDS, lo que permitió evitar los problemas que la vegetación creciendo entre las hileras de viña hubiera provocado en caso de utilizar una aproximación basada en píxeles e índices de vegetación. El procedimiento OBIA es totalmente automático, auto-adaptativo a diferentes situaciones en el campo y permite calcular información del cultivo exportable en los formatos de tabla, vectorial o ráster. Los resultados demuestran una gran precisión en la clasificación de las cepas, en torno al 90-95%, así como pequeños errores en la estimación de la altura de la viña (RMSE de 0,18 m de media). Además, el algoritmo puede calcular la posición, área proyectada y volumen de cada cepa del viñedo, lo que aumenta el potencial de esta tecnología para desarrollar estrategias relacionadas con la tecnología basada en aplicación variable de fitosanitarios dirigidos a la parte aérea del cultivo.

Jorge Torres Sánchez realizó sus estudios de Ingeniero de Montes en la ETSIAM de la Universidad de Córdoba, donde trabajó en el Departamento de Ingeniería Forestal hasta 2008, año en que finalizó sus estudios. Tras esta fase de formación desarrolló durante dos años labores como técnico en EGMASA (empresa pública de gestión medioambiental).

En 2012 se incorporó al Grupo de Teledetección y Agricultura de Precisión (imaPing) del Instituto de Agricultura Sostenible de Córdoba (Consejo Superior de Investigaciones Científicas) bajo la dirección de la Dra. Francisca López Granados. En 2013 comenzó su Tesis Doctoral financiada por el programa FPI (BES-2012-052424), bajo la supervisión de los Dres. Francisca López Granados y José Manuel Peña Barragán, y cuyos objetivos se han desarrollado en dos proyectos aprobados por el Mº de Economía y Competitividad (AGL2011-30442-C02-01 y AGL2014-52465-C4-4-R).

Durante su etapa predoctoral ha expuesto sus trabajos en Congresos Nacionales e Internacionales relacionados con el control de malas hierbas o la agricultura de precisión como el *XV Congreso de la Sociedad Española de Malherbología* (Sevilla, 2015) o la *12th Conference on Precision Agriculture* (Sacramento, USA, 2014). Sus aportaciones en Congresos Internacionales han sido merecedoras de varios premios. También ha publicado los resultados de su Tesis Doctoral en varias revistas de investigación incluidas en el *Science Citation Index* y especializadas en varias disciplinas (teledetección, sensorización, computación, agricultura de precisión).

Parte de su labor investigadora se ha desarrollado en instituciones extranjeras realizando estancias de investigación en la *Maison de la Télédétection* (Montpellier, Francia) bajo la supervisión del Dr. Sylvain Labbé y en el *Z_GIS Department of Geoinformatics* (Salzburgo, Austria) bajo la supervisión del Dr. Stefan Lang.